Centrifuge modelling of drained lateral pile - soil response

Application for offshore wind turbine support structures

Rasmus Tofte Klinkvort

PhD Thesis

Department of Civil Engineering

2012

DTU Civil Engineering Report R-271 (UK)
2012

DTU Civil Engineering
Department of Civil Engineering

Centrifuge modelling of drained lateral pile - soil response

- Application for offshore wind turbine support structures

Rasmus Tofte Klinkvort

Ph.D. Thesis

Department of Civil Engineering
Technical University of Denmark

2012

Supervisors:

Associate Professor Ole Hededal, Technical University of Denmark - DTU, Denmark
Professor Sarah M. Springman, Swiss Federal Institute of Technology - ETH Zurich, Switzerland

Assessment Committee:

Professor Jürgen Grabe, Technical University Hamburg-Harburg - TUHH, Germany
University Lecturer Byron Byrne, University of Oxford, England
Associate Professor Anette Krogsbøll, Technical University of Denmark - DTU, Denmark

Centrifuge modelling of drained lateral pile - soil response
-Application for offshore wind turbine support structures

Printed by DTU-Tryk
Department of Civil Engineering
Technical University of Denmark
ISBN: 9788778773579
ISSN: 1601-2917

Preface

This thesis is submitted as a partial fulfilment of the requirements for the Danish Ph.D. degree. The work title of the project has been "Cyclic laterally response of wind turbine monopile foundation in saturated sand". The thesis is divided into two parts. The first part introduces the research field, discusses the methodology, highlights the major findings and provides an overview of the work carried out within this project along with a discussion. The second part is a collection of papers that constitute the basis of the work and describe the work in greater detail and serves as scientific documentation.

Lyngby, the 29$^{\text{th}}$ of June 2012

Rasmus Tofte Klinkvort

Preface to published version

The thesis was defended at a public defence on Wednesday the 17th of October 2012. Official opponents were Professor Jürgen Grabe, Technical University Hamburg-Harburg - TUHH, University Lecturer Byron Byrne, University of Oxford and Associate Professor Anette Krogsbøll, Technical University of Denmark. Subsequently the Ph.D. degree was awarded from the Technical University of Denmark. Compared to the original submitted version of the thesis a number of minor editorial corrections have been implemented and the status of some of the papers on which the thesis is based has changed from submitted to accepted.

Oslo, the 1th December 2012

Rasmus Tofte Klinkvort

Acknowledgements

I acknowledge the supervision and inspiration given to me by my supervisor Associate Professor Ole Hededal. As a part of the Ph.D. studies, I went to ETH Zurich working with their Geotechnical group. The time at ETH was inspiring and I would like to thank Professor Sarah M. Springman for sharing her knowledge of centrifuge modelling with me. Furthermore, I thank Caspar Thrane Leth for the introduction to centrifuge modelling and discussions concerning laterally loaded piles.

To maintain focus on the scientific content of the thesis, a well-written thesis is important. For helping me with proofreading the manuscript, I would like to give a big thanks to Einar Thór Ingólfsson and Morten Møller van Gils Hansen.

Abstract

The installation and foundation cost of offshore wind turbines is substantial, and today energy from offshore wind is not competitive with energy from more classical energy production methods. The goal of this research project has been to develop simple engineering tools, which can be used in the design of a technical optimal and cost beneficial solution for an offshore wind turbine foundation and thereby reduce the price of energy from offshore wind turbines. The methodologies developed in this thesis hopefully contribute to a better understanding within this field.

Monopiles are one of the most popular foundation methods today for offshore wind turbines. These piles are often installed in dense sand at water depths ranging from 10-30 meters. A monopile is a single, large diameter tubular steel pile. The current design methodology originates from tests on long slender piles but is also used for monopiles today. Therefore, it appears that the methodology for monopiles lacks scientific justification and a better understanding of rigid piles is needed.

More than 70 centrifuge tests on laterally loaded rigid model piles have been carried out in connection with this thesis to get a better understanding of rigid piles. The tests have been performed in homogeneously dense dry or saturated Fontainebleau sand in order to mimic simplified drained offshore soil conditions.

Approximately half of the tests have been carried out to investigate the centrifuge procedure in order to create a methodology of testing that enables the transformation of result from tests in model scale to prototype scale. The grain size to pile diameter ratio, the non-linear stress distribution and the pile installation was identified from this investigation as important parameters in reliable scaling of centrifuge results.

The remaining tests were used to investigate the pile - soil interaction to gain a better in-sight into the complex problem. A monotonic test series was carried out initially and then pile - soil interaction curves were deduced from these tests and compared with methodologies used today. The results indicate that the current methodologies can be improved and a modification

to the methodology has been proposed. Secondly, a cyclic test series was carried out. The accumulation of displacement and the change in secant stiffness of the total response of these tests were evaluated. A simple mathematical model was proposed to predict the accumulation of displacement and change in secant stiffness using the observations seen in the centrifuge.

With the centrifuge test observation as basis, a cyclic pile - soil interaction element was developed. The element can be used in Winkler type analysis where the soil is modelled as spring elements and the rest of the structure as beam elements. The model was calibrated against monotonic and cyclic centrifuge tests. The element predicts the hysteresis seen on element level in an acceptable way, but does not predict the accumulation of displacements and change in secant stiffness as seen in the experiments. The element used in a dynamic analysis gives an estimate of the frictional soil damping. The capabilities of the element were demonstrated by a series of free decay simulations where the logarithmic decrement could be calculated afterwards.

All together, the methodologies developed in this thesis can be directly used in the design of offshore monopiles, with a scientific justification based on centrifuge model scale tests.

Resumé

Omkostningerne for havvindmølle fundamenter er store og i dag er energi fra havvindmøller, ikke konkurrencedygtig med energi fra mere klassiske energi produktionsmetoder. Målet med dette forskningsprojekt er at udvikle simple tekniske værktøjer, der kan bruges i udformningen af en teknisk optimal og omkostningseffektiv løsning for et havvindmølle fundament og derved være med til at gøre prisen på energi fra havvindmøller lavere. De udviklede metoder i denne afhandling bidrager til en bedre forståelse inden for dette område.

Monopæle er i dag en af de mest populære fundaments metoder til havvindmøller. Disse pæle er ofte installeret i tætpakket sand på vanddybder, der spænder fra 10-30 meter. En monopæl er en cylindrisk stålpæl med stor diameter. De nuværende design metoder stammer fra test på lange, slanke pæle, men bruges i dag også til design af monopæle. Det videnskabelige grundlag for design af monopæle er mangelfuldt og en bedre forståelse af opførelsen af stive monopæle er derfor nødvendig.

I forbindelse med denne afhandling er der udført mere end 70 centrifuge test for at få en bedre forståelse af opførelsen af tværbelastede stive pæle. Alle tests er blevet udført i homogent tætpakket tørt eller vandmættet Fontainebleau sand for at efterligne drænede jordbundsforhold.

Omkring halvdelen af forsøgene er udført for at undersøge centrifuge udførelses teknikken med henblik på at skabe en metode til at transformere resultater fra forsøg i model skala til resultater i prototype skala. Fra denne undersøgelse blev forholdet mellem kornstørrelse og pæle diameter, den ikke-lineære spændingsfordeling og pæleinstallationen identificeret som vigtige parametre i en pålidelig skalering af centrifuge resultaterne.

Resten af testene blev anvendt til at undersøge pæl-jord interaktionen og derved få et større indblik i det komplekse problem. Først blev en statisk test serie gennemført hvorfra pæl - jord interaktions kurver blev udledt og sammenlignet med eksisterende metoder. Resultaterne viste, at de nuværende metoder kan forbedres, og en modifikation af metoden blev foreslået. Dernæst blev en cyklisk test serie udført, hvorfra akkumulering af flytning og ændring i sekant stivhed af den samlede reaktion blev målt. En simpel matematisk

model til at forudsige akkumulering af flytning og ændring i sekant stivhed blev foreslået baseret på observationer set i centrifugen.

Med resultaterne fra centrifugen som grundlag blev et cyklisk pæl - jord interaktions element udviklet. Elementet kan bruges i en Winkler-type analyse, hvor jorden er modelleret som fjedre elementer og resten af strukturen, som bjælker elementer. Modellen blev kalibreret til de statiske og cykliske centrifuge forsøg, og elementet forudsiger hysterese set på element niveau i en acceptabel form. Modellen kan dog ikke forudsige akkumuleringen af flytninger og ændringer i sekant stivhed, som det var observeret i centrifuge forsøgene. Elementet kan anvendes i en dynamisk analyse, hvor det kan bruges til at giver et skøn over jorddæmpningen fra friktion. Opførelsen af elementet blev demonstreret ved en række frie svingnings simuleringer, hvor det logaritmiske dekrement bagefter kunne beregnes.

Metoderne udviklet i denne afhandling kan anvendes direkte i designet af offshore monopæle, med et videnskabeligt belæg baseret på centrifuge forsøg udført i model skala.

Contents

Additional work (not included in the thesis)

- R. T. Klinkvort. Single piles under lateral loading, Lecture notes in: Advanced Geotechnical Engineering, DTU - Civil engineering 2008
- R. T. Klinkvort. Monopile foundations for offshore wind turbines, Department of Civil Engineering, Annual Report 2010
- R. T. Klinkvort. Centrifuge modeling of monopiles, 20th European Young Geotechnical Engineers Conference 2010
- R. T. Klinkvort. Hvordan funderes næste generation af havvindmøller, Danskernes Akademi, Invited lecture in DR2. Broadcasted in televison january 2010.
  Homepage:
  `http://www.dr.dk/DR2/Danskernes+akademi/Natur_Matematik/Hvordan_funderes_den_naeste_generation_af_havvindmoeller.htm`
- R. T. Klinkvort, C. T. Leth & O. Hededal. Centrifuge modelling of monopiles in dense sand at The Technical University of Denmark, Eurofuge 2012
- C T Leth S. P. H. Sørensen, R. T. Klinkvort, A. H. Augustesen, L. B. Ibsen and O. Hededal. A snapshot of present research at AAU and DTU on large-diameter piles in coarse-grained materials, Nordic Geotechnical Meeting, NGM2012 2012

Nomenclature

α	Hardening parameter
α	Non-dimensional accumulation of displacement constant
δ	Logarithmic decrement
η	Increase in gravity
γ'	Effective unit weight
κ	Secant stiffness accumulation rate
ω	Rotational frequency
ϕ'	Effective angle of friction
ϕ'_{cr}	Critical state angle
ρ	Sand density
σ'_1	Vertical stress in triaxial test
σ'_3	Radial stress in triaxial test
σ'_v	Effective vertical stress
$\tilde{H}$	Normalised horisontal shear force
$\tilde{K_s}$	Secant stiffness from monotonic test
$\tilde{P}$	Normalised horisontal shear with K_p
$\tilde{p}$	Normalised soil resistance, K
$\tilde{y}$	Normailised pile displacement
ζ_b	Non-dimensional magnitude of the cyclic loading

ζ_c	Non-dimensional characteristic of the cyclic loading
A	Empirical depth factor
C_u	Coefficient of uniformity
CO_2	Carbon dioxide
d	Diameter of pile
d_{50}	Average grain size
E_p	Elasticity modulus pile
E_s	Elasticity modulus sand
e_{max}	Maximum void ratio
e_{min}	Minimum void ratio
E_{py}	Initial stiffness of pile - soil interaction curve
g	Natural gravity acceleration
G_s	Specific gravity of particles
H	Horisontal shear force / Total response
H	Step function
H_{wave}	Lateral wave load
H_{wind}	Lateral wind load
I	Pile installation
I_p	Moment of inertia pile
K	Earth pressure coefficient
k	Initial subgrade modulus
K_0	Earth pressure coefficient at rest
K_N	Secant stiffness to a given load cycle
K_p	Passive earth pressure coefficient by Rankine
K_q^0	Earth pressure coefficient at shallow depth by Brinch Hansen

K_q^∞ Earth pressure coefficient at greater depth by Brinch Hansen

$K_{ult,API}$ Ultimate earth pressure coefficient by API

$K_{ult,BH}$ Ultimate earth pressure coefficient by Brinch Hansen

$K_{ult,B}$ Ultimate earth pressure coefficient by Broms

l_e Load eccentricity

l_L Pile penetration

M Bending moment

m Bending moment in pile

N Number of cycles

N_s Scaling factor

p Soil resistance

p' Effective mean pressure

p_u Current soil yield strength

p_u^{drag} Soil drag capacity

p_u^{face} Soil resistance build up

p_u^{virgin} Soil resistance virgin curve

P_{max} Maximum cyclic load

P_{min} Minimum cyclic load

P_{mon} Bearing capacity from monotonic test

R Centrifuge radius

R_t Centrifuge radius to sand surface

t Pile thickness

T_b Non-dimensional cyclic load function

T_c Non-dimensional cyclic load function

Y Overall displacements

y	Pile displacement
$y*$	Corrected displacement
y_{bt}	Artificial starting point of virgin curve
z	Depth in soil profile

Part I

Extended summary

Chapter 1

Introduction

As a consequence of recent climatic changes, the focus on alternative sustainable energy has increased in the past decade. It is widely accepted that the emission of carbon dioxide (CO_2) is one of the key reasons for global warming. Renewable energy sources generally have a low CO_2 impact and are therefore a good and sustainable tool in the fight against global warming.

1.1 Offshore wind farms

Several energy-producing alternatives are available, and one of these alternative sources is energy from wind turbines, Figure 1.1. Wind turbines generate a small amount of CO_2 emission only from the construction and installation of the turbine, and are today the second largest contributor to sustainable energy production, (Agency, 2009). Onshore wind turbines are easy to install and are today combatable with fossil energy production. There are some environmental concerns, including visual impact, noise and the risk of bird collision. In particular, the low visual impact but also larger production rates are drivers for offshore wind turbines. The wind conditions at sea level are smooth, and the low wind shear and steeper gradient of wind speed, subjects the offshore wind turbine to smaller turbulence. Low wind turbulence will increase the lifetime of a wind turbine and the production is about 50% larger compared to onshore turbines due to larger wind turbines, (Agency, 2008).

The installation and foundation costs of offshore wind turbines are greater than those of onshore wind turbines, and today energy from offshore wind is not competitive with energy from more classical energy production methods. Despite the extra cost, several offshore wind turbine farms have been estab-

***Figure 1.1**: Offshore wind turbine park, under construction, Picture from: http://apps1.eere.energy.gov/news/news_detail.cfm/news_id=15982*

lished, but if the development in offshore wind farms shall succeed, the price on energy has to become competitive. As seen in Figure 1.2, the price of the support structure for an offshore installed wind turbine is about 20% of the total cost. If this ratio can be cut down by improvement of technical solutions, the total price of an offshore wind turbine and the price of electricity from wind turbines can be reduced.

The goal of this research project is to develop simple engineering tools, which can be used in the design of a technically optimal and cost beneficial solution for offshore wind turbine foundation.

1.2 Loads on offshore wind turbines

Offshore wind turbines are placed in a harsh environment with loads from wind and waves acting on the structure. The wind turbine is a tall and slender construction and is therefore dynamically sensitive. A sketch of the primary forces acting on a wind turbine can be seen in Figure 1.3. The primary forces on an offshore wind turbine are lateral loads from wind and waves, shown in

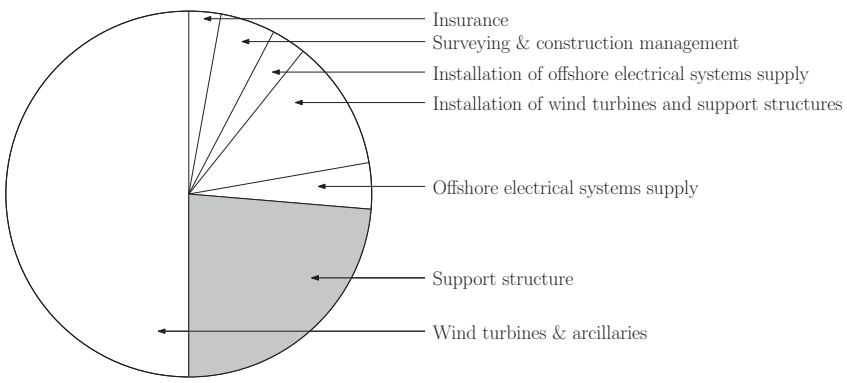

***Figure 1.2**: Schematic view of the cost of a offshore wind turbine, reproduced from: http://www.wind-energy-the-facts.org/en/part-i-technology/chapter-5-offshore/wind-farm-design-offshore/*

Figure 1.3 as H_{wind} and H_{wave}. The two forces will both result in random cyclic lateral reactions in the foundation. A typical power spectrum of the forces acting on an offshore wind turbine is given in Figure 1.4. The loading frequencies from wind and waves are given here, with a peak wave frequency of about 0.1 Hz and a peak wind frequency of about 0.01Hz. The rotor frequency range, often called 1P, and the blade passing frequency range from a three-blade wind turbine, called 3P, are also shown in Figure 1.4. It is important in the design to achieve a first natural frequency of the structure which lies outside these frequencies. This is normally achieved through a design where the entire wind turbine structure has an eigenfrequency in between 1P and 3P, normally called a soft-stiff structure. Considering typical turbines this range is rather narrow, and can be difficult to obtain, special for wind turbines installed at large water depths.

The design of a foundation supporting an offshore wind turbine is carried out in four design limit states, e.g. DNV (2011):

a Ultimate limit state, ULS - Total collapse of the foundation

b Serviceability limit state, SLS - Permanent rotation of turbine tower exceeds limits

c Fatigue limit state, FLS - Material collapse due to large number of cycles

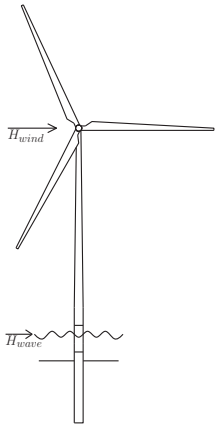

***Figure 1.3**: Force resultants on offshore wind turbine*

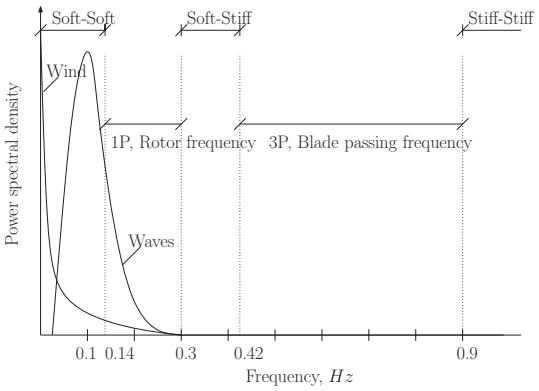

***Figure 1.4**: Typical range of forcing frequencies for an offshore wind turbine, (DNV, 2011)*

d Accident limit state, ALS - Total collapse of foundation from e.g. ship impact

A robust design tool should be capable of handling these design limit states. This includes a description of the ultimate bearing capacity of the foundation in the ULS/ALS situation, which should consider the effects of cyclic loading from different directions and the corresponding accumulation of rotation in SLS situation. In the FLS situation, it should give a good prediction of the stiffness of the foundation and thereby also the eigenfrequency of the total wind turbine structure. Furthermore, an accurate description of the soil damping is beneficial for all design states due to the load reduction in the resonance regimes.

1.3 Monopile support for offshore wind turbines

Different foundation concepts can be chosen in order to support the offshore wind turbine. This thesis will concentrate on the monopile concept as, installed in dense sand. Dense sand is a typical offshore site condition in the North Sea; here waves have compacted sand to a relative density of around 90% and more.

Monopiles are the most widely used foundation method for offshore wind turbines. These piles are often installed in dense sand at water depths ranging from 5-30 meters. A monopile is a single large diameter tubular steel pile driven 4 to 6 times its diameter into the seabed. The diameter of the piles ranges from 4-6 meters. A picture of a monopile before installation is

Figure 1.5*: Picture of one of the monopiles used at Walney Wind Farm, Credit: Dong Energy*

shown in Figure 1.5. These piles are driven vertically into the seabed and a transition piece is placed on the top of the monopile, which can correct small rotations during installation. The transition piece is connected to the monopile by a grouted connection and the wind turbine is mounted on top of the transition piece. It is assumed in the stability design of the monopile foundation that these connections are rigid, neglecting any deformation in the connection. As a simplification, the monopile can therefore be treated as a short rigid pile with a relatively large lateral load eccentricity.

1.4 Work hypothesis

A laterally loaded rigid circular pile, with a relative high ratio of shear force to bending moment is investigated in this thesis, neglecting the vertical load.

The investigation is carried out for both monotonic and uni-directional cyclic load scenarios in dense sand. The monotonic and the cyclic loading are applied quasi static and it is assumed that no pore pressure develops. The effect of pore pressure accumulations and bi-directional cyclic loading are therefore outside the scope of this thesis.

To establish a work hypothesis, it is important to recognize how soil resistance is acting on the rigid monopile. When a pile is laterally loaded, it will start to move and the soil will resist this movement. The bearing capacity of a laterally loaded pile is an interaction between the pile displacement and the resistance of the soil also known as soil-pile interaction. A sketch of a monopile is shown in Figure 1.6. The monopile is loaded at seabed with a combination of horizontal shear force (H) and bending moment ($M = l_e \cdot H$). The applied load is carried by the monopile as a combination of soil pressures

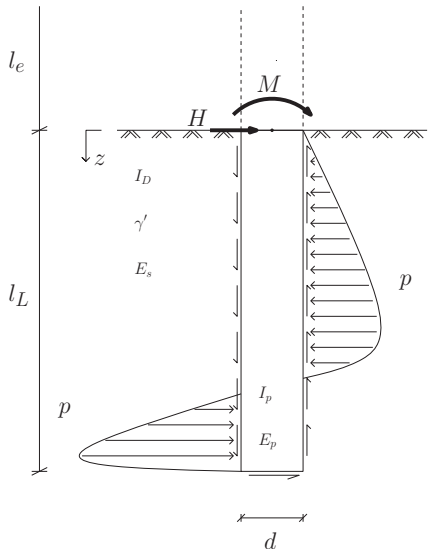

***Figure 1.6**: Sketch of forces acting on a laterally loaded pile*

and friction acting on the pile. The soil response from these forces needs to be seen from a 3 dimensional perspective. A sketch of the pressures acting on a pile cross section is shown in Figure 1.7. The pile is subjected to soil pressure and friction on the side of the pile. To simplify the 3 dimensional friction and pressure distributions all these factors are merged into one single soil resistance, sometimes called the modulus approach. The soil resistance, (p) can then be calculated as the effective stress at a given depth ($\sigma'_v = \gamma' \cdot z$)

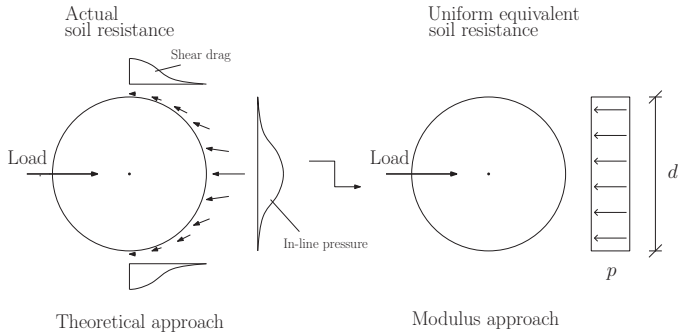

***Figure 1.7**: Sketch of soil pressure approximation in a cross section of the pile, after (Smith, 1987)*

times an earth pressure coefficient (K) integrated over the width of the pile (d),(Briaud et al. (1983) and Smith (1987)). This can be written as:

$$p = K \cdot d \cdot \sigma'_v \tag{1.1}$$

It is important to recognize that the earth pressure coefficient also incorporates the friction acting on the pile from both horizontal and vertical directions. The parameter can be seen as the difference in the active and passive soil pressure including the friction acting on the pile. This is illustrated in Figure 1.7 where the actual stress distribution is shown to the left, whereas the simplification, which is used in the general approximation in (1.1), is shown to the right.

It is the behavior of the simplified non-dimensional soil resistance K, which is important for the total performance of the monopile foundation and is therefore the focus of this study. This can be done by looking either directly at K, or by looking at the total response of the pile, knowing that the capacity of the pile is a function of the soil resistance.

$$H = \int_0^{l_L} K \cdot d \cdot \sigma_v \, dz \tag{1.2}$$

The hypothesis of this thesis is that the modulus approach shown in (1.1) is independent of the pile diameter. The non-dimensional soil resistance K is therefore a function of a set of independent parameters as shown in equation (1.3) if full similarity in the geometry is kept constant (const.=$\frac{e_L}{d}$ & const.=$\frac{E_p I_p}{E_s d^4}$). Scaled models can therefore be used in the investigation of K.

$$K = f(\phi', z/d, I, N, \zeta_b, \zeta_c) \tag{1.3}$$

Here ϕ' is the effective angle of friction of the sand, z/d is the normalized depth in the soil, I is installation of the pile, N is the number of load cycles, ζ_b is the magnitude of the cyclic loading and ζ_c is the characteristic of the cyclic loading.

By planning a test program that investigates the influence of the different parameters independently, the function showed in (1.3) can be determined. When the influence is known, a model is set up which can handle the four design limit states and can be used to provide a better technical solution for a monopile supporting an offshore wind turbine.

Chapter 2

Background review

With the increase in offshore oil and gas structures in the fifties, focused research began to derive the response of laterally loaded piles. The methods developed at that time are still the basis for offshore monopile design today. This chapter will present the methodology and will be divided into three sections. The first section presents methodologies for calculation of the ultimate bearing capacity. The following section presents examples on formulations of the pile-soil interaction. Finally, the state of the art research on monopiles for offshore wind turbines is presented.

2.1 Ultimate bearing capacity

The bearing capacity of a laterally loaded pile can be found knowing the distribution and magnitude of the soil resistance acting on the pile. The soil resistance is determined using the simplification shown in equation (1.1). Broms (1964) presented a very simple method to calculate the bearing capacity of a rigid laterally loaded pile in sand. He assumed an increasing soil resistance acting only on the opposite side of the applied load of the pile. To ensure moment equilibrium a single force is needed at the pile tip. The earth pressure coefficient has to be calculated to determine the soil resistance and is defined as 3 times the passive Rankine pressure as shown (2.1).

$$K_{ult,B} = 3 \cdot K_p = 3 \cdot \tan^2(45 + \phi'/2) \tag{2.1}$$

When the ultimate soil resistance distribution is known, the maximum capacity of the pile can be found by moment equilibrium around the pile toe, for details see Broms (1964).

In reality, the soil resistance profile is not as simple as that assumed by Broms (1964). A method with a soil resistance acting on both sides of a

rigid pile was presented by Hansen (1961). This approach is slightly more sophisticated and thereby also more complex to use. Based on plasticity theory, Hansen (1961) operates with two different kinds of failure mechanisms when defining the soil pressure coefficient. A failure at shallow depth where the pile pushes the soil up (K_q^0) and a failure at greater depth where the pile pushes the soil around the pile (K_q^∞). The failure at shallow depth can be described as:

$$K_q^0 = e^{\pi/2+\phi' \tan\phi'} \cos\phi' \tan(45^o + \phi'/2) - e^{-(\pi/2-\phi')\tan\phi'} \cos\phi' \tan(45^o - \phi'/2) \tag{2.2}$$

and the failure at greater depth is given by

$$K_q^\infty = N_c \cdot d_c^\infty \cdot K_0 \cdot \tan\phi' \tag{2.3}$$

where:

$$N_c = (e^{\pi \tan\phi'} \tan^2(45^o + \phi'/2) - 1) \cot\phi' \tag{2.4}$$
$$d_c^\infty = 1.58 + 4.09 \tan^4\phi' \tag{2.5}$$
$$K_0 = 1 - \sin\phi' \tag{2.6}$$

This is combined in a function which ensures a smooth transition from shallow to failure at greater depth.

$$K_{ult,BH} = \frac{K_q^0 + K_q^\infty \alpha_q \frac{z}{d}}{1 + \alpha_q \frac{z}{d}} \tag{2.7}$$

The value α_q is a parameter which controls the transition from shallow failure to failure at greater depth and is defined by:

$$\alpha_q = \frac{K_q^0}{K_q^\infty - K_q^0} \cdot \frac{K_0 \sin\phi'}{\sin(45^o + \phi'/2)} \tag{2.8}$$

In this approach the soil is divided into a set of layers and a rotation point can then be calculated using moment equilibrium. The maximum capacity of the pile can be calculated by a horizontal equilibrium when the rotation point of the pile is known, for details see Hansen (1961).

The method recommended by design codes, (API, 2007; DNV, 2011) was developed for slender piles. In contrast to the original formulation, the method shown here has been slightly rearranged in order to fit into the more general framework used in this thesis. This is similar to the method by Hansen (1961). This method is a full plastic solution assuming two different failure mechanisms, one at shallow depth and one at greater depth. However,

the ultimate earth pressure is found in this approach as the minimum of two expressions given as:

$$K_{ult,API} = A \cdot \min \begin{cases} (C_1 \cdot \frac{z}{d} + C_2) & \text{failure at shallow depth} \\ C_3 & \text{failure at greater depth} \end{cases} \tag{2.9}$$

The lateral bearing capacity coefficients are calculated from the solution by Reese et al. (1974).

$$C_1 = \frac{(1 - \sin(\phi')) \cdot \tan(\phi') \cdot \sin(45^o + \frac{\phi'}{2})}{\tan(45^o - \frac{\phi'}{2}) \cdot \cos(\frac{\phi'}{2})} + \frac{\tan^2(45^o + \frac{\phi'}{2}) \cdot \tan(\frac{\phi'}{2})}{\tan(45^o - \frac{\phi'}{2})} \tag{2.10}$$
$$+ ((1 - \sin(\phi') \cdot \tan(45^o + \frac{\phi'}{2}) \cdot (\tan(\phi') \cdot \sin(45^o + \frac{\phi'}{2}) - \tan(\frac{\phi'}{2}))$$

$$C_2 = \frac{\tan(45^o + \frac{\phi'}{2})}{\tan(45^o - \frac{\phi'}{2})} - \tan^2(45^o - \frac{\phi'}{2}) \tag{2.11}$$

$$C_3 = (1 - \sin(\phi')) \cdot \tan(\phi') \cdot \tan^4(45^o + \frac{\phi'}{2}) \tag{2.12}$$
$$+ \tan^2(45^o - \frac{\phi'}{2}) \cdot (\tan^8(45^o + \frac{\phi'}{2}) - 1)$$

A is an empirical parameter which was used to fit full-scale results on slender piles and was found to be $A = \left(3.0 - \frac{0.8z}{d}\right) \geq 0.9$ for monotonic loading and $A = 0.9$ for cyclic loading.

In Figure 2.1 the soil resistance profiles together with the normalized profile for the three different methodologies are shown. The soil resistance profiles are generated for a pile with a diameter of $d = 3m$, penetration depth of $l_L = 6d$, load eccentricity of $l_e = 15d$ installed in dense sand with a effective unit weight of $\gamma' = 10kN/m^3$ and a maximum angle of friction of $\phi' = 38^o$. The three different methodologies can then easily be compared and basic observations are here described. The method by Broms (1964) only has a constant soil resistance profile on one of the sides. The method by Hansen (1961) has the same starting value as Broms (1964), but increases with depth. The method used by API (2007) starts with a smaller initial resistance compared to the two other methods, then increases with depth to a point where the resistance is approximately the same as in the method by Hansen (1961), here it start to decrease to point approximately identical with Broms (1964) and then it starts to increase again. This behavior is due to the empirical factor A which decreases to a normalized depth of $z = 2.625d$, after this point it has a constant value of 0.9. From a situation like this, it is seen that the methodology by Hansen (1961) gives the highest bearing

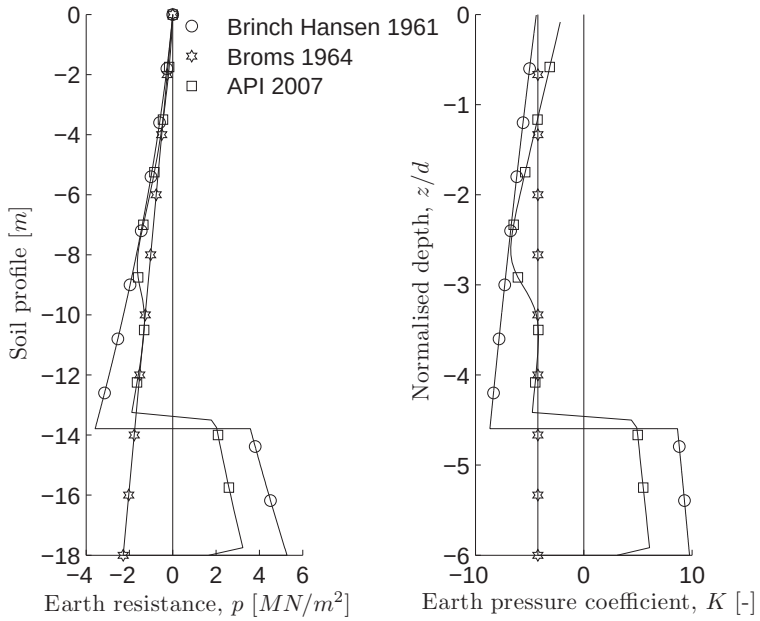

***Figure 2.1**: Comparison of soil resistance profiles at failure*

capacity followed by the method by API (2007) and the simplest method by Broms (1964) also gives the smallest capacity.

Three methodologies to calculate the ultimate soil resistance have here been presented, thus there exist several other methodologies e.g. Meyerhofs et al. (1981) and Norris and Abdollaholiaee (1990).

2.2 Pile - soil interaction

Today, the design of monopiles for offshore wind turbines is carried out by modelling the pile as a beam and the soil as a system of uncoupled non-linear springs, API (2007). A sketch of the approach is shown in figure 2.2. The soil is modeled as a set of independent soil layers represented by springs. The characteristics of these springs, which describe the soil resistance, p, as a function of the displacement, y, are defined as pile-soil interaction springs. This method has been used successfully in pile design for offshore oil and gas platforms in many years. The design methodology originates from field tests on long slender piles with a small load eccentricity, (Reese and Matlock, 1956;

McClelland and Focht, 1956). Although this methodology was originally

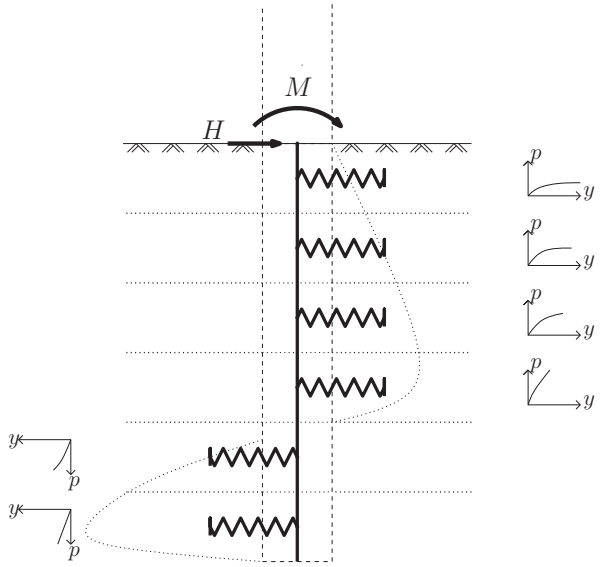

***Figure 2.2**: Sketch of the modelling approach used today*

calibrated to slender piles, it is used today for design of large diameter stiff monopiles.

Murchison and O'Neill (1984) investigated four different ways of computing the pile-soil interaction curves for sand. The best of these four was a method invented by Parker and Reese (1970) and reformulated by Murchison and O'Neill (1984). The method was superior to the other methods in finding the pile deflection and the maximum moment on ten different full-scale tests. A method invented by Scott (1980) performed better in the determination of the depth to the maximum moment Murchison and O'Neill (1984). The approximation made to simulate the p-y relationship for sand is given in equation (2.13), which is rearranged in order to fit into the general modulus approach.

$$K = K_{ult} \cdot \tanh\left[\frac{k \cdot z}{\sigma'_v} \cdot \frac{1}{K_{ult}} \cdot \frac{y}{d}\right] \tag{2.13}$$

A different shape of the curves was used by Kim et al. (2004). They compared 6 different methodologies to compute the curves with a set of 1g tests, and found that hyperbolic function proposed by Kondner (1963), and

shown in (2.14), gave the best predictions of the test results.

$$K = \frac{y/d}{\frac{\sigma'_v}{k \cdot z} + \frac{1}{K_{ult}} \cdot \frac{y}{d}} \tag{2.14}$$

The two methods are similar in the way that both of them only require two parameters, the non-dimensional stiffness, and the ultimate earth pressure coefficient to generate the curves. The value of the soil resistance is then found using (2.13) or (2.14), together with (1.1).

The non-dimensional earth pressure coefficient, K, is described by three factors; the ultimate earth pressure coefficient K_{ult}, the non-dimensional stiffness, $\frac{k \cdot z}{\sigma_v}$ and the non-dimensional displacement, $\frac{y}{d}$. The design codes (API, 2007; DNV, 2011) recommend using an ultimate earth pressure coefficient (K_{ult}), as presented by Reese et al. (1974), but in principle the methods by (Broms, 1964; Hansen, 1961) can also be used in both methods.

The initial modulus of subgrade reaction, k can be found using a curve, as shown in API (2007). From Figure 2.3, it can be seen that there are two different curves, one for dry and one for saturated sand. It should also be noticed that there is a direct link between relative density and angle of friction, whereas it is not dependent on stress level. This is in contrast to the general accepted observation of Bolton (1986).

Non-linear springs are used in a numerical model for the design of monopiles for offshore wind turbines and enable the designer to calculate a static load response curve for a given pile. The effect of cyclic loading is taken into account through the factor A. Thereby, the maximum bearing capacity used in a ULS/ALS calculation can be found. This results in one overall stiffness and one maximum deformation/rotation due to cyclic loading, which is used in the SLS & FLS analysis.

2.2.1 Comments on recent design methodology

The main limitation of the current design methodology for monopiles is that it uses a semi-empirical approach, based on testing on slender piles. The monopile foundation for offshore wind turbines tends to behave in a more rigid way. This is illustrated in Figure 2.4, showing a comparison between a rigid pile and a slender pile. It can be seen that a rigid pile tends to rotate around a rotation point and thereby generates soil pressure over the total length of the pile. A slender pile will not have a single rotation point, rather the pile deflects around multiple rotation points. The load is mainly taken by the upper layers and no deflection will develop at the pile toe. The effect of

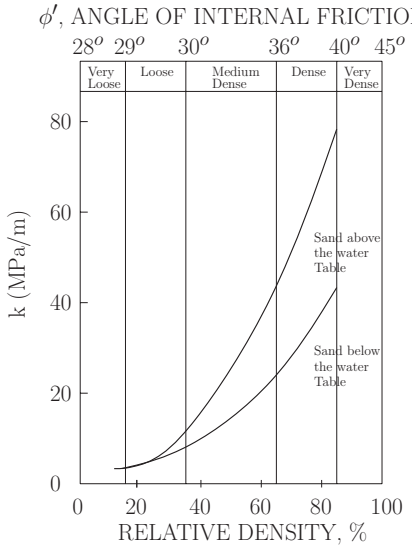

***Figure 2.3**: Initial subgrade modulus as a function of angle of friction, after DNV and RISØ (2001)*

moving from a slender pile behavior to a more rigid pile behavior can change the response of the pile (Poulos and Hull, 1989). Using a semi-empirical approach that is not calibrated to the given pile behavior should be avoided. The main differences between the original test piles and the piles used today for wind turbines are; a) the diameter of the piles is 5-10 times larger, b) they behave in a rigid way and c) the ratio between moment and shear force is much larger. Five main effects have to be investigated in order to verify that the current practice is valid also for rigid large diameter monopiles for offshore wind turbines. 1) The diameter effect, does the non-dimensional soil resistance change if the diameter of the pile is changed? 2) How does the vertical effective soil stress influence the response of the pile? 3) The failure mechanism of the sand changes down through the soil but is it also affected of by how the load is applied? 4) The influence from cyclic loading. In short:

- Diameter, $K = f(d)$?
- Stress, $K = f(\sigma'_v)$?
- Failure mechanism, $K = f(z/d)$ or $K = f(l_e/d)$?
- Cyclic loading, $K = f(N, \zeta_b, \zeta_c)$?

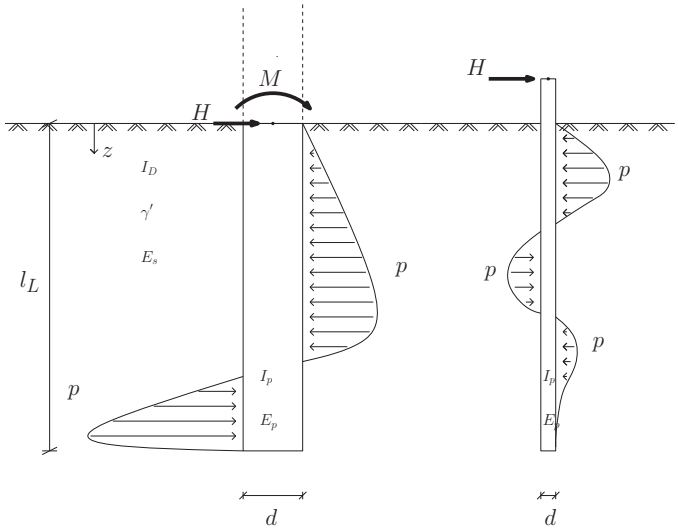

***Figure 2.4**: Monopile vs. offshore pile*

The three first items can be investigated by monotonic tests and the cyclic loading from waves and wind is normally investigated by quasi-static cyclic load tests. The influence on the ultimate capacity is crucial for all of the four points, but the stiffness is even more important for monopiles supporting wind turbines.

To investigate these effects, it is important to secure that only the factor which is under investigation is changed. As an example; if the diameter effect is investigated, only the diameter of the pile should be changed, full similarity in the geometry should be kept,($const. = \frac{l_L}{d}$, $const. = \frac{l_e}{d}$ & $const. = \frac{E_p I_p}{E_s d^4}$) and also identical soil conditions should be retained.

2.3 Recent research

Significant research has been carried out in the past to improve the understanding of monopile behavior. A table with pile dimensions and load conditions is given in table 2.1 to a give an quick overview of some of this research. The different types of experimental models are here defined; "1g" for a scaled experiment performed at 1g, "ηg" is a scaled experiment performed in a centrifuge, "fs" denotes full-scale measurements and "num" denotes numerical simulations. The investigations are divide into two sections: One

concerning the monotonic response, and one for the cyclic response. Only a short presentation of the research is provided here and common findings are highlighted.

***Table 2.1**: Schematic representation of the review*

Author	Model	Proto. Dia. d [m]	Load ecc. l_e/d	Pene. depth l_L/d	Num. of cycle N [-]
Lesny and Wiemann (2006)	num	1-6	?	6.5-10.6	1
Sørensen et al. (2009)	num	1-7	?	2.9-20	1
Augustesen et al. (2009)	num	4	5.2	6	1
A.-R. and Achmus (2005)	num	7.5	0.2-1	2.7-4	1
Fan and Long (2005)	num	0.3-1.2	0.5	34.4	1
Zhang et al. (2005)	fs-ηg	?	0-27	4.4-16	1
Ashford and Juirna.. (2003)	fs	0.4-1.2	0.4-1.2	10-20	1
Hald et al. (2009)	fs	5	?	6	1
Achmus et al. (2009)	num	1.9	8.8-13.7	7.7-9.5	10000
LeBlanc et al. (2010a)	1g	4	4	5.4	65000
Leblanc et al. (2010b)	1g	4	4	5.4	1000
Peralta and Achmus (2010)	1g	-	4	3.3-8.3	10000
Cuéllar et al. (2009)	1g	7.5	4	4	5000000
Li et al. (2010)	ηg	5	14.4	5	1000
Rosquöet et al. (2007)	ηg	0.72	16.7	3.4	44

2.3.1 Monotonic response

The monotonic response has been investigated by different authors and the conclusions of the findings are contradictory. The ultimate capacity was studied by Zhang et al. (2005), who collected data from 17 different tests both centrifuge and full-scale. They presented a method to determine the ultimate capacity of a pile. The model consists of a contribution from the side friction and the resultant soil pressure. The best result was obtained by using Rankine's passive soil pressure coefficient squared for the ultimate soil pressure.

The initial stiffness was investigated by Ashford and Juirnarongrit (2003) and Fan and Long (2005) and they agreed with the original assumption by Terzaghi (1955) that there is no effect from the diameter on the initial

stiffness of the pile-soil interaction curves. This is also the conclusion reached by Pender et al. (2007), who compared a series of full-scale tests stating that the apparent diameter size effect is a consequence of the distribution of the soil modulus. On the other hand, numerical modelling by Lesny and Wiemann (2006) and Sørensen et al. (2009) suggests an effect of changing the diameter on the initial stiffness of the pile-soil interaction curves.

The general tendency for the different research performed on monopiles is that the current design values of the subgrade modulus, k as shown in figure 2.3, are too large, e.g. Rosquöet et al. (2007), Lesny and Wiemann (2006), Abdel-Rahman and Achmus (2005) and Augustesen et al. (2009). The problem with these findings is that they contradict the findings from full-scale monitoring on monopiles, which states that the recommended value is too small, Hald et al. (2009).

2.3.2 Cyclic response

Cyclic loading is a complex load situation and as a first attempt many researchers have investigated the over all response of piles to understand the problem. LeBlanc et al. (2010a) performed a 1g experiment on a scaled monopile subjected to cyclic lateral loading. Accumulation of rotation and change in secant stiffness was observed. The accumulation model was assumed to follow a power law. This was proposed earlier by Long and Vanneste (1994) for slender piles and was also seen by the test by Peralta and Achmus (2010). On the other hand accumulation of displacements observed in centrifuge tests by Rosquöet et al. (2007) and Li et al. (2010), were seen to follow a logarithmic trend.

As an extension of previous studies, Leblanc et al. (2010b) further developed the model to handle random cyclic loading. The model is based on Miner's rule and was validated by a set of experiments with the same setup as used in LeBlanc et al. (2010a). The total framework from (LeBlanc et al., 2010a; Leblanc et al., 2010b) enables the designer to calculate accumulation of rotation and increase in stiffness if the monotonic load-response curve and the load-history is known.

Another scale experiment was performed by Cuéllar et al. (2009). They performed one cyclic load test on a monopile installed in saturated dense sand loaded with 5.000.000 one-way cycles. The magnitude of the cyclic loading was selected to correspond to offshore conditions for a monopile supporting a wind turbine. The main result of this investigation was that the accumulation of rotation changed after around 100.000 cycles. By using colored sand and by performing a vertical cut in the sand next to the pile after the test, an indication of the sand movement in front of the pile was obtained. They

concluded that a convective domain was created and sand was traveling from sand surface and down to a given point in the sand layer and then up again.

No cyclic pile-soil interaction curves for monopiles were found in the investigated literature. In seismic engineering attention has been paid to cyclic interaction curves for long slender piles. Cyclic curves have been derived from centrifuge tests by Rosquöet et al. (2007) where a change in stiffness was found and these curves showed hysteretic behavior. They concluded that the ultimate soil resistance decreases due to the cyclic loading of the sand.

Achmus et al. (2009) developed a 3D finite element model of a monopile to predict the response from cyclic loading. Cyclic triaxial tests were used to calibrate the elasto-plastic Mohr–Coulomb constitutive model. This was achieved by degradation of the soil stiffness that allows the pile to accumulate displacements. Design charts were developed from different calculations using this finite element model. These charts can be used to predict the accumulation of displacement for a monopile supporting an offshore wind turbine.

2.3.3 Comments to recent research

Different research activities have been presented and there is not clear agreement on how to deal with possible diameter effects, failure mechanisms etc. The increase in subgrade modules was seen to increase proportionally with the depth by Ashford and Juirnarongrit (2003) and Fan and Long (2005). However, the investigations were based on slender piles. Lesny and Wiemann (2006) and Sørensen et al. (2009) report a diameter effect, in their research the geometrical similarity was not kept constant, which could influence the failure mechanisms. The different observations reported show that there is still a need to improve the knowledge of rigid laterally loaded monopiles, not only for cyclic loading but also for monotonic loading. A more general model describing the soil pile interaction is needed. The model by Achmus et al. (2009) uses a degradation model of the stiffness, which means that the cyclic response becomes softer with the number of cycles. This is not the behavior seen from physical tests and the model can therefore only be used to predict the accumulation of displacement and not the stiffness of the pile - soil interaction.

The response of a monopile supporting an offshore wind turbine is still not well described and more research is therefore needed. In order to investigate the response of a monopile, it is important to investigate the different effects, one at a time. Only in this way, is it possible to determine the effect of each parameter. In the establishment of a more general model that can handle both monotonic and cyclic loading, it could be relevant to use methodologies

from seismic design. This could be a Winkler model with a cyclic spring element. Such an element is capable of handling cyclic loading and introduces frictional damping into the system. In this respect, inspiration from the models by Boulanger et al. (1999) and Taciroglu et al. (2006) seems to be appropriate.

Chapter 3

Methodology

Using different methodologies to investigate a given problem will often lead to more reliable results. A triangulation where the problem is investigated using different methods is preferable. This is illustrated in Figure 3.1.

Full scale testing or monitoring is one method that can be used. The big advantage of such a method is that the testing is performed on a real size structure. This secures that what you measure is a real physical event in the scale that you want to investigate. The disadvantage is that it can be difficult to estimate the soil profile and the load conditions. Furthermore, it is also an expensive way of testing or monitoring. This will often lead to only one or very few tests, still the results from these tests are, if uncertainties can be controlled, of high credibility.

On the other hand, testing on a scaled model enables the researcher to create artificial scaled soil profiles; the loading is easier to control and it is cheaper to carry out due to the smaller scale, which makes it possible to perform more tests. Testing on a scaled model is also a real physical event, but the results from these tests have to be translated to a larger scale, which can be challenging. The price is smaller and the number of tests can be increased. The results from these tests have, if scaling issues are controlled, reasonable credibility.

A third method is to create a numerical model, which can be used in similar investigations. This is a relatively cheap method, which makes it possible to investigate a large number of possible scenarios. Another advantage in numerical modelling is that it gives the researcher the possibility to look in details into the soil-pile response, e.g. stress - strain curves at a given point. The disadvantage is that this is not a real physical event; this means that constitutive models are required that reflect the real physical behavior during the event. If the numerical model can be validated and the parameters calibrated to real physical events, the method has a good credibility.

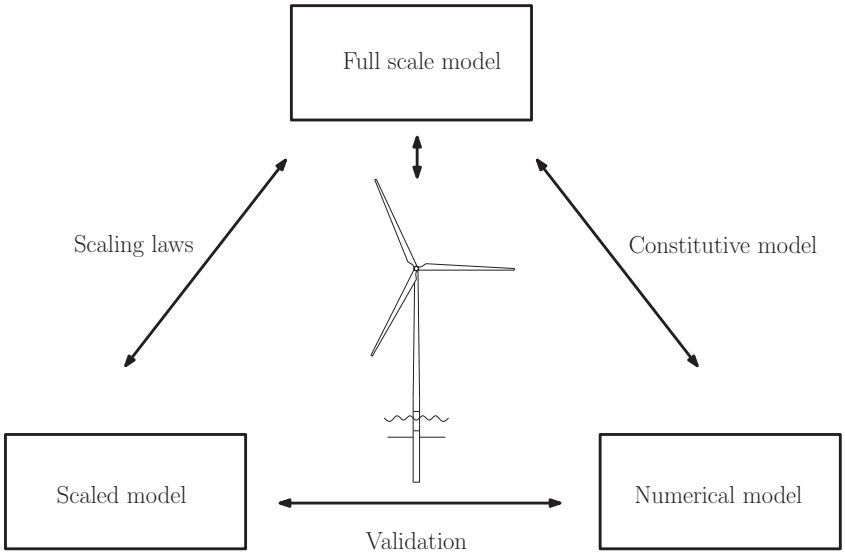

***Figure 3.1**: Schematic view of research strategy*

Evidently, different research methods can be used and the advantages from the different methods can be combined. It is preferable to combine all three methods, although this might be prevented by cost and time. In this thesis, numerical and physical modelling is used to investigate the pile-soil interaction for laterally loaded monopiles. This enables calibration and verification between the physical event and the numerical model and thereby gives a good robust tool in the investigation of the problem. Numerical modelling has not been a part of this thesis, therefore only results presented in (Svensson, 2010; Zania and Hededal, 2011, 2012) will be used.

3.1 Physical modelling

The intention of physical modelling is to study the behavior of a given prototype. Physical modelling can be performed as full-scale testing but is often used in a reduced scale. The physical modelling presented in this thesis will be based on a set of centrifuge model tests. Dimensional analysis is used here to deduce dimensional products, which are used to transform model observation to prototype. These non-dimensional products should be identical and scale independent, this implies that a possible diameter effect is neglected.

3.1.1 Dimensional analysis

The basic idea in dimensional analysis is that the governing parameter is a function of a set of known independent variables. The goal of the analysis is to reduce the number of parameters and to form dimensionless groups, which can be used in the extrapolation to prototype, Fuglsang and Ovesen (1988b).

The basis for the dimensional analysis is the Buckingham Theorem, which states that if an equation is dimensionally homogeneous, it can be transformed to a set of dimensionless products, Langhaar (1951).

The governing parameters should be identified in a dimensional analysis. This requires some initial knowledge of the problem, which can be found in e.g. Reese and Impe (2001), Randolph (2003) or Bhattacharya et al. (2011). The response is assumed to depend on a set of parameters for a laterally loaded stiff monopile, as shown in (**??**). Only quasi-static monotonic and cyclic loading will be investigated in this thesis. This implies that no inertia forces are affecting the response and also that only the fully drained case is considered.

First, the governing parameters controlling the total response of a laterally loaded pile are identified. The total response is governed by the applied lateral load, H, the corresponding displacement, Y, the geometry and material of the pile and the sand behaviour. The pile geometry is described by; penetration depth, l_L, load eccentricity, l_e, diameter, d, and by the moment of inertia, I_p. The pile material is described by the stiffness, E_s, and the surface roughness of the pile, R_a. Finally the sand is described by; submerged unit weight γ'', sand stiffness, E_s, and the mean sand particle size d_{50}. These parameters can be expressed in terms of three dimensions, mass $[m]$, length $[L]$ and time $[T]$. The parameters with the corresponding dimensions are shown in table 3.1. It is chosen here to use the diameter of pile and sand grains, d

Table 3.1*: Controlling parameters for the total response of a laterally loaded pile and the corresponding dimensions*

H	Y	l_e	l_L	d	I_p	E_p	R_a	γ'	E_s	ϕ'	d_{50}
$\frac{[M][L]}{[T]^2}$	$[L]$	$[L]$	$[L]$	$[L]$	$[L]^4$	$\frac{[M]}{[T]^2[L]}$	$[L]$	$\frac{[M]}{[T]^2[L]^2}$	$\frac{[M]}{[T]^2[L]^2}$	$[-]$	$[L]$

$[L]$, d_{50} $[L]$ and unit weight, γ' $[M]/([T]^2[L]^2)$ as normalisation parameters and non-dimensional ratios can then be created. The non-dimensional ratios are shown in table 3.2. The non-dimensional ratios for the stiffness of pile and sand are combined together with the non-dimensional ratio for moment of inertia. The outcome of the dimensional analysis can then be written in a form whereby the normalised applied load is derived as a function of a set

***Table 3.2**: Non-dimensional ratios*

$\frac{H}{\gamma' d^3}$	$\frac{Y}{d}$	$\frac{l_e}{d}$	$\frac{l_L}{d}$	$\frac{I_p}{d^4}$	$\frac{E_p}{\gamma' d}$	$\frac{R_a}{d_{50}}$	$\frac{E_s}{\gamma' d}$	ϕ'	$\frac{d}{d_{50}}$

of non-dimensional ratios, which should be identical at model and prototype scale in order to avoid scale effects Langhaar (1951), Fuglsang and Ovesen (1988a) and Wood (2004). This is shown in equation (3.1).

$$\frac{H}{\gamma' d^3} = f\left(\frac{Y}{d}, \frac{l_e}{d}, \frac{l_L}{d}, \phi, \frac{E_p l_p}{E_s d^4}, \frac{R_a}{d_{50}}, \frac{d_{50}}{d}\right) \tag{3.1}$$

An identical approach can be carried out for the local pile-soil resistance. For the local response it is chosen to use the diameter of pile and sand grains, d $[L]$, d_{50} $[L]$ and effective vertical stress, σ'_v $[M]/([T]^2[L])$ as normalisation parameters. The result of this analysis is shown in (3.2).

$$\frac{p}{\sigma'_v \cdot d} = f\left(\frac{y}{d}, \frac{l_e}{d}, \frac{l_L}{d}, \frac{z}{d}, \phi, \frac{E_p l_p}{E_s d^4}, \frac{R_a}{d_{50}}, \frac{d_{50}}{d}\right) \tag{3.2}$$

The non-dimensional parameters found from the dimensinal analyses is here shown, first the non-dimensional horizontal shear force:

$$\tilde{H} = \frac{H}{\gamma' d^3} \tag{3.3}$$

Remembering the definition of the soil resistance shown in equation (1.1), the non-dimensional soil resistance turns out to be identical to the earth pressure coefficient K:

$$\tilde{p} = K = \frac{p}{\sigma'_v \cdot d} \tag{3.4}$$

The geometrical dimensions are all divided with the diameter, leading to the non-dimensional displacement, Y for the total displacement and y for the local displacement, given as:

$$\tilde{Y} = \frac{Y}{d} \quad \tilde{y} = \frac{y}{d} \tag{3.5}$$

All of the non-dimensional ratios are shown in Figure 3.2. The hypothesis is that the normalized response is identical if all these quantities are identical. For a more in-depth review of dimensional analysis see e.g. Wood (2004).

Two Abaqus models were created by Svensson (2010) and Zania and Hededal (2011) to demonstrate the scaling methodology and the overall response of the piles are presented here. The first model was identical to a

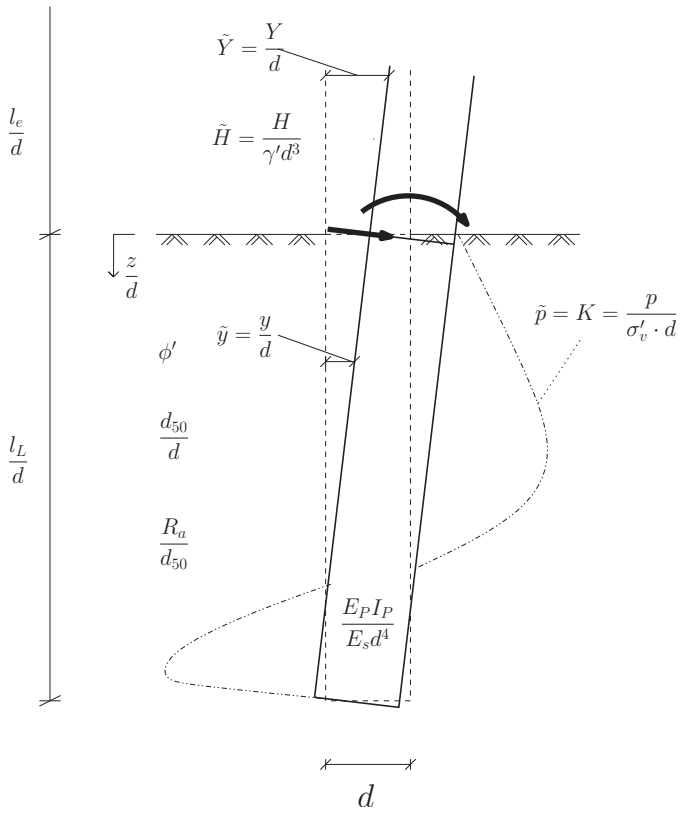

***Figure 3.2**: Sketch of pile and governing parameters*

centrifuge experiment made on a pile with a diameter of $d = 28mm$, Svensson (2010). The second model was made as the equivalent prototype with a diameter of $d = 2m$, Zania and Hededal (2011). The results from the two calculations shown in the respective scales can be seen in Figure 3.3. Here it can be seen that the magnitude of the responses is very different. The normalized responses are shown in Figure 3.4. It can be seen that if full similarity between the models is achieved, the normalized results from tests at different scales are identical.

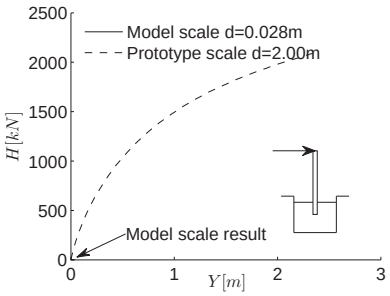

***Figure 3.3**: Abaqus calculation in model and prototype scale*

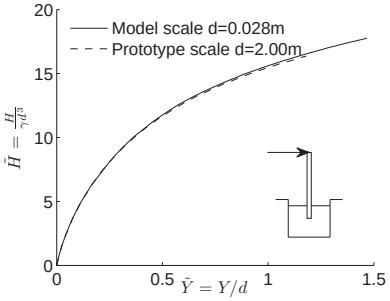

***Figure 3.4**: Normalized response of Abaqus calculations*

Similarity

A function of independent dimensionless parameters was identified from the dimensional analysis. The principle is that if all these dimensionless parameters are kept constant, identical normalized results are achieved, independent of scale. The geometrical size of the model is easy to scale down still maintaining full similarity. The properties of the sand (ϕ' & E_s) on the other hand are stress dependent, which implies that identical stresses in model and prototype are needed, in order to maintain similarity. Gravitational acceleration can be increased to achieve this by increasing the effective density corresponding to the geometrical scaling factor (N_s). This can be achieved in a centrifuge. The last parameter in (3.1), the ratio between the grain size and pile diameter, is very difficult to maintain constant between model and prototype. If the grain-size is reduced according to the linear length scale the mechanical properties of the soil are likely to be changed. Sand with the same grain-size is chosen as in a prototype case. The influence from the lack of similarity therefore has to be investigated.

3.2 Centrifuge modelling

The soil sample is placed in a centrifuge to secure stress similarity. The rotation of the centrifuge will introduce an increased gravitational force. The geotechnical centrifuge at DTU is a beam centrifuge, shown in figure 3.5. The centrifuge facility at DTU was constructed in 1976 and has been upgraded over the years. The capacity of the beam centrifuge is approximately 100 g ton and is capable of providing an artificial gravitation of around 90g,

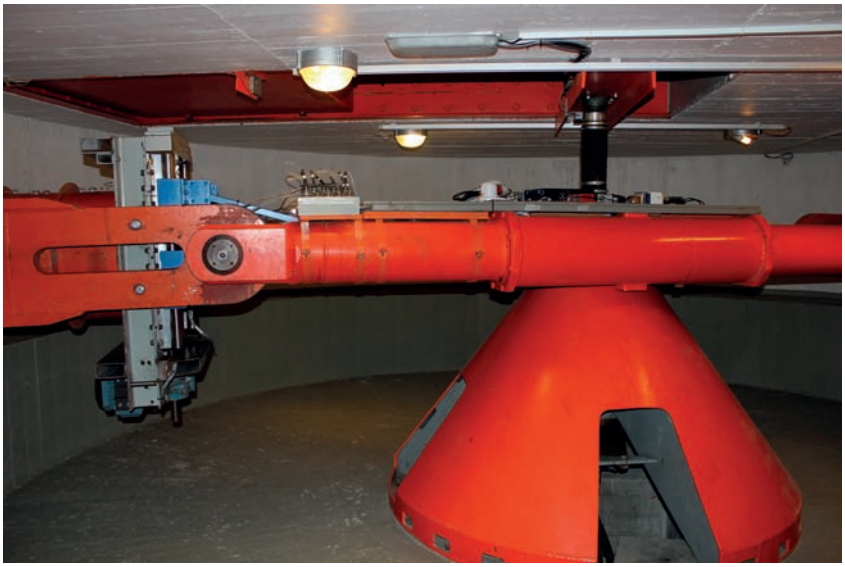

***Figure 3.5**: Picture of the geotechnical centrifuge at DTU under testing*

Fuglsang and Nielsen (1988). The maximum arm or radius of the centrifuge is 2.63 m. The increase in gravity (η) can be calculated from Newton's second law of motion as:

$$\eta = R\omega^2/g \tag{3.6}$$

In (3.6), R is the radius to the point of interest, ω is the rotational frequency and g the natural gravity acceleration. The model monopile is placed in the soil container and a loading actuator is mounted on top of the soil barrel. The load setup allows for in-flight installation and lateral loading with high eccentricity. The changes was made to simulate full-scale conditions better and because initial observation reported by (Klinkvort et al., 2010; Klinkvort and Hededal, 2010) indicated that it was important to the modelling.

The monopile is installed in-flight by a jack with a deformation controlled rate of 2 mm/s. The pile ready for installation is shown in Figure 3.6. The jack is electrically powered and has a capacity of 20 kN. After monopile installation, the jack is removed and a beam has to be mounted for lateral loading. The fully equipped monopile, which is ready for a lateral load testing is shown in Figure 3.7. A sketch of the setup is shown in Figure 3.8. The radius to the sand surface with this setup is $R_t = 2.221m$. This is the basis load setup as used today, and the main results presented in this thesis are

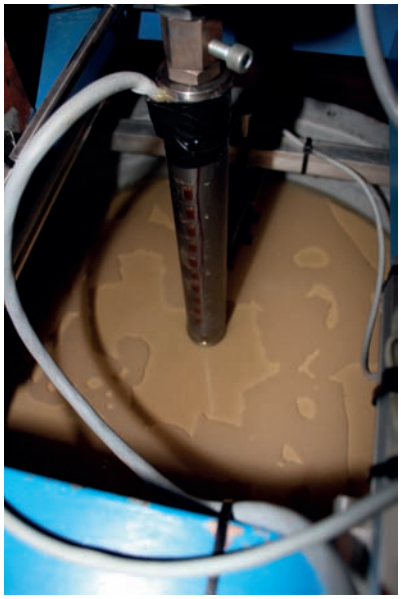

***Figure 3.6**: Photo of the setup before installation*

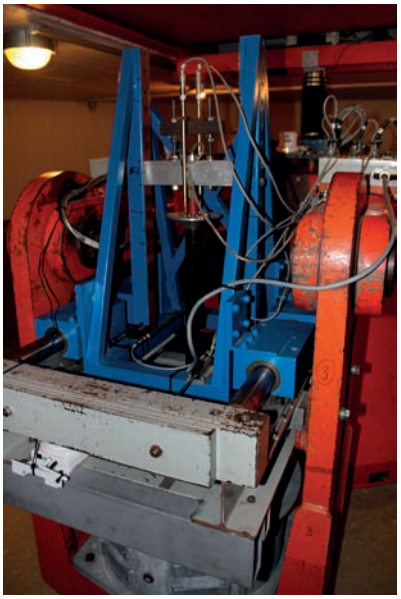

***Figure 3.7**: Photo of the setup before laterally loading*

all derived from this setup.

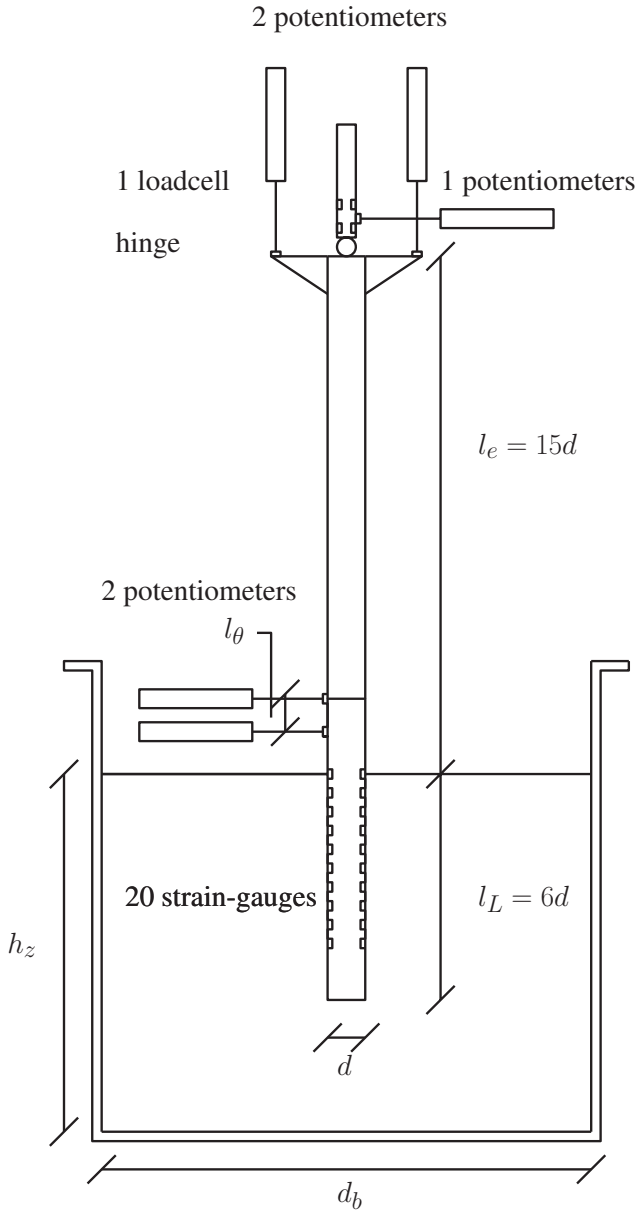

***Figure 3.8**: Sketch of centrifuge test setup*

The loading configuration provides a flexible setup, which enables the use of different piles. In Figure 3.7 the pile mounted with strain-gauges is shown. Two strain-gauge mounted piles have been developed to investigate the pile - soil interaction. These two piles are shown in Figures 3.9 and 3.10.

***Figure 3.9**: Photo of the model monopile mounted with five strain-gauge half bridges*

***Figure 3.10**: Photo of the model monopile mounted with ten strain-gauge half bridges*

The first pile shown in Figure 3.9 has a $24mm$ solid steel core. Five Wheatstone half-bridges are glued on this steel core and then a $2mm$ epoxy layer is applied, resulting in a total diameter of $28mm$. The five Wheatstone strain-gauge bridges are placed with a spacing of one diameter, starting one

diameter under sand surface. The construction of the second pile shown in Figure 3.10 is similar. Here the steel core is $36mm$ and the total diameter reaches $40mm$ with the epoxy coating. 10 strain-gauge Wheatstone bridges are mounted with a spacing of a diameter starting with the first level at sand surface. The piles a calibrated to a known applied moment and the moment in the pile can then be derived from the strain-gauge Wheatstone bridges during testing. From these measurements the pile-soil interaction can be calculated.

The formulation of the beam-column on a flexible foundation was derived by Hetenyi (1946) and is shown here for a pile without any axial loading component.

The governing differential equation neglecting the axial force is written as:

$$0 = E_p I_p \frac{d^4 y}{dz^4} - E_{py} y \tag{3.7}$$

In this equation: $E_p I_p$=pile bending stiffness, E_{py} Stiffness of the pile - soil interaction, y=lateral deflection of the pile at a point z along the length of the pile. The bending moment in the pile is found from integration of (3.7) twice.

$$m = E_p I_p \frac{d^2 y}{dz^2} \tag{3.8}$$

It can be seen from (3.8) that the moment integrated twice with respect to the stiffness is the deflection. This is written as:

$$y = \int \int \frac{m}{E_p I_p} dz dz \tag{3.9}$$

and from (3.7), it can be seen that the soil resistance can be found by differentiating the moment twice.

$$p = \frac{d^2 m}{dz^2} \tag{3.10}$$

It is here important to remember that the soil resistance p is not only the soil pressure, but the total resistance from vertical/horizontal frictions, active/passive soil pressures. The soil resistance p is therefore easily used in the modulus approach shown in (1.1).

The procedure is to fit the moment distribution with a sixth order polynomial and afterward calculates the pile displacement and soil resistance from this. Different methodologies in the fitting of the moment distribution were carried out e.g. Yang and Liang (2006). The sixth order polynomial was chosen because it could be fitted to the measured moment distribution with

a high degree of precision and that afterwards it is easy to integrate and differentiate.

The sixth order polynomial is written as:

$$m(z) = c_6 z^6 + c_5 z^5 + c_4 z^4 + c_3 z^3 + c_2 z^2 + c_1 z + c_0 \tag{3.11}$$

The displacement of the pile can be found by a double integration of the moment fit. The two integration constants turn, out to be the rotation and the displacement at soil surface,

$$y = y_0 - \theta_0 z - (\frac{c_6 z^8}{56} + \frac{c_5 z^7}{42} + \frac{c_4 z^6}{30} + \frac{c_5 z^5}{20} + \frac{c_2 z^4}{12} + \frac{c_1 z^3}{6} + \frac{c_0 z^2}{2})/EI \tag{3.12}$$

The soil resistance is found to be a double differentiation of the moment fit. This is written as:

$$p = 30c_6 z^4 + 20c_5 z^3 + 12c_4 z^2 + 6c_3 z + 2c_2 \tag{3.13}$$

The pile-soil interaction can then be found, knowing the boundary conditions at the sand surface. As shown in Figure 3.8, the displacement and rotation is measured above the sand surface. These measurements therefore have to be scaled down to the sand surface. This is easily done due to the linear moment distribution in the monopile above sand surface.

The loading setup of the monopile is based on a feedback controlled LabView code which controls and collects the data under testing. This setup can perform deformation controlled monotonic testing, deformation and force controlled cyclic testing, and it can perform CPT testing and pile installation when mounted with the loading jack. The sample rate of the data is $10Hz$, which is needed in the feedback control algorithm. It consists of 16 channels for strain-gauge measurements, 16 channels for potentiometer measurements, and two output channels used to control the loading equipment under testing.

3.3 Soil testing

The centrifuge tests are all performed in dense homogeneous Fontainebleau sand with a relative density of approximately 90%, in order to model the North Sea offshore conditions. Leth et al. (2008) has collected classification parameters for the Fontainebleau sand, which can be seen in Table 3.3.

A series of triaxial tests have been performed together with the classification parameters. In addition to the classification tests 9 tests have been carried out on specimens all with a relative density of $I_D = 0.9$. Four of the

***Table 3.3**: Classification parameters for the Fontainebleau sand*

Specific gravity of particles	G_s	2.646
Minimum void ratio	e_{min}	0.548
Maximum void ratio	e_{max}	0.859
Average grain size	d_{50}	0.18
Coefficient of uniformity	C_u	1.6

tests were performed on dry samples and five of the tests were performed on fully saturated samples. The triaxial apparatus uses a sample height ($70mm$) equal to diameter and is constructed according to Jacobsen (1970).

Volume response from the four tests performed on dry samples was difficult to measure. For this reason, only maximal mobilized angle of friction was found from these tests. From the five tests performed on fully saturated samples, maximum angle of friction, angle of dilation and the stiffness of the sample was determined. The maximum angle of friction was found assuming no cohesion in the sand as:

$$\sin \phi'_{max} = \frac{(\sigma'_1/\sigma'_3)_{max} - 1}{(\sigma'_1/\sigma'_3)_{max} + 1} \tag{3.14}$$

The results from the triaxial testing are shown in Figure 3.11. The maximum angle of friction is shown to the left and it can be seen that the results from the tests on saturated and dry sand are almost identical. This concludes that the drained behaviour is identical for saturated and dry sand. It can also be seen that the angle of friction decreases with increasing pressure. The relation proposed by Bolton (1986) to calculate the maximum triaxial angle of friction, is written as:

$$\phi'_{max} = \phi'_{cr} + 3 \cdot (I_D(10 - ln(\frac{p'}{1kPa})) - 1) \tag{3.15}$$

Assuming a critical state angle of $\phi'_{cr} = 30^o$ seems to capture the behaviour of the tested sand well. This equation is therefore used in the analysis of the physical modelling. Gaudin et al. (2005) performed triaxial tests on Fontainebleau sand also for the application into centrifuge modelling. A critical state angle of friction was measured to be around 30^o, which fits with the observations found in this study. From equation (3.15) it can be seen that the maximum angle of friction is a function of the relative density I_D and the mean pressure p'. The unloading - reloading stiffness is also shown in Figure 3.11, like the maximum angle of friction the stiffness of the sand is

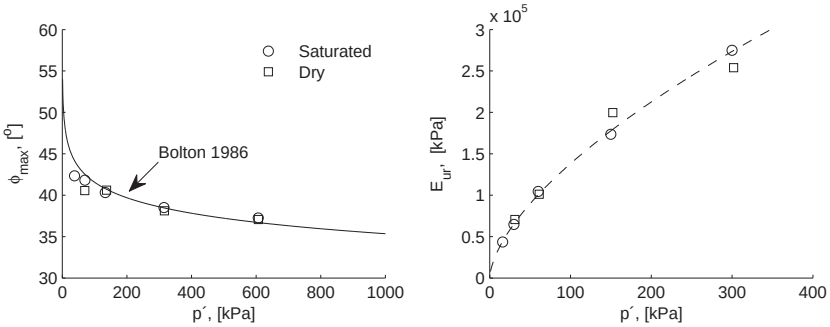

***Figure 3.11**: Results from triaxial tests on Fontainebleu sand*

also depending of the soil pressure. The stiffness as a function of the mean soil pressure can be written as:

$$E_{ur} = E_0 \cdot \left(\frac{p'}{100\text{kPa}} \right)^{0.6226} \tag{3.16}$$

Here $E_{0,ur} = 138070$kPa for the unloading reloading stiffness.

3.4 Methodology validation

A research strategy was presented at the start of this chapter in order to investigate the pile - soil response of a offshore wind turbine foundation. Scale experiments in a centrifuge constitute the main part of this research. The transformation of the data from one scale to another is crucial for the research and this section tries to validate or render the given methodology probable. The results from these tests are presented in the papers Klinkvort et al. (2012) and Klinkvort and Hededal (2012b). The drawing in Figure 3.12 can be used to illustrate how the different centrifuge tests are used in this process. The diameter of the model piles ranges from $d = 16 - 40$mm and the prototype monopiles that is investigated is ranges from $d = 1 - 5$m, and the difference in scale is up to a factor of 125.

In order to validate the transformation of results from model scale to prototype scale, a methodology called "modelling of models" was used, Ovesen (1975). The principle is to model the same prototype monopile with different sized model monopiles. Nearly full similarity in the models is achieved by changing the acceleration level in the centrifuge and identical non-dimensional response should be observed. Only the ratio between grain size and pile diameter is changed. These tests are shown in Figure 3.12 as squares.

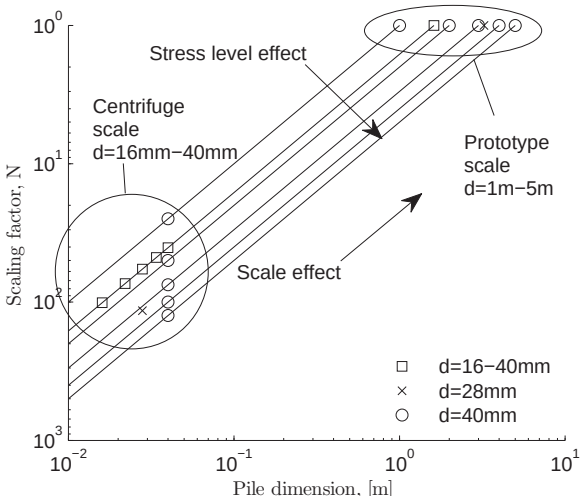

***Figure 3.12**: Schematic view of model scale and prototype scale*

The effect from changing the stress field was investigated after the "modelling of models". Here different stress fields corresponding to different prototype diameters were applied to the laterally loaded monopile, shown in Figure 3.12 as circles. In tests likes this, the stress dependent soil behavior can be investigated and the influence from this can be determined.

Different tests were carried out as a last part of the validation test program to investigate the influence of stiffness, roughness and scaling approach.

In total, 37 tests were performed and the total test program can be seen in table 3.4. Most of the tests were monotonic tests performed on smooth solid steel piles. Five cyclic tests were also performed indicated by a "c" notation in the table. Two tests were performed on a hollow steel pile indicated by an "h" and one test was performed on a sandblasted pile, in order to introduce a rough surface, this is indicated by an "r". Test performed in water saturated sand is indicated by an "s". Characteristic of the sand are given the table by I_D and γ', the geometry of the model monopile is given by d, l_e, and l_L, the scaling factor N_s and acceleration at which the pile was installed at.

***Table 3.4**: Test program. c=cyclic, h=hollow, r=rough, s=saturated*

Test no.	I_D	Effective unit weight, $[kN/m^3]$	Model. dia. d [mm]	Load ecc. l_e/d	Pen. depth l_L/d	Scaling factor N_s	Install. accel. $[g]$
1	0.86	16.4	16	2.5	6	62.5	1
2	0.86	16.4	22	2.5	6	45.5	1
3	0.90	16.6	28	2.5	6	35.7	1
4	0.83	16.4	34	2.5	6	29.4	1
5	0.92	16.6	40	2.5	6	25	1
6 c	0.80	16.5	16	2.5	6	62.5	1
7 c	0.90	16.6	22	2.5	6	45.5	1
8 c	0.90	16.6	28	2.5	6	35.7	1
9 c	0.86	16.4	34	2.5	6	29.4	1
10 c	0.94	16.7	40	2.5	6	25	1
11	0.92	16.7	16	15	6	62.5	1
12	0.92	16.7	16	15	6	62.5	1
13	0.84	16.4	22	15	6	45.5	1
14	0.86	16.5	28	15	6	35.7	1
15	0.90	16.6	34	15	6	29.4	1
16	0.89	16.6	40	15	6	25	1
17	0.90	16.6	16	15	6	62.5	η
18	0.84	16.4	22	15	6	45.5	η
19	0.96	16.8	28	15	6	35.7	η
20	0.89	16.5	34	15	6	29.4	η
21/21s	0.89/0.94	16.4/10.4	40	15	6	25	η
22	0.85	16.4	22.4-21.8	15	6	45.5	η
23	0.90	16.6	28.7-27.7	15	6	35.7	η
24	0.91	16.6	35.0-33.5	15	6	29.4	η
25	0.84	16.4	41.4-39.3	15	6	25	η
26	0.93	16.7	40	15	6	25	$\eta/3$
27	0.93	16.7	40	15	6	50	$\eta/3$
28	0.89	16.5	40	15	6	75	$\eta/3$
29	0.86	16.4	40	15	6	100	$\eta/3$
30	0.95	16.8	40	15	6	125	$\eta/3$
31 h	0.93	16.7	40	15	6	75	$\eta/3$
32 h	0.88	16.5	40	15	6	75	$\eta/3$
33 r	0.89	16.5	40	15	6	75	$\eta/3$
34	0.83	16.3	40	15	6	75	$\eta/3$
35 s	0.83	10.1	40	15	6	75	$\eta/3$
36	0.89	16.6	40	15	6	75	$\eta/3$
37 s	0.99	10.5	40	15	6	75	$\eta/3$

3.4.1 Scale effects

Three factors are of particular interest in the "modelling of models" analysis. First of all, the minimum ratio between in this case monopile diameter and average grain-size diameter. This investigates the influence of using the same sand in model and prototype and thereby not having similarity in the modelling of the sand grain-sizes, Ovesen (1975).

Secondly, the effect of not having completely identical stress distributions is relevant. The height of the centrifuge soil model introduces a parabolic non-linear increase in soil stresses. In comparison with the linear increase that occurs in prototypes, this implies small stress errors between model and prototype. The error is often not larger than 2-3 % and is therefore usually neglected, Schofield (1980).

Finally, the effect of installation is investigated. In-flight installation is important for the vertical response of axially loaded piles. Several studies have shown that the installation method is important for the lateral response as well, Craig (1985) and Dyson and Randolph (2001). The majority of centrifuge tests on laterally loaded monopiles are still performed on piles installed at 1g, e.g. Remaud (1999), Ubilla et al. (2006) and Li et al. (2010).

The "modelling of models" technique has been used before for laterally loaded piles e.g. Remaud (1999) and Nunez et al. (1988), but not for stiff monopiles for wind turbines and normally only the grain-size effect is investigated. Monopiles for wind turbines are different from normal laterally loaded piles because they are short stiff piles subjected to a large degree of bending moment. According to the scaling catalogue from "TC2 -Physical Modelling in Geotechnics" Garnier et al. (2007), no grain size effect was detected in "modelling of models" if the ratio between pile diameter and average grain size was larger than 45, Remaud (1999) or 60, Nunez et al. (1988) for laterally loaded piles. Both of these test series were performed on long slender piles and the results from these tests should be used with caution for short stiff piles.

Klinkvort and Hededal (2010) performed "modelling of models" on five stiff monopiles as an initial study. The test data from these tests are shown in table 3.4 as tests no. 1-10. All piles were installed at 1g and here a relationship between stiffness/strength and applied gravity was reported, indicating scale effects. The indication of scale effects was investigated in more detail and the results from this investigation are shown in the following.

Grain size effects

Five tests were performed on piles ranging from $d = 16 - 40mm$, installed at 1g, (Test no. 11-16). The results can be seen in 3.13. It is noticeable that the response for the $d = 16mm$ pile is different from all of the others. The

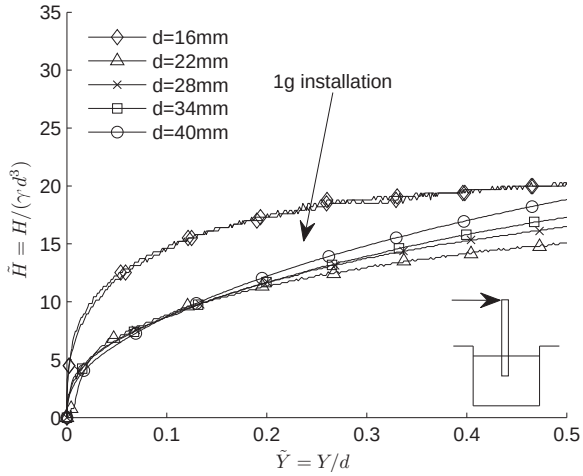

***Figure 3.13**: Grain-size effect on piles installed at 1g, Test no. 11-16*

test with $d = 16mm$ in diameter pile was repeated with identical results. The tendency for the $d = 16mm$ pile is that it shows a large initial stiffness and that it seems to reach a failure plateau. This is clearly an outlier and it is concluded that the ratio between diameter of monopile and diameter of average grain size $d/d_{50} = 88$ is too small, which leads to a grain size effect. This ratio is 30% higher than reported by Remaud (1999).

It can be seen for the four other piles that the response is more or less identical until a point of $0.1d$ deflection. At this point, the piles behavior starts to deviate. The capacity of the piles with large diameter increases more rapidly than the piles with smaller diameter. The difference between $d = 22mm$ and $d = 40mm$ is about 25% at a deflection of $0.5d$. It was not possible to model identical responses with different sized monopiles with 1g installation of the monopiles.

Installation effects

The same five piles were tested with an in-flight installation procedure, (Tests no. 17-21). The $d = 16mm$ pile showed the same behavior as the 1g installed

pile. This confirms the observation that the ratio of diameter of pile to diameter of average grain size is too small. The $d = 16mm$ pile is therefore not shown on the further plots. The lateral response of the 1g - and in-flight installed piles can be seen in Figure 3.14. It is clearly seen that the piles installed in-flight show a larger initial stiffness and higher bearing capacity. This is in agreement with the observations made by Craig (1985) and Dyson and Randolph (2001). For the piles installed in-flight, the response seems more identical than the piles installed at 1g, but a scale effect is seen with larger initial stiffness for the smallest piles. This is most evident for the pile with $d = 22mm$. Also here it was not possible to model identical responses.

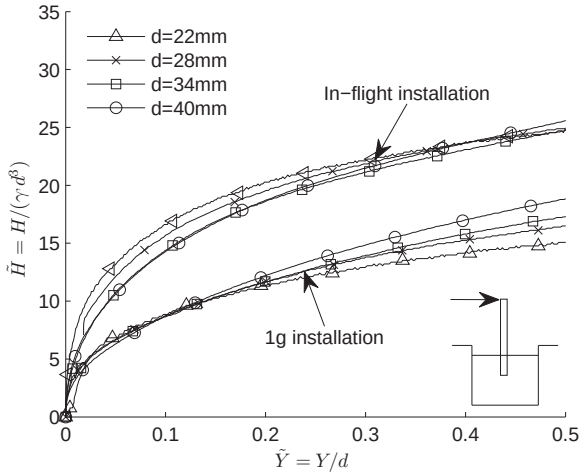

Figure 3.14*: Effect of installation at different stress levels, Tests no. 17-21*

Non-linear stress distribution effect

The increase in gravity depends on the radius to the strongbox, as it is mounted in the centrifuge and is therefore not constant through a soil sample due to the increase in radius. This introduces a nonlinear stress distribution in the centrifuge soil sample. The stress distribution in the centrifuge soil sample can be written as:

$$\sigma = \int_0^z \rho\omega^2(R_t + z)dz = \rho\omega^2 z(R_t + z/2) \tag{3.17}$$

Where R_t is the radius to the sand surface and z is the distance from sand surface to the point of interest in the sand sample. The stress distribution for

a laterally loaded pile is here modelled, so identical stresses are achieved at the depth z=2/3L, to minimize the stress error, Taylor (1995). This implies that soil stresses are too small above this point and too large below, as illustrated in Figure 3.15.

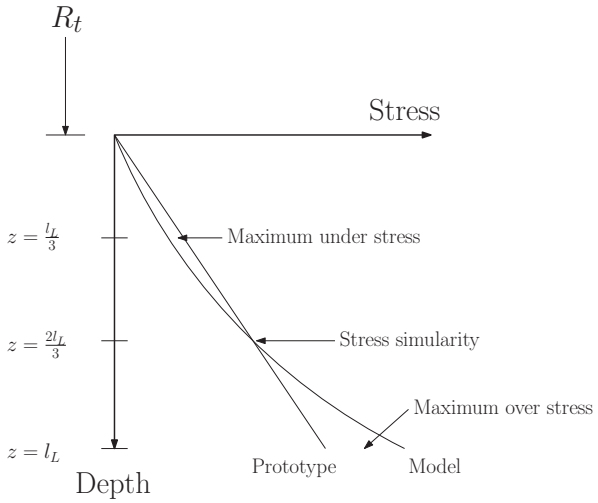

***Figure 3.15**: Stress distribution difference between prototype and centrifuge model*

To see if the small difference in stress distribution is the reason for failure in the "modelling of models" approach, conical shaped piles were designed to counteract the change in g-field. Recalling (1.1) for the soil resistance,

$$p = K \cdot d \cdot \sigma'_v \tag{3.18}$$

It can be seen that if the soil stress σ'_v is too small compared to prototype, the diameter d can be increased in order to achieve a constant soil resistance p. With this in mind, five conical shaped monopiles were made so the soil resistance was identical with prototype, (Tests no. 22-25).

The load deflection curves for the conical shaped piles are plotted in Figure 3.16, showing that, a very good agreement was achieved for the results.

This demonstrates that if the diameter is larger than $22mm$, the pile is installed in-flight and the non-linear stress distribution is taken into account, one prototype monopile can be modelled using different sized piles. This is fundamental and shows that the scaling approach seems valid, and that no diameter effect is present in this range.

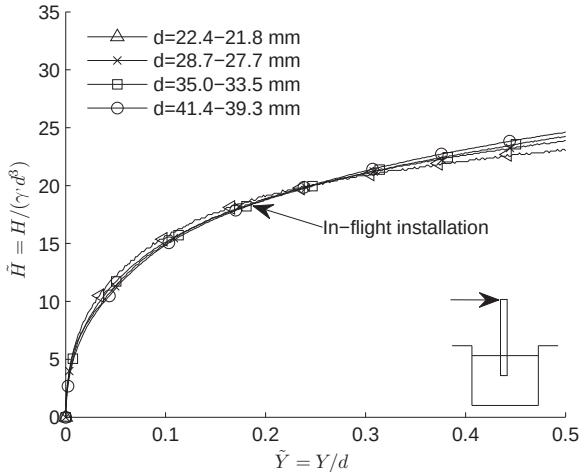

Figure 3.16*: Effect of using conical shape piles installed in-flight, Tests no. 22-25*

Stress level effect

Five different tests on a pile with a diameter of $d = 40mm$ where performed to investigate the stress level effect. The stress levels were chosen to correspond offshore monopiles ranging from 1 to 5 meters in diameter (Test no. 26-30). The overall load - displacement response can be seen in 3.17. Here it is seen that the pile subjected to the smallest stress level has the highest non-dimensional bearing capacity. The pile with the second lowest stress level has the second highest bearing capacity, whereas it seems that the last three piles have identical non-dimensional responses. From the triaxial tests it was seen, that the angle of friction is dependent on stress. A representative angle of friction was calculated for the entire test series. This was carried out using the average relative density and the pressure calculated at a pile depth at 2/3 of the total length. Here it can be seen that the tests performed at low stress levels have a higher mobilized angle of friction. To take this non-linearity into account, Rankine's passive earth pressure coefficient is introduced in the normalisation process shown in equation (3.19).

$$K_p = \tan^2(45 + \phi'/2) \tag{3.19}$$

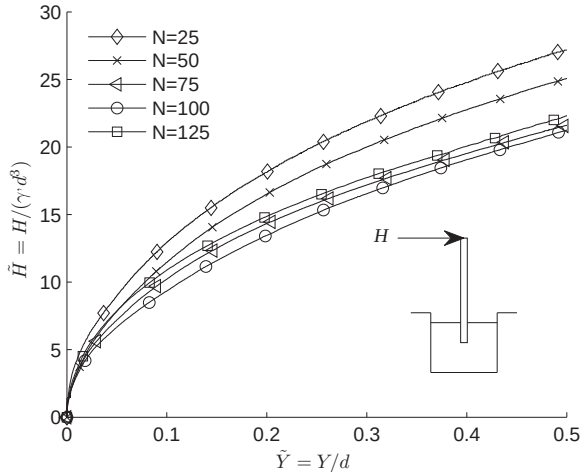

***Figure 3.17**: Effect from different stress levels, $d = 40mm$, Tests no. 26-30*

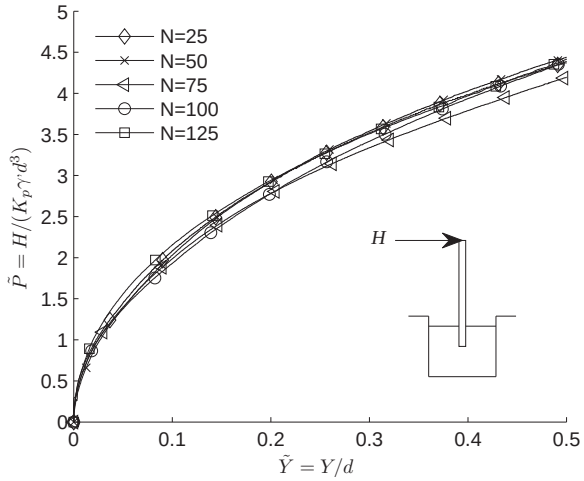

***Figure 3.18**: Effect of the normalisation with Rankines passive earth pressure coefficient, $d = 40mm$, Tests no. 26-30*

The non-dimensional load can then be redefined to be:

$$\tilde{P} = \frac{\tilde{H}}{K_p} = \frac{H}{K_p \cdot \gamma' \cdot d^3} \tag{3.20}$$

In Figure 3.18, the overall response with the new normalization is shown. Here, the response from the five different tests merge into one single characteristic curve. This shows that the nonlinear soil behavior, in these tests, can be taken into account only using the strength parameter. With this normalization one test can be used for any given prototype diameters. Here it is demonstrated that this is valid in the range of $d = 1 - 5$ meters, but it is assumed that this is also valid for larger diameters.

Stiffness effect

Two tests were performed with a hollow monopile in order to investigate the influence from using a solid steel monopile instead of a hollow monopile. The hollow monopile was made of steel and the diameter was $d = 40mm$ and the thickness was $t = 2mm$. A comparison between the response from the solid monopiles and the hollow monopiles was made and can be seen in Figure 3.19. Two tests were made and the results shows that the overall

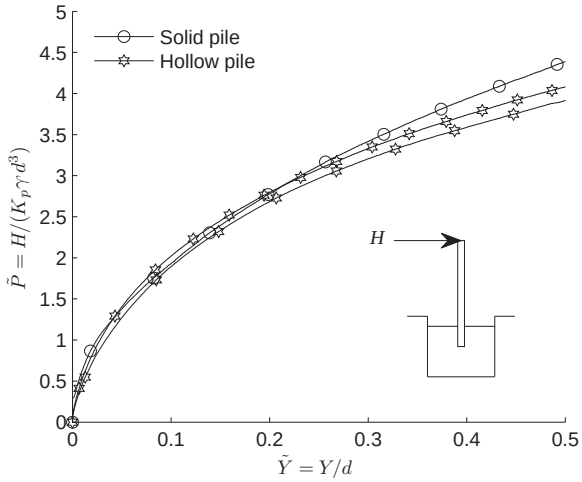

Figure 3.19*: The lateral response from a solid and hollow pile, Test no. 28 & 31-32*

response is identical with the one from the solid pile (Test no. 28 & 31-32). Two conclusions can be drawn from this; first the stiffness of the piles tested is so stiff that they behave in a rigid manner with identical response as a consequence. This was also the conclusion from the numerical study done by Zania and Hededal (2011). Secondly, the influence from installation of a

hollow pile where soil will be trapped inside the pile seems negligible.

The non-dimensional stiffness ratio of a pile, neglecting the stiffness of the sand inside the pile, can be calculated by the criteria by Poulos and Hull (1989):

$$\frac{E_p I_p}{E_s l_L^4} = \begin{cases} > 0.208 & \text{Rigid pile behavior} \\ < 0.0025 & \text{Slender pile behavior} \end{cases} \tag{3.21}$$

The non-dimensional stiffness ratio has been calculated from the solid and hollow monopiles and is compared with fictive prototype conditions in table 3.5. The stiffness of the sand is high, but corresponds to the observations seen in the triaxial tests. From table 3.5 it can be seen that model and

***Table 3.5**: Test program for validation of methodology*

Scale	Pile diameter d [m]	Pile thickness, t [m]	Pile penetration l_L [m]	Pile stiffness E_p [MPa]	Soil stiffness E_s [MPa]	$\frac{E_p I_p}{E_s l_L^4}$
Model	0.04	0.02	0.24	210000	100	0.079
Model	0.04	0.002	0.24	210000	100	0.047
Proto	4	0.05	24	210000	100	0.007
Proto	6	0.1	24	210000	100	0.052

prototype piles all have a non-dimensional stiffness ratio which is bigger than the slenderness criteria. Also it can be seen that they are all smaller than the rigid criteria meaning all piles behave in between a pure rigid and a pure slender pile. However, identical response for the piles with different stiffness ratios indicates that these piles behave in a rigid fashion. Two prototype stiffness ratios have been calculated first for a $d = 4m$ diameter monopile compatible with the piles at e.g. Horns Rev 2 in Denmark and for a monopile with a diameter of $d = 6m$, compared with some of the monopiles installed most recently in e.g. the British sector. From Table 3.5, it can be seen that the monopiles installed today are getting closer to the rigid pile criteria and that the stiffness ratio for the hollow pile corresponds well with the stiffness for the prototype monopiles. With the similar response for the solid and hollow monopiles in mind it therefore seems valid to assume that the stiffness of the solid model monopiles represents a prototype monopile supporting a wind turbine.

Roughness effect

The model piles used in the later investigation of the soil - pile interaction are a strain-gauge mounted solid piles with a $2mm$ epoxy coating, which makes the pile very smooth. The influence of shaft friction was investigated by sandblasting the surface of one pile and comparing the results with the data from the smooth piles (Test no. 28 & 33). The sand blasted sand surface was created in order to mimic the surface of a prototype monopile. The results

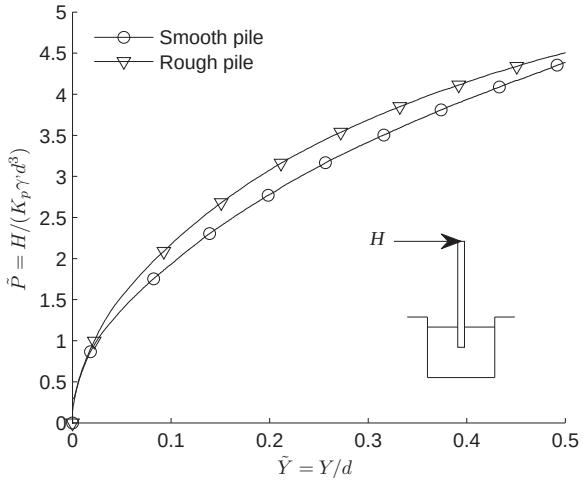

Figure 3.20*: Effect of pile roughness, $d = 40mm$, Test no. 28 & 33*

can be seen in Figure 3.20, where the normalized response is shown. It can be seen that the response from the sand blasted pile is stiffer compare the smooth pile although both appear approaching a similar large strain capacity. It is therefore expected that the results of the stiffness obtained from the tests in this thesis are smaller compared to prototype.

Effect of in-flight installation at low elevated stress level

From the "modelling of models" test series, it was seen that in-flight installation of the monopile is necessary in order to avoid scale effects. The jack, driving the piles in-flight has a 20 kN limit, corresponding to the force needed for pile with a stress distribution for a prototype diameter $d = 2m$. For current investigation into pile - soil interaction it was chosen to install these monopiles at an elevated stress level corresponding to one third of the stress level at which the lateral loading was performed. The effect from in-flight

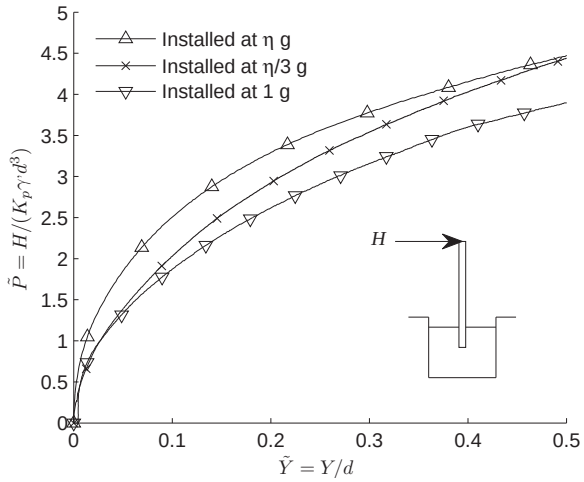

***Figure 3.21**: Effect of installation at different stress levels, Test no. 16 & 21 & 26*

installation at a lower stress level is shown for three piles in Figure 3.21. The three piles are installed respectively at $1g$, full in-flight stress ηg and at a lower stress level $\eta/3$ g. As seen before the in-flight installed monopile has a stiffer response and a larger capacity than the 1g installed monopile. The monopile installed at lower stress level shows a stiffer response than the 1g installed monopile, but has a smaller stiffness than the monopile installed at full stress level. After deformation of around half a diameter the response converges with the pile installed at full stress level. It is concluded from this plot that the piles installed at a third of the full stress level has a smaller initial stiffness, but the capacity is almost identical with the monopile installed at full stress level.

3.4.2 Scaling approach

The scaling approach in this thesis is designed so that tests under dry conditions can be interpreted as if they were performed under saturated conditions. The basic assumption is that for a quasi-static test, no excess pore pressure will develop. With no excess pore pressure identical effective stress distribution can be achieved in the model and prototype. This can be written as:

$$\sigma'_{v,p} = \gamma'_{sat} \cdot z_p = \eta \cdot \gamma'_{dry} \cdot z_m \;\Rightarrow\; \eta = \frac{\gamma'_{sat} \cdot z_p}{\gamma'_{dry} \cdot z_m} = \frac{\gamma'_{sat}}{\gamma'_{dry}} \cdot N_s \tag{3.22}$$

The increase in gravity η and the geometrical scaling factor $N_s = \frac{z_p}{z_m}$ are not identical due to the difference in effective densities. This modelling technique was used by Li et al. (2010). Four monotonic tests were performed, two

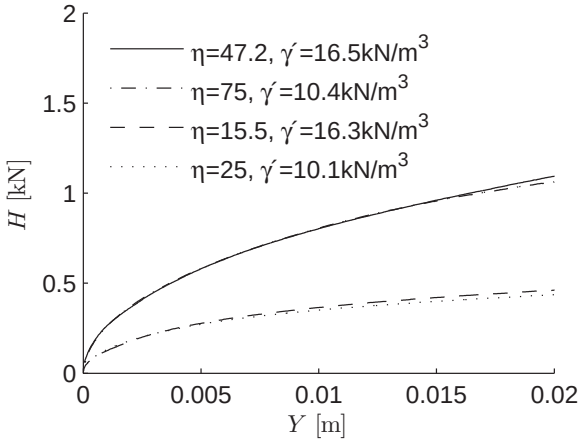

***Figure 3.22**: Verification of scaling approach, Test no. 21 & 21s & 28 & 35*

in saturated sand and two in dry sand with stress levels corresponding to respectively 1 and 3 meter diameter piles. The response of the two tests with a stress distribution corresponding to a one meter diameter pile and the two tests with stress distributions identical to a three meter diameter monopile, can be seen in Figure 3.22 at model scale, which show identical responses. Even though the relative density is not identical for these pairs of tests, the difference is so small that it does not affect the results. This confirms the scaling approach provided that fully drained conditions are achieved.

3.4.3 Measurement uncertainties

Testing is always affected by uncertainties; this section tries to quantify the different uncertainties and the effect of these. Two types of measuring devices are used, potentiometers and strain-gauge based load devices. All potentiometers and strain-gauge devices have been calibrated several times during the period of the thesis shoving a linear response each time with only small deviations in the calibration constants. The scatter on the data from the potentiometers is around $1/100mm$ and the error in the calibration constant is estimated to be around 0.5%. The scatter of the the data obtained from

strain-gauge based devices is around 1N for the load cell used for laterally loading and around 1Nm for the strain gauge mounted piles. The error in these measurements is a bit larger and estimated to be 2%

The validation process shows that using the instrumentation and the given test methodology identical responses can be modelled. This shows that tests are repeatable with identical results as a consequence. This is what is sought after and these results demonstrate that the uncertainties involved in testing can be neglected.

The tests presented previously have all looked at the overall pile response. The pile - soil interaction response in this thesis is derived from the moment distribution in the pile. While the deflection of these pile - soil interaction curves are well described, it is important to remember that the soil resistance and the corresponding distribution due to the double differentiation can be affected by uncertainties of up to 35%, Rosquoët et al. (2010).

3.5 Summary of methodology validation

37 tests have been performed in order to validate the centrifuge modelling approach. Different factors have been identified and have to be taken into account when the centrifuge tests are used in the investigation of piles in prototype scale. The conclusions are here listed:

1. Identical responses can be modelled using the "modelling of models" approach if, the diameter is larger than $22mm$, the pile is in-flight installed and the non-linear stress distribution is taken into account.

2. Using Rankines passive earth pressure coefficient as a normalisation parameter, one centrifuge test can be interpreted as a pile with diameters in the range of $d = 1 - 5$ meters.

3. The solid and hollow model piles shows identical responses.

4. Rough pile shows a stiffer response compared to a smooth pile

5. Piles installed at a third of the full stress level have a smaller initial stiffness but the capacity is almost identical with the monopile installed at full stress level.

6. Using an effective stress scaling approach test in dry sand can represent saturated drained conditions.

Chapter 4

Pile - soil interaction results

The centrifuge modelling approach was validated in the previous chapter by a series of simple monotonic load tests. The tests were performed on solid steel piles with no instrumentation and only the total pile response was of interest. To investigate the pile - soil interaction in more details, monotonic and cyclic tests have been performed on instrumented model piles. 37 tests have been performed in this investigation , see table 4.1.

9 monotonic and 6 cyclic test were performed as an initial study of on a $d = 16mm$ monopile (Test no. 38-52), these tests are presented in Klinkvort et al. (2010). The load setup was changed based on the conclusion drawn from this study and a new load control algorithm was written in order to have a better control of the cyclic loading.

A test series consisting of one monotonic and seven cyclic tests was performed on a $d = 28mm$ pile, the initial analysis of these test was presented in Klinkvort et al. (2011),(Test no. 53-60). Four test were afterwards performed on the same pile with a few deformation controlled (dc) load cycles, (Test no. 54-60). The few number of strain-gauge bridges on the $d = 28mm$ pile makes the interpretation of the interaction difficult and only pile - soil interaction curves from one depth can be deduced.

It is easier to investigate and interpret interaction curves from different levels for the pile with ten strain-gauge bridges ($d = 40mm$). The influence of load eccentricity on the pile - soil interaction was examined by carrying out five test with different load eccentricities were carried out, (Test nr 65-69), Klinkvort and Hededal (2012b).

Finally, five supplementary cyclic tests were carried out; two in dry sand and three in saturated sand (Test no. 70-74), presented in Klinkvort and Hededal (2012a), together with the results in Test no. 53-60.

***Table 4.1**: Test program. c=cyclic, h=hollow, r=rough, s=saturated*

Test nr	I_D	Effective density, $[kN/m^3]$	Pile dia. d [mm]	Load ecc. l_e/d	Pene. depth l_L/d	Scaling factor N_s	Install. accel. $[g]$
38	0.94	16.6	16	2.5	10	62.5	1
39	0.91	16.5	16	2.5	8	62.5	1
40	0.90	16.6	16	2.5	6	62.5	1
41	0.89	16.4	16	4.5	10	62.5	1
42	0.94	16.6	16	4.5	8	62.5	1
43	0.91	16.4	16	4.5	6	62.5	1
44	0.94	16.6	16	6.5	10	62.5	1
45	0.94	16.6	16	6.5	8	62.5	1
46	0.93	16.5	16	6.5	6	62.5	1
47 c	0.92	16.6	16	2.5	10	62.5	1
48 c	0.91	16.5	16	2.5	8	62.5	1
49 c	0.93	16.6	16	2.5	6	62.5	1
50 c	0.94	16.6	16	4.5	8	62.5	1
51 c	0.92	16.5	16	4.5	6	62.5	1
52 c	0.96	16.6	16	6.5	6	62.5	1
53	0.96	16.8	28	15	6	115	1
54 c	0.84	16.4	28	15	6	115	1
55 c	0.86	16.4	28	15	6	115	1
56 c	0.93	16.7	28	15	6	115	1
57 c	0.86	16.4	28	15	6	115	1
58 c	0.84	16.4	28	15	6	115	1
59 c	0.86	16.4	28	15	6	115	1
60 c	0.80	16.2	28	15	6	115	1
61 dc	0.81	16.3	28	15	6	115	1
62 dc	0.95	16.4	28	15	6	115	1
63 dc	0.82	16.3	28	15	6	115	1
64 dc	0.85	16.4	28	15	6	115	1
65 s	0.87	10.2	40	17.25	6	75	$\eta/3$
66 s	0.87	10.2	40	15	6	75	$\eta/3$
67 s	0.87	10.2	40	12.75	6	75	$\eta/3$
68 s	0.94	10.4	40	10.5	6	75	$\eta/3$
69 s	0.90	10.6	40	8.25	6	75	$\eta/3$
70 c	0.93	16.7	40	15	6	75	$\eta/3$
71 c	0.94	16.7	40	15	6	75	$\eta/3$
72 c s	0.97	10.4	40	15	6	75	$\eta/3$
73 c s	0.87	10.2	40	15	6	75	$\eta/3$
74 c s	0.94	10.4	40	15	6	75	$\eta/3$

4.1 Monotonic loading

The monotonic loading is used to determine the monotonic pile - soil interaction curves as well as being reference to the cyclic tests. From the total response it was seen that it was possible to take the stress dependent soil behavior into account by introducing the passive Rankine coefficient. This is also used in the normalization of the soil resistance p but here $K_p(z)$ is a function of the given depth. The revised normalized soil resistance is written as:

$$\tilde{p} = \frac{K}{K_p} = \frac{p}{K_p \cdot \gamma' \cdot z \cdot d} = \frac{p}{K_p \cdot \sigma'_v \cdot d} \tag{4.1}$$

It is possible to compare results performed at different stress levels with this simple normalization. This is first demonstrated in Figure 4.1 for the total response. Here the total response of the $d = 40mm$ pile compared with the response from the $d = 28mm$ pile is shown. The normalized displacement of the pile is plotted against the normalized force on Figure 4.1. The monotonic tests in dry and saturated sand performed on different sized models show approximately identical results. Looking at the pile - soil response shown in Figure 4.2, the pile with a diameter of $d = 28mm$ shows initially the same response as the two other piles, but the response starts to deviate from a pile displacement above $0.05d$. A reason for the deviation could be that the $d = 28mm$ pile is installed at $1g$, whereas the $d = 40mm$ piles are installed at an elevated stress field. As demonstrated by Dyson and Randolph (2001) and in Figure 3.21 in the previous chapter $1g$ installation leads to a softer response.

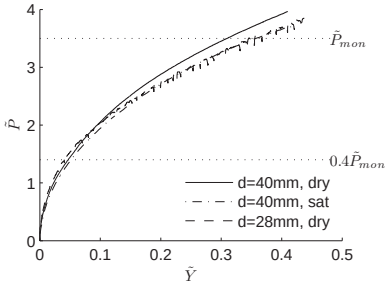

***Figure 4.1**: Total lateral monotonic response, Test no. 28 & 53 & 66s*

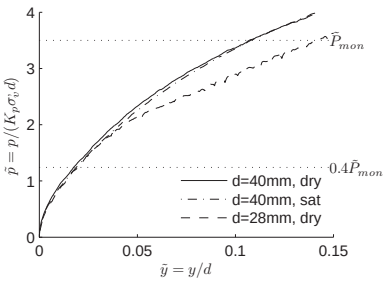

***Figure 4.2**: Pile - soil interaction monotonic response, $z = 2d$, Test no. 28 & 53 & 66s*

It can be seen from Figure 4.1 that the ultimate capacity was not reached for any of the tests. Therefore a rotation criterion was used to define the

reference bearing capacity. Failure was defined at a rotation of 4 degrees for the piles with a diameter of $d = 40mm$. The maximum normalized force is shown Figure 4.1 as a dotted line. The monotonic response from the three tests is identical at load level less than 40 % of maximum. Since all cyclic tests were performed below this level the results from both of the piles was used in the cyclic analysis. The same tendency is seen if the pile - soil interaction is compared, this is shown Figure 4.2. This confirms that the interaction curves also can be compared.

4.1.1 Stress distribution effect

The normalized interaction curves from five tests with different stress distributions, identical with prototype piles with diameters ranging from 1-5 meters, are shown in Figure 4.3, Klinkvort and Hededal (2012b). Normalized

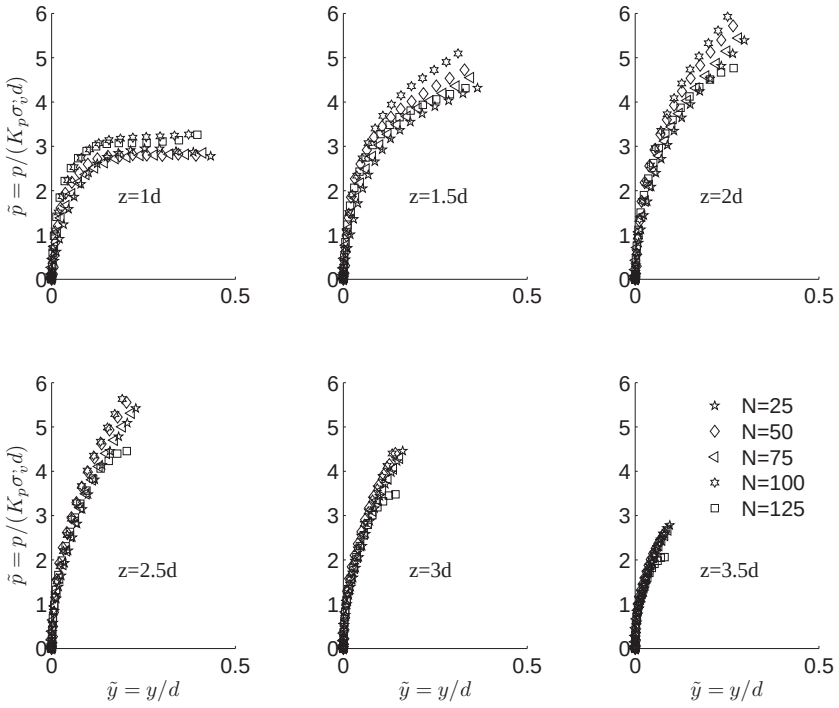

***Figure 4.3**: Monotonic test results on d=40mm pile with five different stress distributions at different normalised depths, Test no. 26-30*

interaction curves are shown separately from the six different depths. It is seen that the normalized pile - soil interaction curves show a high degree of similarity as for the total response. It is concluded from this that the normalized pile - soil interaction responses have similar normalized behaviour, no matter of the stress level. By normalizing the results only through the angle of friction it is demonstrated that the stress level can be taken into account. These curves can then be used for any given prototype stress level, when the stress level effect is taken into account.

Depth effect

A comparison of the effect of depth can be made, this is shown in Figure 4.4, here the soil pile interaction from three different tests in three different depths but with same vertical stress can be seen. Looking at Figure 4.4, it

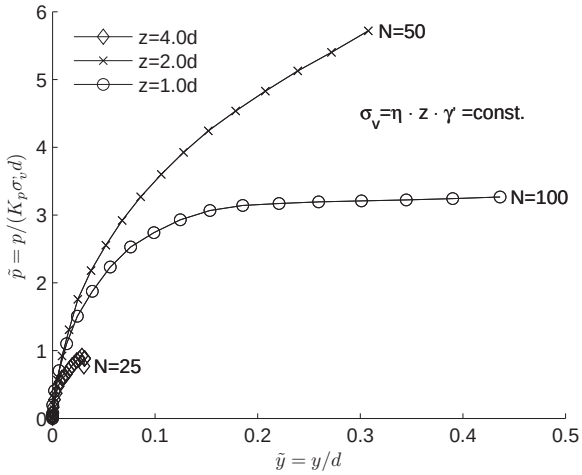

***Figure 4.4**: Identical vertical stress in different depths, $d = 40mm$ pile installed in dry sand, Test no. 26-27 & 29*

is clearly seen that the ultimate earth pressure coefficient is not constant as assumed by Broms (1964) and Zhang et al. (2005). The curves at depths of $z = 1d$ and $z = 4d$ both show that the piles have reached the ultimate capacity, whereas the curve located at $z = 2d$ has not reached the ultimate capacity. The ultimate capacity from $z = 1d$ and $z = 4d$ curves are also very different, with a very small normalized capacity for the lower one, but the initial normalized stiffness is for all three curves almost identical. This

clearly shows that the pile - soil interaction is not only dependent on the vertical stress but also on the depth. The very small capacity at depth of $z = 4d$ also indicates that the distance to the rotation point is important.

It is also clear from this that it is important to have full similarity when comparing results, in order to document one effect. For example, comparing a pile - soil interaction curve $4m$ down in the soil from $1m$ diameter pile with a pile - soil interaction curve $4m$ down in the soil from a $6m$ in diameter pile does not makes sense, because full similarity is not achieved and identical responses cannot be expected.

4.1.2 Load eccentricity effect

The load eccentricity of the resultant force component will change due to the nature of the lateral loads. This was investigated by comparing five tests performed on piles with a stress distribution identical with a $3m$ diameter prototype, but with different load eccentricities, Klinkvort and Hededal (2012b). The five tests were all performed in water saturated sand and on a pile with load eccentricities ranging from $l_e = 8.25d - 17.25d = 330 - 690mm$. Using the normalization strategy described in (4.1), the results from the five tests are shown in Figure 4.5. As for the five tests with different stress distributions, the results from changing the load eccentricity is shown for the six strain-gauge levels. Again it seems like the responses are similar, no matter the load eccentricity. Scatter is seen in the results, but no systematic trend is observed and the curves seem to merge with the increasing soil stress with depth. It is therefore concluded from these tests that the soil-pile interaction dos not change due to load eccentricity. This is identical with the assumption recommended by API (2007).

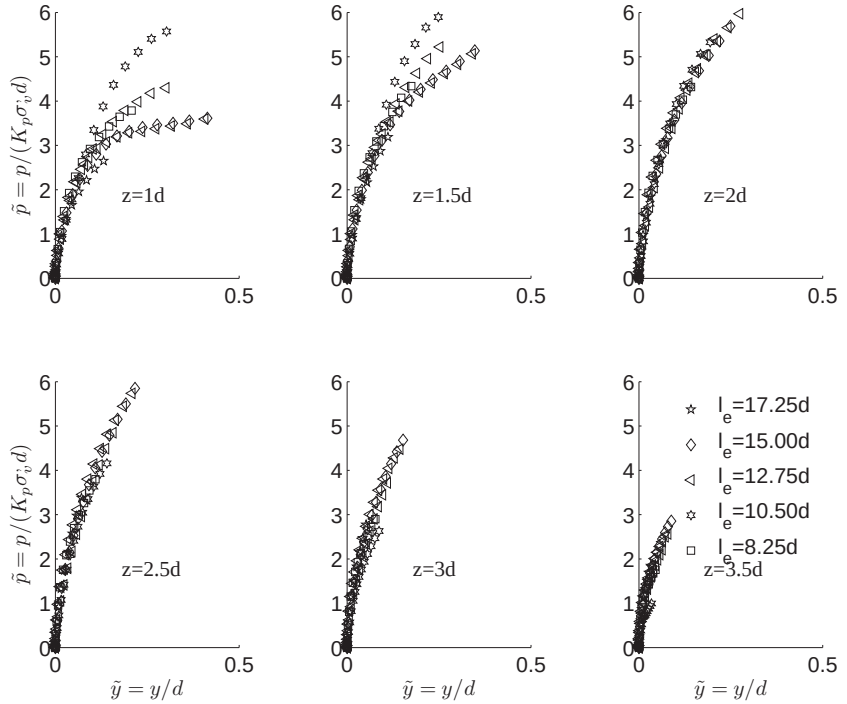

Figure 4.5*: Monotonic test results from $d = 40mm$ pile installed in saturated sand with five different load eccentricities, Test no. 65-69*

4.1.3 Comparison with numerical models

Ten different monotonic tests were carried out with different stress distributions and with different load eccentricities. The normalized responses from these tests should be identical, which was demonstrated in Figure 4.3 and 4.5. These results are compared with a numerical 3D finite element calculation Zania and Hededal (2012) and a Winkler calculation using the recommendations from API (2007). The 3D finite element (FE) calculation was carried out on a $2m$ diameter solid steel pile with a load eccentricity of $l_e = 15d$, and a penetration of $l_L = 6d$. The sand was modelled as Mohr-Coloumb material and the material parameter was deduced from the same triaxial test as shown in Figure 3.11. The interface between pile and soil was modelled using a Coulomb friction law with an angle of friction of $\delta = 21^o$. The FE model and the centrifuge tests with a stress distribution identical to a 2 meter di-

ameter pile have full similarity and the results can therefore be compared. For more details of the numerical model, see Zania and Hededal (2012). A calculation using the API (2007) methodology has been performed. Here, an initial subgrade modulus of $k = 40MPa/m$, which was obtained from Figure 2.3. The results of the two calculations can be seen together with the centrifuge results in Figure 4.6. The pile-soil interaction response using the

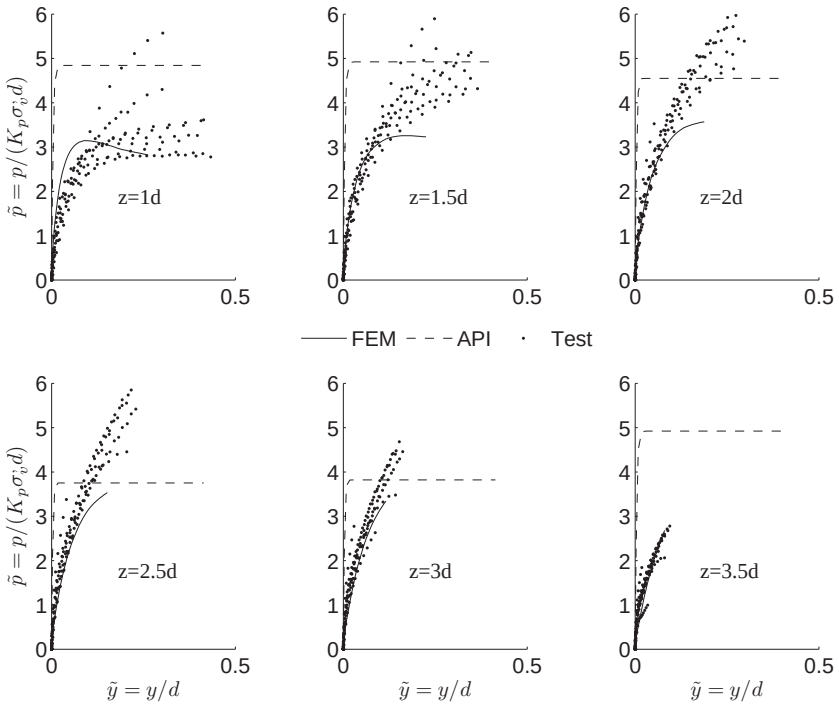

Figure 4.6*: Monotonic centrifuge test results (Test no. 26-30 & 65s-69s) compared against FE model analysis carried out on a representative prototype case and an API model*

methodology proposed by API (2007) overestimates the initial stiffness in a high degree, the ultimate capacity is overestimated in $z = 1d$ depths and underestimated in $z = 1.5 - 3d$, this is clearly seen in Figure 4.6. The FE calculation predicts the stiffness of the test result in a better way than the API (2007) methodology, but it can be seen that the stiffness of the curve in shallow depth is too high, at the medium depth acceptable and is to low in greater depths. The maximum capacity is predicted well at the shallowest

depth, but seems to have been underestimated at the lower levels.

The test results from the ten tests can be represented by a single set of generic curves, which has been shown in Figure 4.7. It can be seen that a maximum soil resistance was only reached in the upper layer $z = 1d$, even though the pile has been displaced more than $0.5d$ at sand surface. The initial slopes of the pile - soil interaction curves were all similar and can be represented by $\tilde{E}_{py}/K_p = 100$. A constant normalized initial stiffness is identical with the assumption proposed by API (2007). In the same way,

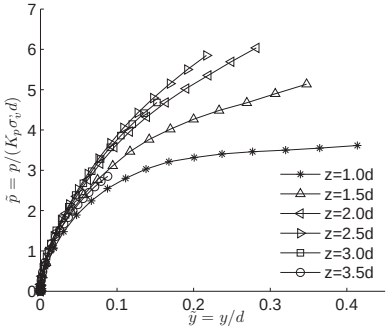

***Figure 4.7**: Generic pile - soil interaction curves from centrifuge test no. 66s*

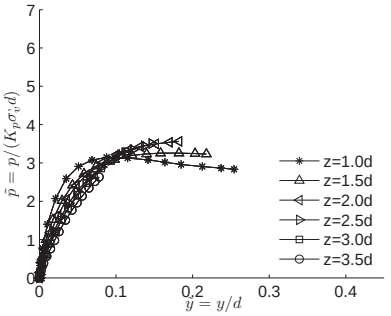

***Figure 4.8**: Pile - soil interaction curves from finite element model*

the results from the FE model are shown in Figure 4.8. Here it is seen that more of the curves have reached a maximum capacity and also that the normalized stiffness is decreasing with increasing depth, in contrast to the recommendation from API (2007). It should also be noticed that the maximum capacity is around 3 which is the value Broms (1964) proposed.

The magnitude of the pile - soil interaction curves from the centrifuge tests and the numerical calculations are in the same order of magnitude. This validates, in some way, the results from the two methods. The results from the centrifuge are from a real physical event and the credibility of these tests is therefore higher. The FE model needs to be improved in order to achieve better results, which can be used in the analysis of the laterally loaded monopile.

4.1.4 New monotonic pile - soil interaction model

The results from the tests were compared with methodologies of API (2007) and Kondner (1963), but here with an initial stiffness of $\tilde{E}_{py}/K_p = 100$. The

two types of curves were compared and disagreements between models and results were still seen. A new way to compute pile - soil interaction curves is introduced here. It uses the formulation proposed by Kondner (1963) and the calculation of ultimate capacity is identical with the method proposed by API (2007), but the calculation of the empirical depth factor A, is changed in order to match the results. The calculation of A is shown in (4.2), Klinkvort and Hededal (2012b).

$$A = 0.9 + 1.1 \cdot H \tag{4.2}$$

The parameter H is a step function and controls the transition from 2 in the upper parts to 0.9 at greater depths.

$$H = \frac{1}{2} + \frac{1}{2} \tanh\left(9 - 3\frac{z}{d}\right) \tag{4.3}$$

The new formulation is shown in Figure 4.9 and compared with the formulations proposed by API (2007) and Georgiadis et al. (1992). It can be seen

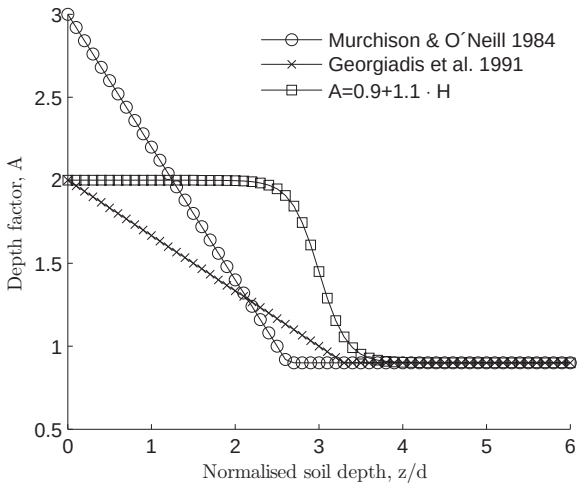

***Figure 4.9**: New calculation of the empirical depth factor A*

that all of the three functions are in the same range. The formulation by Georgiadis et al. (1992) is similar to the one by API (2007) and decreases linearly to 0.9, whereas the one showed in (4.2) has a more abrupt change from 2 to 0.9. The centrifuge results and the Kondner (1963) model using the new calculation of A are shown in Figure 4.10 together with the models by API (2007) and Kondner (1963), using the standard formulation of A.

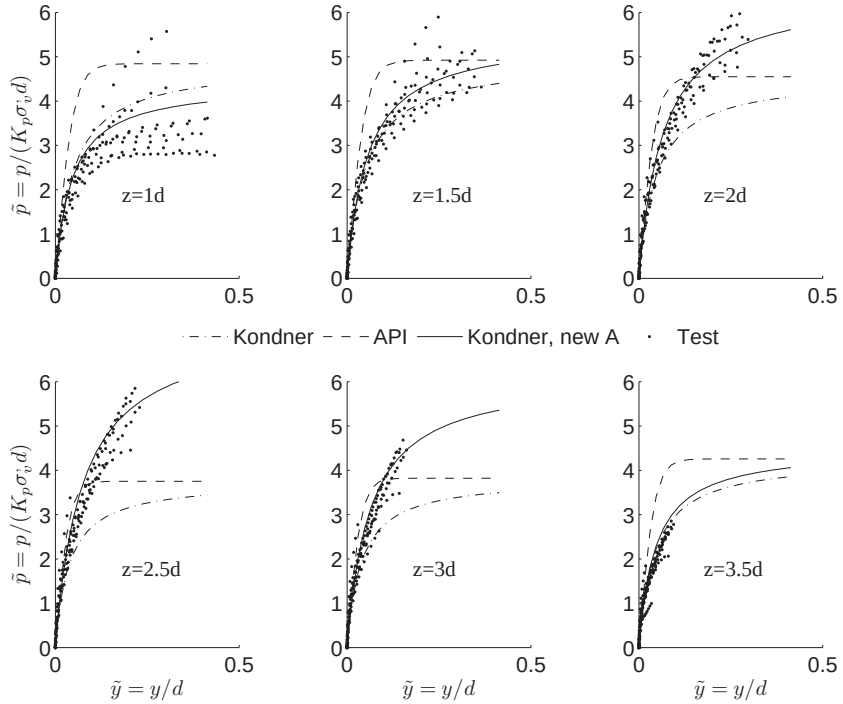

***Figure 4.10**: Pile - soil interaction models in comparison with centrifuge test data, Test no. 26-30 & 65s-69s*

It can be seen from Figure 4.10 that using the standard value of A leads to slight overestimation of the capacity in the top layers and underestimation in the lower layers. Using the new value of A shown in (4.2), together with the hyperbolic function proposed by Kondner (1963), provides a model with a high degree of the similarity to the test observations. It is therefore recommended to use the formulation calibrated here in a ULS analysis.

4.2 Cyclic loading - total response

As a first attempt to understand the cyclic pile - soil response, a test series with focus on the total response was carried out. First, an analysis of the tests no. 54-60 was carried out, Klinkvort et al. (2011). These tests were supplemented by five extra tests and a more general analysis was carried

out, Klinkvort and Hededal (2012a). Twelve cyclic tests were performed, (Test no. 54-60 & 70-74) and together with the monotonic test shown in Figure 4.1, (Test no. 28 & 53 & 66s) they provide the basis for the analysis. The monotonic tests were used as a reference for the cyclic tests. Firstly seven cyclic tests were performed on the $d = 28mm$ pile in dry sand, from these tests the non-dimensional functions were established. This was done by changing the load amplitude of the cyclic loading (η_b), while keeping the characteristic of the cyclic loading (ζ_c) constant. Afterwards, the effect of the characteristic of the cyclic loading was investigated by changing ζ_c, while keeping ζ_b constant. Later, two tests on a $d = 40mm$ pile were performed to investigate the influence of number of cycles and three tests were used to perform cyclic tests in saturated sand. Although tests were performed on different sized piles and in dry or saturated conditions, the non-dimensional functions determined from all the tests proved representative for the entire test series.

4.2.1 Model framework

In order to investigate the accumulation of displacements and change in secant stiffness the cyclic loading is load controlled. In each load cycle the maximum and minimum value of the load ($\tilde{P}_{max,N}, \tilde{P}_{min,N}$) and the displacement ($\tilde{Y}_{max,N}, \tilde{Y}_{min,N}$) can be obtained. A schematic cyclic response is shown in Figure 4.11. The maximum displacement and the cyclic secant stiffness from each cycle can therefore be determined. The maximum displacement is found as the displacement when the load is at the maximum of each cycle and the cyclic secant stiffness is found as the slope of a straight line between the extremes for every cycle, see Figure 4.11.

Having determined the bearing capacity of the pile from a monotonic test, ($\tilde{P}_{mon}$), the cyclic loading can be described by two non-dimensional parameters, (Long and Vanneste (1994), Rosquöet et al. (2007) and LeBlanc et al. (2009)).

$$\zeta_b = \frac{\tilde{P}_{max}}{\tilde{P}_{mon}} \quad \zeta_c = \frac{\tilde{P}_{min}}{\tilde{P}_{max}} \tag{4.4}$$

The value ζ_b defines the load amplitude relative to the maximum bearing capacity under monotonic conditions, $\tilde{P}_{mon}$, and ζ_c defines the characteristic of the cyclic loading.

Displacement evolution model

The cyclic loading is described by the parameters (ζ_b, ζ_c), the maximum displacement from the number of cycles (N) may then be determined from

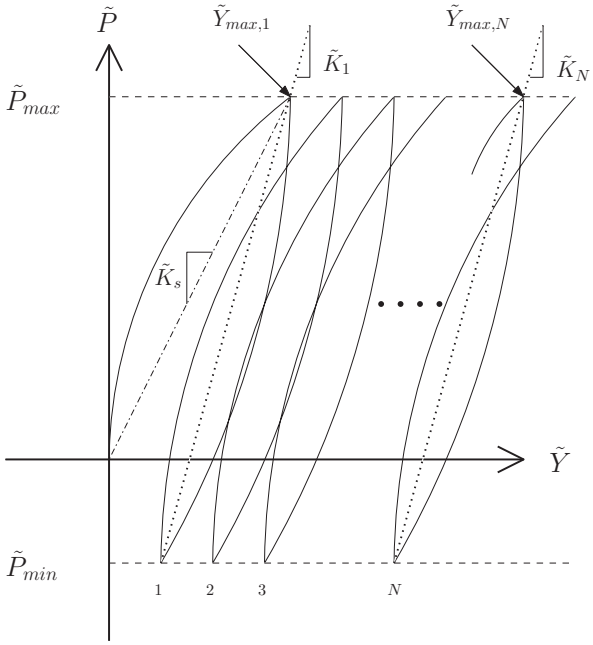

***Figure 4.11**: Schematic drawing of determination of secant stiffness and maximum accumulation of displacement*

a power function,

$$\tilde{Y}_{max,N} = \tilde{Y}_{max,1} \cdot N^{\alpha} \tag{4.5}$$

The coefficient, α is dependent, both on the load characteristic described by ζ_c, and the magnitude of the loading described by ζ_b. Assuming the two effects to be independent, the value of α can be calculated as a product of two non-dimensional functions.

$$\alpha(\zeta_c, \zeta_c) = T_c(\zeta_c) \cdot T_b(\zeta_b) \tag{4.6}$$

The first function, T_c, depends on the load characteristic, ζ_c, and the second function, T_b, depends on the load magnitude, ζ_b.

Secant stiffness evolution model

The cyclic secant stiffness in every cycle may be described by a logarithmic function;

$$\tilde{K}_N = \tilde{K}_1(1 + \kappa \cdot \ln(N)) \tag{4.7}$$

In (4.7), κ is the accumulation rate, $\tilde{K}_1$ is the cyclic secant stiffness for the first cycle and $\tilde{K}_N$ is the cyclic secant stiffness for cycle number N. As for the accumulation of displacements, it is chosen to describe the value of κ by two independent non-dimensional functions.

$$\kappa(\zeta_c, \zeta_c) = \kappa_c(\zeta_c) \cdot \kappa_b(\zeta_b) \tag{4.8}$$

The non-dimensional cyclic secant stiffness at the first cycle, $\tilde{K}_1$, is found using the secant stiffness of the monotonic response.

$$\tilde{K}_s(\zeta_b) = \frac{\tilde{P}_{max}}{\tilde{Y}_{max}} \tag{4.9}$$

This value is appropriately scaled by $\tilde{K}_c(\zeta_c)$, which depends on the cyclic load characteristic, i.e.

$$\tilde{K}_1(\zeta_c, \zeta_c) = \tilde{K}_c(\zeta_c) \cdot \tilde{K}_s(\zeta_b) \tag{4.10}$$

The input to the two evolution models can be established from a monotonic test combined with the non-dimensional functions, $(T_c(\zeta_c), T_b(\zeta_b)$,$\kappa_c(\zeta_c), \kappa_s(\zeta_b)$ and $\tilde{K}_c(\zeta_c), \tilde{K}_b(\zeta_b))$. These functions can be determined empirically by a series of cyclic load tests.

4.2.2 Evolution of displacements

The accumulation of displacement may be described by a power function. The maximum deflection for all cycles plotted together with the power fit is shown in Figure 4.12. It can be seen that the power fit captures the accumulation of displacement well. The results, together with the non-dimensional cyclic load characteristics, can be seen in Table 2 in Klinkvort and Hededal (2012b). The value of α can be calculated using two non-dimensional cyclic functions, as shown in (4.6). By normalizing $T_c = 1$ for pure one-way loading, $\zeta_c = 0$, the non-dimensional function T_b can be found from a series of tests where T_b is changed.

$$\alpha(\zeta_c = 0, \zeta_b) = 1 \cdot T_b(\zeta_b) \tag{4.11}$$

When T_b is determined the function T_c may be found by performing a series of tests with a constant ζ_b and then dividing the results with the T_b function, i.e.

$$T_c(\zeta_c) = \frac{\alpha}{T_b(\zeta_b)} \tag{4.12}$$

The result of this analysis can be seen in Figure 4.13. It was chosen to force

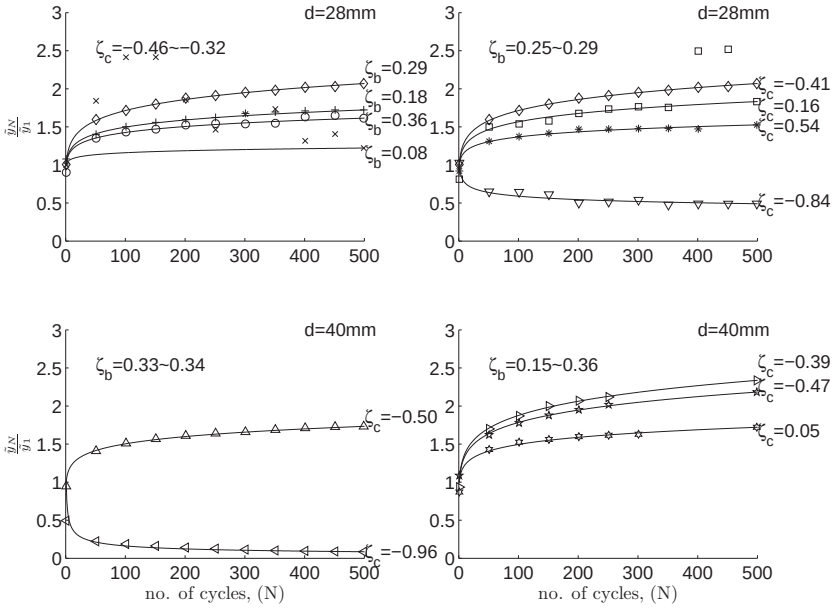

***Figure 4.12**: Accumulation of displacements, under load controlled cyclic loading for a pile with a load eccentricity of $l_e = 15d$ and penetrated to $l_L = 6d$, Test no. 54-60 & 70-74*

the values of T_b to be a straight line and then to plot the corresponding value of T_c. The linear dependency of the load magnitude can be seen in (4.13).

$$T_b(\zeta_b) = 0.61\zeta_b - 0.013 \tag{4.13}$$

The function T_b cannot be negative, hence cyclic loading with a small magnitude $\zeta_b \leq 0.02$, will lead to a value $T_b = 0$, implying that the pile-soil interaction is reversible and no accumulation of displacements will occur. Figure 4.13 shows results for the cyclic load characteristic function. The results seem to follow a third order polynomial, see (4.14).

$$T_c(\zeta_c) = (\zeta_c + 0.63)(\zeta_c - 1)(\zeta_c - 1.64) \tag{4.14}$$

The function ensures that $\alpha = 0$ for monotonic loading, $\zeta_c = 1$. The maximum value of the function is found at $\zeta_c = -0.01$, which means that the most damaging load situation is when the monopile is loaded in a more or less pure one-way loading. When $\zeta_c \leq -0.63$, the function T_c becomes negative, which means that the accumulation of displacement is reversed and the pile moves towards its initial position.

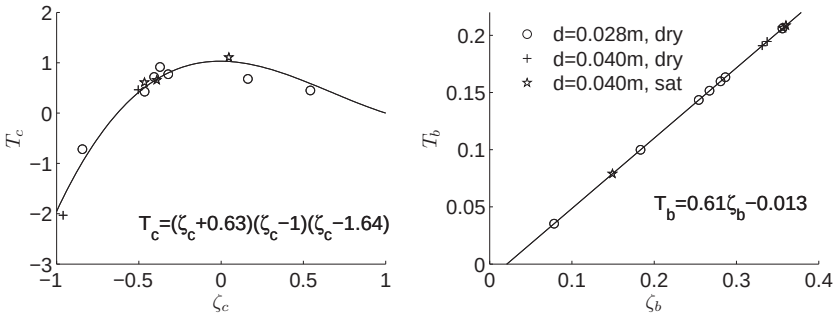

Figure 4.13*: Non-dimensional function to determine the displacement accumulation rate for a pile with a load eccentricity of $l_e = 15d$ and penetrated to $l_L = 6d$*

Since both dry and saturated conditions have been used in the tests, this shows that all tests behave as if they where fully drained and the chosen scaling approach seems valid also for quasi static cyclic loading. It can be concluded from the non-dimensional functions that the accumulation coefficient α is increasing with increasing magnitude of the cyclic loading and that the most damaging cyclic load orientation lies in the range of $-0.4 \leq \zeta_c \leq 0$. The displacement for the first cycle is easily found from a monotonic test, and only depends on the load magnitude. It is possible to estimate the displacement to a given number of cycles using (4.5) given the monotonic load-displacement curve together with the non-dimensional functions shown in (4.13) and (4.14).

4.2.3 Evolution of secant stiffness

The secant stiffness is plotted against the number of cycles in Figure 4.14. It shows that the logarithmic function seems to describe the changes in secant stiffness reasonably. The results of the logarithmic fits can also be been seen in Table 2, in Klinkvort and Hededal (2012a). The determination of the non-dimensional functions follows the same methodology as described for the displacements. The results are shown in Figure 4.15. A linear dependency of the load magnitude is found;

$$\kappa_b(\zeta_b) = 0.05\zeta_b + 0.02 \tag{4.15}$$

(4.15) implies that an increase in the cyclic load magnitude leads to an increase in the accumulation secant stiffness accumulation rate, κ . Having

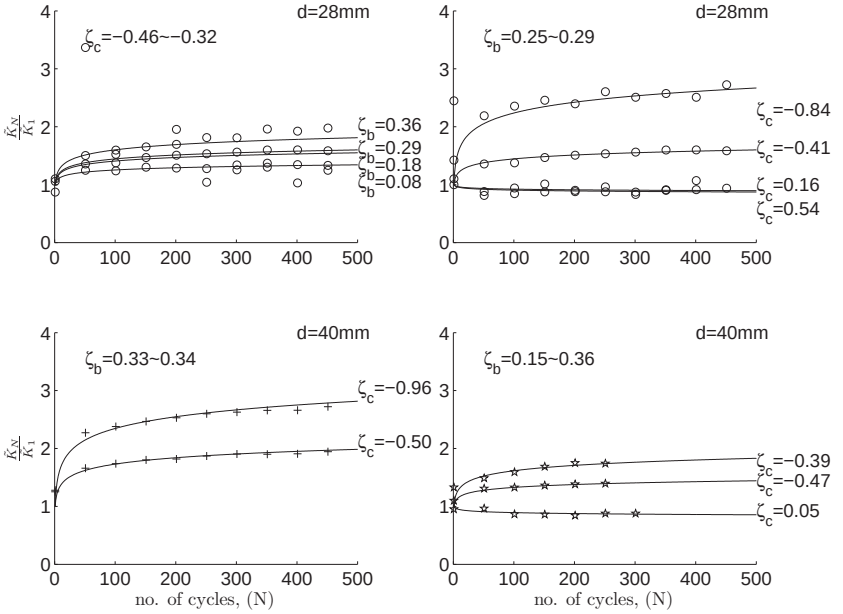

Figure 4.14*: Change in cyclic secant stiffness, under load controlled cyclic loading for a pile with a load eccentricity of $l_e = 15d$ and penetrated to $l_L = 6d$, Test no. 54-60 & 70-74*

determined κ_b, the values of κ_c are plotted and it is seen that a linear fit seems to capture the trend, see (4.16).

$$\kappa_c(\zeta_c) = -6.92\zeta_c + 1 \tag{4.16}$$

It can be seen that going from one-way to two-way loading will lead to an increasing accumulation of stiffness.

The initial cyclic secant stiffness is found by considering the results of a monotonic test and cyclic tests with varying amplitude. The function $\tilde{K}_s(\zeta_b)$ is established directly from the monotonic load-displacement curve. The function $\tilde{K}_c(\zeta_c)$ is then evaluated from the cyclic tests. The results are shown in Figure 4.16, and it can be seen that a second order polynomial describes the variation of $\tilde{K}_c(\zeta_c)$,

$$\tilde{K}_c(\zeta_c) = 1.64\zeta_c^2 + 3.27\zeta_c + 3.27 \tag{4.17}$$

From this equation, it should be recognized that the initial stiffness due to cyclic loading is stiffer than the monotonic stiffness. Depending on the

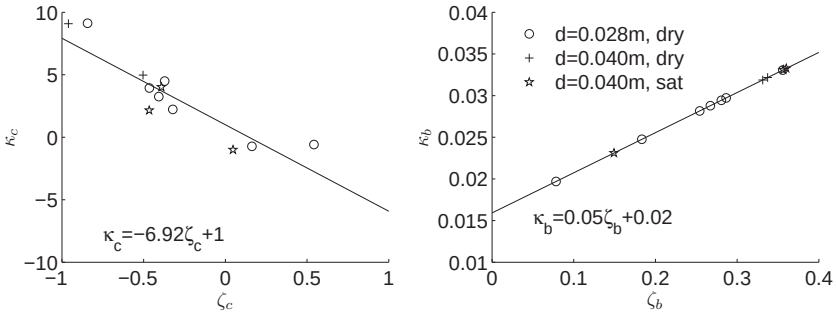

***Figure 4.15**: Non-dimensional functions to calculate the cyclic stiffness accumulation rate for a pile with a load eccentricity of $l_e = 15d$ and penetrated to $l_L = 6d$*

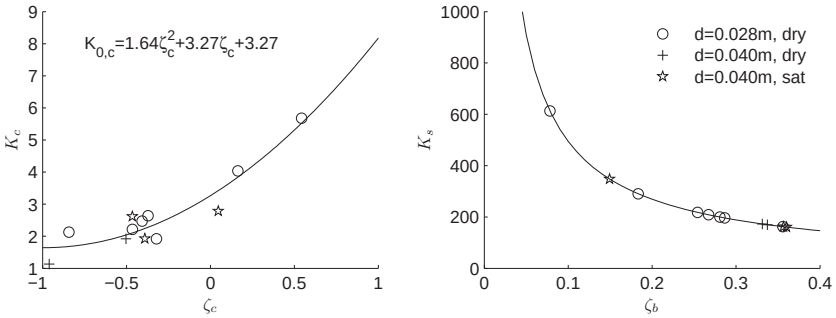

***Figure 4.16**: Non-dimensional functions to calculate the cyclic initial stiffness for a pile with a load eccentricity of $l_e = 15d$ and penetrated to $l_L = 6d$*

characteristic of the cyclic loading, the initial cyclic secant stiffness may be 2 to 8 times the monotonic secant stiffness.

4.2.4 Concluding remarks

Two key issues were investigated for the design of a monopile support for an offshore wind turbine, accumulation of displacements and the change in secant stiffness. It was clearly seen that the accumulation of displacement and secant stiffness is affected by the characteristic of the cyclic loading, and by the load amplitude.

An empirically based design procedure for a monopile installed in dense saturated sand has been given, but should only be used for drained condi-

tions. The design procedure can be applied for any load amplitude, load characteristic and number of cycles. Together with three sets of non-dimensional functions, the procedure only needs a monotonic response to be determined in order to address the accumulation of displacement and the change in stiffness. This gives a very simple design procedure, which is superior the given methodology used in the industry today.

4.3 Cyclic pile - soil interaction response

The total response from load controlled cyclic loading was documented in the previous section and a model to predict the accumulation of displacement and the change in stiffness was given. Cyclic pile - soil interaction curves were generated in order to investigate the soil resistance in more details. First four tests were performed with deformation controlled few cycles, (test no. 61-64), and force controlled test with a high number of cycles where performed afterwards (test no. 70-74).

4.3.1 Deformation controlled cyclic loading

Four deformation controlled tests were performed on the $d = 28$mm pile in order to investigate the cyclic soil resistance, (Test no. 61-64). The tests was carried out with five cycles with a maximum deformation of $Y_{max} = 0.5d$ at pile top, and then five cycles to a maximum deformation of $Y_{max} = 1.0d$. The characteristic of the cyclic loading was designed so the four test would represent different load scenarios going from pure two-way loading to a pure one-way loading. The results shown here will be from the soil layer at $z = 2d$ and the results will be plotted together with the monotonic response shown in Figure 4.2. The monotonic response from the $d = 28$mm pile will on the plot be shown as a thick dark line.

Here is only shown the result of the first tests. The observation seen in this test was general and the observation is therefore also valid for the three other cyclic load scenarios. The test was performed with a deformation controlled loading of five cycles each loaded to $0.5d$ two-way and then five cycles with deformation of $1.0d$ two-way, (Test no. 61). This is equivalent to the non-dimensional cyclic parameter $\zeta_c = -1$. The test result can be seen in Figure 4.17. It can be seen that the first loading of the pile follows the results from the monotonic test, which is here called virgin loading. When the load is reversed, an elastic unloading of the pile is seen. This is followed by a small plateau where the load is more or less constant followed by an increase in resistance until the response seems to follow the opposite virgin

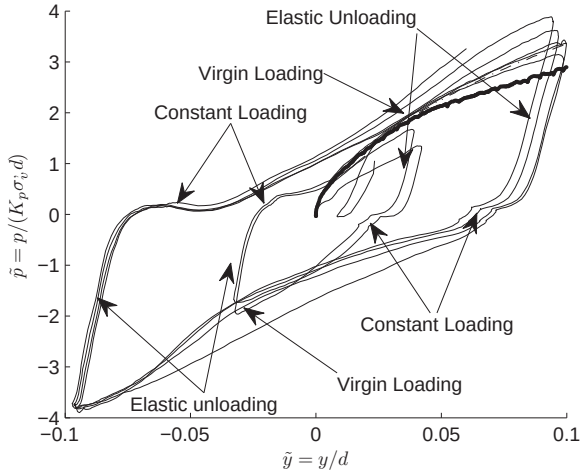

***Figure 4.17**: Cyclic non-dimensional p-y curves $\zeta_c = -1$, $z = 2d$, Test no. 61*

curve again. When the load is reversed again an elastic unloading followed by a plateau is again seen. This behavior seems to be identical for all of the five cycles. It can also be seen that the soil resistance increases due to cyclic loading.

4.3.2 Force controlled cyclic loading

Force controlled cyclic loading was applied to the $d = 40mm$ pile and the cyclic pile - soil interaction was observed for six soil depths. The loading magnitude applied to these piles is much smaller than the previous deformation controlled tests, the cyclic loading was carried out at a maximum cyclic load level of approximately 35% of the monotonic capacity, corresponding to the serviceability loading of a offshore wind turbine. Two tests are shown here to demonstrate some general observations.

Cyclic interaction curves $\zeta_c \approx -1$

Interaction curves are presented from six depths and the interaction between soil resistance and depths can be seen. The two-way loading test is shown in Figure 4.18, (Test nr 71). The force control allows the pile to accumulate displacements/rotations. The pile - soil interaction curves from the first three cycles and after 1000 cycles are shown in Figure 4.18. It can be seen that

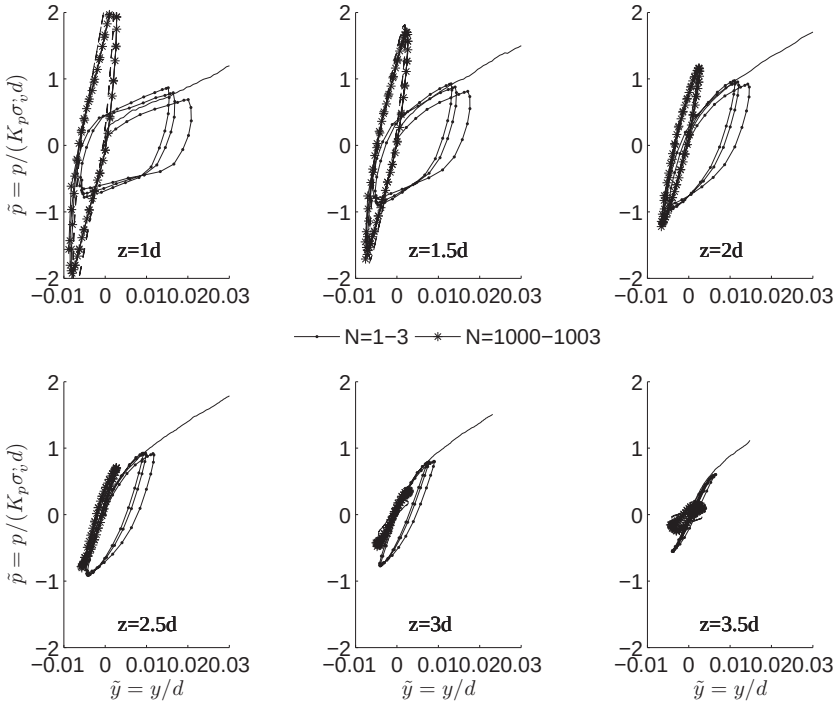

Figure 4.18*: Non-dimensional pile - soil interaction curves from cyclic two-way loading, $\zeta_c = -1$. Test pile dimensions; $d = 40mm$, $l_e = 15d$, $l_L = 6d$ and $N_s = 75$ installed in dry sand, Test no. 71*

mean displacement of each cycle moves backwards, this was also the case for the total response. It can also be seen that no degradation of the sand is occurring due to the cyclic loading. The capacity is increasing due to densification. The load carrying soil pressure is shifting so the soil in the upper parts are carrying more and more and the soil resistance mobilization in the lower layers is therefore decreasing. There is a large hysteretic behavior in the three top layers whereas the lower layers is showing a more linear and elastic behavior.

Cyclic interaction curves $\zeta_c \approx -0.5$

The semi two-way loading test is shown in Figure 4.19, (Test no. 70). Cycles between 1-3, 1000-1003 and 10,000-10,003 are here shown. Again, it can be

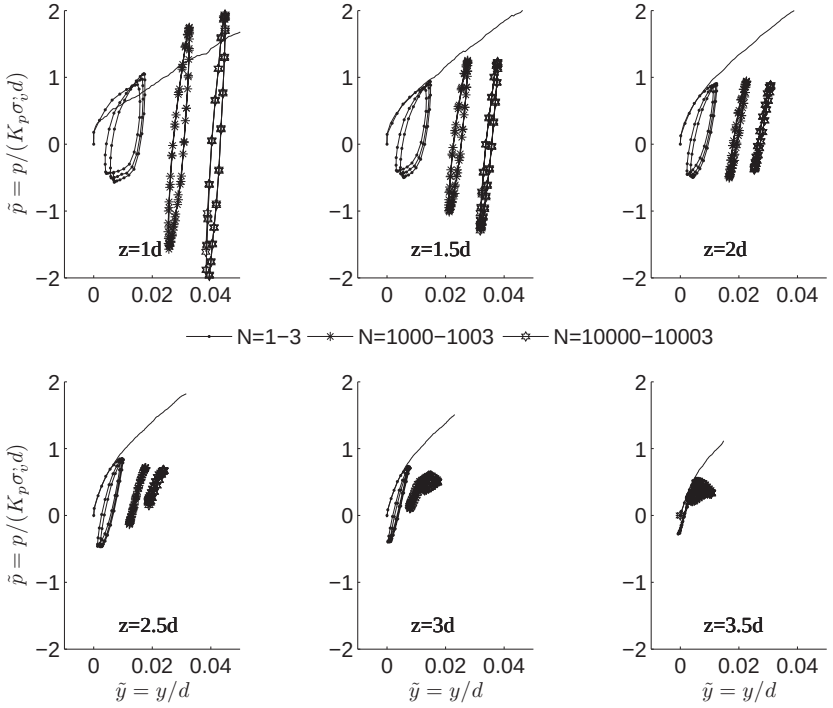

Figure 4.19*: Non-dimensional pile -soil interaction curves from cyclic semi two-way loading* $\zeta_c = -0.5$*. Test pile dimensions;* $d = 40mm$*,* $l_e = 15d$*,* $l_L = 6d$ *and* $N_s = 75$ *installed in dry sand, Test no. 70*

seen that the pile starts to accumulate displacements. The pile was subjected to 10.000 of cycles and accumulation of displacements and hysteric behaviour was still seen for the top layers. Comparing the cyclic interaction curves with the monotonic response, it can be seen that the maximum soil resistance seems to follow the virgin curve. The capacity in the top soil layer is increasing. This rearranges the soil resistance and the layers in the bottom do not have to mobilize soil resistance in the same degree.

4.3.3 General observations

It was seen from all of the tests that the virgin loading was following the monotonic test results. It was also observed that the cyclic capacity due to the cyclic loading always was the same or a bit above the monotonic response,

this was also seen on the total response in Klinkvort et al. (2010). From this it is concluded that the monotonic response on the safe side can be used as yield surface while the soil resistance in a given point is controlled by its displacement. It can be seen from all the tests, that the cyclic loading approaches a mean value where the cycles are symmetric around, and also hysteresis is seen in all cycles. The unloading is always linear and the stiffness is always much stiffer compared to the initial stiffness of the virgin curve when the pile is unloaded. The remobilisation of soil pressure after elastic unloading also seems stiffer than the initial virgin curve.

It was seen from the load controlled tests, that the displacement and the stiffness of the pile is strongly affected by the load situation. The pile displacement moves towards its original position for a two-way loading situation, whereas displacements accumulate for a one-way load situation. Hysteresis was seen from both of the test. This was also the case for the test (Test no. 74) with a maximum cyclic load of only 15 % of the capacity.

4.4 Summary of pile - soil interaction results

37 tests have been performed in order to investigate the pile soil interaction. This has been done for both the total and the pile - soil interaction responses. From the monotonic and cyclic centrifuge tests different conclusions can be drawn and are here listed:

1. The use of Rankines passive earth pressure coefficient as a normalization parameter was also seen to merge the pile-soil interaction curves into one set of generic curves.

2. No effect on the earth pressure coefficient K from load eccentricity.

3. Centrifuge and Finite element calculations shows responses in same order of magnitude but initial stiffness and capacity is different.

4. The method proposed by API (2007) was not capable to predict the monotonic centrifuge results in a sufficient degree.

5. A new formulation of the pile - soil interaction was proposed using the shape by Kondner (1963) and a re-calibration of the empirical factor A.

6. The change of displacements and secant stiffness is affected of the characteristic, the magnitude and the number of the cyclic loading

7. For the total cyclic response, a new prediction model based on the centrifuge results was proposed.

8. For the local pile - soil interaction response, four basic behaviors were identified; Virgin loading, elastic unloading, constant loading and that the cycles seems to adjust around a mean value.

Chapter 5

Pile - soil interaction model

The observations from the centrifuge experiments are used to develop a spring element for cyclic pile-soil interaction. The spring element is used in an algorithm based on the finite element framework FemLab, (Hededal and Krenk, 1995). The model is a Winkler model where the pile is modelled as beams and the soil as a system of uncoupled non-linear cyclic springs. The response of the pile subjected to cyclic loads can then be investigated using this model. Additionally a time integration algorithm was implemented in the FemLab framework based on the generalized α method to take the dynamic loading into account (Chung and Hulbert, 1993; Krenk, 1999). Here the total soil - pile - turbine interaction can be investigated; the main purpose of this model is to demonstrate how hysteretic damping can be introduced to the system using the cyclic spring formulation.

5.1 Cyclic pile - soil interaction spring

In seismic engineering, different kinds of cyclic pile - soil interaction formulations have been proposed. An elasto-plastic model proposed by Boulanger et al. (1999), based on a two component set-up in which the loading response is handled by a series connection of springs - one spring handling loading (passive failure mode). Another spring is handling the unloading-reloading properties while it is gradually creating a gap behind the pile. Taciroglu et al. (2006) further developed these ideas and proposed an element consisting of three components; leading-face element, rear-face element and drag-element. The two face-elements are formulated in terms of elasto-plastic springs supplemented with a tension cut-off. The drag element controls the side friction, when the pile is moving inside a cavity during unloading. In contrast to the two models by Boulanger et al. (1999) and Taciroglu et al. (2006), a model is

here presented where the cyclic pile - soil interaction is incorporated into one single spring element. This simplifies the implementation into a standard finite element code. Furthermore, the formulation is based on observation from rigid pile tests, which makes it more suitable for monopiles supporting wind turbines.

From the cyclic tests, basis observations of the cyclic pile - soil interaction was seen. The test $\zeta_c = -0.5$ is shown in Figure 5.1, (Test no. 62). Three types of lines are drawn on top of the result order to show the physics of the spring model. The model consists of 3 parts, shown on the Figure 5.1

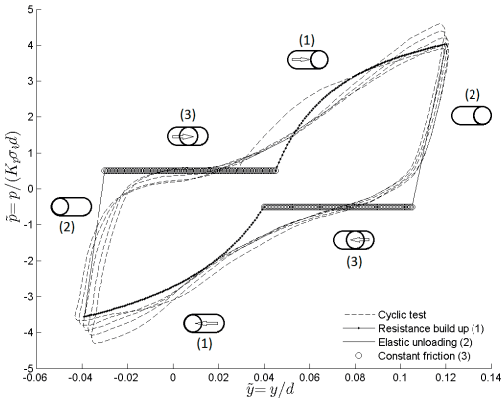

***Figure 5.1**: Cyclic non-dimensional p-y curves, test no. 62*

as (1), (2) and (3). Firstly, a loading phase is seen in which the resistance is building up. Here the pile is pushing the soil and creating a gap behind the pile (1). Secondly, an unloading phase that is more or less linear is seen, and is therefore designed as elastic unloading (2). Finally, a phase where the pile moves towards the initial position in the cavity created behind the pile during initial loading (3). In this phase, it may be assumed that a drag or friction along the side of the pile exists. For a fine-grained soil the gap can be assumed to develop between the two extreme points of the pile movements, this was also the assumption in Hededal and Klinkvort (2010). El Naggar et al. (2005) assumes that this the gap will develop for fine-grained soils, whereas for coarse-grained soils, the soil will cave in and close the gap. From the centrifuge tests, it can be argued that a mechanism in between these two extremes occurs. The sand will fall back, but it will not fill the gap totally. It was also seen from the tests that the soil-pile interaction curves

were symmetrical around the mean value of the two extremes. In this model, the pile will move in the cap until reaching the mean of the two extremes, here the soil resistance starts to build up again.

In order to handle the observation seen in the centrifuge tests, the formulation presented in Hededal and Klinkvort (2010) is here modified. The modified model is basically identical to the model presented in Hededal and Klinkvort (2010), but here change with a new hardening model. This was chose in order to mimic the behaviour seen in the centrifuge experiments in a better way.

Spring behavior

The current yield strength is divided into two parts; one relating the drag contribution, when the pile is moving in the cavity, and one relating the soil resistance build up while the pile is pushing against the soil face.

$$p_u(y*) = p_u^{drag} + p_u^{face}(y*) \tag{5.1}$$

The term p_u^{drag} is the drag capacity, assumed constant here, when the pile is moving in the gap. Below this value the the spring is assumed to be elastic. The second term p_u^{face} is the soil resistance build up, when the pile is in contact with the sand and pushing the face. When there is no contact, the term is zero. A schematic drawing of the model can be seen in Figure 5.2. Here a schematic representation of a cyclic curve is shown together with definitions.

Here is introduced a corrected displacement ($y*$) given as the difference between the current displacement y and the hardening parameter (α). This is done in order to capture the cyclic behavior around a mean value as seen in the experiments.

$$y* = y - \alpha \tag{5.2}$$

The hardening parameter α is given as the mean of the maximum and minimum plastic displacements as shown in Figure 5.2:

$$\alpha = \frac{y_{p,max} + y_{p,min}}{2} \tag{5.3}$$

The additional soil resistance for the face element can then be written as:

$$p_u^{face}(y*) = S(p_i)S(y* - y_{k,i})p_u^{Kondner}(y*) \tag{5.4}$$

The control of the contact is done by introducing the step function, $S(x)$. An approximation of the heavyside step function is used to control if the

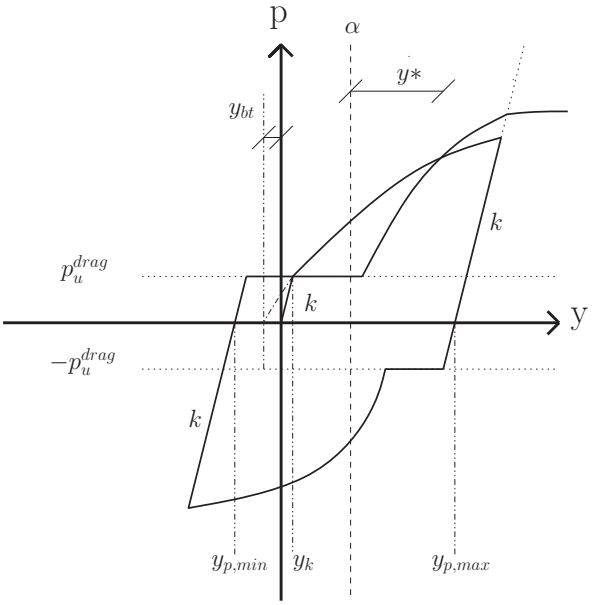

***Figure 5.2**: Schematic drawing of the spring element*

face element is zero or whether resistance is building up. The formula for the approximation can be seen in equation (5.5).

$$S(x) = \frac{1}{1 + e^{-2 \cdot \beta x}} \tag{5.5}$$

The step function is zero when $x < 0$, one half when $x = 0$ and one when $x > 0$. The constant β defines the change from zero to one in the approximation. High β values gives an abrupt change, whereas a smaller value will give a smoother transition from zero to one. A good approximation of the Heaviside function has been prioritised here, and a value of $\beta = 1,000,000$ is used. The values used in the step function are then given as:

$$\begin{array}{llll} p_1 = p & \& & y_{k,1} = y_k & \text{for} \quad y* > 0 \\ p_2 = -p & \& & y_{k,2} = -y_k & \text{for} \quad y* < 0 \end{array} \tag{5.6}$$

And the step functions are written as:

$$\begin{aligned} S(p_i) &= \frac{1}{1 + e^{-2 \cdot \beta p_i}} \\ S(y* - y_{k,i}) &= \frac{1}{1 + e^{-2 \cdot \beta (y* - y_{k,i})}} \end{aligned} \tag{5.7}$$

From the static centrifuge tests, it was seen that the monotonic response seems to follow the hyperbolic relationship proposed by Kondner (1963) using a modified value of A, (4.2). This observation is used to describe the virgin curve in the model.

$$p_u^{virgin} = \frac{y}{\frac{1}{E_{py}} + \frac{y}{p_{ult}}} \tag{5.8}$$

In order to implement this relationship into the framework, the resistance is split into a drag contribution and a face loading contribution.

$$p_u(y*) = p_u^{drag} + p_u^{face}(y*) \tag{5.9}$$

The drag contribution is a constant value and is defined as an input parameter. The face element should follow the virgin curve, when the element is loaded for the first time ($y_{p,min} = 0$). The displacement y for virgin loading can then be defined from (5.2) and (5.3) as:

$$\begin{aligned} y* &= y - \alpha = y - \frac{1}{2}(y - \frac{p}{k}) \\ 2y* &= 2y - y + \frac{p}{k} \\ y &= 2y* - \frac{p}{k} \end{aligned} \tag{5.10}$$

It can be seen from Figure 5.2 that the virgin curve has an artificial starting point and this distance has to be added to the displacement in order to capture virgin curve seen from the experiments. The displacement used in the Kondner (1963) formulation is therefore written as:

$$y = 2y* - \frac{p}{k} + y_{bt} \tag{5.11}$$

The artificial starting point is calculated as:

$$y_{bt} = \frac{p_u^{drag}}{E_{py} \cdot (1 - \frac{p_u^{drag}}{p_{ult}})} - \frac{p_u^{drag}}{k} \tag{5.12}$$

This is used, together with the virgin curve model found from the monotonic test shown in (2.14) and (1.1). Remembering to take the drag contribution into account, the face element is then defined as:

$$p_u^{virgin}(y*) = \frac{2y* - \frac{p}{k} + y_{bt}}{\frac{1}{E_{py}} + \frac{2y* - \frac{p}{k} + y_{bt}}{p_{ult}}} - p_u^{drag} \tag{5.13}$$

The cyclic pile-soil interaction spring element can then be defined. The only extra input parameter, compared to the monotonic calculation, is the extent of the drag contribution and the elastic loading-unloading stiffness. The formulation used here is not a strict elasto-plastic model, because the model can build up soil pressure without any hardening. This discrepancy is chosen in order to represent the observations seen in the experiment.

A schematic drawing of the spring element behavior is shown in Figure 5.3. The element will follow the virgin curve for the first time it is loaded,

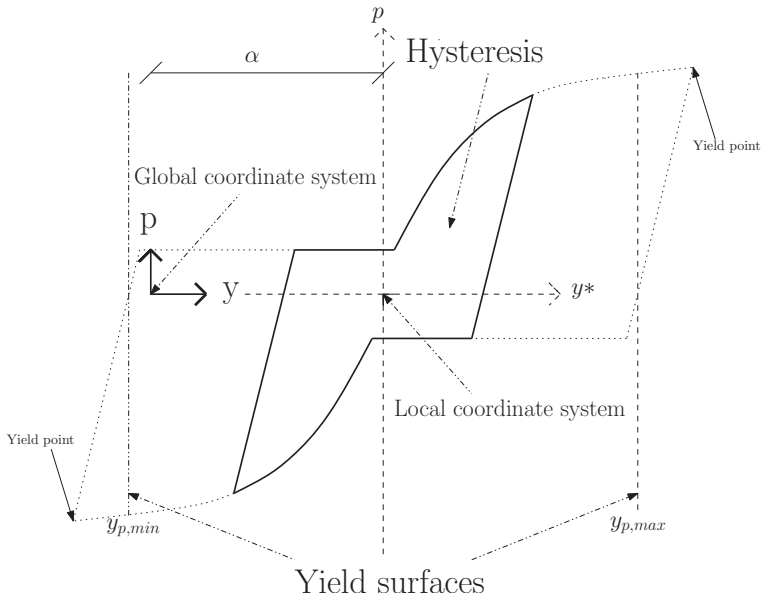

***Figure 5.3**: Schematic demonstration of the cyclic spring*

as seen in the monotonic tests. Subsequently, the element "pushes" the yield surface and the hardening parameter is activated. When the element is working "inside" the yield surface, the element is symmetrical around a local coordinate system, as shown in Figure 5.3. The hysteretic behavior can then develop without any hardening. When the element "pushes" to the yield point again, the increase in soil pressure will again follow the virgin curve, but with a displaced initial starting position.

There are two special phenomena described by this model, both of which are important to appreciate; firstly, even though the element is moving inside the yield surface, the pile - soil response will follow a hysteretic path. Secondly, the soil resistance can also be larger than that defined by the virgin

curve, but never larger than the ultimate capacity.

5.1.1 Calibration and demonstration of response

The cyclic spring model has four input parameters, elastic stiffness k, initial stiffness of the virgin curve E_{py}, maximum capacity p_u and friction capacity p_u^{drag}. The stiffness of the virgin curve and the maximum capacity can be found using e.g. the recommendation from API (2007). It was seen from the cyclic tests that the friction capacity was in the range of 10% of the maximum capacity, whereby $p_u^{drag} = 0.1 \cdot p_u$ is adopted here. The elastic unloading stiffness was seen to be approximately 5 times stiffer than the virgin curve, and so it is assigned $k = 5 \cdot E_{py}^{model}$ in this case. The cyclic interaction model can then be established with the same input parameters as a monotonic calculation.

The response of the spring model is compared with results from the four deformation controlled centrifuge tests, (Test nr 61-64), to demonstrate the performance of the cyclic spring in Figure 5.4. As described above, two different stiffness are defined by the model. The stiffness of the virgin curve is reduced to 60% of the initial stiffness found from monotonic tests, $E_{py}^{model} = 0.6 \cdot E_{py}^{test}$. This is carried out in order to follow the virgin curve seen in the centrifuge tests. The virgin curve of the model seems to reproduce the monotonic test results quite well with this reduction. The elastic unloading also seems to predict the test results with a high degree of accuracy for all of the tests.

The model assumes that a representative friction term remains constant, and it can be seen from the test results that accuracy is acceptable, but that this assumption is probably too simplistic. The model performs well for the three first load scenarios, but for the last load scenario, shown in the low right corner (D) in Figure 5.4, the model predicts a stiffer reloading response and significant hysteresis that was not measured. In general, the model seems to represent the key observations seen from the centrifuge tests at element level.

The pile - soil interaction spring is implemented in a cyclic quasi-static finite element analysis to compare the pile - soil interaction model with a cyclic centrifuge experiment. The pile is modelled as a solid steel pile with a diameter of $d = 3$m, load eccentricity of $l_e = 15d = 45$m and a penetration of $l_L = 6d = 18$m. The soil is uniform sand with a relative density of $I_D = 0.9$. The corresponding angle of friction is calculated using the expression by Bolton (1986) presented in (3.15). There is full similarity between the non-dimensional ratios in centrifuge and numerical models. The stiffness of the monotonic response was found to be $\tilde{E}_{py}/K_p = 100$, whereas the stiffness

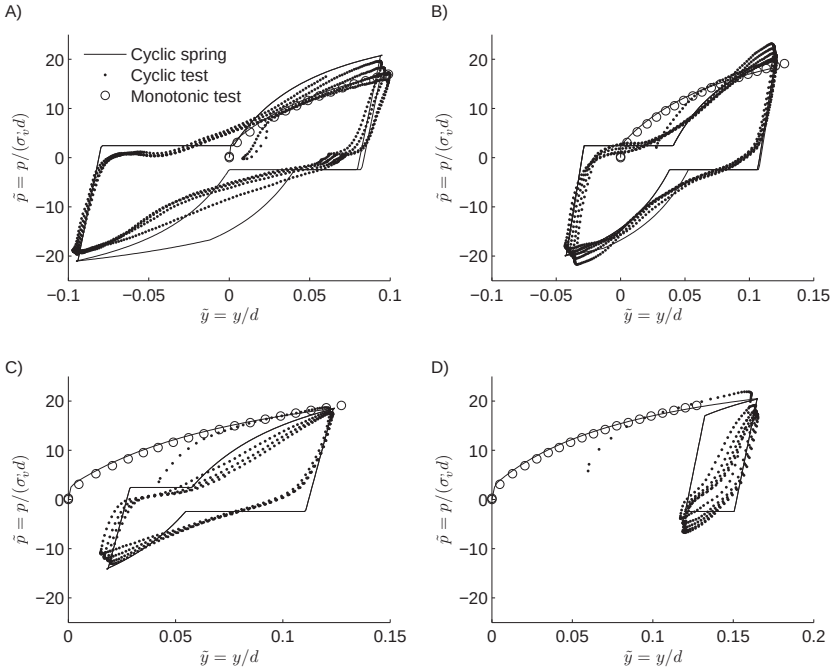

***Figure 5.4**: Demonstration of the cyclic spring, d=3.2m & z=2d & $\phi = 42^o$, Test no. 61-64*

of the virgin curve and the elastic unloading reloading stiffness was described above. It was observed in the centrifuge tests that the overall displacements and secant stiffness were changing due to cyclic loading, and were dependent on the characteristics of the loading perturbation and the number of cycles. Furthermore, the effect from number of cycles is not reproduced very accurately by the numerical model, so that only data for the first couple of cycles are shown here in the first instance.

One simulation has been carried out to demonstrate the response of the model, and the findings are compared with the centrifuge results in test no. 71. The simulation was carried out with five load controlled cycles corresponding to test no. 71. The total response of the first couple of cycles is shown in Figure 5.5. It can be seen here that the model follows the virgin curve with a high degree of accuracy. When the load is reversed, the model shows a much softer response than was seen in the tests. It should be remembered that the deflection in the tests is measured with a mechanical

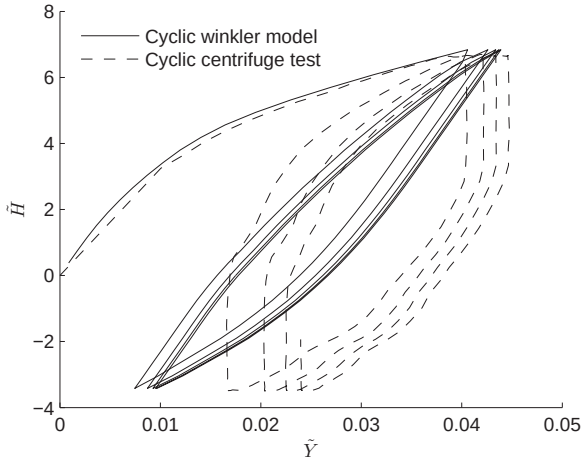

Figure 5.5*: Comparison between the results obtained from the centrifuge test and the Winkler model with the cyclic spring, for the overall response. Test no. 71*

potentiometer. If there is just a small clearance in the contact between the pile and the potentiometer, this will record less displacement and imply an unloading phase that is stiffer than reality. The small increase in deflection after load reversal indicates this. At the end of the half cycle, the model underpredicts the displacement slightly, and yet the response seems to be simulated to an acceptable degree. The hysteresis seen in the centrifuge test is larger than the predicted by the model simulation. This shows that the model will underestimate the damping in the soil.

The pile - soil interaction curves previously shown in Figure 4.19 is re-plotted, together with the results from the numerical simulation, and shown in Figure 5.6. A good simulation of the pile - soil interaction is seen in the six depths representing the soil layers. It is seen that the cyclic spring element does not change, due to number of cycles, to the same degree as seen in the centrifuge tests. The hysteresis measured in the tests changes shape due to the increase in capacity of the sand, and the response is also getting stiffer. A qualitative assessment indicates that the hysteresis loops maintain an area that is approximately constant.

The prediction of the accumulation of displacement and the change in secant stiffness is not modelled sufficiently accurately by the cyclic model. It is therefore recommended to use the total response model for the total response in order to address accumulation of displacements.

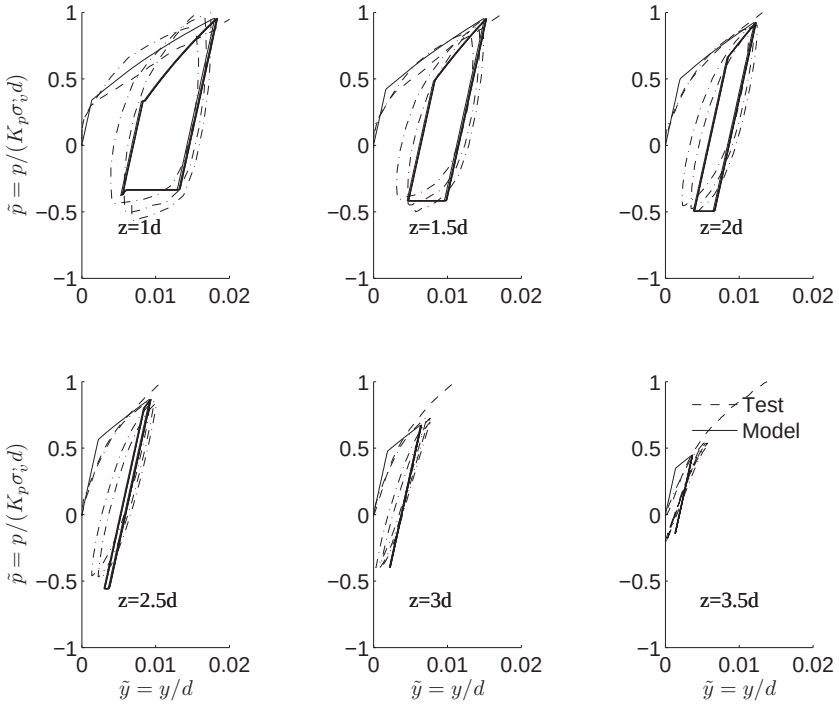

***Figure 5.6**: Comparison of the centrifuge test and Winkler model with the cyclic spring, for the local response. Test no. 71*

5.2 Dynamic model

The cyclic spring represents the hysteretic behaviour seen in the centrifuge experiments, shown in Figure 5.4 and 5.6. The hysteretic behaviour represents friction damping in the soil, and this parameter can be very difficult to access. To give an estimate of the soil damping in the sand, the finite element framework FemLab was extended with a time integration scheme.

The time integration scheme uses the generalized α procedure, described in e.g. Krenk (1999) and Krenk (2009). Both the acceleration and the force term are formed by weighted means between t_n and t_{n+1}, Chung and Hulbert (1993) in this methodology. The basis of the α procedure is the Newmark (1959) formulation, which uses a γ and a β for forward weighting. The generalized α method introduces two additional parameters α_m and α_f. The parameter α_m describes the relative weight of the old inertia term, and the

parameter α_f describes the relative weight of the old force term. The values of these parameters have been taken as $\alpha_m = \alpha_f = \gamma = 1/2$ and $\beta = 1/4$ for the dynamic calculations presented in this thesis.

The foundation, structure and wind turbine are modelled as a beam and the cyclic spring formulation is used for the soil. A simple model of a Horns Rev wind turbine is used, Figure 5.7, with a sketch of the simplification presented in Figure 5.8. The pile is penetrated $24m$ into the sand and the

***Figure 5.7**: Photo of the Horns rev wind turbine*

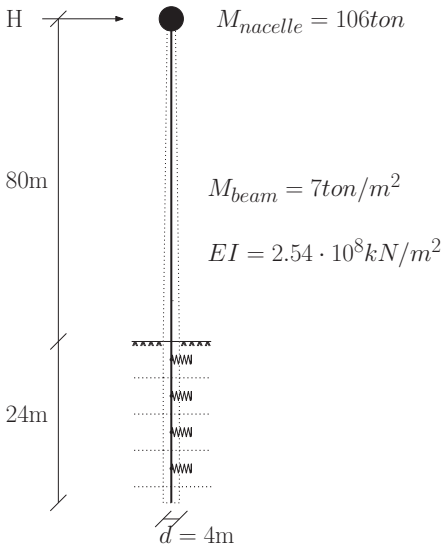

***Figure 5.8**: Sketch of numerical model*

structure above is modelled as a beam with a constant cross section, and thereby also constant mass distribution and stiffness. The nacelle is located $80m$ above the sand surface and has a weight of $106ton$. The stiffness and masses correspond with the values reported by Augustesen et al. (2009). The structure above the sand surface is modelled as 40 Bernoulli Euler beam elements with a distributed mass. The structure under sand surface is modelled as 24 Bernoulli Euler beam elements with a distributed mass and a spring is attached at each node in the soil.

5.2.1 Validation of dynamic model

The general α procedure introduces some beneficial numerical high frequency damping into the model. A free decay test was performed with springs set

to respond only elastically to investigate the numerical damping in the algorithm. No viscous damping is applied the model and the numerical damping is therefore the only damping contribution in this case.

The free vibration of the first mode of the model shown in Figure 5.8 can also be treated as a single degree of freedom (SDOF) system. The displacement response of the nacelle is therefore compared to the analytical solution of a single degree of freedom system. The free response of an undamped single degree of freedom system can be given as:

$$\ddot{x} + \omega_o^2 x = 0 \tag{5.14}$$

The homogeneous solution to the free oscillations, Chopra (2007) is given entirely in terms of the initial conditions as:

$$\begin{aligned} x &= x_0 \cos(\omega_0 t) + \dot{x}\omega_o^{-1} \sin(\omega_0 t) \\ \dot{x} &= -x_0\omega_0 \sin(\omega_0 t) + \dot{x} \cos(\omega_0 t) \end{aligned} \tag{5.15}$$

The solution given in (5.15) is calculated entirely in terms of the initial conditions. The solution to the undamped vibration therefore only needs the natural angular frequency and the initial displacement and velocity as input parameters. The initial Eigen frequency of the combined soil - monopile - turbine structure was determined by solving the Eigen value problem of the multi degree of freedom (MDOF) system, and the first natural Eigen frequency was found to $f = 0.37Hz$. This places the structure in the soft-stiff region with a first Eigen frequency between 1P and 3P as shown in Figure 1.4. This is used as an input parameter in the calculation of the SDOF system, together with the displacement at the point where the force is removed. At this point, the loading is very slow and the velocity of the displacements is set as zero. Elastic springs was used in this analysis and the results are shown in Figure 5.9. The force is applied in steps and reaches a maximum after 10 seconds, at this time the force is removed and the structure is free to vibrate. The applied load and the displacement of the nacelle is shown in Figure 5.9. The the MDOF and SDOF simulations give identical responses, which validate the dynamic FE model and confirm that the numerical high frequency damping is negligible for the first vibration mode.

5.2.2 Estimation of soil damping

In the fatigue analysis of a wind turbine damping plays a huge role and is often critical for offshore wind turbines, Andersen et al. (2012). The fatigue analysis is carried out using an aero elastic code (e.g. Flex5 - Øye (1996) or HAWK2 - Larsen and Hansen (2007)) where soil damping often is introduced

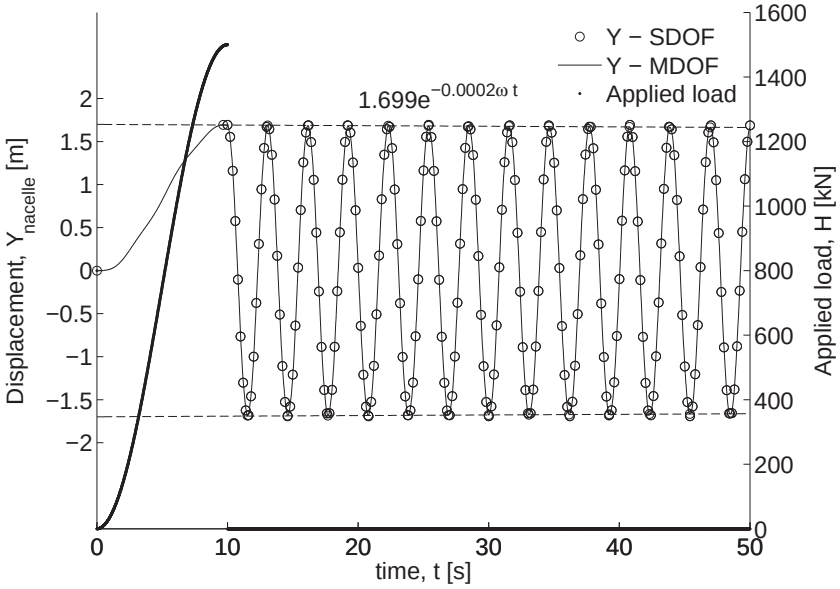

***Figure 5.9**: Free decay modelling of Horns Rev 2 wind turbine with elastic springs, the response at nacelle is showed together with the applied load*

as viscous damping. Soil damping consists of two parts; one from radiation viscous damping and one from friction in the soil. For sand the main damping contribution is from friction, Bolton and Wilson (1990). The soil damping is difficult to access, but several studies shows that the soil damping is higher than expected, e.g. Tarp-Johansen et al. (2009); Versteijlen et al. (2011); Devriendt et al. (2012).

A series of free decay tests have been simulated to demonstrate how the pile - soil interaction spring element introduces soil damping to the entire wind turbine structure. Soil properties are adopted that represent the behaviour of the sand used in the centrifuge. Input parameters for the cyclic spring element are found as described above. An initial subgrade modulus, as proposed by API (2007), and derived from in Figure 2.3 as $k = 40000kN/m^2$ was adopted for a sand with a relative density of $D_r = 0.9$.

In total, 6 simulations were carried out. The response from the test where the pile is loaded to 1500kN, and released afterwards to vibrate, can be seen in Figure 5.10.

The displacement at the first cycle and the displacement after ten cycles

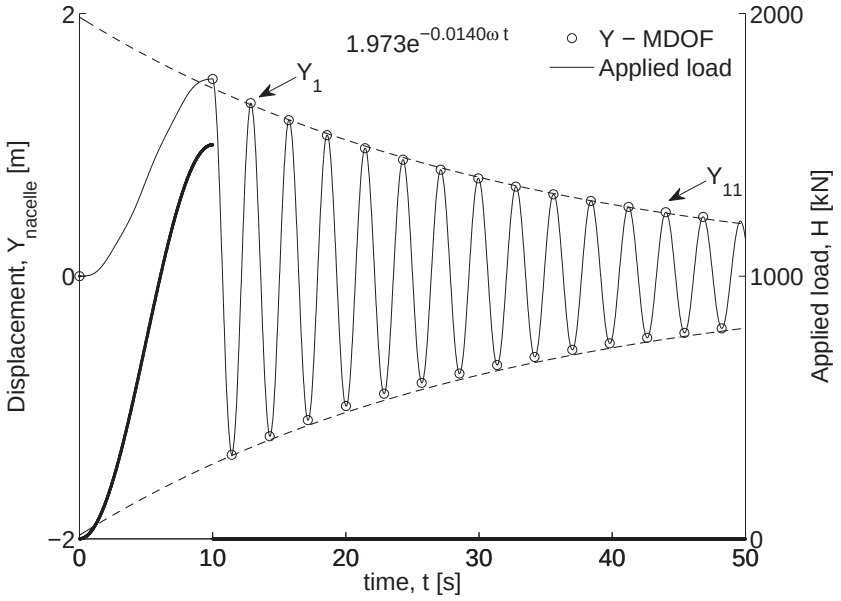

***Figure 5.10**: Free decay modelling of Horns Rev 2 wind turbine*

is used to calculate a mean logarithmic decrement to estimate the damping of the first mode. This is done as:

$$\delta = \frac{1}{10} ln \left(\frac{Y_1}{Y_{1+10}} \right) \tag{5.16}$$

It can be seen clearly from the figure that the displacement is decreasing due to the damping. The results from the six tests are shown in Table 5.1. From Table 5.1 it can be seen that the response from the simulation with elastic springs shown in Figure 5.9 has a small amount of numerical damping 0.06%. This is so small that it is negligible. It is also clearly seen that, that the damping is dependent on the size of the displacements. Large displacements lead to greater damping and small displacements cause less damping. This is not a surprise and confirms that it is too simple to assume constant damping in the soil.

The results from Table 5.1 are shown in Figure 5.11. It is seen that the damping decrement can be estimated using a logarithmic function and the pile displacement at sand surface. This model can be used to estimate the

***Table 5.1**: Logarithmic decrement from free decay simulations*

P_{max} $[kN]$	Y_{max} $[m]$	$y_{surface}$ $[m]$	element $[-]$	Y_1 $[m]$	Y_{11} $[m]$	δ $[\%]$
1500	1.6990	0.0668	elastic	1.4095	1.4015	0.06
1500	1.4932	0.0386	cyclic	1.3228	0.5741	8.3
1000	0.9790	0.0233	cyclic	0.8765	0.4026	7.8
500	0.4768	0.0098	cyclic	0.4355	0.2309	6.3
250	0.2330	0.0041	cyclic	0.2194	0.1434	4.3
125	0.1146	0.0018	cyclic	0.1118	0.0933	1.8

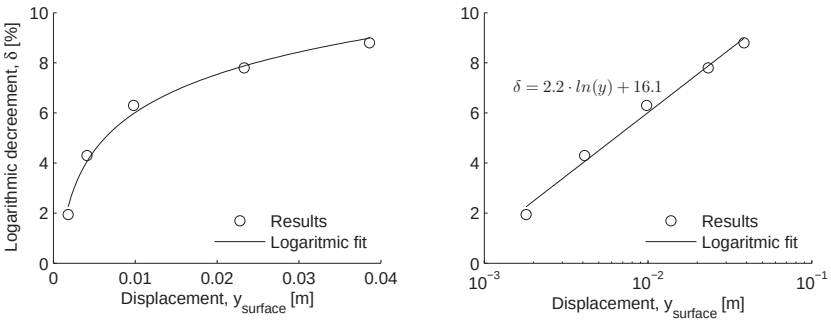

***Figure 5.11**: Logarithmic decrement as a function of displacement*

equivalent viscous damping for the first mode which can be adopted in the wind turbine calculation in the aero elastic code.

The optimal solution is to implement the cyclic spring directly in an aero elastic code. Then the friction based damping is introduced in a more realistic way.

5.3 Summary of pile - soil interaction model

A cyclic spring element has been developed and implemented in a quasi-static cyclic code and also in a dynamic code. The spring element has been calibrated against both deformation controlled and load controlled tests. In the dynamic code, the element has been used to estimate the soil damping that arises from friction. Different conclusions can be drawn from calibration and the subsequent demonstration of the performance of the spring element, and these are listed below:

1. The cyclic spring element only needs 4 parameters, which are reduced to two with the current calibration.

2. The cyclic spring element represents the initial hysteresis seen in centrifuge experiments.

3. The change of secant stiffness and accumulation of displacement from the number of cycles is not modelled with sufficient accuracy.

4. In a dynamic analysis, the element can be used to estimate the soil damping

Chapter 6

Discussion

Offshore monopiles are situated in saturated soil conditions. The centrifuge test series was primarily carried out in dry dense sand. Choosing an effective stress scaling approach enables piles installed under saturated conditions to be modelled using dry sand. This was demonstrated by four monotonic tests. A direct comparison between cyclic tests performed in dry and saturated conditions was not carried out, but no difference was registered when inspecting the non-dimensional functions derived from testing in dry and saturated conditions. The scaling approach therefore seems valid. It is important to recognize that the results only are valid for drained loading conditions. Testing in water saturated sand does not represent full-scale drainage, which means that the water flow in the centrifuge setup is occurring η times faster compared to the prototype and it is therefore unlikely that pore pressures can build up at the current rate of loading. The possible accumulation of pore pressure therefore has to be studied in more detail.

6.1 Monotonic loading

The initial stiffness and the maximum bearing capacity are important design parameters in the design of a monopile supporting an offshore wind turbine for a monotonic load situation. The design methodology used today relies on empirical tests on slender piles. Pile - soil interaction curves were deduced from these tests and are also used today for large diameter, stiff monopiles. The validity of the extrapolation of these curves seems to lack scientific justification.

The diameter effect has only been investigated in the centrifuge scale, and here no diameter effect was seen. The diameter effect in prototype scale cannot be investigated in a centrifuge experiment, simply because this type

of experiment uses a scaled down model. A possible effect from using large diameter piles can only be investigated using prototype dimensions. In a given situation where full-scale tests have to be compared, it is important to achieve full similarity between the tests.

Not only the diameter, but also the stress levels are increased in full-scale tests on large diameter laterally loaded monopiles, compared to the original tests. Five centrifuge tests were performed on one model monopile subjected to increasing stress levels. It was clearly seen from the tests that by taking the stress dependent soil behaviour into account with a simple normalization, the stress level did not affect the normalized response. The normalized result from one centrifuge test can then be compared to a pile with any given diameter. The effect from both diameter and stress level can be decoupled using the proposed normalization, and a possible diameter effect can then be investigated in a full-scale test.

Normalized pile - soil interaction curves from centrifuge tests with different load eccentricities were also compared, and the results from the tests showed a high degree of similarity, regardless of the load eccentricity. It was therefore possible to relate all of the different tests to one generic pile - soil interaction model, no matter the load eccentricity. It therefore seems like the change in bending moment to shear force ratio does not affect the pile - soil interaction.

6.1.1 Initial stiffness

There is a wide consensus that the stiffness of sand found in a triaxial test can be described by a power law. This was also seen in (3.16). As a first approximation, it is therefore also natural to try to convert the observation seen in the triaxial test to the pile - soil interaction. The linear increase of the initial stiffness in the model seems too simple from this perspective and should instead follow the power law seen in the triaxial test. This has also been tried in this thesis, but no correlation between triaxial and centrifuge results could be given. It is hard to identify the exact reason why a disagreement between triaxial tests and the results from the centrifuge exists, but it is likely to be related to difference in initial stress states, future stress paths and other issues linking to the various assumptions and more complex pile - soil interaction issues.

It is proposed in this thesis to calculate the initial stiffness using the effective stress level. This enables the calculation of E_{py} with only one initial subgrade modulus function, which is valid both for dry and saturated sand. Having an effective density of $10kN/m^3$ leads to an initial subgrade modulus of $k = 5000kN/m^3$, which is significantly smaller than the proposed value

of $k = 40000kN/m^3$. The initial stiffness is affected by the installation procedure and pile installed in-flight at the right stress level would have a greater stiffness. The value found from this study is very small but it is confirming the order of magnitude seen in other centrifuge tests. The linear increase with depth above a point of 3.5d is clear from the tests presented in this thesis, whereas the order of magnitude of the initial subgrade modulus needs to be investigated further.

6.1.2 Maximum bearing capacity

It was clear from the centrifuge tests that the ultimate capacity is not well predicted by any of the methodologies, (Broms (1964) Hansen (1961) or API (2007)). In the formulation of the ultimate capacity by API (2007), the minimum value is used of the theoretical calculation of failure at shallow or greater depths. For monopiles supporting offshore wind turbines installed in dense sand, the piles are all relative short and the ultimate capacity is always calculated following the method for shallow failure. The failure mechanism is therefore not correct and the value of A plays a huge role.

The use of an empirical factor in the calculation of the ultimate capacity clearly shows that the theoretical assumption lacks accuracy. A pragmatic approach is chosen here where this factor is calibrates to the tests. It would thus be preferable to develop a theoretical approach, where an empirical factor is avoided. In this perspective, the formulation by Hansen (1961) seems to be a better choice. An empirical factor is not used here and the formulation secures a failure transition from shallow to greater depth. No clear conclusions can be drawn though from this study, and this point should be investigated further.

6.2 Cyclic loading

A simple framework for the prediction of displacements and secant stiffness has been proposed. This framework was calibrated by a set of centrifuge tests in order to determine a set of non-dimensional functions. The centrifuge tests represent simplifications of the complex soil - water - structure - wind interaction problem and these simplifications are discussed in connection with offshore prototype monopile conditions.

Between 250-500 load cycles were applied during the main part of the tests in this study involved 250-500 load cycles. Three tests were performed with more than 500 cycles; one test with 1000 cycles on the $d = 28mm$ pile and two tests on the $d = 40mm$ pile with respectively 3000 and 10000 numbers of

cycles. From these tests it was seen that accumulation of displacement and secant stiffness was well described with the predictions based on the first 500 cycles. The accumulation of displacement for the test with 10000 cycles is shown in 6.1 It therefore seems reasonable to use the results for up to 10000

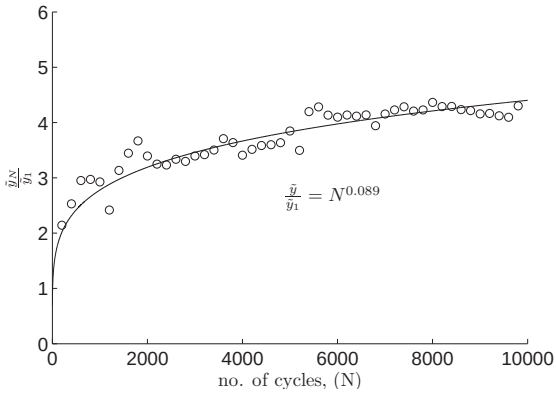

***Figure 6.1**: Accumulation of displacements, 10000 cycles*

cycles. This is still below the number of cycles for the fatigue limit state ($N = 10^7$), but it is an improvement compared to the original design method which is based on tests with fewer than 50 cycles.

In general, the model framework is similar to the one proposed by LeBlanc et al. (2010a), but differences between the models are seen. One of the main findings from the 1g experiments by LeBlanc et al. (2010a) was that the most damaging load situation was for two-way loading, i.e. $\zeta_c = -0.6$. The present centrifuge test series does not show this trend, instead it indicates that one-way loading, $\zeta_c = 0$, is the most damaging one. From the tests by LeBlanc et al. (2010a) accumulation of rotation was seen regardless of the characteristic of the loading. This is also in contrast to the observation done in this study, where it was seen that the pile starts to move back against its initial position for pure two-way loading. This observation was also done by Rosquoët et al. (2010) who performed centrifuge tests on long slender piles. One explanation of these disagreements can be the fact that the tests performed by LeBlanc et al. (2010a) was carried out in loose sand in order to model the maximum angle of friction correctly. The sand in the 1g experiments thus most likely starts to compact when loaded. Tests performed in a centrifuge, model stresses and relative densities correctly, so the dilatant behaviour of sand is therefore better accounted for, see e.g.

Springman (2000).

The correct modelling of stresses, together with the chosen simplification, indicates that the findings from the study in this thesis are reliable and can be used in the predictions of the behaviour of prototype monopiles.

6.3 Cyclic spring model

A simple cyclic spring element has been presented and the performance of the element has been compared with results from centrifuge experiments. The element predicts the hysteresis seen at element level in an acceptable way but does not predict the accumulation of displacements and change in secant stiffness, as seen in the experiments. Soil damping from friction is hard to address and is also dependent upon the magnitude of the loading, Hald et al. (2009). The spring element takes this into account. A logarithmic decrement of 1-8% of soil damping of the first natural vibration mode was added from simple free decay tests. This is in accordance with the observation seen in Versteijlen et al. (2011).

Soil damping is especially important in fatigue analysis and it is believed that applying this cyclic element in an aero elastic calculation will reduce the resonance loads. Especially, when the waves and wind are misaligned and the aerodynamic damping is small, Schløer et al. (2012). The material used in the monopile can be reduced if the loads are lower, making the monopile cheaper. This has to be validated by simulations.

The spring element still needs some improvement, in order to handle the accumulation of deflection and the change in secant stiffness, as observed in the centrifuge.

Chapter 7

Conclusions

The response of a laterally loaded pile has been investigated in this thesis. The investigation has been carried out with the application as a supporting structure for an offshore wind turbine in mind. To narrow down the scope, only a pile installed in homogeneously saturated sand has been investigated and the possible accumulation of the pore pressure has been deliberately neglected. Hence, only the drained case is investigated here.

The design of a monopile supporting an offshore wind turbine is carried out for different design limit states. Design methodologies have been presented through this thesis, which can be used for a better technical solution for a monopile supporting an offshore wind turbine.

The scientific validation of this methodology is based on a set of 74 different centrifuge experiments on laterally loaded model piles. About half of the tests have been used in order to investigate the transformation of centrifuge results to prototype scale. This has primarily been carried out using the "Modelling of Models" technique. Scale effects were identified and centrifuge modelling procedures were developed in order to achieve a reliable modelling technique.

Once this has been established, the pile - soil interaction was investigated with a range of monotonic and cyclic centrifuge tests. The ultimate limit state was investigated by a series of monotonic tests. A formulation of the monotonic pile-soil interaction was obtained from the observations seen in these test. This formulation can be used in a standard Winkler model and predicts the displacement from a given lateral load. The serviceability limit state has been investigated by a series of cyclic load tests. A model to predict the overall displacement and secant stiffness of the foundation from cyclic loading has been proposed from these tests. The model only needs a monotonic test to determine an input parameter, which can be found using the Winkler approach described above.

A cyclic spring element has been developed and can be used in monotonic, cyclic and dynamic calculation. This is needed in the design of the fatigue limit states. The spring element has been developed from cyclic centrifuge test observations and describes the cyclic pile - soil interaction. The element predicts the hysteresis seen in the different soil layers acceptably, but does not model the accumulation of displacement and change in secant stiffness seen in the centrifuge experiments very well.

It is recommended here that the cyclic spring element is implemented in an aero elastic code. This code can be used in the fatigue analysis and in the load analysis. When this analysis is carried out, the monotonic model can be used to calculate a static response and the cyclic model for overall displacements can be used to estimate the permanent displacements. The design limit states can thereby all be represented by models developed in this thesis.

Outlook

Doing the three years of my Ph.D. studies, I have gained an insight into a complex soil - structure interaction problem. With the centrifuge setup as my main investigation tool, I have tried to identify different important parameters for the interaction problem of a laterally loaded pile. This outlook tries to describe my current understanding of the interaction problem, and especially in which direction further investigations should be performed.

A large part of my project has been about the centrifuge methodology and how to transfer these results to a prototype scale. This can be done by a dimensional analysis and is not only a tool for scaling of results, but also a tool that should be used in order to understand scaling problems. From industry and research communities, concerns about the use of pile - interaction curves for large diameter piles have been cited: this is known as the diameter effect. Through my three years of work, I have not seen a paper where the diameter effect has been threated and full similarity has been achieved between the investigated models. It is therefore very difficult to know if such an effect exists. It is my belief that a finite element calculation cannot capture a possible diameter effect. This was also illustrated in this thesis by having identical normalised response from two numerical simulations of laterally loaded piles at two different scales. I suspect that only full-scale testing may be attempted in order to investigate and document a possible diameter effect.

Pore pressure accumulation is also a factor that needs to be investigated as a matter of urgency. If possible pore pressure accumulations have to be investigated in a centrifuge; both loading frequency and permeability have to be scaled with the increase in gravity in order to achieve full similarity with the prototype. The permeability can be decreased by changing the liquid used in the centrifuge test to e.g. silicon oil. The loading frequency is hard to scale and with the current setup at DTU I do not think it is possible to perform loading at this frequency. I think the solution for this is to perform centrifuge tests in oil saturated sand, with a load frequency as high as possible. The results from these tests should then be calibrated against a cyclic numerical model. The numerical model can then be used for

the final scaling of the observation. The numerical model should be cable of handling the interaction between structure soil and water.

The centrifuge tests performed during this thesis have all been carried out with the focus on initial stiffness and maximum capacity. This has implied that a solid pile has been used in order to capture the soil failure. The initial stiffness of the pile - soil response is more crucial for wind turbines than the ultimate capacity. I will recommend that a hollow pile is used in the further centrifuge tests. The installation force for a hollow pile is smaller and the softer response will help the interpretation of the initial stiffness. The focus should be the initial stiffness and the displacement magnitude should be very small $y < 1/100d$. With a pile with a diameter of $d = 40mm$, this leads to maximum deformations at sand surface of $y < 0.4mm$. This set some demands on the displacement measurements.

A load setup is needed with in-flight installation at the correct stress level followed by lateral load testing without stopping the centrifuge. This approach will lead to less manual work with the setup after the pile is installed and thereby also lower disturbances in the soil package. The demand for installation and lateral loading in one handling of the package, and the precision of the deflection measurements required, implies that two new contactless measurement devices will be needed. Laser LVDT's with the appropriate accuracy and range would be the obvious choice.

This thesis has mainly concerned centrifuge modelling, although I have briefly discussed the used of other methodologies in thesis as well as here in the outlook. I think it is important to remember that no methodology is perfect and that different methodologies should always be used for reliable research.

Lyngby, the 29$^{\text{th}}$ of June 2012

Rasmus Tofte Klinkvort

Bibliography

K. Abdel-Rahman and M. Achmus. Finite element modelling of horizontally loaded monopile foundations for offshore wind energy converters in germany. In *International Symposium on Frontiers in Offshore Geotechnics (ISFOG)*, 2005.

M. Achmus, Y.-S. Kuo, and K. Abdel-Rahman. Behavior of monopile foundations under cyclic lateral load. *Computers and Geotechnics*, 36(5):725–735, 2009. M3: 10.1016/j.compgeo.2008.12.003.

International Energy Agency. *Energy Technology Perspectives 2008: Scenarios and Strategies to 2050*. Organisation for Economic Co-operation and Development, Jul 08 2008. ISBN 9789264041424.

International Energy Agency. *Energy Technology Perspectives 2010*. Organisation for Economic Co-operation and Development, Jul 01 2009. ISBN 9789264085978.

L. V. Andersen, M. J. Vahdatirad, M. T. Sichani, and J. D. Sørensen. Natural frequencies of wind turbines on monopile foundations in clayey soils - a probabilistic approach. *Computers and Geotechnics*, 43:1–11, 2012.

API. *API RP 2A-WSD Recommended practice for planning, designing, and constructing fixed offshore platforms - Working stress design*, 2007.

S. A. Ashford and T. Juirnarongrit. Evaluation of pile diamter effect on initial modulus of subgrade reaction. *Journal of geotechnical and geoenvironmental engineering*, 129:234–242, 2003.

A. H. Augustesen, K. T. Brødbæk, M. Møller, S. P. H. Sørensen, L. B. Ibsen, T. S. Pedersen, and L. Andersen. Numerical modelling of large-diameter steel piles at Horns Rev. In *Proceedings of the Twelfth International Conference on Civil, Structural and Environmental Engineering Computing*, 2009.

S. Bhattacharya, D. Lombardi, and D. M. Wood. Similitude relationships for physical modelling of monopile-supported offshore wind turbines. *International Journal of Physical Modelling in Geotechnics*, 11:58 –68, 2011.

M. D. Bolton. Strength and dilatancy of sands. *Geotechnique*, 36(1):65–78, 1986.

M. D. Bolton and J. M. R. Wilson. Soil stiffness and damping. *Structural Dynamics*, 1:209–216, 1990.

R. W. Boulanger, C. J. Curras, B. L. Kutter, D. W. Wilson, and A. Abghari. Seismic soil-pile-structure interaction experiments and analysis. *Journal of Geotechnical and Geoenvironmental Engineering*, 125:750–759, September 1999.

J.-L. Briaud, T. D. Smith, and B. J. Meyer. Using the pressuremeter curve to design laterally loaded piles. *Proceedings - Annual Offshore Technology Conference*, 1:495–502, 1983.

B. Broms. Lateral resistance of piles in cohesionless soils. *ASCE – Proceedings – Journal of the Soil Mechanics and Foundations Division*, 90:123–156, 1964.

A. K. Chopra. *Duynamics of structures - Theory and applications to earthquake engineering*. Prentice Hall, 2007.

J. Chung and G. M. Hulbert. A time integration algorithm for structural dynamics with improved numerical dissipation: The generalized-alpha method. *Journal of applied mechanics*, 60(2):371–375, 1993. ISSN 15289036.

W. H. Craig. Installation studies for model piles. *Proceedings of a Symposium on the Application of Centrifuge Modelling to Geotechnical Design.*, pages 441–456, 1985.

P. Cuéllar, M. Baeßler, and W. Rücker. Ratcheting convective cells of sand grains around offshore piles under cyclic lateral loads. *Granular Matter*, 11(6):379–390, 2009. M3: 10.1007/s10035-009-0153-3.

C. Devriendt, P. J. Jordaens, G. D. Sitter, and P. Guillaume. Damping estimation of an offshore wind turbine on a monopile foundation. In *EWEA*, 2012.

DNV. *Design of offshore wind turbine structures*, volume DNV-OS-J101. Det norske Veritas, 2011.

DNV and RISØ. *Guidelines for Design of Windturbines*, 2001.

G. J. Dyson and M. F. Randolph. Monotonic lateral loading of piles in calcareous sand. *Journal of Geotechnical and Geoenvironmental Engineering*, 127(4):346–352, 2001. M3: 10.1061/(ASCE)1090-0241(2001)127:4(346).

M. H. El Naggar, M. A. Shayanfar, M. Kimiaei, and A. A. Aghakouchak. Simplified bnwf model for nonlinear seismic response analysis of offshore piles with nonlinear input ground motion analysis. *Can. Geotech. J.*, 42 (2):365–380, 2005. ISSN 12086010.

C.-C. Fan and J. H. Long. Assessment of existing methods fro predicting spoil response of laterally loaded piles in sand. *Computers and Geotechnics*, 32: 274–289, 2005.

L. D. Fuglsang and J. Nielsen. Danish centrifuge hardware and usage. *Centrifuges in Soil Mechanics*, pages 93–95, 1988.

L. D. Fuglsang and N. K. Ovesen. *The application of the theory of modelling to centrifuges studies*. Balkema, Rotterdam, 1988a.

L. D. Fuglsang and N. K. Ovesen. The application of the theory of modelling to centrifuge studies. *Centrifuges in Soil Mechanics*, pages 119–138, 1988b.

J. Garnier, C. Gaudin, S. M. Springman, P. J. Culligan, D. Goodings, D. Konig, B. Kutter, R. Phillips, M. F. Randolph, and L. Thorel. Catalogue of scaling laws and similitude questions in geotechnical centrifuge modelling. *International Journal of Physical Modelling in Geotechnics*, 7 (3):1–23, 2007.

C. Gaudin, F. Schnaid, and J. Gamier. Sand characterization by combined centrifuge and laboratory tests. *International Journal of Physical Modelling in Geotechnics*, 5:42–56, 2005.

M. Georgiadis, C. Anagnostopoulos, and S. Saflekou. Centrifugal testing of laterally loaded piles in sand. *Canadian Geotechnical Journal*, 29(2): 208–216, 1992.

T. Hald, C. Mørch, L. Jensen, C. L. Bakmar, and K. Ahle. Revisiting monopile design using p-y curves. results from full scale measurements on Horns Rev. *Proceedings of European Offshore Wind 2009 Conference*, 2009.

J. B. Hansen. Ultimate resistance of rigid piles against transversal forces. *Geoteknisk Institut – Bulletin (Danish Geotechnical Institute – Bulletin)*, 1(12):5–9, 1961.

O. Hededal and R. T. Klinkvort. A new elasto-plastic spring element for cyclic loading of piles using the p-y curve concept. *Numerical Methods in Geotechnical Engineering : NUMGE 2010*, pages 883–888, 2010.

O. Hededal and S. Krenk. Femlab, matlab toolbox for the finite element method. Aalborg University, May 1995.

M. Hetenyi. *Beams on Elastic Foundation: Theory with Applications in the Fields of Civil and Mechanical Engineering*. University of Michigan Press, 1946.

M. Jacobsen. *New oedometer and new triaxial apparatus for firm soils*. Geoteknisk Institut, 1970.

B. T. Kim, N.-K. Kim, W. J. Lee, and Y. S. Kim. Experimental load-transfer curves of laterally loaded piles in nak-dong river sand. *Journal of Geotechnical and Geoenvironmental Engineering*, 130(4):416–425, 2004. M3: 10.1061/(ASCE)1090-0241(2004)130:4(416).

R. T. Klinkvort and O. Hededal. Lateral response of monopile supporting an offshore wind turbine. Submitted for publication, 2012a.

R. T. Klinkvort and O. Hededal. Monotonic soil-structure interaction of monopile support for offshore wind turbines. Submitted for publication, 2012b.

R. T. Klinkvort, C. T. Leth, and O. Hededal. Centrifuge modelling of a laterally cyclic loaded pile. *Physical Modelling in Geotechnics*, pages 959–964, 2010.

R. T. Klinkvort, O. Hededal, and M. Svensson. Laterally cyclic loading of monopile in dense sand. *Proceedings of the 15th European Conference on Soil Mechanics and Geotechnical Engineering*, 2011.

R. T. Klinkvort, O. Hededal, and S. Springman. Scale effects in centrifuge modelling of monopiles. Submitted for publication, 2012.

R.T. Klinkvort and O. Hededal. Centrifuge modelling of offshore monopile foundation. *Frontiers in Offshore Geotechnics II*, pages 581–586, 2010.

R. L. Kondner. Hyperbolic stress-strain response; cohesive soils. *ASCE – Proceedings – Journal of the Soil Mechanics and Foundations Division*, 89: 115–143, 1963.

S. Krenk. Dynamic analysis of structures - numerical time integration. Technical report, Course on Non-Linear Analysis of Frame Structursc, 1999. Course on Non-Linear Analysis of Frame Structurs, 1999.

S. Krenk. *Non-linear Modeling and Analysis of Solids and Structures*. Cambrigde University Press, 2009.

H. L. Langhaar. Dimensional analysis and theory of models. Technical report, John Wiley & Sons, 1951.

T. J. Larsen and A. M. Hansen. *How 2 HAWC2, the user's manual*, 2007.

C. LeBlanc, G. T. Houlsby, and B. W. Byrne. Response of stiff piles in sand to long-term cyclic lateral loading. *Geotechnique*, -:–, 2009.

C. LeBlanc, G. T. Houlsby, and B. W. Byrne. Response of stiff piles in sand to long-term cyclic lateral loading. *Geotechnique*, 60(2):79–90, 2010a. M3: 10.1680/geot.7.00196.

C. Leblanc, B. W. Byrne, and G. T. Houlsby. Response of stiff piles to random two-way lateral loading. *Geotechnique*, 60(9):715–721, 2010b. M3: 10.1680/geot.09.T.011.

K. Lesny and J. Wiemann. Finite-element-modelling of large diameter monopiles for offshore wind energy converters. In *Geo Congress*, 2006.

C. T. Leth, A. Krogsbøll, and O. Hededal. Centrifuge facilities at danish technical university. In *15th Nordic Geotechnical Meeting*, 2008.

Z. Li, S. K. Haigh, and M. D. Bolton. Centrifuge modelling of mono-pile under cyclic lateral loads. *Physical Modelling in Geotechnics*, pages 965–970, 2010.

J. H. Long and G. Vanneste. Effects of cyclic lateral loads on piles in sand. *Journal of Geotechnical Engineering*, 120:225–244, 1994.

B. McClelland and J. A. Focht. Soil modulus for laterally loaded piles. *American Society of Civil Engineers – Proceedings – Journal of the Soil Mechanics and Foundations Division*, 82, 1956.

G. G. Meyerhofs, K. Mathur, and A. J. Valsangk. Lateral resistance and deflection of rigid walls and piles in layered soils. *CAN. GEOTECH. J.*, 18:159–170, 1981.

J. M. Murchison and M. W. O'Neill. Evaluation of p-y relationships in cohesionless soils. In *Proc., Symposium of Analysis and Design of Pile Foundations, ASCE, San Fransisco*, pages 174–191, 1984.

N. M. Newmark. Method of computation for structural dynamics. *ASCE – Proc (J Eng Mechanics Div)*, 85:67–94, 1959.

G. Norris and P. Abdollaholiaee. Bef - studies with the strain wedge model. part a. *Proceedings of the 1990 Annual Symposium on Engineering Geology & Geotechnical Engineering*, pages 13A.1–13A16, 1990.

I. L. Nunez, R. Phillips, M. F. Randolph, and B. D. Wesselink. Modelling laterally loaded pile in calcareous sand. *Centrifuge 88*, pages 353–362, 1988.

N. K. Ovesen. Centrifugal testing applied to bearing capacity problems of footings on sand. *Geotechnique*, 25(2):394–401, 1975.

F. Parker and L. Reese. Experimental and analytical study of behavior of single piles in sand under lateral and axial loading - research report no. 117-2. Technical report, Center for Highway Research, The University of Texas, 1970.

M. J. Pender, D. P. Carter, and S. Pranjoto. Diameter effects on pile head lateral stiffness and site investigation requirements for pile foundation design. *Journal of Earthquake Engineering*, 11(1), 2007. SP:.

P. Peralta and M. Achmus. An experimental investigation of piles in sand subjected to lateral cyclic experiments. In *Physical Modelling in Geotechnics*, 2010.

H. Poulos and T. Hull. The role of analytical geomechanics in foundation engineering. *Foundation Engineering: Current principles and Practices, ASCE, Reston*, 2:1578–1606, 1989.

M. F. Randolph. Science and empiricism in pile foundation design. *Geotechnique*, 53(10):847–875, 2003. M3: 10.1680/geot.53.10.847.37518.

L. C. Reese and . F. Van Impe. *Single Piles and Pile Groups Under Lateral Loading*. A. A. Balkema, 2001.

L. C. Reese and H. Matlock. Non-dimensional solutions for laterally-loaded piles with soil modulus assumed proportional to depth. In *Proceedings of eighth Texas Conference on Soil Mechanics and Foundation Engineering*, 1956.

L. C. Reese, W. R. Cox, and F. D. Koop. Analysis of laterally loaded piles in sand. In *Offshore Technology Conference*, 1974.

D. Remaud. *Pieux sous charges latérales: Etude Experimentale de l'effect de groupe*. PhD thesis, Ecole Centrale de Nantes, 1999.

F. Rosquöet, L. Thorel, J. Garnier, and Y. Canepa. Lateral cyclic loading of sand-installed piles. *Soils and Foundations*, 47, no 5:821–832, 2007.

F. Rosquoët, L. Thorel, J. Garnier, and M. Khemakhem. P-y curves on model piles: Uncertainty identification. In *Physical Modelling in Geotechnics*, pages 997–1002, 2010. ISBN 978-0-415-59288-8.

S. Schløer, H. Bredmose, H. B. Bingham, and J. T. Larsen. Effects from fully nonlinear irregular wave forcing on the fatique life of an offshore wind turbine and its monopile foundation. In *Proceedings of the ASME, International Conference on Ocean, Offshore and Artic Engineering, OMAE*, 2012.

A. N. Schofield. Cambridge geotechnical centrifuge operations. *Geotechnique*, 30(3):227–268, 1980.

R. F. Scott. Analysis of centrifuge pile tests: Simulation of pile driving. Research report, american petroleum institut osapr project 13, California Institute of Technology, 1980.

T. D. Smith. Pile horizontal soil modulus values. *Journal of Geotechnical Engineering*, 113(9):1040–1044, 1987.

S.P.H. Sørensen, K. T. Brødbæk, M. Møller, A. H. Augustesen, and L. B. Ibsen. Evaluation of the load-displacement relationships for large-diameter piles in sand. In *Proceedings of the Twelfth International Conference on Civil, Structural and Environmental Engineering Computing*, 2009.

S. M. Springman. Discussions - displacement of structures adjacent to cantilever sheet pile walls. *Soils and Foundations*, 40(5):149, 2000. ISSN 00380806.

M. Svensson. Load amplitude effects on cyclically loaded monopile. Master's thesis, Technical University of Denmark, 2010.

E. Taciroglu, C. Rha, and J. W. Wallace. A robust macro element model for soil pile interaction under cyclic loads. *Journal of geotechnical and geoenvironmental engineering*, Vol. 132(No. 10):p. 1304–1314, October 2006.

N.J. Tarp-Johansen, L. Andersen, E. Damgaard, B. Kallesøe, and Sten Frandsen. Comparing sources of damping of cross-wind motion. In *European Offshore Wind*, 2009.

R. N. Taylor. *Centrifuges in modelling: principles and scale effects*. Blackie Academic & Professional, 1995.

K. Terzaghi. Evaluation of coefficients of subgrade reaction. *Geotechnique*, 5(4):297–326, 1955.

J. Ubilla, T. Abdoun, and T. Zimmie. Application of in-flight robot in centrifuge modeling of laterally loaded stiff pile foundations. *Physical Modelling in Geotechnics*, 1:259–264, 2006.

W.G. Versteijlen, A. Metrikine, J.S. Hoving, E.H. Smidt, and W.E. De Vries. Estimation of the vibration decrement of an offshore wind turbine support structure caused by its interaction with soil. In *Proceedings of the EWEA Offshore 2011 Conference, Amsterdam, The Netherlands*, 2011.

D. M. Wood. *Geotechnical modelling*. Spon Press, 2004.

K. Yang and R. Liang. Methods for deriving p-y curves from instrumented lateral load test. *Geotechnical testing journal*, 30:1–8, 2006.

S. Øye. Flex4 simulation of wind turbine dynamics. In *28th IEA Meeting of Experts, Concerning State of the Art of Aeroelastic Codes for Wind Turbine Calculationsn.*, 1996.

V. Zania and O. Hededal. The effect of soil-pile interface behaviour on laterally loaded piles. In *Proceedings of the Thirteenth International Conference on Civil, Structural and Environmental Engineering Computing*, 2011.

V. Zania and O. Hededal. Friction effects on lateral loading behavior of rigid piles. In *GeoCongress 2012 - State of the Art and Practice in Geotechnical Engineering*, 2012.

L. Zhang, F. Silva, and R. Grismala. Ultimate lateral resistance to piles in cohesionless soils. *Journal of Geotechnical and Geoenvironmental Engineering*, 131(1):78–83, 2005. M3: 10.1061/(ASCE)1090-0241(2005)131:1(78).

Part II

Papers

Paper I

"Centrifuge modelling of offshore monopile foundation"

R.T. Klinkvort & O. Hededal

Published in: *Frontiers in Offshore Geotechnics II, 2010*

Frontiers in Offshore Geotechnics II – Gourvenec & White (eds)
© 2011 Taylor & Francis Group, London, ISBN 978-0-415-58480-7

Centrifuge modelling of offshore monopile foundation

R.T. Klinkvort & O. Hededal
Technical University of Denmark, Copenhagen, Denmark

ABSTRACT: Today one of the most used concepts for wind turbine foundation is the monopile. The foundation concepts for these monopiles on deeper water is uncertain and consequently the design needs to be conservative leading to uneconomic designs. This paper describes a total number of 6 static and 5 cyclic centrifuge tests on a laterally loaded monopile in dry sand. The prototype dimension of the piles was modelled to a diameter of 1 meter and penetration depth on 6 meter. The test series were designed in order to investigate the scaling laws in the centrifuge both for monotonic and cyclic loading. It was not possible in the tests to reproduce the same prototype response for both the monotonic and the cyclic loading. It was not clear if this scatter in prototype data was due to normal measurement uncertainties or if the response is depending on the scaling factor.

1 INTRODUCTION

Single large diameter tubular steel piles commonly denoted monopiles is today a very used foundation method for offshore wind turbines. The design of these monopiles is commonly based on the theory of laterally loaded piles which relies on empirical data originated from the oil and gas industry, Reese and Matlock (1956) & McClelland and Focht (1958). The lateral capacity is determined by modelling the pile as a beam and the soil as a system of uncoupled springs, this is known as aWinkler model. The springs are described by p-y curves defining the load-displacement relationship for the interaction between soil and pile, API (1993). The formulation of these curves was originally calibrated to slender piles, but is today even used for design of large diameter monopiles with a slenderness ratio L/D as low as 5. The monopiles used for wind turbine foundations thus act as stiff piles. Therefore it is relevant to investigate the behavior of stiff piles in more detail. The tests series presented in this paper is an initial program that intends to investigate the response of model monopiles subjected to different artificial gravities in a centrifuge. The concept called modelling of models is used to investigate the response from five different piles which are scaled to the same prototype dimensions.

2 CENTRIFUGE MODELLING

When performing centrifuge tests an artificial gravity is applied to a model test setup. This is done to ensure that the stress field in the model is similar to the stress field in the prototype. This is important in model testing due to the non-linearity of the stress-strain relations of soils. To apply the artificial gravity the model is placed at the end of a rotating arm. The acceleration in a specified point in the model is given by the angular rotation speed (ω) and the distance (R) from the rotational axis. The ratio between gravity (g) and artificial gravity is described by the gravity scale factor (N).

$$N = R\omega^2/g \tag{1}$$

In centrifuge modelling two key issues are represented, the scaling laws and the scaling errors.

2.1 *Scaling laws*

To transform results from test carried out on models to prototypes the dimensional analysis can be used, Langhaar (1951). The foundation for the dimensional analysis is Buckingham's Π theorem. From this, dimensionless parameters can be determined. These dimensionless parameters have to be the same for the prototype and the model to have full similarity. If all governing laws of similitude are in place a true model is obtained. This implies that stresses and strains are scaled by a factor of 1, deflection and lengths is scaled by a factor of N, forces are scaled by a factor of N^2 and so on; see e.g. Taylor (1995).

2.2 *Scale effects*

In physical modelling it is seldom possible to produce a model where all details of the model is scaled correctly in the prototype. Therefore some approximations have to be made. These differences are called scale effects and are important to be aware of when the test results are interpreted. Model studies are not perfect and it is important to understand this. Two main effects will be presented here. The first is the stress distribution. Looking at Equation 1 on the preceding page it can be seen that the applied gravity is depending on the distance to the rotational axis.

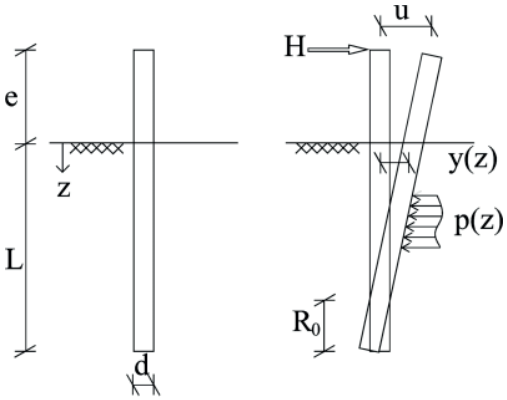

Figure 1. Sketch of pile.

This distance will increase through the model. In the prototype the stresses will increase linearly due to the constant gravity field, whereas the stresses in the model will increase parabolically. To minimize this error the radius is defined from center to a depth of 2/3 of the pile penetration depth, Stuit (1995).

When performing centrifuge modelling it is not possible to scale the sand grain diameter correctly, since this will imply a difference in friction angle and cohesion. Therefore, when considering bearing capacity, it is most often necessary to use the same sand in the model as in the prototype. This causes the sand grains to be scaled by a factor of N in the model. This is known as the particle size effect. The grain size effect has been investigated with "modelling of models". Particle size effect has been tested for laterally loaded piles by Hoadley et al. (1981) and they found that a "model diameter/ grain size diameter" ratio of 50 and above gave a good agreement. Remaud et al. (1998) found that a ratio over 60 was enough to avoid particle size effects. Both of these studies were performed on long slender piles. Nunez et al. (1988) performed modelling of models on tension piles. They found that the smaller piles tested at high accelerations gave consistently higher capacity than larger piles tested at smaller accelerations. They explain this difference with installation effects and differences in wall thickness and conclude that the effect from particle size is not significant.

3 EXPERIMENTS

As the first of a larger test series on monopiles a series of modelling of models have been performed to analyze the response of a monopile in relation to the applied gravity. The test program was performed on five solid steel piles with a diameter between 16–40 mm and penetration depths between 96–240 mm which were all scaled to a prototype pile with a diameter of $d = 1$ m and penetration depth $L = 6$ m.

In figure 1 a sketch of the test pile can be seen. In Table 1 the dimension of the five piles and the scaling factor is shown. This should scale all the piles to the same prototype pile.

Table 1. Dimensions and scaling factor for the piles.

d [mm]	e [mm]	L [mm]	N [–]
16	40	96	62.5
22	55	132	45.5
28	70	168	35.7
34	85	204	29.4
40	100	240	25

Table 2. Classification parameters for the Fontainebleau sand.

Specific gravity of particles	G_s	2.646
Minimum void ratio	e_{min}	0.548
Maximum void ratio	e_{max}	0.859
Average grain size	d_{50}	0.18
Coefficient of uniformity	C_u	1.6

Table 3. Void ratio for the different tests.

d [mm]	16	22	28	34	40
Monotonic	0.58/0.57	0.58	0.57	0.59	0.56
Cyclic	0.59	0.56	0.56	0.58	0.55

All monotonic and cyclic tests were performed in dry Fontainebleau sand. Leth et al. (2008) has collected classification parameters for the Fontainebleau sand which can be seen in table 2 on the next page. The average grain size of the Fontainebleau sand is 0.18 mm. With pile diameter ranging from 16 mm to 40 mm this leads to a "model diameter/ grain size diameter" ratio ranging from 88 to 189.

The centrifuge at DTU uses a spot pouring hopper (SPH) for the preparation of the sand sample. Due to the geometry of the container and pile the sand is prepared using a circular travelling loop as described in Zhao et al. (2006). The sand is installed in a container with a inner diameter of 50 cm and a height of 49 cm. A new sample is prepared for each of the tests. CPT tests have been carried out to validate the pouring method. All these CPT tests showed the soil sample has a good homogeneity in the container.

After the sand is prepared, the pile is installed at 1 g. It must be expected that the sand is compacted in a higher degree around the pile, for large piles than for small piles. When the tests are carried out it must be expected that the stresses in the sand is so high that potential preconsolidated areas disappears. Installing the pile at 1 g. is therefore intended to minimize the effects from the installation.

A total of 11 centrifuge tests have been performed: six monotonic and five cyclic. For all the tests the relative density was found to vary in the range 0.8–0.94. A table with the different void ratios can be seen in table 3 on the following page. The relative densities

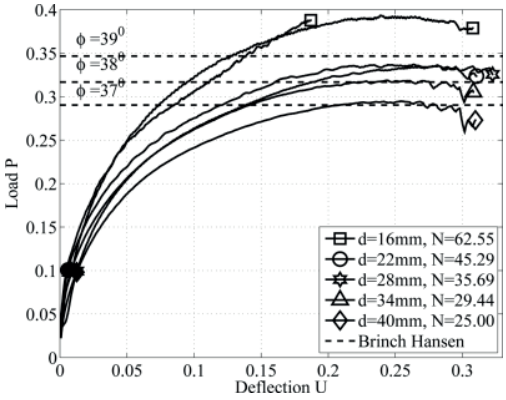

Figure 2. Normalized plot with the five static tests.

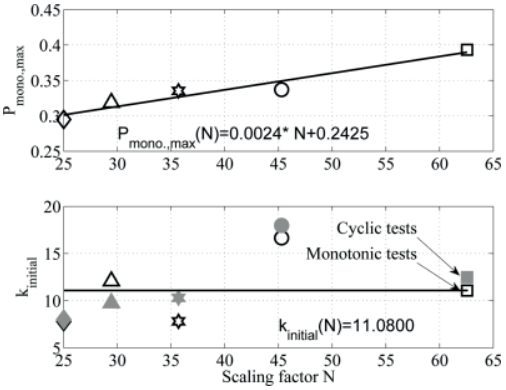

Figure 3. Normalized plot bearing capacity and initial stiffness as a function of the scaling factor.

are calculated by knowing the weight and the volume of the sand sample. The average value for both the static and cyclic tests is for the relative density $I_D = 0.924$ and a void ratio of $e = 0.57$ leading to a triaxial frictional angle of $\phi = 38°$.

3.1 *Monotonic tests*

The force and deflection is normalized, to compare the general pile behavior. On the y-axis the normalized force is plotted. This is found as shown in equation 2.

$$P = \frac{H}{\gamma \cdot L^3} \tag{2}$$

On the x-axis the normalized deflection is plotted. This is shown in equation 3

$$U = \frac{u}{L} \tag{3}$$

In figure 2 the observation of the monotonic loading can be seen. Remember that all the test is scaled to same prototype and the response from the different tests should be identical. However a variation in the results can be seen. The test performed at 62.5 g showed a significantly high bearing capacity therefore a second test on the $d = 16$ mm was performed to validate the response. The second test confirmed the response.

Interpretation method 1: Looking at figure 2 you could say that the pile with a diameter of $d = 16$ mm shows a much higher capacity than the other piles and thereby indicates that the pile diameter particle diameter is too small. If this pile is neglected an acceptable scatter of the results is obtained. From this a bearing capacity for the prototype pile could be expected to be $P_{max} \approx 0.32$. This will be called interpretation method 1. On figure 2 the bearing capacity according to Hansen (1961) is shown for three different frictional angles. This indicates small change in frictional angle can be the reason for this scatter. On the other hand using the result from the pile with a diameter of $d = 16$ mm it can be seen that the maximum bearing capacity is increasing with the applied gravity. This could indicate that the linear scaling which is assumed is problematic.

Interpretation method 2: The maximum bearing capacity and the initial stiffness is plotted on figure 3 against the scaling factor. The maximum capacity is found as the maximum value found on figure 2 and the initial stiffness is found at the point where the applied load is $P = 0.1$. This is shown on figure 2 as the black markings. From figure 3 it seems to be a clear linear relationship between the maximum bearing capacity and the scaling factor. Looking at the initial stiffness of the load deflection response no clear relationship is seen. The variance of the stiffness could though indicate that a constant stiffness from the tests could be expected. Here is also plotted the initial stiffness found from the cyclic testing which support this conclusion.

Four of the piles were mounted with measuring of the pile head rotation, if the pile is assumed to behave as a rigid pile, the pile movement can be described according to equation 4.

$$y(z) = u - \theta(e + z) \tag{4}$$

The assumption of the pile behaves like a rigid pile is satisfied according to Poulos and Hull (1989) if the stiffness of the sand is lesser than $E_s = 35$ MPa. If the pile should act as a slender pile then the soil stiffness should be over $E_s = 3090$ MPa. Even if the stiffness of the sand is larger than 35 MPa it is expected that the pile will be located close to the rigid boundary. Therefore it is assumed that the pile behaves as a stiff pile. From this assumption the point of rotation can be found knowing the deflection of the pile u and the rotation θ. The normalize point of rotation measured from pile tip is plotted in figure 4. Due to practical reasons the rotation of the 16 mm pile could not be measured. All the piles shows that the normalized point of rotation is located below the pile tip at initial deflection and the pile is therefore sheared through the sand. After some deformation the rotation point moves up and is located

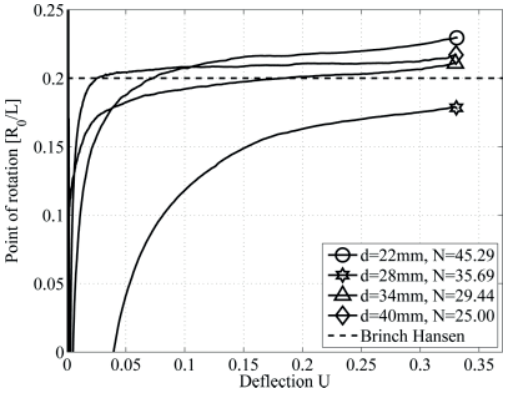

Figure 4. Point of rotation.

in the pile where it is stabilized until failure. From figure 4 no clear relation between normalized point of rotation and scaling factor can be seen. It seems like for all the piles that the rotation point stabilizes around a value of 0.22 except the pile with a diameter of $d = 28$ mm which haves a lower rotation point that the others. Using the theory of Hansen (1961) the rotation point is calculated to 0.2 which is close to the observation. It seems like all the piles is moving in the same manner.

3.2 *Cyclic tests*

The cyclic tests were performed with 500 force controlled cycles. To investigate the effects from cyclic loading this paper uses a method describe in LeBlanc (2009) to described the cyclic loading. The load characteristics are denoted ζ_b and ζ_c. They are determined as shown in equation 5.

$$\zeta_b = \frac{P_{max}}{P_{monotonic}} \qquad \zeta_c = \frac{P_{min}}{P_{max}} \tag{5}$$

Here P_{max} and P_{min} are the maximum and minimum applied force in the cyclic loading. $P_{monotonic}$ is the maximum bearing capacity found from the corresponding monotonic test.

The amount of the applied load depends on the interpretation of the monotonic test. The cyclic loading was performed as individual tests, with five different maximum capacities according to the monotonic tests shown on figure 2 on the preceding page. It was the intension to perform the cyclic test with a $\zeta_b = 0.40$ and a $\zeta_c = 0$ but due to the control system it has not been possible to perform tests with exactly the same load characteristics. However the load characteristics can also be calculated assuming a constant bearing capacity for the monotonic tests. The characteristics of the cyclic loading for the tests series for the two types of interpretation can be seen on Figure 4. For the cyclic loading the accumulation of deflection and the change in secant stiffness is calculated. This is done as showed on figure 5. For every cycle the maximum and minimum values of load and the deflection is found. From this the average deflection can be calculated as shown in equation 6 and the secant stiffness can be calculated as shown in equation 7.

Table 4. Load characteristics for the cyclic tests.

N	$P_{mono.,1}$	$P_{mono.,2}$	$\zeta_{b,1}$	$\zeta_{b,2}$	ζ_c
62.6	0.32	0.39	0.53	0.44	−0.04
45.3	0.32	0.34	0.52	0.49	−0.05
35.7	0.32	0.34	0.44	0.44	−0.02
29.4	0.32	0.32	0.41	0.42	−0.02
25.0	0.32	0.29	0.41	0.44	−0.10

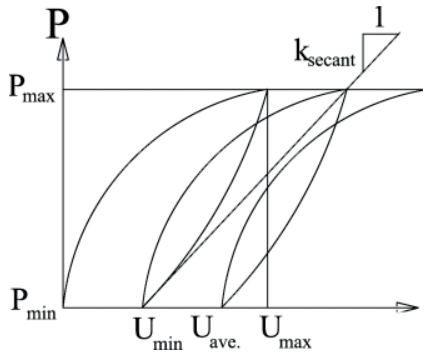

Figure 5. Schematic illustration of average deflection and secant stiffness.

$$U_{average} = \frac{U_{max} + U_{min}}{2} \tag{6}$$

$$K_{secant} = \frac{P_{max} - P_{min}}{U_{max} - U_{min}} \tag{7}$$

The best fit to the accumulation of deflection was done with a power fit as proposed by Long and Vanneste (1994), cf. equation 8.

$$U_{average}(n) = u_0 \cdot n^{\alpha} \tag{8}$$

Here u_0 is the accumulated deflection at the first cycle and α is an empirical coefficient which controls the shape of the curve. n is the number of cycles. The accumulated deflection for a given cycle is defined as the average value for the cycle. The values of the coefficient to the proposed formula can be seen in Table 5. If interpretation method 1 is used the accumulation depends on the load characteristic. ζ_c is nearly constant for all the tests expect test on $d = 40$ mm. It must therefore be expected to see a relation between ζ_b and the coefficient to the power fit. A linear relationship is assumed which leads to the following equations.

$$u_0(\zeta_b) = 0.0300 \cdot \zeta_b + 0.0002 \tag{9}$$

$$\alpha(\zeta_b) = 0.3170 \cdot \zeta_b + 0.1585 \tag{10}$$

Table 5. Empirical constant for accumulation of the deflection from the cyclic testing.

d	u_0	α
16	0.016	0.324
22	0.015	0.315
28	0.010	0.339
34	0.015	0.245
40	0.012	0.256

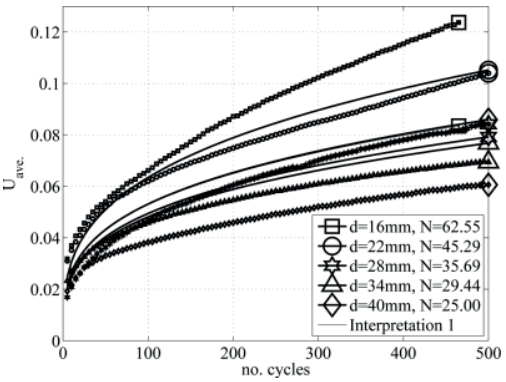

Figure 6. Accumulation of average deflection with interpretation method 1 prediction.

If on the other hand interpretation method 2 is used a linear relationship between the coefficients for the power fit and the scaling factor can be assumed. This leads to following equations.

$$u_0(N) = 0.0001 \cdot N + 0.0096 \tag{11}$$

$$\alpha(N) = 0.0018 \cdot N + 0.2266 \tag{12}$$

On figure 6 the accumulation of the deflection for cyclic testing is seen. Here is also shown the prediction as proposed in equation 8 for the interpretation methods 1. The prediction for the interpretation methods 2 can be seen in Figure 7. None of the methods give good predictions, but it seems that interpretation method 2 is the best. It should again be noted that the cyclic loading is performed according to the maximum bearing capacity found from the monotonic tests. This means that the piles are not loaded to the same prototype loads. The maximum prototype load for the small pile with the large scaling factor is therefore larger than the large pile with the small scaling factor.

Lin and Liao (1999) proposed a logarithmic fit to the change in secant stiffness as shown in equation

$$K_{secant}(n) = k_0 + \kappa \cdot ln(n) \tag{13}$$

Here k_0 is the secant stiffness at the first cycle and κ is an empirical coefficient which control the shape of the curve. n is the number of cycle. A formulation like

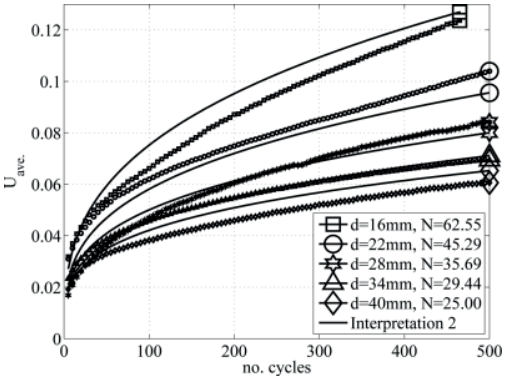

Figure 7. Accumulation of average deflection with interpretation method 2 prediction.

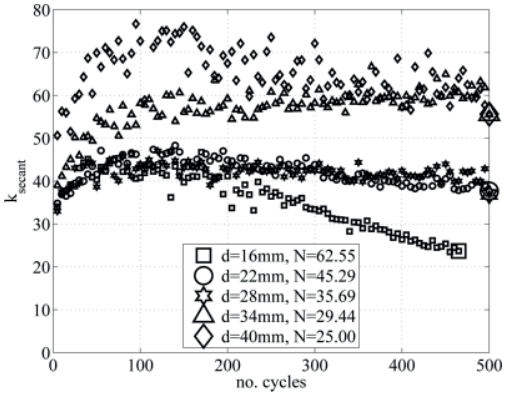

Figure 8. Change in secant stiffness.

this fits the first 100 cycles for the 5 cyclic tests, but as it can be seen in Figure 8 the secant stiffness starts to decrease or stabilize after 100 cycles. It has not been possible to fit the entire number of cycles cyclic. Looking at Figure 8 it can be seen that the secant stiffness is changing from test to test. The secant stiffness is large for the large piles and smaller for the small piles. The explanation for the difference can again be explained for interpretation method 1 as high ζ_b values gives small secant stiffness. Using method 2 high scaling factor gives high secant stiffness. No clear dependency is seen for the two interpretation methods.

4 CONCLUSIONS

A test series of modelling of models have been performed for both monotonic and cyclic loading. It has not been possible for the two loading types to reproduce exactly equal prototype response. The results have been analyzed in two ways; one as a normal scatter in the response, and one using a dependency of the scaling factor. It seems like the scaling factor affects the results but it is not clear. Nunez et al. (1988) reports

also higher capacity for the small piles tested at high g levels and more tests have to be conducted. The fact that the piles in this test series are acting as stiff piles could be an explanation of the difference from previously modelling of models tests. More tests have to be conducted in order to clarify the scaling laws for these stiff laterally loaded piles.

REFERENCES

API (1993). *Recommended Practice For Planning, Designing and Construction Fixed Offshore Platforms* – Load and Resistance Factor Design. American Petroleum Institute.

Hansen, J. B. (1961). The ulitimate resistance of rigid piles against transversal forces. *Danish Geotechnical Institute, Copenhagen, Denmark Bulletin NO. 12*, 5–9.

Hoadley, P. J., Y. O. Barton, and R. H. G. Parry (1981). Cyclic lateral load on model pile i a centrifuge. In *Proceedings of the Tenth International Conference on Soil Mechanics ans Foundation Engineering*, Volume Vol. 1.

Langhaar, H. L. (1951). Dimensional analysis and theory of models. Technical report, John Wiley & Sons.

LeBlanc, C. (2009). *Design of Offshore Wind turbine Support Structures*. Ph. D. thesis, Aalborg University.

Leth, C. T., A. Krogsbøll, and O. Hededal (2008). Centrifuge facilities at danish technical university. In *15th Nordic Geotechnical Meeting*.

Lin, S. S. and J. C. Liao (1999). Permanent strains of piles in sand due to cyclic lateral loads. *Journal of Geotech. and Geoenv. Engng. 125 No. 9*, 798–802.

Long, J. H. and G. Vanneste (1994). Effects of cyclic lateral loads on piles in sand. *Journal of Geotechnical Engineering 120*, 225–244.

McClelland, B. and J. A. Focht (1958). Soil modulus for laterally loaded piles. *Journal of the soil mechanics and foundations division – Proceedings of the American Society of Civil Engineers* -, 1–22.

Nunez, I. L., P. J. Hoadley, M. F. Randolph, and J. M. Hulett (1988). Driving and tension loading of piles in sand on a centrifuge. In *Centrifuge 88*.

Poulos, H. and T. Hull (1989). The role of analytical geomechanics in foundation engineering. *Foundation Engineering: Current principles and Practices, ASCE, Reston 2*, 1578–1606.

Reese, L. C. and H. Matlock (1956). Non-dimensional solutions for laterally loaded piles with soil modulus assumed proportional to depth. *Proceedings of the 8th Conference on Soil Mechanics* -, 1–41.

Remaud, D., J. Garnier, and R. Frank (1998). Pieux sous charges lat'erales: étude de léffect de groupe. *5. Journées Nationales Génie Civil Génie Côtier, Toulon*, pp. 369–376.

Stuit, H. G. (1995). *Sand In The Geotehcnical Centrifuge*. Ph. D. thesis, Technische Universiteit Delft.

Taylor, R. N. (1995). *Centrifuges in modelling: principles and scale effects*. Blackie Academic & Professional.

Zhao, Y., K. Gafar, M. Elshafie, A. Deeks, J. Knappett, and S. Madabhushi (2006). Calibration and use of a new automatic sand pourer. In *Physical modelling in Geotechnics, 6th ICPMG '06*, pp. p. 265–270.

Paper II

"Scaling issues in centrifuge modelling of monopiles"

R. T. Klinkvort, O. Hededal & S. Springman

Accepted for publication in: *International Journal of Physical modelling in Geotechnics, 2012*

Scale effects in centrifuge modelling of monopiles

Rasmus T. Klinkvort[1], Ole Hededal[2] and Sarah M. Springman[3]

1) Ph.D. research student, Dept. of Civil Engineering, Technical University of Denmark, Sec. of Geotechnics and Soil Mechanics, Brovej Building 118, 2800 Kgs. Lyngby, Denmark. Phone: (+45) 25 38 78 13, rakli@byg.dtu.dk.

2) Associate Professor, Dept. of Civil Engineering, Technical University of Denmark, Sec. of Geotechnics and Soil Mechanics, Brovej Building 118, 2800 Kgs. Lyngby, Denmark. Phone: (+45) 45 25 50 20, olh@byg.dtu.dk.

3) Professor, Institute for Geotechnical Engineering, Swiss Federal Institute of Technology – Zurich , Sec. of Geotechnics, HIL C13.1, 8093 Zurich, Switzerland. Phone: +41 (44) 633 38 05, sarah.springman@igt.baug.ethz.ch

Keywords: *Centrifuge modelling, Foundations, Piles and piling, Sands, Renewable energy.*

Date written: Wednesday, July 25, 2012

Date revised: -

Number of words: 5040 (without abstract, tables, figure and references)

Number of pages: 27

Number of figures: 10

Number of tables: 3

Abstract

Offshore wind turbine generating capacity is increasing and new wind farms are being constructed in deeper and deeper waters. A popular foundation concept for offshore wind turbines is the monopile. A reformulation of the design concept based on rigid piles is needed if this foundation concept is to function effectively in deeper waters at an affordable cost and over the lifetime of the structure. Centrifuge modelling offers a tool for testing monopiles, and this paper deals with three different and important issues for centrifuge testing on monopiles for offshore wind turbines. A series of centrifuge model tests has been conducted on cylindrical stiff model monopiles that were installed at 1g and in-flight before being loaded laterally as well as on conical model piles installed in-flight. All model tests were performed in normally consolidated dense dry sand, simulating drained condition. The tests confirmed three important issues for centrifuge modelling of monopiles for offshore wind turbines. Firstly, to avoid any noticeable grain-size effect, the geometric ratio between average grain-size in poorly graded soils and pile diameter has to be larger than 88. Secondly, the non-linear stress distribution with depth, which is often neglected, has to be taken into account in the analysis of the lateral response. Finally, the pile lateral load-displacement tests confirm that both stiffness and strength increase following in-flight installation and that in-flight installation is needed to avoid any scale effects. This paper illustrates how these three issues are important factors in achieving reliable centrifuge modelling, which is capable of scaling model observations to prototype.

Introduction

Generating capacity from offshore wind turbines is increasing and new wind farms are being constructed in deeper and deeper waters. A popular foundation concept for such offshore wind turbines is the monopile. This is a large diameter hollow steel pile that is driven into the ground to a depth of 5-6 times the diameter. It acts in a rigid manner when subjected to the lateral loads that are transferred to the foundation from the wind turbine with a significant eccentricity. Notwithstanding the rigidity of modern monopiles, today's design method is calibrated for slender piles and should be reformulated to enable this foundation concept to succeed in deeper waters. This justifies the current research on monopiles.

Centrifuge modelling offers a low-cost tool, compared to prototype testing, which allows model observations of the response of offshore foundations to be scaled up effectively to prototype dimensions. The centrifuge modelling technique has been used with success for a range of different offshore foundation problems, and has been used in order to establish design procedures (e.g. Springman (1993), Dean et al. (1998), De Nicola and Randolph (1999), Phillips (2002), Martin (2002), Cassidy et al. (2004) and Bienen et al. (2009)).

Scale effects have been investigated by Nunez et al. (1988), Terashi (1989), Bouafia and Garnier (1991) and Remaud (1999) for long, slender piles that have been loaded laterally, in order to develop reliable modelling techniques. No investigation seems to have been carried out into scale effects for rigid monopiles loaded with a high moment to shear ratio. Therefore, an investigation has been performed in this study into the scaling issues for a monopile.

A centrifuge modelling methodology has been established whereby model observations can be used to analyse a prototype monopile. The investigations have been based on a modelling technique that uses different sizes of piles and stress distributions to simulate the same prototype response, so that any scale effects can be identified. This is known as modelling of models, (Ovesen 1975) and is adopted in this paper for piles of five different sizes.

This paper deals with three different important aspects when performing centrifuge modelling of laterally loaded monopiles for offshore wind turbines: scaling of grain-sizes, installation effects and nonlinearity of the g-field.

Scale effects in the centrifuge

Dimensional analysis is commonly used to transform results from model to prototype scale (Fuglsang and Ovesen 1988), however this requires some knowledge of the relevant phenomena to be able to determine the governing parameters for lateral loading of piles, e.g. (Hansen 1961) and (Randolph 1981). Quasi-static lateral loading of the monopile is assumed in this analysis, with no pore pressure build up during loading, so that the problem can be analysed as an effective stress problem (Li et al. 2010). The outcome of a dimensional analysis can then be written in a form whereby the normalised applied load is derived as a function of a set of non-dimensional ratios, which should be identical at model and prototype scale in order to avoid scale effects (Langhaar 1951), (Fuglsang and Ovesen 1988) and (Wood 2004).

$$\frac{H}{\gamma' \cdot d^3} = f\left(\frac{Y}{d}, \frac{l_L}{d}, \frac{l_e}{d}, \frac{E_s l_L^4}{E_p I_p}, \frac{d}{d_{50}}, \frac{q_c - \gamma \cdot z}{\gamma' \cdot z}, \phi'\right) \qquad (1)$$

A sketch of a laterally loaded pile (Figure 1) is used to define the parameters used in Equation 1.

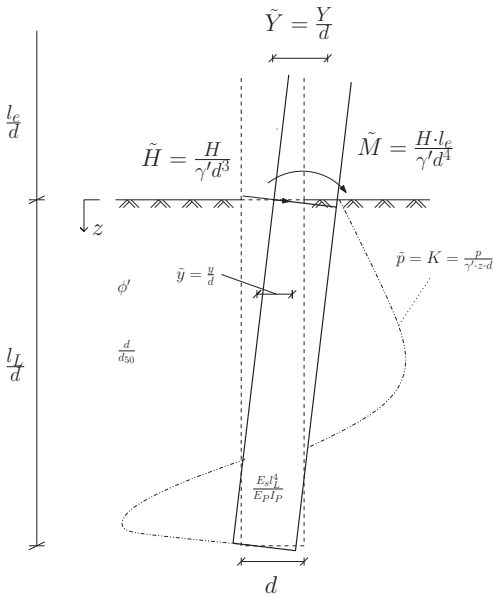

Figure 1 Sketch of laterally loaded pile with key non-dimensional groups

The dimensions of the pile ($l_L / d, l_e / d$) are scaled with the length scale ratio $N_s = d_p / d_m$ (ratio between prototype and model diameter). The non-dimensional stiffness ratio $E_s l_L^{\,4} / E_p I_p$ is also easily obtained from having the same material and stress field in the model and prototype. However, using identical soil in model and prototype, while intended to ensure identical mechanical behaviour in model and prototype, leads to a scaling problem for the size of the grains, e.g. (Gui and Bolton 1998) . The soil resistance in sand is derived from a combination of effective stress and friction, (Briaud et al. 1983) and (Smith 1987), however friction is dependent upon behaviour at particulate scale, and this can be affected by roughness (Garnier and Konig 1998), dilatancy (Bolton 1986) and grain crushing (McDowell and Bolton 1998). A minimum ratio between pile diameter and average grain-size diameter d / d_{50}, in this case, is needed to ensure that the soil behaves in a consistent manner at all geometrical scales, (Ovesen 1975).

In-flight installation is important to replicate the vertical response of axially loaded model piles (Ko, Atkinson et al. 1984). Several studies have shown that the installation method is important for the lateral response as well (Craig 1985, Dyson and Randolph 2001). The majority of centrifuge tests on laterally

loaded monopiles are still performed on piles installed at 1g, e.g. (Remaud 1999), (Ubilla et al. 2006) and (Li et al. 2010). The process that occurs at particulate scale during pile installation is complex, with significant displacement of the sand grains combined with particle abrasion and crushing, (Randolph, Dolwin et al. 1994), (De Nicola and Randolph 1999), (McDowell and Bolton 2000), (White and Bolton 2004), (White and Lehane 2004) and (Weber et al. 2010). The non-dimensional installation stress for the model, $\tilde{Q} = \left(q_c - \gamma \cdot z\right) / \left(\gamma' \cdot z\right)$ should have similarity with the prototype in order to replicate these effects correctly, (Gui and Bolton 1998) and (Bolton, Gui et al. 1999).

The model is placed in a centrifuge to increase the acceleration as a multiplicator η of gravity and to achieve stress levels identical to the prototype. The increase in gravity can be calculated using equation 2. See e.g. (Schofield 1980).

$$\eta = \frac{\omega^2 R}{g} \qquad (2)$$

where ω is the angular frequency of the centrifuge, R is the radius of the rotation measured to a selected point of reference and g is the earth's gravity. Equation 2 demonstrates that acceleration increases with radius, implying that soil density also increases with depth although the vertical stresses in a prototype are assumed to increase linearly. An effective radius $R_e = R_t + l_L/3$ corresponding to 1/3rd of the pile penetration was chosen so that vertical stresses were identical in a model and prototype at a depth of 2/3rds of the pile penetration. This was chosen to minimize the under-stress above R_e and the over-stress below it (Taylor 1995), derived from the difference between linear prototype and parabolic non-linear model (Equation 3) vertical stresses.

$$\sigma_v \approx \rho \cdot \varpi^2 \cdot z \cdot (R_t + \frac{z}{2}) \qquad (3)$$

This implies stress errors between model and prototype of less than 2-3 % for ratios of model depth to effective radius less than 1/15 so that these are usually neglected (Schofield 1980).

The three issues presented above can be studied by performing centrifuge tests on different sized model piles with a stress distribution corresponding to the same prototype. This is called “modelling of models”. This technique has been used before for laterally loaded piles e.g. (Barton 1985), (Nunez et al. 1988), (Terashi 1989) and (Remaud 1999) to investigate solely the grain-size effect.

(Garnier et al. 2007) developed a scaling catalogue for “TC2 –Physical Modelling in Geotechnics” and noted that no grain size effect was detected in “modelling of models” if the ratio between pile diameter and average grain size was larger than 45 (Nunez et al. 1988) or 60 (Remaud 1999) for laterally loaded piles. However, both of these test-sets were performed on long slender piles and the results from these tests should be used with caution for short stiff piles such as monopoles, which are subjected to a high ratio between bending moment and shear force by the wind turbines.

Klinkvort and Hededal (2010) performed “modelling of models” on five stiff monopoles, with ratios between the pile diameter and average grain size larger than 88. All piles were installed at 1g, and scale effects were obtained from relationships between stiffness/strength and applied gravity.

Experimental method

The centrifuge experiments were carried out in a beam centrifuge at the Technical University of Denmark (DTU). The centrifuge, Figure 2, has a radius of 1.7m to the swing and 0.521m from the swing to the sand surface, so that the net radius to the sand surface is R_t=2.221m.

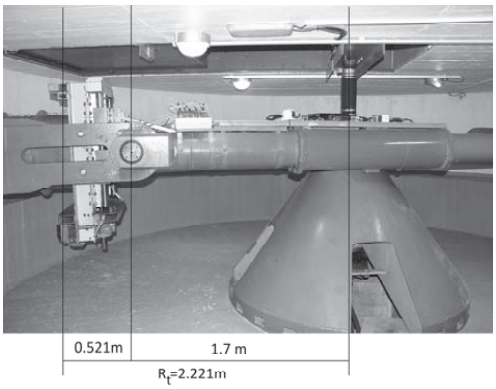

Figure 2 Photograph of the beam centrifuge at DTU

A circular strong box is placed on the swing and a load actuator is mounted on top. The maximum payload of the strongbox and load actuator is 100 gton.

A multipurpose load actuator was mounted on the strongbox container to apply either axial or lateral load to the pile with only small changes to the setup, which consists of a tower which can be moved back and forth perpendicular to the soil surface. A jack, with a capacity of 20kN that operates at a speed of 2mm/s with a maximum stroke of 250 mm, can be mounted between two columns in the tower for CPT tests and for pile installation. A beam can be mounted in the tower to apply lateral loading to the piles, controlled through a feedback loop. Deformation or force controlled loading can be applied and is defined by the user.

The actuator applied one-way, vertical load to the pile until a penetration of 6d was reached, whereupon the vertical jack was removed and the lateral beam was mounted. A sketch of the lateral load actuator and the circular strongbox can be seen Figure 3.

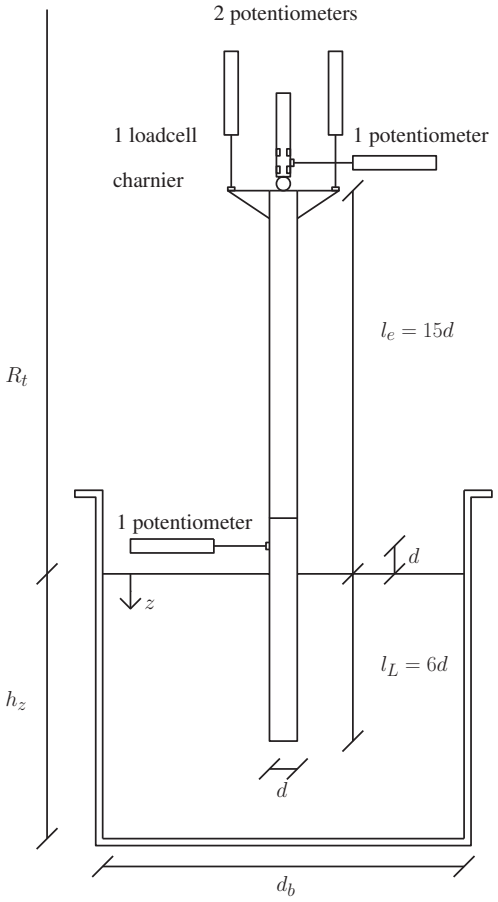

Figure 3 Sketch of the lateral load setup

The diameter of the circular strongbox is d_b=0.52m and the depth of the sand layer is h_z=0.388m. The lateral load was applied to the pile head through a hinge connected to a load cell with a capacity of 2kN. The lateral displacement and the rotation of the pile head was measured by three potentiometers, see Figure 3. One additional displacement measurement was carried out close to the sand surface using a potentiometer. The lateral loading of the piles was controlled so a deformation of 0.5d, measured at the potentiometer close to the sand surface, was achieved in 30 secs. All potentiometers and strain-gauge based load cells were calibrated before and after the tests and showed a high degree of identical linearity.

This setup provided a flexible solution, although it was necessary to stop the centrifuge for the piles installed in-flight to remove the jack and remount the beam for lateral loading. The sand package is affected by this load cycle and leads to a densification of the sand. (Leth 2011) showed, using the DTU centrifuge, that the sand surface will settle around 0.2mm for a density and load cycle similar to one reported in this paper.

The pile testing procedure for the piles installed in-flight was as follows:

1. the soil sample was prepared using a spot pouring hopper and dry pluviation;
2. the package was then mounted in the centrifuge swing;
3. the gravity in the centrifuge is then increased to the level for the given pile (see Table 3) and the pile was installed.

The centrifuge was then stopped and the lateral loading beam was mounted, together with load cell and potentiometers. The centrifuge is again spun up to the given gravity and the monotonic lateral load test is then performed. The test procedure for the piles installed at 1g was quite similar, although the pile was installed at 1g after the centrifuge followed a loading-unloading cycle to and from the required g-level, so there was always one loading cycle.

The test series consisted of 5 monotonic tests with 1g installation of cylindrical piles, 5 monotonic tests with in-flight installation of cylindrical piles and 4 tests performed on piles with a conical shape that were installed in-flight. The conical piles had a circular cross section and the largest diameter at the sand surface. The test programme is shown in Table 3, where dimensions, the increase in acceleration, laterally loading speeds and the relative density used in the different tests can be seen.

The tests were carried out on solid steel piles at a stress distribution identical to a prototype dimension of d=1m in dry sand. The penetration and load eccentricity was kept constant at l_L=6d and l_e=15d for all of the tests. The choice of using solid steel piles, which do not replicate a real wind turbine monopile, was made to ensure that the tested pile would be completely rigid and so that the pile stiffness would be known. The increase in gravity in the sand sample was not constant due to the increase in centrifuge radius with the depth

in the sand sample, which introduced a non-linear stress distribution. It was therefore not possible to model the linear increase seen in the prototype and four conical piles were designed to take account of these small stress errors. Nonetheless, the pile was constructed to be wider in the part where the stresses are too small and the diameter is smaller in the part where the stresses are too high, see Table 3. Full similarity for the forces acting on the different piles is achieved when the stresses are integrated over the width of the pile.

Additionally, one in-flight and one 1g tests was performed using a CPT penetrometer, (Leth 2011) here mounted with a flat tip to investigate the installation procedure in more detail.

Experimental results

Sand properties

The centrifuge experiments were carried out in dry Fontainebleau sand, which is a uniform silica sand from France, consisting of fine and rounded particles, (Leth 2011). The classification data can be seen Table 1.

Specific gravity of particles [g/mm^3]	G_s	2.644
Minimum void ratio	e_{min}	0.532
Maximum void ratio	e_{max}	0.851
Average grain size [mm]	D_{50}	0.21
Coefficient of uniformity	C_U	1.6

Table 1 Classification data for Fontainebleau sand

The average relative density is derived from the total weight and volume of the sand sample for the different tests, and is shown in Table 3. There is a slight change in the density between the different tests but it is believed that this change in relative density, will not affect the results greatly.

Five isotropic consolidated drained triaxial (axial) compression tests were performed on Fontainebleau sand with a relative density of 0.9 and specimen dimensions of HxD=70x70mm, (Jacobsen 1970) to obtain the mechanical properties of the sand. The triaxial tests were carried out with smooth end platens, and deformations were measured within the triaxial chamber.

q' [kPa]	p' [kPa]	ϕ'_{max} [^{o}]	ψ'_{max} [^{o}]
66	38	42.3	16.9
120	70	41.8	16.8
220	133	40.3	14.9
495	315	38.5	13.8
920	607	37.2	12.7

Table 2 Triaxial data at failure

The maximum angle of friction and the maximum angle of dilation were determined from these tests, see Table 2, and the former corresponded well with the predictions made by (Bolton 1986) using Equation 4 and a critical state angle of $\varphi'_{cr}=30^o$, which was not measured and was therefore chosen in order to fit the results. (Bolton 1986) notes that an empirical estimate of the critical state angle of friction for quartz sand is close to 33°, which contradicts earlier findings by (Ovesen 1975) and the Danish Code (DS415 1977) that imply a value closer to 30°, (Springman 2008). In another study by (Gaudin et al. 2005), Fontainebleau sand was tested to determine the critical state angle, which was found to be identical to 30° as well. The value 10 in Equation 4 represents the crushing strength of quartz sand.

$$\varphi'_{\max} \approx \varphi'_{cr} + 3\left(D_r\left(10 - \ln(p')\right) - 1\right) \qquad (4)$$

The triaxial tests showed that both the maximum angle of friction and the angle of dilation are a function of the relative density, crushing strength and the mean stress in the sand, with increased values for denser packings, stronger particles and lower mean stresses.

Centrifuge tests

15 centrifuge tests were carried out. The dimensions and effective scaling factors for the different piles can be seen in Table 3. Model dimensions of the model pile are given together with the corresponding effective scaling factor (η), lateral load velocity (v) and average relative density (D_r) achieved in the tests.

Test ID	d [mm]	l_L [mm]	l_e [mm]	η [-]	v [mm/s]	D_r [%]
T-01	11.2	250	-	89.3	-	84
T-01	11.2	250	-	1	-	84
T-02	16	96	240	62.5	0.266	92
T-03	22	132	330	45.5	0.366	84
T-04	28	168	420	35.7	0.466	86
T-05	34	204	510	29.4	0.566	89
T-06	40	240	600	25.0	0.666	89
T-07	16	96	240	62.5	0.266	90
T-08	22	132	330	45.5	0.366	86
T-09	28	168	420	35.7	0.466	84
T-10	34	204	510	29.4	0.566	96
T-11	40	240	600	25.0	0.666	89
T-12	22.4-21.8	132	330	45.5	0.366	84
T-13	28.7-27.7	168	420	35.7	0.466	90
T-14	35.0-33.5	204	510	29.4	0.566	91
T-15	41.4-39.3	240	600	25.0	0.666	84

Table 3 Dimensions and scale factors for the test piles

Pile installation

The resistance to pile installation is affected by the tip resistance and the shaft friction acting along the pile, (Randolph et al. 1994). A model piezocone (CPTU), with a diameter of 11.3mm and a length of 300mm, was fitted with a flat tip to simulate pile installation. Strain-gauge bridges were mounted on load cells on the shaft and directly behind the tip to measure tip resistance and combined resistance from tip + shaft friction. Pore pressure was measured behind the tip (Leth 2011). The mini piezocone was subjected to a stress field in dry sand identical to that for a prototype monopile, with a diameter of 1m. The tip resistance is compared with the total driving stress q_p, which is calculated from the driving force F divided by the pile area. Tip resistance

q_c is found as the force at pile tip divided by pile area. The results from driving stress and tip resistance can be seen in Figure 4.

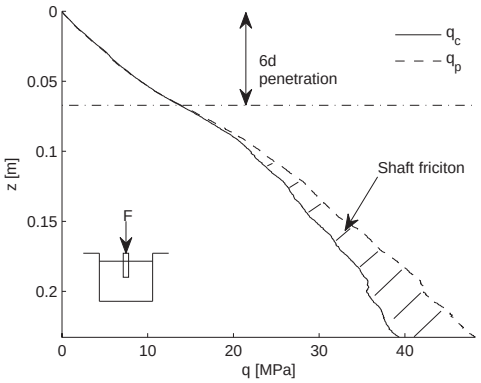

Figure 4 Installation resistance of CPT with flat tip, cone pressure versus penetration

The force acting on the pile for 1g installation was too small to give meaningful results and is therefore not shown. The driving stress and the tip stress are identical to approximately 100 mm depth in the soil sample, before any shaft friction is mobilised, and the rate of increase of the tip resistance is decreasing below this depth. This is probably due to a change from a shallow failure mechanism in the upper part of the pile penetration to a combined failure mode in end bearing and shaft friction in the deeper part of the pile penetration, (Gui and Bolton 1998). The shallow failure is related to a mechanism similar to one known from bearing capacity theory with rupture lines going from pile tip to sand surface; (Vesic 1963) calls this general shear failure. The failure at greater depth is related to a combination of grain crushing, followed by cylindrical cavity expansion, and is interpreted by (Vesic 1963) as a local shear failure. A horizontal line is shown in Figure 4 at a depth of 62.7 mm to indicate the depth of 6 pile diameters. This corresponds to the penetration depth of the piles for this investigation and suggests that the shaft friction has not been mobilised sufficiently for pile installation to a maximum depth of 6d. It therefore seems valid to assume that the pile tip stress q_c and the forcing stress q_p are identical. This enables the calculation of the pile tip stress as:

$$q_c \approx q_p = \frac{F}{\pi/4 \, d^2} \qquad (5)$$

This approximation is used in the entire test series in the analysis of pile installation.

1g pile installation

The force measured during 1g installation is plotted in Figure 5. The data was logged continuously at a sampling frequency of 10 Hz for all of the tests.

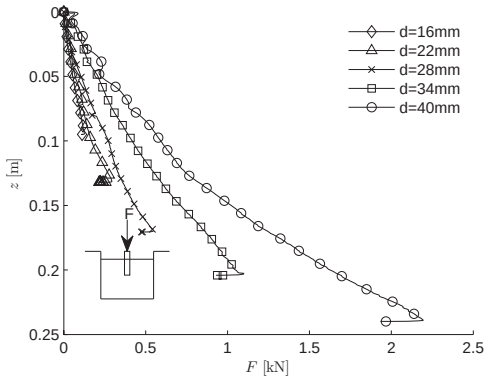

Figure 5 Installation of piles at 1g, axial load versus penetration.

The installation resistance curves for the different piles show increasing resistance with depth and are all quite smooth, indicating that the soil sample was homogenous for all tests. Surface heave, with circular rupture lines, was seen on the surface around the piles for all those installed at 1g, and especially for the larger piles. The stress state for piles installed at 1g is low, which leads to high a degree of dilatancy and volume increase for dense sands, especially for the shallow mechanism. This was also observed from the five triaxial tests performed in connection with this study. The surface heave is closely related to this fundamental sand behaviour.

In-flight installation

The force required to install the piles in-flight is shown in Figure 6. All piles were installed at the same stress levels. Here, too, the curve shows increase in load with depth and the results implies that a homogenous sample has been prepared. No surface heave was observed in soil around piles installed in-flight, confirming

the hypothesis of the surface heave at 1g installation is related to dilatancy of the sand, whereas local crushing occurs during pile installation at the higher stresses and suppresses dilatancy.

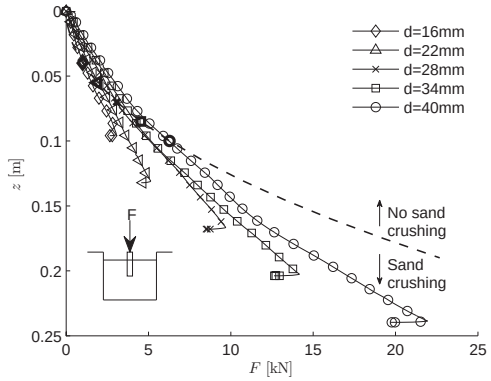

Figure 6 Installation of piles in-flight, axial load versus penetration

This is consistent with Equation 4.

The pile tip stress is around 10 times greater than for a pile installed at 1g. (McDowell and Bolton 1998) showed that the tensile strength of sand grains can be exceeded under compression, and also crushing of grains was reported to occur at a pile tip stress of 5 MPa (Yang et al. 2010). A pile tip stress of 5 MPa is reached at a depth of approximately 2.5 pile diameters and below for the piles installed in-flight. This zone is shown in Figure 6 as a dashed line.

A normalisation procedure was used to interpret the pile installation further, as proposed by (Bolton et al. 1993) for interpretation of CPT tests. The tip stress is normalised with soil stresses and the depth z is normalised by the pile diameter.

$$\tilde{Q} = \frac{q_c - \sigma_v}{\sigma'_v} \qquad (6)$$

$$\tilde{Z} = \frac{z}{d} \qquad (7)$$

The vertical stress is found using equation 2 for in-flight installation at a scaling factor of η, and is defined as shown in equation 8 for 1-g installation.

$$\sigma_v = \rho \cdot g \cdot z \qquad (8)$$

The total stresses are equal to the effective stresses for the dry sand and it is possible to compare the installation procedures at 1g and in-flight with this normalisation procedure.

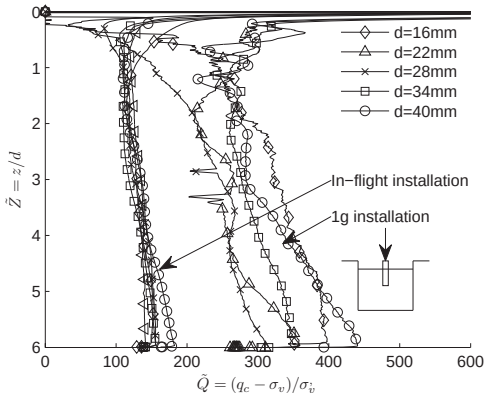

Figure 7 Normalisation of pile installation, normalised end bearing resistance versus normalised depth

The comparison is shown in Figure 7 where it is seen that that installations at 1g produces a large scatter in the normalised tip stress due to the very low mean stress during installation. The data acquisition also becomes less precise at low vertical stresses.

Normalisation of the tip stress indicates that no scale effects are apparent for different pile diameters for the in-flight installation, with only a difference of 5%. A clear scale effect is seen in contrast to this for the 1g installation. (Borghi et al. 2001) reported effects from the diameter on the pile tip stress for piles installed in-flight. The effect caused by the larger diameter was explained by an increase in pile tip stress for smaller piles due to greater frictional force acting along the shaft. The results here do not show any sign of this effect, which indicates that the assumption of low friction is valid. The increase in normalised pile tip stress

indicates that a critical depth was not reached and the assumption of a shallow failure therefore seems appropriate.

Lateral loading

After installation, the piles were loaded laterally and both deflection and force was normalised, according to the dimensional analysis shown in equation 1. The deflection, Y measured one diameter above the sand surface, is normalised by the pile diameter, d.

$$\tilde{Y} = \frac{Y}{d} \qquad (9)$$

The force H applied 15 pile diameters above the sand surface is normalised by the in-flight effective bulk unit weight and the cube of the diameter.

$$\tilde{H} = \frac{H}{\gamma' \cdot d^3} \qquad (10)$$

Grain-size effect

The results of the lateral loading for the cylindrical piles installed at 1g can be seen in Figure 8.

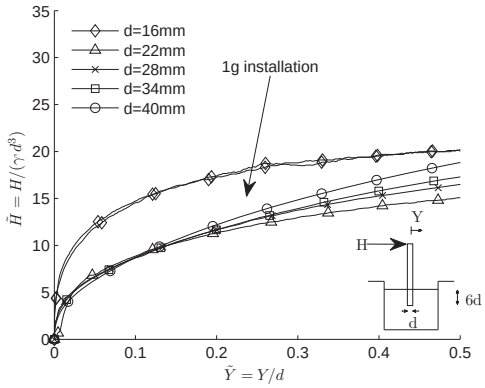

Figure 8 Lateral loading of cylindrical piles, 1g installation, normalised lateral load versus normalised lateral deflection

The response is significantly different for the d=16mm pile compared to the others, showing high initial stiffness before approaching a failure plateau that was higher than the other piles. The test was therefore repeated and identical results were obtained. This is clearly an outlier and it is concluded that the ratio between diameter of the pile and diameter of average grain size d/d_{50}=88 is too small, which leads to a grain size effect. This ratio is 30% higher than reported by (Remaud 1999). The response is more or less identical until a normalised deflection of 0.1 is reached for the four other piles, and the load-deflection curves start to deviate at larger deflections. The capacity of the piles with large diameter increases more rapidly than the piles with smaller diameter and the difference at a deflection of 0.5 d is about 25% between the d=22mm and d=40mm piles, indicating scale effects.

Installation effect

The same five piles were tested with the in-flight installation procedure, and the load-deflection curves are shown in Figure 9.

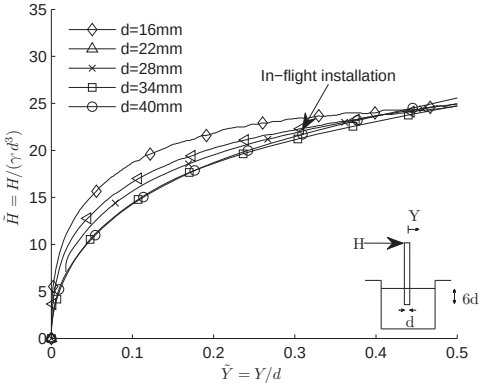

Figure 9 Lateral loading of cylindrical piles, inflight installation, normalised lateral load versus normalised lateral deflection

The response from the 16mm diameter pile shows again a high initial stiffness and approaches a failure plateau at large deflection, even though the tendency is not that clear. It is concluded that the pile is too small. The response for the rest of the piles installed in-flight seems to be more consistent than for the piles installed at 1g, but a scale effect is still seen with larger initial stiffnesses for the smallest piles.

The lateral response of the piles installed both at 1g and in-flight can be seen in Figure 8 and Figure 9, whereby the piles installed in-flight show a greater initial stiffness and higher normalised bearing capacities than the piles installed at 1g. This is in agreement with the observations made by (Craig 1985) and (Dyson and Randolph 2001).

g-field effect

To investigate the influence of g-field, conical shaped piles were designed to counteract the change in g-field with depth, and the load deflection curve is plotted in Figure 10.

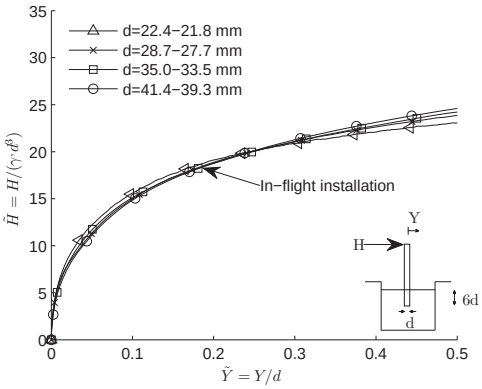

Figure 10 Lateral loading of conical monopiles, inflight installation, normalised lateral load versus normalised lateral deflection

Here only four piles was created, because it was concluded that the d=16m pile was too small. The required installation force, not shown here, for the piles with a conical shape is similar, but are approximately 5% smaller compared to those obtained for the cylindrical piles. A very good agreement between the normalized load-deflection results was achieved. The stiffness of the larger piles increases more rapidly, than the smaller piles, but the effect almost negligible. This demonstrates that it is possible to model the same normalised response using different sized piles.

Discussion

The centrifuge tests represent simplifications of the complex wind-water-structure-soil interaction problem for a monopile supporting an offshore wind turbine and some of these simplifications are discussed here.

Although, an offshore monopile is installed in saturated soil conditions, the centrifuge test series was carried out in dry dense sand to represent an effective stress scaling approach. This modelling technique was also used by (Li et al. 2010). This simplification seems to be appropriate for the investigation of scale effects and the observations made under dry conditions are also believed to be valid for the drained saturated condition.

The stress field applied to the piles corresponds to stresses for a prototype pile with a diameter of d=1m. This stress distribution is therefore smaller compared to the prototype case where pile diameters of 5-6 metres are regularly used in practice. Even though the tests were performed in a lower stress field, it is believed that the observations made here are also valid for higher stress fields.

This study shows that the ratio between pile diameter and average grain size has to be above 88 for a smooth stiff pile, to avoid grain size scale effects. This is nearly 30 % more than the limit recommended by (Garnier et al. 2007), which is based on tests on slender piles. One reason for this increase in ratio could be the fact that the stiff piles load the sand over the whole length of the pile, which is not the case for a slender pile. The ratio between grain size and pile diameter is therefore more important for stiff piles than for slender piles.

The maximum angle of friction and the dilation angle determined from triaxial testing were seen to be controlled by the stress level. This implies that the sand surrounding the piles installed at 1g is subjected to greater dilation than piles installed in-flight. The surface heave around the piles provides convincing evidence. Both (Craig 1985) and (Dyson and Randolph 2001) report an effect from the in-flight installation but it does not seem to be a common procedure in the literature for monopiles. The driving force for the installation of these large diameter piles is probably the reason for this choice. This study shows that not only the stiffness and the strength are smaller using 1g installation. It also finds that the piles are showing scale

effects due to the lack of stress similarity during installation. It is therefore important to perform the installation under soil stresses corresponding to prototype.

A scale effect was seen even for the piles installed in-flight. The explanation for this is suggested to be the non-linear stress distribution, which is not identical for the different tests. This was investigated with conically shaped piles, to take account of the non-linear stress distribution. The conical piles can be viewed as tapered piles with a small taper angle. (El Naggar and Sakr 2000) performed centrifuge tests with tapered piles and showed that the axial response increased with increasing taper angle. A slightly smaller installation force was found for the piles when comparing the installation of the conical piles with the cylindrical ones showed for the conical piles. This is in contrast to the observation seen in (El Naggar and Sakr 2000) and it is believed to be related to the very low taper angle used in this research. The influence of the taper angle is therefore negligible and the installation force is smaller due to a smaller pile tip. Only the lateral response was affected when conical piles were used. The lateral response using conical shaped demonstrated almost identical normalised load-deflection responses. The results supported the hypothesis of the influence of the stress distribution on the lateral response.

Conclusions

The centrifuge modelling technique has been used with success for a number of offshore foundation problems, and it therefore also seems appropriate to use the technique to investigate the lateral response of offshore monopiles for wind turbines. Scale effects have been investigated for laterally loaded piles in order to develop a reliable modelling technique, but these investigations have been for long slender piles. No investigation of scale effects seems to have been carried out to date for rigid monopiles.

This research demonstrated that the concept of ‘modelling of models’ can be used in order to establish a centrifuge modelling procedure whereby model observations can be used to analyse a prototype monopile.

One attempt to model the same lateral normalised response was performed using five different sized piles installed at 1g. The test results showed different normalised responses, indicating the presence of scale

effects. The smallest pile, with a pile diameter of d=16mm, produced a different load-displacement response compared to the other piles and indicated that the ratio between pile diameter and average grain size was too small.

The same five piles were used again but this time the piles were installed in-flight. Scale effects were seen in the normalised lateral response. The smallest pile, with a pile diameter of d=16mm, showed a response comparable with to that for 1g installation, and it was concluded that the pile was too small relative to the grain size. The tests show that the initial stiffness and the maximum bearing capacity were increased with in-flight installation of monopiles, confirming results seen before.

Conical piles were used in a third attempt to perform a successful modelling of models test series. Using conically shaped piles to counteract the effect of the non-linear stress distribution, full similarity of the force acting on the piles can be achieved. The normalised lateral responses showed nearly identical performance and it was therefore possible to model the same prototype behaviour with different pile sizes. The assumption of a linear stress distribution should be used with care.

The test series shows that the ratio of pile diameter to average grain size for centrifuge modelling of monopiles, the non-linear stress distribution and the installation process are key modelling parameters. It is possible to scale centrifuge results of rigid monopiles to prototype scale with due consideration of these effects.

References

BARTON, Y.O., 1985. RESPONSE OF PILE GROUPS TO LATERAL LOADING IN THE CENTRIFUGE. *Proceedings of a Symposium on the Application of Centrifuge Modelling to Geotechnical Design*, pp. 457-473.

BIENEN, B., CASSIDY, M.J. and GAUDIN, C., 2009. Physical modelling of the push-over capacity of a jack-up structure on sand in a geotechnical centrifuge. *Canadian Geotechnical Journal*, **46**(2), pp. 190-207.

BOLTON, M.D., GUI, M.W., GARNIER, J., CORTE, J.E., BAGGE, G., LAUE, J. and RENZI, R., 1999. Technical Notes - Centrifuge cone penetration tests in sand. *Géotechnique*, **49**(4).

BOLTON, M.D., 1986. Strength and dilatancy of sands. *Géotechnique*, **36**(1), pp. 65-78.

BOLTON, M.D., GUI, M.W. and PHILLIPS, R., 1993. Review of Miniature Soil Probes For Model Tests. *Eleventh Southeast Asian Geotechnical Conference*, .

BORGHI, X., WHITE, D.J., BOLTON, M.D. and SPRINGMAN, S., 2001. Empirical pile design based on cone penetrometer data: an explanation for the reduction of unit base resistance between CPTs and piles, *Proceedings of the 5th International Conference on Deep Foundation Practice* 2001.

BOUAFIA, A. and GARNIER, J., 1991. Experimental study of p-y curves for piles in sand. *Proceedings, International Conference "Centrifuge'91"*, pp. 261-268.

BRIAUD, J., SMITH, T.D. and MEYER, B.J., 1983. USING THE PRESSUREMETER CURVE TO DESIGN LATERALLY LOADED PILES. *Proceedings - Annual Offshore Technology Conference*, **1**, pp. 495-502.

CASSIDY, M.J., RANDOLPH, M.F. and BYRNE, B.W., 2004. A comparison of the combined load behaviour of spudcan and caisson foundations on soft normally consolidated clay. *Géotechnique*, **54**(2), pp. 91-106.

CRAIG, W.H., 1985. Installation studies for model piles. *Proceedings of a Symposium on the Application of Centrifuge Modelling to Geotechnical Design*, pp. 441-456.

DE NICOLA, A. and RANDOLPH, M.F., 1999. Centrifuge modelling of pipe piles in sand under axial loads. *Géotechnique*, **49**(3), pp. 295-318.

DEAN, E.T.R., JAMES, R.G., SCHOFIELD, A.N., JAMES, R.G., SCHOFIELD, A.N. and TSUKAMOTO, Y., 1998. Drum centrifuge study of three-leg jackup models on clay. *Géotechnique*, **48**(6), pp. 761-785.

DS415, 1977. Danish Code of Practice for Foundation Engineering. *Danish Technical Press, Copenhagen*, **2nd edition**.

DYSON, G.J. and RANDOLPH, M.F., 2001. Monotonic lateral loading of piles in calcareous sand. *Journal of Geotechnical and Geoenvironmental Engineering*, **127**(4), pp. 346-352.

EL NAGGAR, M. and SAKR, M., 2000. Evaluation of axial performance of tapered piles from centrifuge tests. *Canadian geotechnical journal*, **37**(6), pp. 1295-1308.

FUGLSANG, L.D. and OVESEN, N.K., 1988. The application of the theory of modelling to centrifuge studies. *Centrifuges in Soil Mechanics*, pp. 119-138.

GARNIER, J., GAUDIN, C., SPRINGMAN, S.M., CULLIGAN, P.J., GOODINGS, D., KONIG, D., KUTTER, B., PHILLIPS, R., RANDOLPH, M.F. and THOREL, L., 2007. Catalogue of scaling laws and similitude questions in geotechnical centrifuge modelling. *International Journal of Physical Modelling in Geotechnics*, **7**(3), pp. 1-23.

GARNIER, J. and KONIG, D., 1998. Scale effects in piles and nails loading tests in sand. *Centrifuge 98*, **1**, pp. 205-210.

GAUDIN, C., SCHNAID, F. and GAMIER, J., 2005. Sand characterization by combined centrifuge and laboratory tests. *International Journal of Physical Modelling in Geotechnics*, **5**, pp. 42-56.

GUI, M.W. and BOLTON, M.D., 1998. Geometry and scale effects in CPT and pile design, *Geotechnical Site Charecterization* 1998, Balkema, pp. 1063.

HANSEN, J.B., 1961. Ultimate resistance of rigid piles against transversal forces. *Geoteknisk Institut (Danish Geotechnical Institute -- Bulletin* 12), pp. 5-9.

JACOBSEN, M., 1970. *New oedometer and new triaxial apparatus for firm soils. Geoteknisk Institut (Danish Geotechnical Institute).*

KLINKVORT, R.T. and HEDEDAL, O., 2010. Centrifuge modelling of offshore monopile foundation. *Frontiers in Offshore Geotechnics II*, pp. 581-586.

KO, H.Y., ATKINSON, R.H., GOBLE, G.G. and EALY, C.D., 1984. Centrifuge modelling of pile foundations. *Analysis and Design of Pile Foundations. Proceedings of a Symposium in conjunction with the ASCE National Convention*, pp. 21-40.

LANGHAAR, H.L., 1951. *Dimensional Analysis and Theory of Models.* London: Chapman & Hall.

LETH, C.T., 2011. *Centrifuge modelling of large diameter pile in sand subject to lateral loading.* SR 11-09. http://www.byg.dtu.dk/Publikationer/Byg_rapporter.aspx: DTU Civil Engineering.

LI, Z., HAIGH, S.K. and BOLTON, M.D., 2010. Centrifuge modelling of mono-pile under cyclic lateral loads. *Physical Modelling in Geotechnics*, pp. 965-970.

MARTIN, C.M., 2002. Impact of centrifuge modelling on offshore foundation design. *Constitutive and centrifuge modelling: two extremes*, pp. 135-153.

MCDOWELL, G.R. and BOLTON, M.D., 2000. Effect of particle size distribution on pile tip resistance in calcareous sand in the geotechnical centrifuge. *Granular Matter*, **2**(4), pp. 179-187.

MCDOWELL, G.R. and BOLTON, M.D., 1998. On the micromechanics of crushable aggregates. *Geotechnique*, **48**(5), pp. 667-679.

NUNEZ, I.L., PHILLIPS, R., RANDOLPH, M.F. and WESSELINK, B.D., 1988. Modelling laterally loaded pile in calcareous sand. *Centrifuge 88*, pp. 353-362.

OVESEN, N.K., 1975. Centrifugal testing applied to bearing capacity problems of footings on sand. *Géotechnique*, **25**(2), pp. 394-401.

PHILLIPS, R., 2002. Centrifuge modelling of failures and safe structures. *Constitutive and centrifuge modelling: two extremes*, pp. 183-189.

RANDOLPH, M.F., 1981. Response of flexible piles to lateral loading. *Géotechnique,* **31**(2), pp. 247-259.

RANDOLPH, M.F., DOLWIN, J. and BECK, R., 1994. Design of driven piles in sand. *Géotechnique,* **44**(3), pp. 427-448.

REMAUD, D., 1999. Pieux sous charges latérales: étude expérimentale de l'effet de groupe. *Ph.D. thesis*.

SCHOFIELD, A.N., 1980. Cambridge geotechnical centrifuge operations. *Géotechnique,* **30**(3), pp. 227-268.

SMITH, T.D., 1987. PILE HORIZONTAL SOIL MODULUS VALUES. *Journal of Geotechnical Engineering,* **113**(9), pp. 1040-1044.

SPRINGMAN, S.M., 2008. Niels Krebs Ovesen: his Legacy to Physical Modelling. *Spirit of Krebs Ovesen Session – challenges in geotechnical engineering, Geoteknisk Institut (Danish Geotechnical Institute -- Bulletin* 23).

SPRINGMAN, S.M., 1993. Centrifuge modelling in clay: Marine applications. *4th Canadian Conference of Marine Geotechnics, Newfoundland,* **3** (Invited keynote lecture), pp. 853-896.

TAYLOR, R.N., 1995. *Geotechnical centrifuge technology*. London: Blackie Academic.

TERASHI, M., 1989. Centrifuge modeling of a laterally loaded pile. *Proceedings of the International Conference on Soil Mechanics and Foundation Engineering,* **2**, pp. 991-994.

UBILLA, J., ABDOUN, T. and ZIMMIE, T., 2006. Application of in-flight robot in centrifuge modeling of laterally loaded stiff pile foundations. *Physical Modelling in Geotechnics,* **1**, pp. 259-264.

VESIC, A.B., 1963. Bearing capacity of deep foundations in sand. *National Research Council -- Highway Research Board -- Research Record,* (39), pp. 112-153.

WEBER, T.M., PLOTZE, M., LAUE, J., PESCHKE, G. and SPRINGMAN, S.M., 2010. Smear zone identification and soil properties around stone columns constructed in-flight in centrifuge model tests. *Géotechnique,* **60**(3), pp. 197-206.

WHITE, D.J. and BOLTON, M.D., 2004. Displacement and strain paths during plane-strain model pile installation in sand. *Géotechnique,* **54**(6), pp. 375-397.

WHITE, D.J. and LEHANE, B.M., 2004. Friction fatigue on displacement piles in sand. *Géotechnique,* **54**(10), pp. 645-658.

WOOD, D.M., 2004. *Geotechnical Modelling - applied geotechnics volume 1*. 1 edn. Great Britain: Spon Press.

YANG, Z.X., ZHU, B.T., FORAY, P., JARDINE, R.J., ZHU, B.T., FORAY, P. and TSUHA, C.H.C., 2010. Sand grain crushing and interface shearing during displacement pile installation in sand. *Géotechnique,* **60**(6), pp. 469-482.

Paper III

"Monotonic soil-structure interaction of monopile support for offshore wind turbines"

R. T. Klinkvort & O. Hededal

Submitted for publication -, *2012*

Monotonic soil-structure interaction of monopile support for offshore wind turbines

Rasmus Tofte Klinkvort and Ole Hededal

Abstract: Currently monopiles is the preferred foundation solution for offshore wind turbines. The design of these monopiles relies on empirical data from tests performed on long slender small diameter piles loaded predominantly in shear. In contrast, a monopile is a large diameter relatively short pile, where load is applied with a large eccentricity. With centrifuge tests as the basis, this paper discusses the effects on the non-linear soil-pile interaction in sand from changing the stress level and the load eccentricity. Hence, a test series was carried out to simulate idealised load situations for monopiles supporting an offshore wind turbine. Centrifuge tests were performed on model monopiles subjected to stress levels equal to prototype monopiles with a diameter ranging from 1-5 meters. It was possible to merge these tests into one general response using Rankine's passive earth pressure coefficient as a normalisation parameter. The effect of load eccentricity was investigated by considering five different eccentricities. The main conclusions from these tests were, the initial stiffness of the soil-pile response was increasing linearly and ultimate soil resistance seemed unaffected by the load eccentricity, which is in agreement with the current design methodology. The size of the ultimate soil resistance, the magnitude of the stiffness and the shape of the soil-pile interaction were all different from the current design methodology.

Key words: Monopiles, Monotonic loading, Centrifuge modelling, p-y curves, Sand, Initial stiffness, Ultimate capacity.

1. Introduction

Monopiles are today one of the most popular foundation methods for offshore wind turbines. These piles are often installed in dense sand at water depths ranging from 10-30 meters. A monopile is a single, large diameter tubular steel pile driven 5 to 6 times its diameter into the seabed. The diameter of the piles ranges from 4-6 meters. Monopiles for wind turbines are affected by lateral loads from waves and wind, which subject the pile at seabed level to shear forces and moments corresponding to the load eccentricity; this is illustrated at Figure 1. Today, the design of monopiles is carried out by modelling the pile as a beam and the soil as a system of uncoupled non-linear springs, (API 2007). This method has successfully been used in pile design for offshore oil and gas platforms. The design methodology originates from tests on long slender piles with a small load eccentricity, (Reese and Matlock 1956; McClelland and Focht 1956). Even though this methodology was originally calibrated to slender piles, it is today used for design of large diameter rigid monopiles. Still, the methodology lacks of scientific justification and a better understanding of rigid piles is needed. This is the motivation for current research on monopiles. In this context, centrifuge modelling offers a low-cost tool, compared to prototype testing, and if handled correctly makes it possible to scale model observations to prototype. The centrifuge modelling technique have successfully been used for a number of offshore foundation problems to establish design procedures e.g. (Bienen, Cassidy, and Gaudin 2009; Cassidy, Randolph and Byrne 2004; De Nicola and Randolph 1999).

Fig. 1. Non-dimensional dimensions of a typical offshore wind turbine

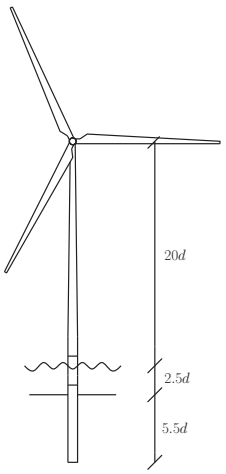

In order to understand the behaviour of a pile, it is important to recognize the stresses acting on the pile. When a pile is moved in a soil continuum, passive earth pressure will act in front of the pile, friction on the side of the pile and active pressure will load the back of the pile. The sum of these components will resist the pile movement. These are three independent forces acting on the pile, but as a simplification the three forces can be combined into one resulting force over the

Received . Revision received . Accepted . Revision accepted .

Rasmus Tofte Klinkvort. Dept. of Civil Engineering, Technical University of Denmark, Sec. of Geotechnics and Geology, Brovej Building 118, 2800 Kgs. Lyngby, Denmark
Ole Hededal. Dept. of Civil Engineering, Technical University of Denmark, Sec. of Geotechnics and Geology, Brovej Building 118, 2800 Kgs. Lyngby, Denmark

DOI: 10.1139/

pile width, (Briaud, Smith and Meyer 1983; Smith 1987). The soil resistance can as a simplification be described as the effective vertical stress (σ'_v) in a given depth, which is found as the effective unit weight (γ') , multiplied the depth in the soil (z), integrated over the diameter of the pile (d), multiplied by an earth pressure coefficient (K) representing the mobilised resistance.

$$[1] \qquad p \approx K \cdot \sigma'_v \cdot d$$

It is important to recognise that the earth pressure coefficient, K, here incorporates the friction on the side of the pile and is therefore the sum of active soil pressure, passive soil pressure and side friction. This modulus approach is used by different researcher's e.g. (Brinch Hansen 1961 ; Broms 1964; Briaud, Smith and Meyer 1983; API 2007).

The earth pressure coefficient is a function of a set of parameters depending on the soil behaviour (ϕ', E_s), pile material (δ, E_pI_p), pile geometry $(\frac{z}{d})$, pile installation $(Inst.)$ and degree of mobilisation $(\frac{y}{d})$. For a rigid monopile this can be written as:

$$[2] \qquad K = f\left(\phi', E_s, \delta, E_pI_p, \frac{z}{d}, Ins., \frac{y}{d}\right),$$

The soil-pile interaction is thus a function of the degree of mobilisation controlled by the normalised displacement of the pile. Especially, the initial stiffness of this function and the ultimate capacity has been investigated by different authors and the conclusions of the findings are contradictory. The ultimate capacity was studied by Zhang, Silva and Grismala 2005 who collected data from 17 different tests; both centrifuge and full scale. They presented a method to determine the ultimate capacity of a pile by using Rankines passive soil pressure coefficient squared for the ultimate soil pressure. The initial stiffness was investigated by Fan and Long 2005 and Ashford and Juirnarongrit 2003,they agreed with the original assumption by Terzaghi 1955, that there is no effect from the diameter on the initial stiffness of the p-y curves. This is also the conclusion by Pender, Carter and Pranjoto 2007 who compared a series of full scale test and states that the apparent diameter size effect is a consequence of the distribution of the soil modulus. On the other hand numerical modelling by Lesny and Wiemann 2006 and Sorensen et al. 2009 suggest an effect of changing the diameter on the initial stiffness of the p-y curves.

The general tendency of the research performed on monopiles is that the current design values of the initial stiffness are too large, e.g. (Rosquot et al. 2007; Lesny and Wiemann 2006; Abdel-Rahman and Achmus 2005; Augustesen et al. 2009. The problem with these findings is that they are not in agreement with the findings from full scale monitoring on monopiles which states that the recommenced value is too small, (Hald et al. 2009).

The purpose of this paper is to investigate the earth pressure coefficient (K) both in terms of initial stiffness, ultimate capacity and shape. The investigation is performed with the application for wind turbine foundation in mind. This means that the tests are performed on rigid piles with a high load eccentricity and a stress distribution corresponding to piles with diameters ranging from 1 to 5 meters. This is in both cases in contrast to the tests that the current practice relies on.

2. Soil-pile interaction

The formulation of the soil-pile interaction used in the analysis of laterally loaded piles have been given special attention since the development of the semi-empirical based method was developed in the 1950^{ies}. A number of different proposals describing the soil-pile interaction have been given, e.g. (Reese, Cox and Koop 1974; Murchison and O'Neill 1984; Norris 1986; Wesselink et al. 1988; Georgiadis, Anagnostopoulos and Saflekou 1992). All of these studies have been on long slender piles.

Here is presented two methods to calculate the pile-soil interactions. The first one, is the API 2007 design method and is based on the formulation proposed by Murchison and O'Neill 1984. The second one, is based on the hyperbolic stress strain response proposed by Kondner 1963. This method was found to be superior to the other methods in the prediction of experiments on laterally loaded piles Georgiadis, Anagnostopoulos and Saflekou 1992 and Kim et al. 2004.

The modulus approach shown in eq. 1 is the basic framework and the original formulations are therefore rewritten to be expressed as an earth pressure coefficient. For both of the methods the soil-pile interaction is a function of initial stiffness, maximum capacity and pile displacement. The calculations of these values are here identical for the two methods and the recommendations from API 2007 is here used. The initial stiffness is given by the subgrade modulus (k) multiplied the depth in the soil (z), and is assumed to increase linear with depth, this is normalised with the vertical effective stress.

$$[3] \qquad \tilde{E}_{py} = \frac{k \cdot z}{\sigma'_v}$$

Reese, Cox and Koop 1974 proposed a methodology to calculate the ultimate capacity K_{ult} using plasticity theory;

$$[4] \qquad K_{ult} = A \cdot \min \begin{cases} (C_1 \cdot \frac{z}{d} + C_2) & \text{shallow depth} \\ C_3 & \text{great depth} \end{cases}$$

Here the coefficients C_1, C_2 and C_3 is found by plasticity theory and is only dependent of angle of friction. The value of K_{ult} is found as the minimum value of the expressions showed in eq. 4. Where the upper expression defines a failure in shallow depths and the lower is failure in great depth. A is an empirical constant which was used to fit the original test results with theory. For monotonic loading $A = \left(3.0 - \frac{0.8X}{D}\right) \geq 0.9$.

The formulation of the non-linear soil-pile interaction spring, also known as the p-y relationship, is expressed by a hyperbolic tangent function in the API 2007 method. Here shown in the normalised form as the earth pressure coefficient.

$$[5] \qquad K = K_{ult} \cdot \tanh\left[\frac{k \cdot z}{\sigma_v} \cdot \frac{1}{K_{ult}} \cdot \frac{y}{d}\right]$$

Alternatively, the hyperbolic equation proposed by Kondner 1963 may be used:

$$[6] \qquad K = \frac{y/d}{\frac{\sigma_v}{k \cdot z} + \frac{1}{K_{ult}} \cdot \frac{y}{d}}$$

The two formulations have identical initial stiffness and ultimate asymptotic capacity but the shape of the functions are different. The applicability of the two formulations will be part of the analyses based on the results from the performed centrifuge tests.

3. Experimental Methodology

A centrifuge test program was designed to investigate the stress level and the load eccentricity effects for a monopile supporting a wind turbine installed in sand, see Table 1. The penetration depth of the pile was for the entire test series kept constant to $l_l = 6d = 240mm$. Ten test were performed; five test in dry sand with a constant load eccentricity of $l_e = 15d = 600mm$ and stress distributions identical with a prototype pile with diameter ranging from d=1m - 5m, and five test in saturated sand with load eccentricities ranging from $l_e = 8.25d - 17.25d = 330 - 690mm$. The pile was loaded at the pile top and the deflection of the pile was measured $2d$ above the sand surface. The centrifuge experiments were carried out using the centrifuge at the Technical University of Denmark. The centrifuge is a beam centrifuge with a radius of $1.7m$ to the swing. In the swing a circular strongbox is placed and the distance from the swing to the sand surface is 0.521 m, (Fuglsang and Nielsen 1988a). A sketch of the basic pile setup ($l_e = 15d$) for laterally loading of a strain-gauge mounted monopile can be seen in Fig. 2. The strong box have a diameter of $d_b = 500mm$ and the height of the sand sample is $h_z = 388mm$. Centrifuge modelling theory is today standard procedure and can be seen in e.g. (Schofield 1980; Fuglsang and Ovesen 1988b).

All piles were installed in-flight, but at a stress level three times smaller than the level at which the monotonic test was performed. This was done due to a 20 kN limit on the jack. The installation at a lower stress level will lead to a softer response; this was demonstrated in Dyson and Randolph 2001, but the effect from a lower installation stress will affect the piles in the same degree and the results are therefore comparable. Pilot test carried out prior to the present study demonstrates that this would not be the case if the pile was installed at 1g. The procedure for the test sequence was to spin the centrifuge up and install the pile. Then the centrifuge has to be stopped to remove the jack and then mount the lateral loading equipment. Afterwards the centrifuge was accelerated again, to a given soil stress level and the monotonic lateral test was performed. It is assumed that the effect of this procedure is negligible.

The pile used in the tests is a solid steel pile with a diameter of $36mm$. Strain-gauges are glued to the pile and protected

Fig. 2. Sketch of the test setup

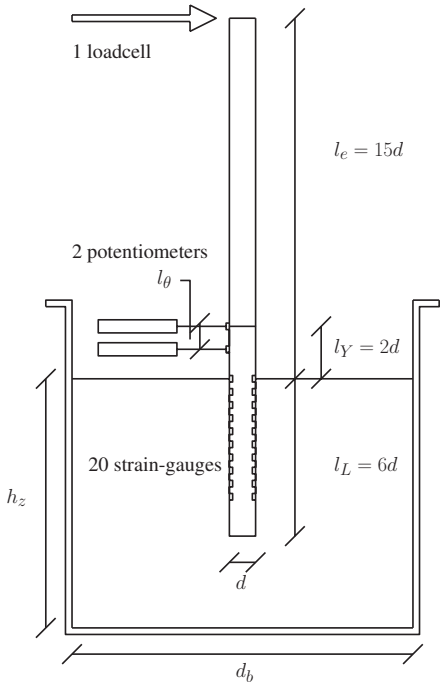

by a $2mm$ epoxy coating. This leads to a total model pile diameter of $40mm$. 20 strain-gauges are mounted on the pile to form 10 half-bridges for moment measurements. The strain-gauge bridges are spaced with half diameter spacing, starting with a bridge at the sand surface, see Fig. 2. The moment distribution measured in the half-bridges was fitted to a 6th order polynomial function by least square regression. From this it was possible to generate p-y curves from the moment distribution. While the deflection of these p-y curves were well described it is important to remember that the soil resistance can be affected by uncertainties of up to 35%, (Rosquot, Garnier and Khemakhem 2010). Hence, care needs to be taken in the deduction of the resistance and displacements. The soil resistance was found by differentiation of the moment distribution twice, and the pile displacement was found by an integration of the moment distribution twice. The p-y curves are very sensitive to the fitting and even small changes in the moment polynomial will due to the double differentiation, change the soil resistance significantly. To avoid effects from boundaries, it was here chosen only to use strain-gauge level $z = 1d - 3.5d$ to generated p-y curves. This ensures that at least two extra moment measurements on both sides of a given strain-gauge bridge were used.

Table 1. Test program

Tests	Scaling factor N	Increase in gravity η	Diameter d [-]	l_e $[d]$	l_L $[d]$	γ' $[kN/m^3]$	I_D $[-]$	ϕ' $[^0]$	Saturated sand
1	25	15.5	0.04	15	6	16.7	0.93	46.3	No
2	50	31.1	0.04	15	6	16.6	0.93	44.2	No
3	75	46.6	0.04	15	6	16.5	0.89	42.3	No
4	100	62.1	0.04	15	6	16.4	0.86	41.0	No
5	125	77.7	0.04	15	6	16.8	0.89	40.9	No
6	75	75	0.04	8.25	6	10.3	0.88	42.2	Yes
7	75	75	0.04	10.50	6	10.4	0.93	43.0	Yes
8	75	75	0.04	12.75	6	10.2	0.87	42.0	Yes
9	75	75	0.04	15.00	6	10.2	0.87	42.0	Yes
10	75	75	0.04	17.25	6	10.2	0.86	42.0	Yes

4. Results

4.1. Sand properties

The centrifuge experiments were carried out in Fontainebleau sand - a uniform silica sand from France - which consists of fine and rounded particles. The classification data can be seen in Table 2, (Leth 2011). Triaxial tests were performed to obtain mechanical properties of the sand. A total of 9 trixial tests have been performed, five tests under saturated conditions and four under dry conditions. All tests with a relative density of, $I_D = 0.9$. The dry and saturated triaxial tests show that maximum angle of friction, (ϕ'_{max}) is a function of the relative density and the effective stress. This is in contrast to the method by API 2007 which states that maximum angle of friction only is a function of the relative density. The maximum angle of friction from these triaxial tests correspond well with the predictions done by Bolton 1986 using a critical state angle of $\phi'_{cr} = 30^o$.

Table 2. Classification parameters for the Fontainebleau sand

Specific gravity of particles	G_s	2.646
Minimum void ratio	e_{min}	0.548
Maximum void ratio	e_{max}	0.859
Average grain size	d_{50}	0.18
Coefficient of uniformity	C_u	1.6

$$[7] \qquad \phi_{max} = \phi_{cr} + 3 \cdot (I_D(10 - In(p')) - 1)$$

The mean effective stress p' was in the centrifuge tests calculated as:

$$[8] \qquad p' = \frac{1}{3}(1 + 2K_0)\sigma'_v \ , K_0 = 1 - \sin\phi'$$

The sand was prepared in the centrifuge container by dry pluvation using a single spot hopper. An average relative density was then calculated from the weight of the sand sample. A representative angle of friction was calculated using Eq. 7 and Eq. 8. The reference pressure p' was found at a soil depth of $z = 2/3l_L$. At this depth full similarity of soil stresses between model and prototype was achieved. The achieved relative density, effective density and representative angle of friction can be seen in Table 1.

4.2. Centrifuge results

4.2.1. Scaling approach

The scaling approach is carried out so tests in dry conditions can be interpreted as if they were performed in saturated conditions. The goal is to achieve identical effective stress distribution in the dry model $(\sigma'_{v,m})$ and the saturated prototype $(\sigma'_{v,p})$. This can be written as:

$$[9] \qquad \sigma'_{v,p} = \gamma'_{sat} \cdot z_p = \eta \cdot \gamma'_{dry} \cdot z_m$$
$$\Rightarrow \ \eta = \frac{\gamma'_{sat} \cdot z_p}{\gamma'_{dry} \cdot z_m} = \frac{\gamma'_{sat}}{\gamma'_{dry}} \cdot N_s$$

Here it can be seen that by increasing the gravity with η identical soil stresses can be achieved in a dry sample compared to a saturated sample for which that gravity is increased by N. The increase in gravity η and the geometrical scaling factor $N = z_p/z_m$ are here not identical. This can be achieved by performing tests at a deformation rate at which no excess pore pressure will develop. This modelling technique was used by Li, Haigh and Bolton 2010 and here it is confirmed by comparing the results from two tests performed in dry and saturated conditions. The result are compared for the two tests with a load eccentricity $l_e = 15d$ with a stress level corresponding to a 3 meter in pile diameter. The results in model scale can be seen in Figure 3. The response of the two tests shows identical responses. This confirms the scaling approach and the test series are comparable in both dry and saturated sand.

4.2.2. Stress level

To investigate the stress level effect, five different tests with stress levels corresponding to offshore monopiles ranging from 1 to 5 meters in diameter were performed. The results are here presented in non-dimensional terms. The global force (H) is

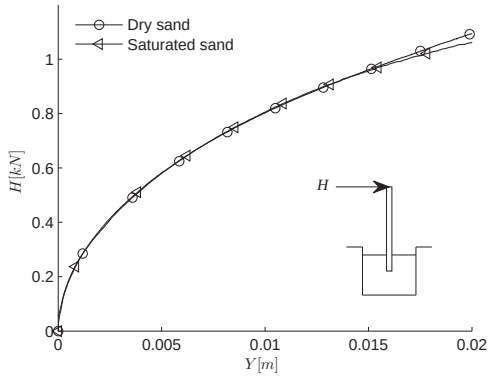

Fig. 3. Comparison of modeling approach, $l_e = 15d$

normalised with the effective density γ' (under centrifuge testing at η g), and the diameter of the pile d.

$$[10] \qquad \tilde{H} = \frac{H}{\gamma' d^3}$$

The overall displacement (Y) measured $l_Y = 2d = 80mm$ above the sand surface is normalised with the diameter of the pile.

$$[11] \qquad \tilde{Y} = \frac{Y}{d}$$

The overall load - displacement response can be seen in Figure 4 from test 1-5. Here it is seen, that the pile subjected to the

Fig. 4. Normalised load deflection response, $l_e = 15d$

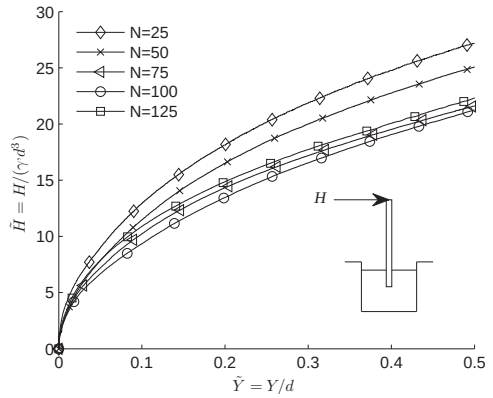

smallest stress level has the highest non-dimensional bearing capacity. The pile with the second lowest stress level has the second highest bearing capacity, whereas it seems that the last three piles have identical non-dimensional responses. From the triaxial tests it was seen that the angle of friction was dependent on pressure and for the entire test series a representative angle of friction was calculated using the average relative density and the pressure calculated at a pile depth at 2/3 of the total length. This was shown in Table 2. Here it can be seen that the tests performed at low stress levels have a higher mobilized angle of friction.

We choose to introduce Rankine's passive earth pressure coefficient.

$$[12] \qquad K_p = tan^2(45 + \phi'/2)$$

The non-dimensional load can be redefined to be:

$$[13] \qquad \tilde{P} = \frac{\tilde{H}}{K_p} = \frac{H}{K_p \gamma' d^3}$$

In Fig. 5 the overall response from test 1-5 with the new normalization is shown. Here the responses from the five different

Fig. 5. Load deflection response normalized with the Rankine earth pressure coefficient, le=15d

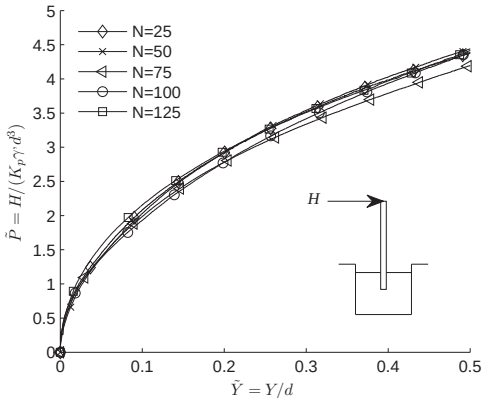

tests merge into one single characteristic curve. This indicates that the effect from stress level can as a simplification be taken into account only through the angle of friction.

The generated p-y curves from the moment distribution are also normalised and again the Rankine coefficient is used.

$$[14] \qquad \tilde{p} = \frac{\tilde{p}}{K_p} = \frac{1}{K_p} \frac{p}{\sigma'_v d}$$

We here recognize the normalised pressure as the earth pressure coefficient introduced in Eq. 1 divided by Rankine's passive earth pressure coefficient. The normalized p-y curves from the five different tests are shown in Fig. 6. Here normalized p-y curves from the six different levels are shown separately. It is seen that the normalized p-y curves from the six different levels show the same high degree of similarity as was found for the overall response. Hence, it may be concluded that the normalized p-y responses have similar normalized behavior no matter of the stress level. It is seen that the stress level can be

Fig. 6. p-y curves for test with different stress distributions, $l_e = 15d$

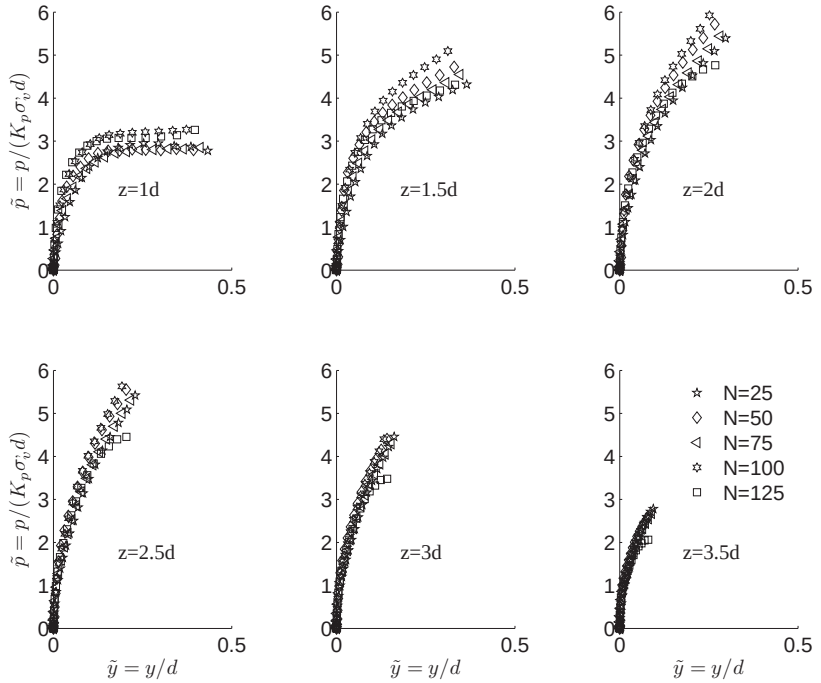

taken into account normalizing the results only using the angle of friction. These curves can then be used for any given prototype stress level, when the stress level effect is taken into account. In contrast to the API 2007 method, we use a different normalization in order to take the stress dependent maximum angle of friction into account.

4.2.3. Load eccentricity effect

The effect from load eccentricity was investigated by comparing five tests performed on piles with a stress distribution identical with a 3 meter in diameter prototype but with different load eccentricities. The five tests were all performed in water saturated sand and on a pile with load eccentricities ranging from $l_e = 8.25d - 17.25d = 330 - 690mm$. Using the normalisation strategy described in Eq. 14 the results from the five tests is shown in Fig. 7. As for the five tests with different stress distributions the results from changing the load eccentricity is shown for the six strain-gauge levels. The responses are similar no matter of the load eccentricity. Scatter is seen in the results but no systematic error is observed and with the increasing soil stress in the depth the curves seems to collapse. It is therefore concluded from these tests that the soil-pile interaction did not change in the five tests. This is identical with the assumption recommended by API 2007.

4.2.4. Generic soil-pile interaction

From the tests it was seen that using the chosen normalisation the effect from stress distribution and load eccentricity can be taken into account. The normalised response can therefore be used in the range of piles with diameter of 1-5 meters and different load eccentricities. Generic normalized p-y curves representative for the ten performed tests are shown in Fig. 8. It can be seen that a maximum soil resistance was only reached in the upper layer $z = 1d$, even though the pile at sand surface has been displaced more than $0.5d$. The initial slopes of the p-y curves were all similar and are found to $\tilde{E}_{py}/K_p = 100$.

5. Discussion

In the design of a monopile supporting an offshore wind turbine, the initial stiffness and the maximum bearing capacity of the pile foundation are important design parameters for a monotonic load situation. The design methodology used today relies on empirical tests on slender piles. From these tests, p-y curves were deducted and are today used also for large diameter, stiff monopiles. The validity of the extrapolation of these p-y curves to the design of monopiles seems to lack a scientific justification. This paper has investigated two effects in this perspective, the stress level and the load eccentricity effects.

Eq. 1 shows the maximum soil resistance is dependent on the pile diameter and the stress level. This research demon-

Fig. 7. Normalized p-y curves for tests with different load eccentricities

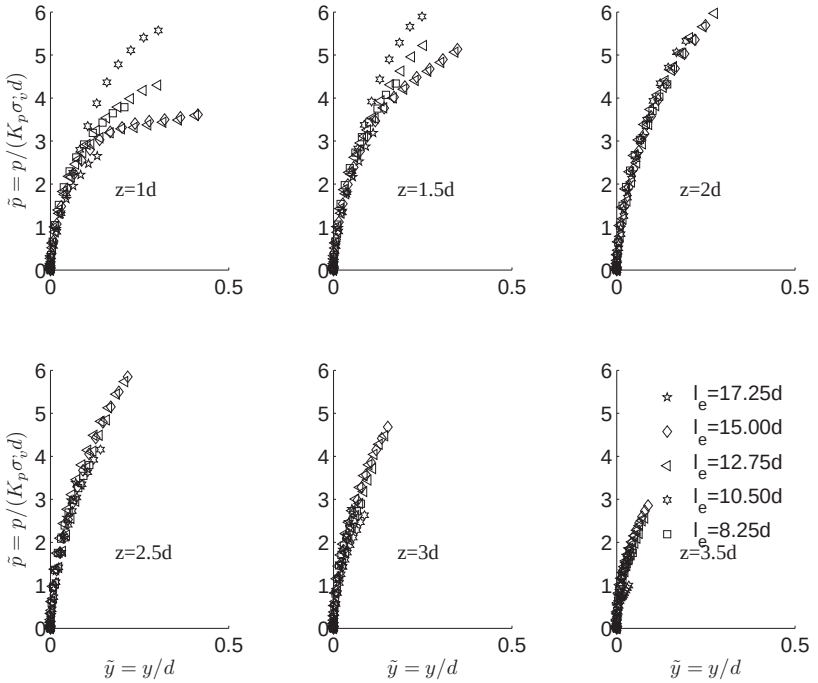

Fig. 8. Normalised general p-y curves for a pile ranging load eccentricities $l_e = 8.25 - 17.25d$ and a diameter ranging from 1-5 m

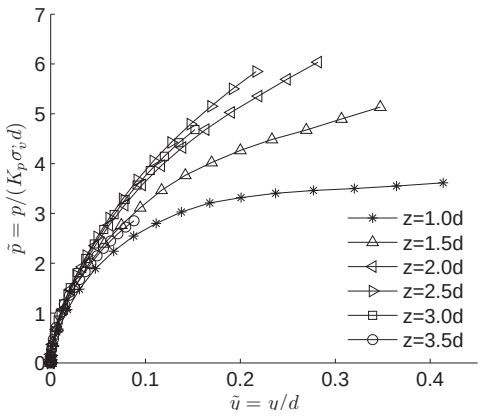

strates that the stress level depending soil behavior can be taken into account by a simple normalisation using the passive Rankine earth pressure coefficient. The effect from changing the diameter of a monopile is still unknown. In a full scale test of a monopile, both the stress level and the pile diameter are increased, compared to the original tests, from e.g. (Murchison and O'Neill 1984). Our research shows that results from a full scale test will not be affected by the stress level if this is taken correctly into account, and a possible diameter effect can thereby be identified.

One could argue that tests performed in dry sand do not represent prototype behaviour for offshore monopiles, but if no pore pressure develops the response of the pile is determined by the effective stresses. This was demonstrated by comparing one tests performed in saturated sand with a test performed in dry sand, shown in Fig. 3. The scaling approach described in Eq. 9 was used, and the responses from the tests were identical in model scale, which confirms the scaling procedure.

This research shows that for the investigated stress levels and for a range of different load eccentricities, the initial stiffness of the p-y curves increases linearly as proposed by API 2007. The corresponding stiffness found from the tests using a representative angle of friction of $\phi' = 42^o$ can therefore be written as:

$$[15] \quad \begin{aligned} E_{py} &= \tilde{E}_{py} \cdot K_p \cdot \sigma_v' \\ &= 100 \cdot tan^2(45^o + 42^o/2) \cdot \gamma' \cdot z \\ &\approx 500 \cdot \gamma' \cdot z \end{aligned}$$

We propose to calculate the initial stiffness using the effective stress level; this enables the calculation of E_{py} with only one initial subgrade modulus function which is valid both for dry and saturated sand. Having an effective density of $10kN/m^3$

leads to an initial subgrade modulus of $k = 5000kN/m^3$, which is significantly smaller than the proposed value of, $k = 40000kN/m^3$ of API 2007. The initial stiffness is affected by the installation procedure and piles installed in-flight at the right stress level would have a larger stiffness. The value found from this study is very small but it is confirming the order of magnitude seen in other centrifuge tests e.g. (Remaud 1999) and (Klinkvort, Leth, and Hededal 2010). From the tests presented in this paper the linear increase with depth is clear, whereas the order of magnitude of the initial subgrade modulus needs to be investigated further.

In the data from the original tests on long slender piles, presented in Murchison and O'Neill 1984 all tests sites were presented by one characteristic angle of friction. Bolton 1986 showed that the angle of friction is dependent on both the relative density and the mean soil pressure. For a homogenous sand sample with a constant relative density, the angle of friction is therefore not constant. The determination of the empirical factor A is therefore due to this probably defined from an assumption that the soil has a constant angle of friction. In Fig. 9 all test data is shown together with the two soil-pile interaction models shown in Eq. 5 and Eq. 6. From the tests it was seen that the normalised initial stiffness was 100 and is therefore used in the models. The ultimate capacity is here calculated using Eq. 4 for both of the models, and, Eq. 7 has been used to calculate the angle of friction for every soil layer. Looking at Fig. 9 it can be seen that the initial stiffness of the two models is well described. The tangential hyperbolic function used in the API 2007 method is though very straight and it starts to deviate the data points early. On the contrary, the hyperbolic function seems to match the measurements in a larger range. The maximum capacity is overestimated in the upper soil layer $z = 1d$, it is reasonable estimated in the soil layer $z = 1.5d$ and it is underestimated in the soil layers from $z = 2 - 3d$.

It is clear that the ultimate capacity is not well predicted, and that all these layers are heavily influenced on the maximum capacity by the empirical parameter A. If one chose to use the assumption of the ultimate capacity shown in Equation 4 a reformulation of the empirical parameter A is needed. To give a better estimate of soil-pile interaction seen in the test, here is chosen to reformulate the parameter A. The step function is here used to give the transition from a value of 2 in the upper layers to a value of 0.9 in the lover layers.

$$[16] \qquad A = 0.9 + H \cdot 1.1$$

$$[17] \qquad H = \frac{1}{2} + \frac{1}{2} tanh\left(9 - 3\frac{z}{d}\right),$$

The hyperbolic function shown in Eq. 6 is used together with the new value of A, shown in Eq. 16. The results are shown in Fig. 9 and here it can be seen that the new model still overpredicts the maximum capacity in the $z = 1d$ layer but only to a minor degree and in the rest of the layers, there seems to be a good agreement.

In Figure 10 different depth factors are plotted. Here is shown the proposed function by Murchison and O'Neill 1984 and recommended by API 2007, the proposed function by Georgiadis, Anagnostopoulos and Saflekou 1992 determined from centrifuge test and the one proposed in Eq. 16. The high start

Fig. 10. Comparison of depth factor

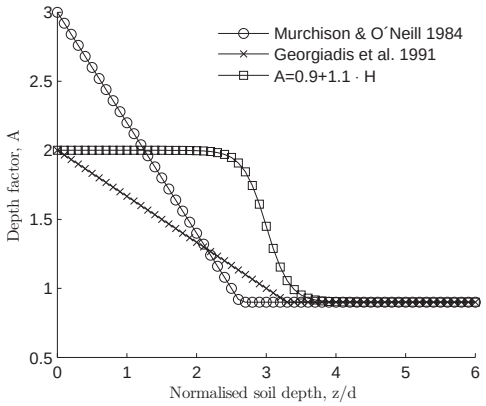

value used in the Murchison and O'Neill 1984 could be addressed to the stress dependent angle of friction. If this is not taken into account, this leads to the use of a too small angle of frictions in the top layers and thereby a high value of A. Nevertheless the inconsistency in the empirical formulation of the empirical depth factor A clearly shows that the formulation of A is site dependent. One therefore has to be very careful when a formulation of A is used on locations different from the place where it was original determined.

In the formulation of the ultimate capacity shown in Eq. 4 the minimum value of the theoretical calculation of failure in shallow or great depth is used. For monopiles supporting offshore wind turbines installed in dense sand the piles are all relative short and the ultimate capacity is thus always calculated as the shallow failure. The failure mechanise is therefore not correct and the value of A plays a huge role. The formulation, shown in Eq. 16, uses a step function and therefore has a steep transition from one value to another. This could indicate the transition from a shallow failure mechanism to a deep failure mechanism. Looking at Fig. 10 it can be seen that transition is about a depth of $3.5d$, and with a rotation point of the pile located around a depth of $4.5d$, it could be argued to use a deep failure mechanism which is closely related to the rotation point of the pile in the lower part. The use of an imperial factor in the calculation of the ultimate capacity clearly shows that the theoretical assumption lacks accuracy. Here is chosen to use a pragmatic approach with calibration of this factor to the tests. It would though be preferable to develop a theoretical approach where an empirical factor is avoided. No clear conclusions can though be drawn from this study and it has to be investigated in more details.

Fig. 9. Comparison of the effect from load eccentricity on the normalized p-y curves

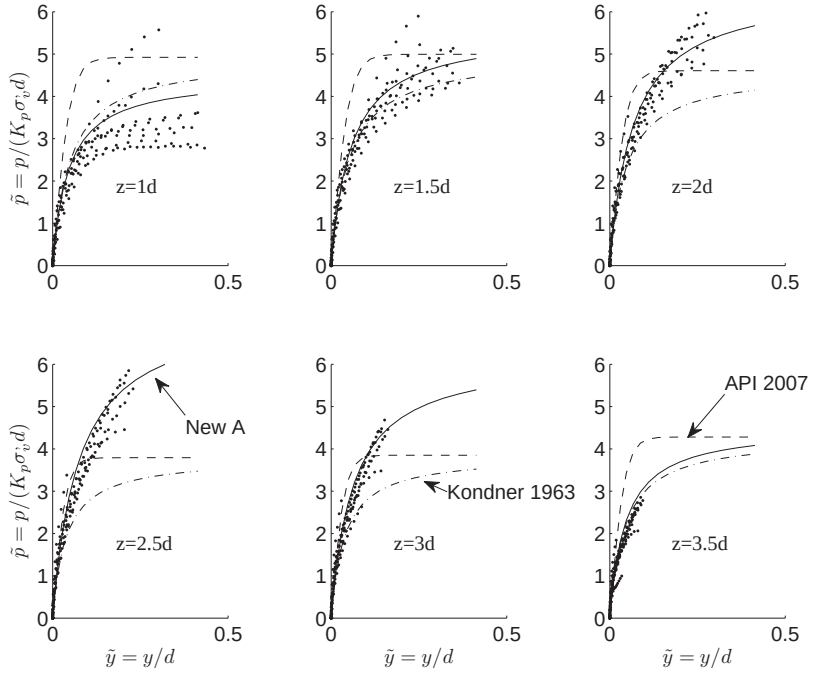

6. Conclusion

Ten centrifuge tests have been used to demonstrate the effect from changing the stress level and the load eccentricity for a monopile installed in sand supporting an offshore wind turbine. Five centrifuge tests were performed on model monopiles subjected to stress levels equal to prototype monopiles with a diameter ranging from 1-5 meters. From the tests it was clearly seen that by taking the different angle of frictions into account as a simple normalisation, the stress level did not affect the normalised response. This enables that the normalised result from 1 centrifuge test can be compared to a monopile with a diameter ranging from 1 to 5 meter.

Normalised p-y curves from tests with different load eccentricities were also compared, and it was here also seen the results from the test shoved a high degree of similarity no matter of the load eccentricity. It was therefore possible to relate all of the ten different tests to one generic soil-interaction model. The model has a constant normalised initial stiffness in accordance with the recommendations in API 2007. The stiffness obtained in this study is one order of magnitude smaller than the recommendations, but in the range of values found from other centrifuge studies.

A new formulation of the depth factor A was proposed and used together with a hyperbolic function, and was seen to fit all of the results with a high degree of accuracy. The new formulation of A with a steep transition from 2 to a value of 0.9, could indicate a transition from one failure mechanism to another. This transition is not seen when using the methodology recommended by API 2007 which for monopiles for wind turbines always uses the shallow failure mechanism in the calculation of the ultimate capacity. This study demonstrated that the empirical related factor sough as initial stiffness and ultimate capacity is dependent on the given test condition and should be used with care when used outside the range of its calibration. Special it seems to be a need of a reformulation of the calculation of the ultimate capacity which capture the right failure mechanism and where a calibration factor as A is not needed.

References

Abdel-Rahman, K. & Achmus, M. 2005. Finite element modelling of horizontally loaded monopile foundations for offshore wind energy converters in Germany, Frontiers in offshore geotechnics; 1ST 2005, , pp. 391-396.

API 2007. API RP 2A-WSD Recommended practice for planning, designing, and constructing fixed offshore platforms - Working stress design.

Ashford, S.A. & Juirnarongrit, T. 2003. Evaluation of pile diameter effect on initial modulus of subgrade reaction, Journal of Geotechnical and Geoenvironmental Engineering, vol. 129, no. 3, pp. 234-242.

Augustesen, A.H., Brodbaek, K.T., Moller, M., Sorensen, S.P.H., Ibsen, L.B., Pedersen, T.S. & Andersen, L. 2009. Numerical mod-

elling of large-diamter steel piles at Horns Rev, Civil Comp -CD Rom Edition.

Bienen, B., Cassidy, M.J. & Gaudin, C. 2009. Physical modelling of the push-over capacity of a jack-up structure on sand in a geotechnical centrifuge, Canadian Geotechnical Journal, vol. 46, no. 2, pp. 190-207.

Bolton, M.D. 1986. Strength and dilatancy of sands, Geotechnique, vol. 36, no. 1, pp. 65-78.

Briaud, J., Smith, T.D. & Meyer, B.J. 1983. Using the pressuremeter curve to design laterally loaded piles, Proceedings - Annual Offshore Technology Conference, vol. 1, pp. 495-502.

Broms, B. 1964. Lateral resistance of piles in cohesionless soils, ASCE - Proceedings - Journal of the Soil Mechanics and Foundations Division, vol. 90, pp. 123-156.

Cassidy, M.J., Randolph, M.F. & Byrne, B.W. 2004. A comparison of the combined load behaviour of spudcan and caisson foundations on soft normally consolidated clay, Geotechnique, vol. 54, no. 2, pp. 91-106.

De Nicola, A. & Randolph, M.F. 1999. Centrifuge modelling of pipe piles in sand under axial loads, Geotechnique, vol. 49, no. 3, pp. 295-318.

Dyson, G.J. & Randolph, M.F. 2001. Monotonic lateral loading of piles in calcareous sand, Journal of Geotechnical and Geoenvironmental Engineering, vol. 127, no. 4, pp. 346-352.

Fan, C. & Long, J.H. 2005. Assessment of existing methods for predicting soil response of laterally loaded piles in sand, Computers and Geotechnics, vol. 32, no. 4, pp. 274-289.

Fuglsang, L.D. & Nielsen, J. 1988. Danish centrifuge hardware and usage, Centrifuges in Soil Mechanics, pp. 93-95.

Fuglsang, L.D. & Ovesen, N.K. 1988. The application of the theory of modelling to centrifuge studies, Centrifuges in Soil Mechanics, pp. 119-138.

Georgiadis, M., Anagnostopoulos, C. & Saflekou, S. 1992. Centrifuge testing of laterally loaded piles in sand, Canadian Geotechnical Journal, vol. 29, no. 2, pp. 208-216.

Hald, T., Mrch, C., Jensen, L., Bakmar, C.L. & Ahle, K. 2009. Revisiting monopile design using p-y curves. Results from full scale measurements on Horns Rev, Proceedings of European Offshore Wind 2009 Conference.

Hansen, J.B. 1961. Ultimate resistance of rigid piles against transversal forces, Danish Geotechnical Institute - Bulletin, no. 12, pp. 5-9.

Kim, B.T., Kim, N., Lee, W.J. & Kim, Y.S. 2004. Experimental load-transfer curves of laterally loaded piles in Nak-Dong River sand, Journal of Geotechnical and Geoenvironmental Engineering, vol. 130, no. 4, pp. 416-425.

Klinkvort, R.T., Leth, C.T. & Hededal, O. 2010. Centrifuge modelling of a laterally cyclic loaded pile", Physical Modelling in Geotechnics, pp. 959-964.

Kondner, R.L. 1963. Hyperbolic stress-strain response; cohesive soils, ASCE - Proceedings - Journal of the Soil Mechanics and Foundations Division, vol. 89, pp. 115-143.

Lesny, K. & Wiemann, J. 2006. Finite-element-modelling of large diameter monopiles for offshore wind energy converters, GeoCongress 2006: Geotechnical Engineering in the Information Technology Age, vol. 2006.

Leth, C.T. 2011. Centrifuge modelling of large diamter pile in sand subject to lateral loading, Technical report, DTU Civil Engineering.

Li, Z., Haigh, S.K. & Bolton, M.D. 2010. Centrifuge modelling of mono-pile under cyclic lateral loads, Physical Modelling in Geotechnics, pp. 965-970.

McClelland, B. & Focht, J., J.A. 1956. Soil modulus for laterally loaded piles. American Society of Civil Engineers -Proceedings - Journal of the Soil Mechanics and Foundations Division, 82, 1956.

Murchison, J.M. & O'Neill, M.W. 1984. Evaluation of p-y relationships in cohesionless soils, Analysis and Design of Pile Foundations.Proceedings of a Symposium in conjunction with the ASCE National Convention, pp. 174-191.

Norris, G. 1986. Theoretically based BEF laterally loaded pile analysis, Numerical Methods in Offshore Piling 3rd International Conference, pp. 361-386.

Pender, M.J., Carter, D.P. & Pranjoto, S. 2007. Diameter Effects on Pile Head Lateral Stiffness and Site Investigation Requirements for Pile Foundation Design, Journal of Earthquake Engineering, vol. 11, no. 1.

Reese, L.C., Cox, W.R. & Koop, F.D. 1974. Analysis of laterally loaded piles in sand, Proceedings of sixth Annual Offshore Technology Conference, Houston.

Reese, L.C. & Matlock, H. 1956. Non-dimensional solutions for laterally-loaded piles with soil modulus assumed proportional to depth, Proceedings of eighth Texas Conference on Soil Mechanics and Foundation Engineering.

Remaud, D. 1999 Pieux sous charges latrales: tude exprimentale de l'effet de groupe, Ph.D. thesis.

Rosquot, F., Thorel, L., Garnier, J. & Khemakhem, M. 2010. P-y curves on model piles: Uncertainty identification, Physical Modelling in Geotechnics, pp. 997-1002.

Rosquoet, F., Thorel, L., Garnier, J. & Canepa, Y. 2007. Lateral cyclic loading of sand-installed piles, Soils and Foundations, vol. 47, no. 5, pp. 821-832.

Schofield, A.N. 1980. Cambridge geotechnical centrifuge operations, Geotechnique, vol. 30, no. 3, pp. 227-268.

Smith, T.D. 1987. Pile horizontal soil modulus values, Journal of Geotechnical Engineering, 1987.

Sorensen, S.P.H., Brodbaek, K.T., Moller, M., Augustesen, A.H. & Ibsen, L.B. 2009. Evaluation of the load-displacement relationships for large-diamter piles in sand, Civil Comp -CD Rom Edition.

Terzaghi, K. 1955. Evaluation of coefficients of subgrade reaction, Geotechnique, vol. 5, no. 4, pp. 297-326.

Wesselink, B.D., Murff, J.D., Randolph, M.F., Nunez, I.L. & Hyden, A.M. 1988. Analysis of centrifuge model test data from laterally loaded piles in calcareous sand, Engineering for calcareous sediments, vol. 1, pp. 261-270.

Zhang, L., Silva, F. & Grismala, R. 2005. Ultimate lateral resistance to piles in cohesionless soils, Journal of Geotechnical and Geoenvironmental Engineering, vol. 131, no. 1, pp. 78-83.

Paper IV

"Centrifuge modelling of a laterally cyclic loaded pile"

R.T. Klinkvort, C.T. Leth & O. Hededal

Published in: *Physical Modelling in Geotechnics, 2010*

Physical Modelling in Geotechnics – Springman, Laue & Seward (eds)
© 2010 Taylor & Francis Group, London, ISBN 978-0-415-59288-8

Centrifuge modelling of a laterally cyclic loaded pile

R.T. Klinkvort, C.T. Leth & O. Hededal
Technical University of Denmark, Copenhagen, Denmark

ABSTRACT: A total number of 9 monotonic and 6 cyclic centrifuge tests on laterally loaded piles in very dense, dry sand was performed. The prototype dimensions of the piles were 1 meter in diameter and penetration depths varying from 6 to 10 meters. The static tests were used to investigate the initial subgrade reaction modulus and as a reference for cyclic tests. For the cyclic tests the accumulation of deflections and the change in secant stiffness of the soil from repetitive loading were investigated. From all the tests carried out accumulations of deflections were seen. From the centrifuge tests it was seen that no reduction occurs of the overall bearing capacity and that deflections accumulate due to cyclic loading. This paper presents test results and discusses the effects from load eccentricity and effects from cyclic loading with focus on accumulations of the deflection and the change in secant stiffness.

1 INTRODUCTION

Over the last decades there has been an increasing focus on alternative sustainable energy. One of these alternative sources is energy from wind turbines. The most widely used foundation method for offshore wind turbines is single large diameter tubular steel piles commonly denoted monopiles. The monopile design has been used in Denmark at the wind turbine parks at Samsø and Horns Rev. The design of monopiles is commonly based on the theory of laterally loaded piles. This theory relies on empirical data originated from the oil and gas industry, Reese & Matlock (1956) & McClelland & Focht (1958). The design for the lateral capacity is carried out by modelling the pile as a beam and the soil as a system of uncoupled springs, known as a Winkler model. The springs are described by p-y curves which defines the load displacement relationship for the interaction between soil and pile, API (1993). The formulation of these curves was originally calibrated to slender piles, but is today even used for design of large diameter monopiles. However, the monopiles used for wind turbine foundations act as stiff piles. Therefore it is relevant to investigate the behavior of stiff piles in more detail. The current test program comprises piles with a prototype diameter of 1 m and penetration depths up to 10 m and is intended to investigate the behavior of the larger monopiles used offshore today.

2 SCOPE OF WORK

Two major loads act on an offshore wind turbine. One due to the wind at the top of the wind turbine and one due to the waves and ice at sealevel. The purpose of the research carried out is to investigate the pile behavior when changing the location of force resultant and the penetration depth. The investigation will for the static tests focus on the initial stiffness of the pile-soil response. The cyclic tests will focus on the gradual change in secant stiffness and the accumulation of deflection as a function of the number of load cycles.

3 DESIGN METHODOLOGY

The method for sand presented here is the one used in API (1993), which is based on the formulation proposed by Murchison & O'Neill (1984).

The p-y relationship for sand is typically approximated by

$$p = A \cdot p_u \tanh\left[\frac{k \cdot X}{A \cdot p_u} y\right] \quad (1)$$

The value k represents the initial modulus of subgrade reaction and X is the distance to soil surface. p_u is the ultimate soil resistance and is found using plasticity theory. A is an empirical constant which is used to fit the test results with theory. For static loading $A = \left(3.0 - \frac{0.8X}{D}\right) \geq 0.9$. For cyclic loading $A = 0.9$.

The initial stiffness of the p-y relationship can be found if p is differentiated with respect to y,

$$E_{py,ini} = \frac{\partial}{\partial y}\left[A \cdot p_u \tanh\left(\frac{k \cdot X}{A \cdot p_u} y\right)\right]_{y=0} = k \cdot X \quad (2)$$

From Equation 2 it can be seen that the design codes uses a initial stiffness of the p-y relationship which is increasing linearly with depth.

4 EXPERIMENTS

The centrifuge test program was performed on solid steel piles with a diameter d = 16 mm and penetration depths between 96–160 mm. The gravity field was increased to obtain a scaling factor of approximately N = 62.5. This resulted in prototype piles with a diameter of d = 1 m and penetration lengths between L = 6–10 m.

The different definitions are shown in Figure 1. The test program for the static and cyclic tests can be seen in Table 1. Here L is the penetration depth, e is the load eccentricity, while m and c indicate monotonic and cyclic test, respectively. All static and cyclic tests were performed in dry Fontainebleau sand. Leth et al. (2008) has collected classification parameters for the Fontainebleau sand which can be seen in Table 2. The average grain size of the Fontainebleau sand is 0.18 mm. The test piles have a diameter of 16 mm. This leads to a "model diameter/grain size diameter" ratio of 16/0.18 = 88. This ratio should be large enough to avoid particle size effects when applying the artificial gravity field according to the observations described in Fuglsang & Ovesen (1988).

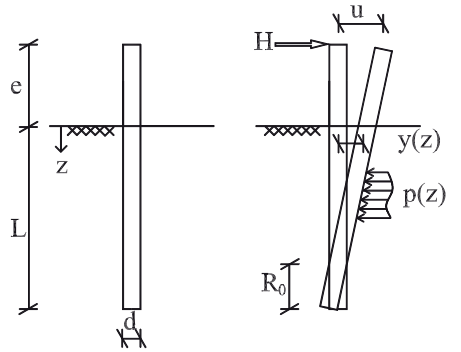

Figure 1. Sketch of pile.

Table 1. Test program for the centrifuge tests.

$e\backslash L$	6d	8d	10d
2.5d	m c	m c	m c
4.5d	m c	m c	m
6.5d	m c	m	m

Table 2. Classification parameters for the Fontainebleau sand.

Specific gravity of particles	G_s	2.646
Minimum void ratio	e_{min}	0.548
Maximum void ratio	e_{max}	0.859
Average grain size	d_{50}	0.18
Coefficient of uniformity	C_u	1.6

A spot pouring hopper (SPH) was used for the preparation of the sand sample. This equipment was developed according to a setup described in Huei-Tsyr et al. (1998). Due to the geometry of the container and pile the sand is prepared using a circular travelling loop as described in Zhao et al. (2006). CPT tests have been carried out to validate the pouring method. All these CPT tests showed the soil sample has a good homogeneity in the container, Gottlieb et al. (2005). After the sand is prepared, the pile is installed at 1 g.

A total of 15 centrifuge tests have been performed: nine monotonic and six cyclic. For all the tests the relative density was found to vary in the range 0.9–0.95 The relative densities are calculated by measuring the weight and the volume of the sand sample. The average value for both the static and cyclic tests is I_D = 0.924 and a void ratio of e = 0.57. It is assessed that the small variation of the density not will affect the results significantly.

4.1 *Monotonic tests*

The force and deflection are normalized to facilitate comparison between the different tests. The normalized force is defined as

$$P = \frac{H}{\gamma . d^3} \tag{3}$$

and normalized deflection is defined as

$$U = \frac{u}{d} \tag{4}$$

In Figure 2 the observation on the change between load with an eccentricity on 6.5d and 4.5d or 2.5d is clear. The tendency is that for load eccentricity of 6.5d and 4.5d the normalized lateral bearing capacity is nearly identical. This indicates that a change in failure mechanism occurs.

More tests have to be conducted in order to clarify how the load eccentricity and pile penetration depth affects the pile-soil failure mechanism.

The design codes assume a linear increase in the initial stiffness with depth as indicated by Equation 2. Several authors have, however, proposed alternative distributions e.g. Lesny & Wiemann (2006) and Haahr (1989). Therefore the increase in initial stiffness is investigated further.

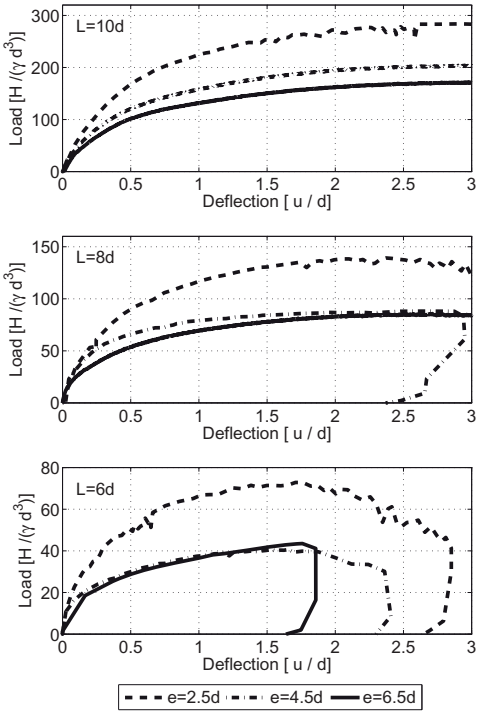

Figure 2. Normalized plot with the nine monotonic tests.

At initial loading the pile is assumed to behave as a rigid pile and only elastic deformations occur in the sand. This implies that the pile deflection can be described knowing the pile head deflection and the rotation.

$$y(z) = u - \theta\,(e + z) \tag{5}$$

In the present setup, the pile may be assumed to behave rigidly if, according to Equation 6 by Poulos & Hull (1989), the stiffness of the sand is less than $E_s = 100\ MPa$.

$$1.48\left(\frac{E_p I_p}{E_s}\right)^{\frac{1}{4}} < L_{inter} < 4.44\left(\frac{E_p I_p}{E_s}\right)^{\frac{1}{4}} \tag{6}$$

The soil reaction on the pile can be described as an initial stiffness times the deflection of the pile.

$$p(z) = -E_{py,\,ini}\,(z)\,y(z) \tag{7}$$

The initial stiffness may be assumed to have a nonlinear variation with depth as e.g. given in Equation 8. Here $n = 1$ corresponds a linear distribution and $n = 0.5$ corresponds to a parabolic distribution.

$$E_{py,ini}\left(\frac{z}{d}\right) = A_n \cdot \left(\frac{z}{d}\right)^n \tag{8}$$

Considering moment and horizontal equilibrium, the constant A_n can be found to be

$$A_n = \begin{cases} \dfrac{144 + 384\left(\dfrac{e}{L}\right) + 288\left(\dfrac{e}{L}\right)^2}{8L}\,\dfrac{H}{u}\dfrac{d}{L}, & n = 1 \\[2ex] \dfrac{75 + 210\left(\dfrac{e}{L}\right) + 175\left(\dfrac{e}{L}\right)^2}{8L}\,\dfrac{H}{u}\sqrt{\dfrac{d}{L}}, & n = 0.5 \end{cases} \tag{9}$$

For the nine static tests the constant An has been calculated using both relations for the development of the initial stiffness. The applied force has been found for the entire test series at an initial deflection of $u/d = 0.1$. The results are presented in Table 3. It must be expected that the soil has the same subgrade modulus for all the tests. Therefore, considering the smaller variation of the constant A_n for $n = 0.5$, it is assessed that the parabolic distribution gives a better description of the initial subgrade modulus. This parabolic distribution is also observed by Haahr (1989) and a distribution with $n = 0.6$ is observed by Lesny & Wiemann (2006).

The design codes prescribe a linear distribution of the initial subgrade reaction. This distribution was found using data from tests on long slender piles. For long slender piles only deformation on the upper part of the pile is seen and it is therefore only in the upper part of the pile data can be withdrawn. The tendency according to initial stiffness seen in the upper part is then extrapolated to the lower part. A linear distribution and a parabolic distribution may be nearly identical in the upper part of the pile but yield large differences in the lower part. The effects on a long slender pile from

Table 3. Calculated subgrade reaction modulus for the nine monotonic tests.

L *[d]*	*e* *[d]*	*An* = 1 *[kPa]*	*An* = 0.5 *[kPa]*
10	2.5	3962	6883
10	4.5	3994	7105
10	6.5	4845	8753
8	2.5	4851	7603
8	4.5	4908	7883
8	6.5	5211	8595
6	2.5	6532	8972
6	4.5	6015	8466
6	6.5	6268	8943

assuming a wrong distribution will therefore not be critical. This is not the case for a short rigid pile.

Sørensen et al. (2009) compared $FLAC^{3D}$ calculations with the p-y approach recommended by design codes. They adopted a distribution proposed by Lesny & Wiemann (2006) which is identical with Equation 8 with $n = 0.6$. They observed that the use of this distribution gave a better fit to the results from the three dimensional numerical model, but more tests have to be conducted in order to clarify the distribution of the initial subgrade reaction.

In Table 4 different values of initial subgrade modulus for dense dry sand is presented. For these values proportional distribution is expected. From this table it can be seen that the values proposed by API (1993) and Reese & Impe (2001) are much larger than the values found by Remaud (1999).

Some of the tests presented here were numerically modelled using the Winkler method by Klinkvort (2009). The best fit to the monotonic curves was done using an initial subgrade modulus of $k = 2.7\ MN/m^3$.

This study and the study by Remaud (1999) both used centrifuge modelling where the deflection is scaled with a factor of N and the force is scaled with a factor of N^2. The scaling factors are found using dimensional theory. More tests have to be conducted in order to clarify results from centrifuge modelling in order to determine the magnitude and distribution of the initial stiffness.

4.2 *Cyclic tests*

In the cyclic tests the pile was subjected to 100 force controlled load cycles. To investigate the influence from previous loading three of the tests were performed in three phases. The first phase with large cycles, second phase with smaller cycles and the third phase with cycles equal to cycles in the first phase. To investigate the effects from cyclic loading this paper uses methods described in LeBlanc (2009) to account for accumulation of deflections and the change in secant stiffness.

A set of load characteristic constant are used to describe the cyclic loading. The load characteristics are denoted ζ_b and ζ_c. They are determined as shown in Equation 10.

Table 4. Comparison of modula of initial subgrade reaction.

	k_{py} [MN/m^3]
API (1993)	83
Reese & Impe (2001)	61
Remaud (1999)	8

$$\zeta_b = \frac{H_{\max}}{H_{\text{static}}} \quad \zeta_c \frac{H_{\min}}{H_{\max}} \tag{10}$$

Here $H_{\max}$ and $H_{\min}$ are the maximum and minimum applied force in the cyclic loading. H_{static} is the maximum bearing capacity found from the static test. ζ_b describes how close the cycles are carried out to the static bearing capacity. $\zeta_b = 1$ is therefore cycles carried out to the maximum bearing capacity. ζ_c describes the direction of the loading. For one-way loading $\zeta_c = 0$ and for two-way loading $\zeta_c = -1$.

In all of the 6 cyclic tests, accumulation of the deflection was seen. The best fit in all the tests was with a power fit as proposed by Long & Vanneste (1994) and LeBlanc (2009), cf. Equation 11.

$$\Delta u(N) = u_0 \cdot N^{\delta} \tag{11}$$

Here u_0 is the accumulated deflection at the first cycle and δ is an empirical coefficient which control the shape of the curve. The accumulated deflection for a given cycle is defined as the average value for the cycle.

A small increase in secant stiffness was observed for the first 100 cycles for all the tests. The best fit to the change in secant stiffness was done with a exponential function cf. Equation 12.

$$\kappa(N) = \kappa_0 \cdot e^{\kappa N} \tag{12}$$

κ_0 describes the initial secant stiffness in the first cycle. κ describes the change in secant stiffness.

Figure 3 shows the results for cyclic testing on the pile with a load eccentricity $e = 2.5d$ and a penetration depth $L = 10d$. This way of analyzing the cyclic tests has been done for all the performed tests.

As it can be seen from Figure 3, the determination of the secant stiffness and accumulation of the deflection involves a great scatter of data. This was also reported by LeBlanc (2009). This is to a some extent attributed the fact that measurements involves differences of small displacements.

The results from the cyclic tests are shown in Table 5. No clear relationship for the coefficients can be seen concerning load eccentricity and penetration depth. Neither do the results show any clear correlation to the loading characteristic constants ζ_b and ζ_c. Table 5 shows that the loading characteristic constants ζ_b and ζ_c has a large difference from test to tests. Therefore it is not possible from the performed test to conclude on the effect of the loading eccentricity and pile penetration, and further tests need to be conducted.

It seems like the development of the secant stiffness can be expressed in a more simple form

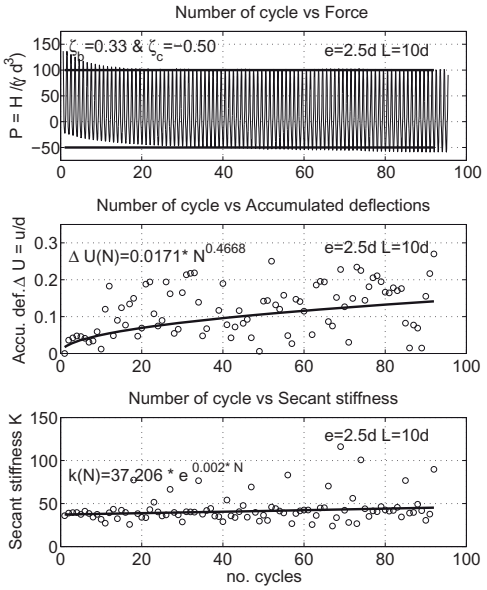

Figure 3. Displacements difference versus secant stiffness for cyclic test $e = 2.5$ & $L = 10d$.

Table 5. Dimensionless results from the cyclic testing.

L	e	ζ_b	ζ_c	Δu_0	δ	κ_0	κ
10	2.5	0.3	–0.5	0.02	0.46	37	0.002
10	4.5	0.3	–0.8	0.04	0.11	6.6	0.018
10	6.5	0.7	–0.6	0.02	0.72	11.4	0.003
8	4.5	1.0	–0.6	0.1	0.31	4.1	0.006
8	6.5	0.8	–0.9	0.1	0.01	2.2	0.000
6	6.5	0.6	–0.8	0.1	0.45	5.7	0.004

than proposed in Equation 12. In the last column in Table 5 κ is shown. For all the tests except the test $e = 4.5$ $L = 10d$, this value is very small. This indicates that the change in secant stiffness is very small and it may be sufficient to described the change in secant stiffness in a linear fashion. For three of the cyclic test ($e = 4.5d$ $L = 8d$, $e = 4.5d$ $L = 6d$ & $e = 6.5d$ $L = 6d$) new cyclic loading was done after the first 100 cycles. The new cyclic testing was done with a smaller amplitude than the first. Only in the test with a load eccentricity of $4.5d$ a decrease in the secant stiffness was seen. It must be expected that when performing a loading series with a smaller amplitude the secant stiffness will decrease as long as no equilibrium in the cyclic loading is found. When the pile has compacted the sand around the pile in a constant manner, the cyclic behavior will stabilize and the secant stiffness will increase. When performing cyclic loading

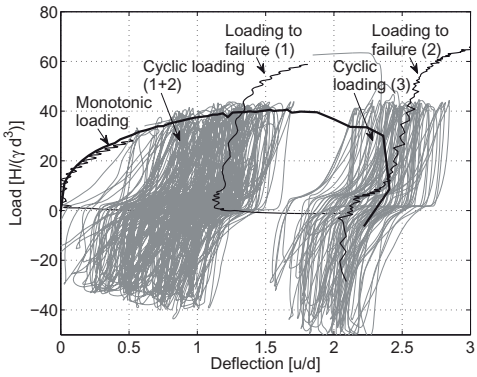

Figure 4. Normalized plot for the cyclic test $e = 4.5d$ & $L = 6d$.

again with a larger amplitude the secant stiffness in all the tests shows an increase.

An example of a cyclic tests series is shown in Figure 4. The plot contains two different tests; the monotonic test and the corresponding cyclic test series. The cyclic test series contains of first 100 cycles, followed with 100 cycles with smaller amplitude. After these cycles, the pile is loaded to failure and unloaded, then 100 cycles are applied again with a monotonic loading to failure at the end.

The pile is loaded to failure twice and it can be seen that the pile reaches a higher bearing capacity than the monotonic test. Cyclic loading is handled in the design codes by a reduction of the static soil resistance. This leads to a reduction of the bearing capacity and the pile—soil stiffness. These tests indicate that no reduction of the bearing capacity will occur.

From the cyclic load series it can also be seen that the secant stiffness increases for the cyclic loading in the investigated cases.

5 CONCLUSIONS

The monotonic tests revealed a relationship between the lateral bearing capacity of the pile and the load eccentricity. This indicates that there are different failure mechanisms for piles with large load eccentricity and piles with smaller load eccentricity. In practise this may be of importance for offshore wind turbines subjected to a combination of wind load from the rotor acting 60–100 m above seabed level and wave forces acting relatively closer to the seabed.

The centrifuge modelling indicates that using the design code recommendations to generate p-y curves led to a overestimation of the pile—soil

stiffness. Due to this observation it is believed that the recommendations to generate the distribution and magnitude of the initial subgrade modulus should be changed. Further research is needed to gain knowledge about this.

From all the cyclic tests carried out, accumulations of deflections were seen. The secant stiffness of every cycle was measured revealing that the cyclic loading led to an increase in secant stiffness. From the centrifuge tests it was clearly seen that no reduction of the bearing capacity of dry sand occurs due to cyclic loading.

It seems like the influence of the location of the applied force on a laterally loaded pile was most critical for the monotonic bearing capacity. It is believed that this also affects the accumulations of deflection and the change in secant stiffness but it was not clearly seen in this research.

REFERENCES

API 1993. *Recommended Practice For Planning, Designing and Construction Fixed Offshore Platforms—Load and Resistance Factor Design.* American Petroleum Institute.

Fuglsang, L.D. & Ovesen, N.K. 1988. *The application of the theory of modelling to centrifuges studies.* Balkema, Rotterdam.

Gottlieb, S., Klinkvort, R.T., Petersen, J. & Christensen, L.K. 2005. Calibration and the use of mini-cpt. Student report, Technical University of Denmark (in Danish).

Haahr, F. 1989. *Interaction between latterally laoded model piles in sand*. Ph.D. thesis, Technical University of Denmark. (in Danish).

Huei-Tsyr, C., Chung-Jung, L. & Hung-Wen, C. 1998. The travelling pluvation apparatus for sand specimen preparation. *Centrifuge 98 1*: p. 143–148.

Klinkvort, R.T. 2009. Laterally loaded piles—centrifuge and numerically modelling. Master's thesis, Technical University of Denmark.

LeBlanc, C. 2009. *Design of Offshore Wind turbine Support Structures*. Ph.D. thesis, Aalborg University.

Lesny, K. & Wiemann, J. 2006. Finite-element-modelling of large diameter monopiles for offshore wind energy converters. In *Geo Congress*.

Leth, C.T., Krogsbøll, A., & Hededal, O. 2008. Centrifuge facilities at danish technical university. In *15th Nordic Geotechnical Meeting*.

Long, J.H. & Vanneste, G. 1994. Effects of cyclic lateral loads on piles in sand. *Journal of Geotechnical Engineering 120*: 225–244.

McClelland, B. & Focht, J.A. 1958. Soil modulus for laterally loaded piles. *Journal of the soil mechanics and foundations division—Proceedings of the American Society of Civil Engineers*: 1–22.

Murchison, J.M. & O'Neill, M.W. 1984. Evaluation of p-y relationships in cohesionless soils. In *Proc., Symposium of Analysis and Design of Pile Foundations, ASCE, San Fransisco*, 174–191.

Poulos, H. & Hull, T. 1989. The role of analytical geomechanics in foundation engineering. *Foundation Engineering: Current principles and Practices, ASCE, Reston 2*: 1578–1606.

Reese, L.C. & Impe, W.F.V. 2001. *Single Piles and Pile Groups Under Lateral Loading*. A.A. Balkema.

Reese, L.C. & Matlock, H. 1956. Non-dimensional solutions for laterally loaded piles with soil modulus assumed proportional to depth. *Proceedings of the 8th Conference on Soil Mechanics*: 1–41.

Remaud, D. 1999. *Pieux sous charges laterales: Etude Ex-perimentale de l'effect de groupe*. Ph.D. thesis, Ecole Centrale de Nantes. (in French).

Sørensen, S., Brødbæk, K.T., Møller, M., Augustesen, A.H. & Ibsen, L.B. 2009. Evaluation of the load-displacement relationships for large-diameter piles in sand. In *Proceedings of the Twelfth International Conference on Civil, Structural and Environmental Engineering Computing*.

Zhao, Y., Gafar, K., Elshafie, M., Deeks, A., Knappett, J. & Madabhushi, S. 2006. Calibration and use of a new automatic sand pourer. In *Physical modelling in Geotechnics, 6th ICPMG '06*, p. 265–270.

Paper V

"Laterally cyclic loading of monopile in dense sand"

R.T. Klinkvort, O. Hededal & M. Svensson

Published in: *Proceedings of the 15th European Conference on Soil Mechanics and Geotechnical Engineering, 2011*

Proceedings of the 15th European Conference on Soil Mechanics and Geotechnical Engineering
A. Anagnostopoulos et al. (Eds.)
IOS Press, 2011

doi:10.3233/978-1-60750-801-4-203

Laterally cyclic loading of monopile in dense sand

Chargement lateral cyclique de monopile dens le sable dense

R. T. Klinkvort[1], O. Hededal and M. Svensson
Technical University of Denmark (DTU)

ABSTRACT

In order to investigate the response from laterally cyclic loading of monopiles a large centrifuge tests series is ongoing at the Technical University of Denmark (DTU). This paper will present some of the tests carried out with a focus on the influence of accumulation of rotation when changing the loading conditions. In these tests the load conditions are controlled by two load characteristics, one controlling the level of the cyclic loading and one controlling the characteristic of the cyclic loading. The centrifuge tests were performed in dense dry sand on a pile with prototype dimensions as following: The diameter of the pile was d = 2 m, the penetration depth of the pile was L = 6 d = 12 m and a load eccentricity of e = 15 d = 30 m. The loading of the pile was performed with a load setup which applies the load on the monopile in a manner that corresponds to the load condition for a monopile used for wind turbine foundation. This is important in order to get the right failure mechanism in the sand. The load frame is controlled with a feedback system which enables force controlled load series. A total number of 8 tests have been carried. In all of the tests, the pile was loaded with 500 load controlled cycles and for the entire test series accumulation of rotation was seen.

RÉSUMÉ

Afin d'étudier la réponse de chargement latéral cyclique de monopieux, une importante série d'essais en centrifugeuse est en cours à l'Université technique du Danemark (DTU). Ce document présente quelques-uns des tests effectués avec un accent sur l'influence de l'accumulation de rotations pour des conditions de chargement variables. Dans ces essais, les conditions de charge sont contrôlées par deux caractéristiques de charge, une contrôlant le niveau de la charge cyclique et l'autre contrôlant l'orientation du chargement cyclique. Les essais en centrifugeuse ont été effectués sur un pieu situé dans du sable dense et sec ; le pieu a les dimensions suivantes : d = 2 m de diamètre, profondeur de L = 6 d = 12 m et excentricité de la charge de e = 15 d = 30 m.
Le chargement du pieu a été réalisé avec une configuration de charge qui applique la charge sur le monopieu d'une manière correspondant au chargement rencontré lors de l'utilisation d'un monopieu comme fondation d'une éolienne. Ceci est important afin d'obtenir le mécanisme de rupture correct dans le sable. Ce cadre de chargement est contrôlé à l'aide d'un système de rétroaction qui permet des séries de chargement contrôlées par la force. Un total de 8 essais a été effectué. Dans tous les tests, le pieu a été chargé avec 500 cycles contrôlés par la force et une accumulation de la rotation a pu être notée pour toute la série de tests.

Keywords: Foundations, monopiles, centrifuge testing, sand, load-amplitude effects

[1] Corresponding Author.

1 INTRODUCTION

Monopiles are today one of the most popular foundation methods for offshore wind turbines. The monopile is a single large diameter tubular steel pile driven 5 to 6 times the diameter into the seabed. The water depth for installation of wind turbines is increasing. The design methodology for monopiles therefore needs a reformulation if the monopile concept shall succeed into deeper waters. Monopiles for wind turbines are affected by lateral loads from waves and winds which subject the pile at seabed with shear forces and corresponding moments due to the load eccentricity. The design for these loads is today done by model the pile as a beam and the soil as a system of uncoupled non-linear springs. From this e.g. rotation of the monopile can be calculated. This method has successfully been used in pile design for offshore oil and gas platforms. The design methodology originates from tests on long slender piles, [1] & [2]. In the case of monopile foundation for wind turbines the relationship proposed by [3], showed in equation 1, is often used. Even though these curves were originally calibrated to slender piles, they are still used for design of large diameter monopiles with a slenderness ratio L/D as low as 5. With a slenderness ratio of 5 the monopile for wind turbine foundation acts as a stiff pile. Therefore it is relevant to investigate the behaviour of stiff piles in more detail. The tests series presented in this paper are a part of a program that intends to investigate the response of monopiles subjected to cyclic loads.

2 SCOPE OF WORK

The loading condition for a monopile for offshore wind turbines is dominated by environmental loads from waves and wind. These loads act on the monopile in a cyclic manner with a variation in amplitude as well as orientation. This study investigates the effect from load orientation and amplitude. For the design of a monopile foundation for wind turbines, three issues are important; the accumulation of rotation, the change in secant stiffness and the damping in the soil. Here we will focus on the accumulation of the rotation.

3 DESIGN METHODOLOGY

The design method for sand presented here [3] is based on the formulation proposed by [4]. As described, the pile is modelled as a beam and the soil is modelled as non-linear springs. The formulation of the spring also known as the p-y relationship is typically for sand approximated by

$$p = A \cdot p_u \cdot tanh\left[\frac{k \cdot z}{A \cdot p_u} y\right] \quad (1)$$

The value k represents the initial subgrade reaction modulus and z is the distance to soil surface. p_u is the ultimate soil resistance as determined by plasticity theory. A is an empirical constant which is used to fit the test results with theory. For static loading $A = (3.0\text{-}0.8X/D) \geq 0.9$. For cyclic loading $A = 0.9$. The non-linear system is typically defined and solved using an FE program.

4 EXPERIMENTS

The centrifuge test program was performed with a solid steel pile. The pile was made of a 24 mm steel core with a 2 mm epoxy coating leading to a total diameter of d = 28 mm. The load eccentricity e and the penetration depth of the pile was also kept constant as e = 15d and L = 6d. The response of the pile is influenced by load eccentricity and penetration depth which was shown in [5]. Therefore a load setup which applies the load in a way similar to a wind turbine foundation is used. A more detail description of the test setup is given in [6]. A sketch of the pile with definitions is shown in figure 1.The centrifuge is used to increase the gravity so soil stresses corresponds to a pile with a diameter of 2 meters. Scaling laws for the test are quite standard, see e.g. [7].

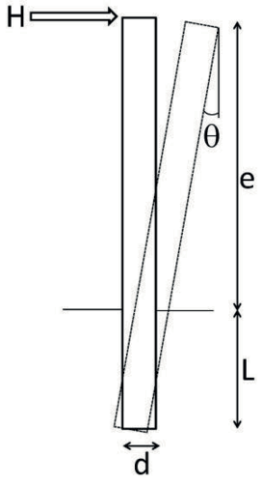

Figure 1. Sketch of pile

The static and all cyclic tests were performed in dry Fontainebleau sand. The classification parameters shown in Table 1 are taken from [7].

Table 1. Classification parameters for the Fontainebleau sand

Specific gravity of particles, G_s	2.646
Minimum void ratio, e_{min}	0.548
Maximum void ratio, e_{max}	0.859
Average grain size, d_{50}, in mm	0.18
Coefficient of uniformity, C_u	1,6

The test pile has a diameter of 22 mm. This leads to a "model diameter/grain size diameter" ratio of 22/0.18 = 122. This ratio should be large enough to avoid particle size effects when applying the artificial gravity field according to the observations described in [8].

A spot pouring hopper was used for the preparation of the sand sample. After the sand is prepared, the pile is installed at 1 g. Only one test is carried out per soil sample.

A set of non-dimensional parameters are used to describe the applied cyclic loads. This approach is similar to the one chosen by [9].

$$\zeta_b = \frac{H_{max}}{H_{mon}} \quad , \quad \zeta_c = \frac{H_{min}}{H_{max}} \tag{2}$$

Here, H_{mon} is the maximum bearing capacity found from a monotonic test, H_{min} is the minimum force in cyclic loading and H_{max} is the maximum force in cyclic loading. The value ζ_b is thus a measure of how close the cyclic loading is to the maximum bearing capacity, and ζ_c is defining the characteristic of the cyclic loading. From these non-dimensional parameters a test program was designed. The procedure for the test program was to start with a monotonic test (T1). From this test the maximum bearing capacity was found. Then four cyclic tests were performed changing ζ_c, the load orientation (T2-T5). From these four tests the most critical load orientation was found and used for the last four cyclic tests (T3, T6-T8). In this test series the effect of load amplitude is investigated by changing ζ_b. A total number of eight centrifuge tests were carried out - one monotonic and 7 cyclic. All cyclic tests were carried out with 500 cycles except one of the test which was performed with 1000 cycles (T7).

4.1 Installation of piles

After the sand is prepared the piles are jacked into the soil at 1g. Figure 2 shows the jacking force measured during installation. It can be seen that the sand samples are homogeneous and that deviation can be attributed mainly to the variation in void ratio. From this it is concluded that the soil samples for all the performed tests can be assumed identical. The installation data of T6 was not recorded - the relative density for this test was found to I_D=0.84.

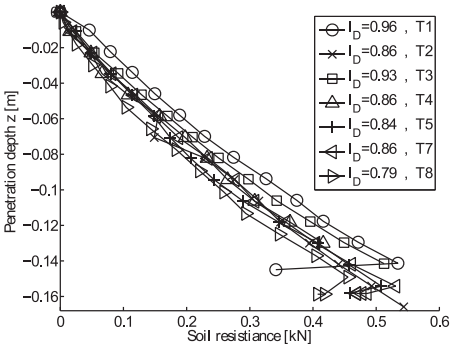

Figure 2. Monotonic test results.

4.2 Monotonic test

The monotonic test (T1) was performed as a deformation controlled test where the pile was moved at a constant rate until a displacement of one diameter at sand surface was reached. The

displacement, the applied force and the rotation were recorded. In Figure 3 the result from the monotonic load test can be seen. Here the rotation of the pile top is plotted against the applied force. As it can be seen from the figure no maximum capacity is reached. Therefore a rotation criterion was used for define the failure.

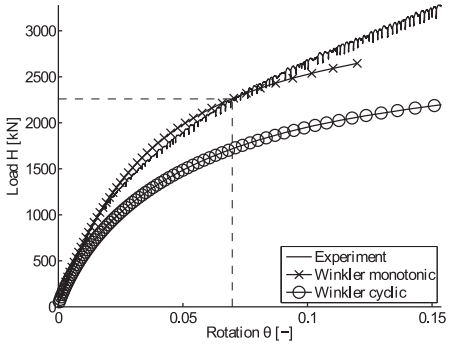

Figure 3. Monotonic test results.

The failure is defined at a rotation of 4 degrees = 0.0698 rad. The maximum prototype load is thus found to be H_{mon}=2295 kN. The Winkler model is here fitted to the monotonic test and shows therefore a good agreement with the experiments. For comparison, the load-displacement curve for cyclic loading is also shown at figure 3. Note that the design methodology leads to a general reduction in capacity of stiffness, but does not take load orientation, load level and number of cycles into account for cyclic loading.

4.3 Cyclic tests

With the maximum capacity found from the monotonic test, the values for the cyclic testing can be determined. The cyclic loading is carried out using a feedback control system. A sinusoidal signal is generated according to the non-dimensional parameters wanted. Due to the feedback control system it is not always that the pile response is exactly as wanted. This can lead to difference between the measured non-dimensional parameters and the planned.

In figure 4 an example of a cyclic test series is shown. A small difference in maximum and minimum values can be seen. This is due to difficulties in the feedback control. From a test like this maxima and minima from every cycle can be found.

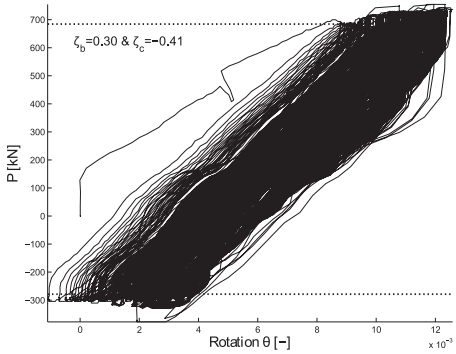

Figure 4. Load deflection result for cyclic test T3.

When the extremes are found, deflection, rotation, damping and secant stiffness from every cycle can be determined. Figure 5 shows the maximum rotation from every cycle of test T3. The accumulation of rotation may be fitted to a power function, see equation (3). This corresponds with observations done in [10].

$$\frac{\theta_{max,N}}{\theta_{max,1}} = N^{\alpha} \tag{3}$$

Some scatter in the data can be seen, but the power function seems to capture the accumulation of rotation quite well, see Figure 5. This is the case for all the cyclic tests performed in this test series.

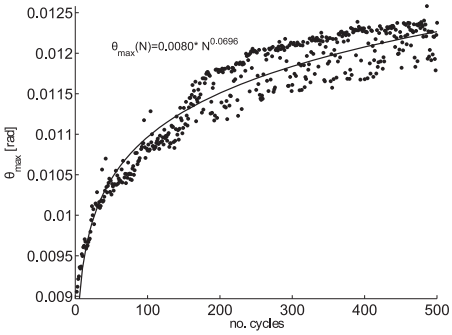

Figure 5. Maximum rotation from every cycle, test T3

From Figure 5, it can be seen that an asymptotic value of the rotation is not reached. Even for test number T7 with 1000 identical cycles it

was not possible to assess that an asymptotic value was reached. Hence, tests with an even larger number of cycles should be carried out in order to get a more reliable estimate on the accumulation law.

4.3.1 Load orientation, ζ_c

To investigate the load orientation, four cyclic tests was performed. Recently, [9] reported that a ζ_c value of -0.6 was the most critical one, based on tests carried out as 1g test.

Table 3. Centrifuge test program, N = number of cycles

ζ_c	ζ_b	N	α	Test nr.
-0.84	0.28	500	0.0154	T2
-0.41	0.30	500	0.0696	T3
0.17	0.30	500	0.0307	T4
0.55	0.30	500	0.0227	T5

To investigate this, four tests were performed, with the non-dimensional cyclic parameters as listed in Table 3. ζ_b is more or less kept constant and the influence from changing ζ_c can therefore be seen.

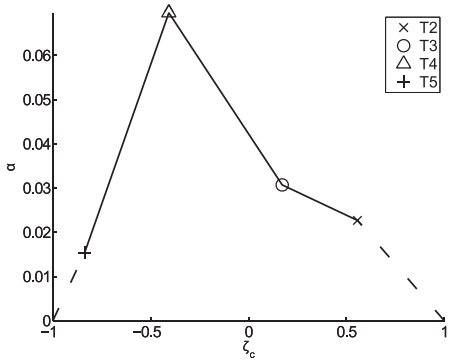

Figure 7. Load orientation effects from cyclic tests.

The results from the power fit of the first four cyclic tests can be seen in Table 3 and Figure 7. It confirms the observation made by [9]. A cyclic load situation between one-way and two loading results in larger accumulation of rotation compared with pure one-way loading. It was therefore chosen to continue the cyclic testing with a ζ_c=-0.4.

4.3.2 Load amplitude, ζ_b

Having identified the most critical load orientation, the effect from the load amplitude was investigated. The non-dimensional cyclic parameters and the results from the four tests can be seen in Table 4.

Table 4. Centrifuge test program, N = number of cycles

ζ_c	ζ_b	N	α	Test nr.
-0.36	0.08	500	0.0132	T6
-0.31	0.20	500	0.0406	T7
-0.41	0.30	500	0.0696	T3
-0.46	0.38	500	0.1148	T8

It is clear that an increase in amplitude leads to an increase in accumulation of rotation. Even though it has not been possible to keep ζ_c constant for the four tests, it is seen in Figure 8 that the deviation does not seem to affect the result. A power function seems to be a good approximation. This deviates with the 1g experiments from [9], where a linear relationship is reported. The power function furthermore ensures that no accumulations occur for a ζ_b=0 which seems more appropriate.
The power function can be written as:

$$\alpha(\zeta_b, \zeta_c) = A \cdot {\zeta_b}^{B(\zeta_c)} \tag{4}$$

A and B was found to A=0.4 and $B_{\zeta c=-0.41}$=1.37. The value A is independent of the load orientation and amplitude.

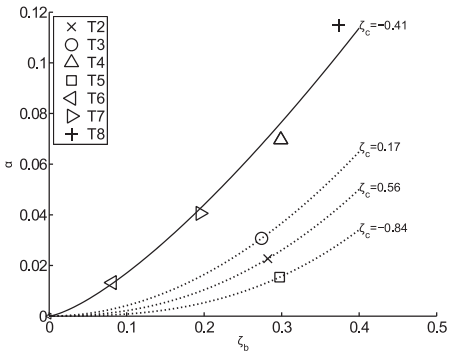

Figure 8. Rotational accumulation parameter.

The value B can be found and calculated from Figure 7 in the following way.

First the α-value for a given load orientation is found using Figure 7. This value is used in Equation 5 with the A value found from the test on load amplitude effects.

$$B(\zeta_c) = \frac{ln\left(\frac{\alpha(\zeta_c)}{0.4}\right)}{\ln(0.3)} \quad (5)$$

When B is found, Equation 4 can be used to determine the rotational accumulation parameter α, for the given load situation.

5 EXAMPLE

The maximum rotation is wanted for a 2 m in diameter monopile. The cyclic loading is pure one-way loading (ζ_c=0) and has and amplitude of 25% of the maximum bearing capacity (ζ_b=0.25). The pile is subjected to 10^7 cycles which is the fatigue limit state. The maximum bearing capacity was found to be H=2295 kN, giving H_{max} = 2295 · 0.25 = 574 kN. The maximum rotation for this load for the first cycle can then be found from Figure 3 as: $\theta_{max,1} = 0.008$. From Figure 7, the rotational accumulation parameter α for ζ_c=0 can be found to α=0.04. This is used in Equation 5, and the B value is found to:

$$B = \frac{ln\left(\frac{0.04}{0.4}\right)}{\ln(0.3)} = 2.9 \quad (5)$$

The rotational accumulation parameter α, for the given load situation (ζ_b=0.25) can then be calculated by Equation 4:

$$\alpha = 0.4 \cdot 0.25^{2.9} = 0.007 \quad (6)$$

The maximum rotation for the monopile subjected to 10^7 cycles can then be found using equation 3 to:

$$\theta_{max} = 0.008 \cdot (10^7)^{0.007} = 0.009\, rad \quad (7)$$

6 CONCLUSIONS

A series of cyclic centrifuge tests was carried out at the geotechnical centrifuge at DTU. One of the key issues for the design of a monopile for wind turbine was investigated. It was clearly seen that the accumulation of rotation is highly affected by the characteristic of the cyclic loading, and by the load amplitude. A design procedure for monopile with a diameter of 2 m has been given and can be applied for any load amplitude, orientation and number of cycles. This is not the case for the current design methodology.

All the cyclic tests do not reach a steady state and it can therefore be concluded that 500 cycles is not enough. This should therefore be increased in further cyclic centrifuge tests.

REFERENCES

[1] L. C. Reese & H. Matlock, Dimensional Solutions for Laterally Loaded Piles with Soil Pile Modulus Assumed Proportional to depth, Proceedings of the 8th Conference on Soil Mechanics (1956), 1-41

[2] B. McClelland & J. A. Focht, Soil modulus for laterally loaded piles, Journal of the soil mechanics and foundation division – Proceedings of the American Society of Civil Engineers (1958), 1-22

[3] API RP 2A-WSD, Recommended Practice for Planning, Designing and Constructing Fixed Offshore Platforms - Working Stress Design (2000)

[4] J. M. Murchison & M. W. O'Neill, Soil modulus for laterally loaded piles in sand, Journal of Geotechnical Engineering Vol.120 (1984), 174-191

[5] R. T. Klinkvort C. T Leth & O. Hededal, Centrifuge modeling of a laterally cyclic loaded pile, International Conference on Physical Modelling in Geotechnics - 7th, (2010), 959-964

[6] R. T. Klinkvort, Centrifuge modelling of monopiles, Geotechnical Engineering 20, View of Young European Geotechnical Engineers (2010)

[7] C. T Leth, A. Krogsbøll & O. Hededal, Centrifuge facilities at Danish Technical University, 15th Nordic Geotechnical Meeting (2008)

[8] J. Garnier et al., Catalogue of scaling laws and similitude questions in centrifuge modelling, International Journal of Physical Modelling in Geotechnics Vol 7 III (2007)

[9] C. Leblanc, G. T. Houlsby & B. W. Byrne, Response of stiff piles in sand to long-term cyclic lateral loading, Géotechnique 60 no 2 (2010), 79-90

[10] R. T. Klinkvort & O. Hededal, Centrifuge modelling of offshore monopile foundation, Frontiers in Offshore Geotechnics II (2010), 581-586

Paper VI

"Lateral response of monopile supporting an offshore wind turbine"

R. T. Klinkvort & O. Hededal

Accepted for publication in: *Geotechnical Engineering, 2013*

Lateral response of monopile supporting an offshore wind turbine.

Rasmus Tofte Klinkvort[1] and Ole Hededal[2]

1) Ph.D. research student, Dept. of Civil Engineering, Technical University of Denmark, Sec. of Geotechnics and Geology, Brovej Building 118, 2800 Kgs. Lyngby, Denmark. Phone: (+45) 25 38 78 13, rakli@byg.dtu.dk.

2) Associate Professor, Dept. of Civil Engineering, Technical University of Denmark, Sec. of Geotechnics and Geology, Brovej Building 118, 2800 Kgs. Lyngby, Denmark. Phone: (+45) 45 25 50 20, olh@byg.dtu.dk.

Date written: Monday, June 25, 2012

Date revised: -

Number of words: 4455

Number of pages: 21

Number of figures: 10

Number of tables: 2

Abstract

One of the geotechnical challenges for a monopile supported offshore wind turbine is to create a foundation design procedure that incorporates the effects of cyclic loading from wind and waves in a safe and easy way. Improved procedures may enable the use of monopiles on deeper waters, securing still a robust and cost beneficial foundation design. In order to develop new design procedures it is essential to understand the pile-soil interaction. With centrifuge tests as the basis, this paper discusses the effects of the soil-pile interaction with the focus on accumulation of displacements and change in secant stiffness in dense sand. Hence, a centrifuge test series simulating idealised cyclic load on a monopile supporting an offshore wind turbine was carried out. The validity of these centrifuge tests is discussed and a simple design procedure for the prediction of the accumulation of displacements and change in secant stiffness based on the results from the centrifuge tests is presented.

Keywords: Renewable energy, Offshore engineering, Geotechnical engineering

Notations

d:	Diameter of pile	H :	Applied lateral load
l_e:	Load eccentricity	$\tilde{P}$:	Normalised applied load
l_L:	Pile penetration depth	$\tilde{K}$:	Normalised secant stiffness
φ'_{max}:	Maximum angle of friction	ζ_b, ζ_c :	Load characteristic parameters
φ'_{cr}:	Critical state angle of friction	N :	Number of cycles
I_D:	Relative density	α, κ :	Evolution parameter
p':	Mean pressure	T_b, T_c :	Dimensionless functions
η :	Gravity scaling factor	κ_b, κ_c :	Dimensionless parameters
N_s:	Geometrical scaling factor	$\tilde{K}_s, \tilde{K}_c$:	Dimensionless parameters
Y :	Pile displacement		
$\tilde{Y}$:	Normalised pile displacement		

INTRODUCTION

Today one of the most common foundation methods for offshore wind turbines is the monopile. The monopile is a single, large diameter tubular steel pile with a diameter of 4-6 meters, driven to a depth 5-6 times the diameter into the seabed. Wind turbines are affected by lateral cyclic loads from waves and winds, which at seabed subject the pile to shear forces and bending moments. The combined loads on the wind turbine have to be supported by the foundation, (Byrne, Houlsby 2003).

The pile design for the lateral loads is today normally based on a Winkler model where the pile is modelled as a beam and the soil as a system of uncoupled non-linear springs, e.g. (API 2007). From this, one overall displacement and stiffness of the monopile can be calculated. This procedure neither takes the number of cycles nor the characteristics and the magnitude of the cyclic loading into account. The design methodology originates from tests on long slender piles with a few number of cycles, (Reese, Matlock 1956) & (McClelland, Focht 1956). Even though calibrated to slender piles, the method is – without modifications – applied in the design of large diameter monopiles. Furthermore, since the dynamic response of the integrated structure - turbine, tower and foundation – is sensitive to stiffness and displacements of the soil pile system, it is important to take such variation into account in the design.

Several studies on the cyclic response of laterally loaded piles have been reported (Briaud, Smith & Meyer 1983), (Long, Vanneste 1994) & (Lin, Liao 1999) . Still, the number of investigations is limited and the majority of studies have been carried out on long slender piles. The performance of monopiles subjected to cyclic loading was investigated by (LeBlanc, Houlsby & Byrne 2010) in a series of 1g model tests. They found that the evolution of rotation and stiffness depends on the number of cycles, as well as on the magnitude and the characteristic of the load cycles. With these findings in mind, this paper propose a model which can be used to determine displacement and stiffness depending on the number of cycles, the magnitude and the characteristic of the load cycles. The model is based on a set of centrifuge tests.

MODEL FRAMEWORK

The cyclic response of a pile can be described in terms of pile head displacement, *Y*, and the applied lateral load of the pile, *H*. Normalising these parameters enables comparison of results across scale. Here it is chosen to normalise with the diameter of the pile and the effective density γ'.

$$\tilde{Y} = \frac{Y}{d} \qquad \& \qquad \tilde{P} = \frac{H}{\gamma' \cdot d^3}$$

Equation 1

A schematic response of a pile for constant amplitude cyclic loading is shown in Figure 1. In each load cycle the maximum and minimum value of the load ($\tilde{P}_{\max,N}$, $\tilde{P}_{\min,N}$) and the displacement ($\tilde{Y}_{\max,N}$, $\tilde{Y}_{\min,N}$) can be obtained. The maximum displacement and the cyclic secant stiffness from each cycle can therefore be determined. The maximum displacement is found as the displacement when the load is at the maximum of each cycle and the cyclic secant stiffness is found as the slope of a straight line between the extremes for every cycle, see Figure 1.

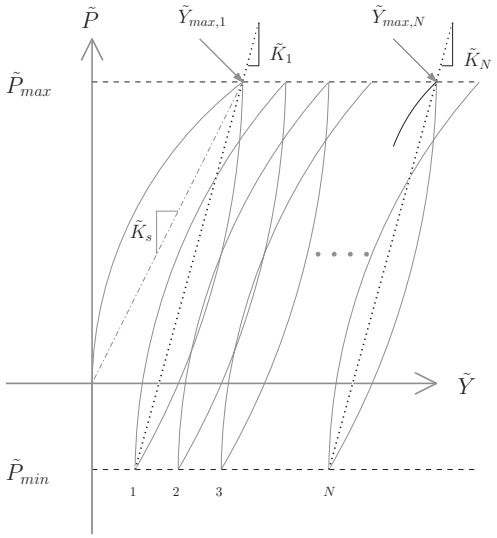

Figure 1 Schematic drawing of determination of secant stiffness and maximum accumulated displacement.

Having determined the bearing capacity of the pile from a monotonic test, ($\tilde{P}_{mon}$), the cyclic loading can be described by two non-dimensional parameters.

$$\zeta_b = \frac{\tilde{P}_{\max}}{\tilde{P}_{mon}} \qquad \zeta_c = \frac{\tilde{P}_{\min}}{\tilde{P}_{\max}}$$

Equation 2

The value ζ_b defines the load amplitude relative to the maximum bearing capacity, $\tilde{P}_{mon}$, and ζ_c defines the characteristic of the cyclic loading.

Evolution models

Having cyclic loading described by the parameters (ζ_b, ζ_c), the maximum displacement from the number of cycle (*N)* may be determined from a power function,

$$\tilde{Y}_{\max,N} = \tilde{Y}_{\max,1} \cdot N^{\alpha}$$

Equation 3

The coefficient, α, is dependent both on the load characteristic described by ζ_c and the magnitude of the loading described by ζ_b. Assuming the two effects to be independent, the value of α can be calculated as a product of two non-dimensional functions.

$$\alpha(\zeta_c, \zeta_b) = T_c(\zeta_c) \cdot T_b(\zeta_b)$$

Equation 4

The first function, T_c, depends on the load characteristic, ζ_c, and the second function, T_b, depends on the load magnitude, ζ_b.

The cyclic secant stiffness in every cycle is described by a logarithmic function;

$$\tilde{K}_N = \tilde{K}_1\left(1 + \kappa \cdot \ln(N)\right)$$

Equation 5

In Equation 5, κ is the accumulation rate, $\tilde{K}_1$ is the cyclic secant stiffness for the first cycle and $\tilde{K}_N$ is the cyclic secant stiffness for cycle number *N*.

As for the accumulation of displacements, it is chosen to describe the value of κ by two independent non-dimensional functions.

$$\kappa\left(\zeta_c, \zeta_b\right) = \kappa_c(\zeta_c) \cdot \kappa_b(\zeta_b)$$

Equation 6

The non-dimensional cyclic secant at the first cycle, $\tilde{K}_1$, is found using the secant stiffness of the monotonic response.

$$\tilde{K}_s(\zeta_b) = \frac{\tilde{P}_{\max}}{\tilde{Y}_{\max}}$$

Equation 7

This value is appropriately scaled by $\tilde{K}_c(\zeta_c)$ which depends on the cyclic load characteristic, i.e.

$$\tilde{K}_1\left(\zeta_c, \zeta_b\right) = \tilde{K}_c(\zeta_c) \cdot \tilde{K}_s(\zeta_b)$$

Equation 8

The input to the two evolution models can be established from a monotonic test combined with the non-dimensional functions, $(T_c(\zeta_c), T_b(\zeta_b)$, $\kappa_c(\zeta_c), \kappa_b(\zeta_b)$ and $\tilde{K}_c(\zeta_c), \tilde{K}_s(\zeta_b))$. These functions can be empirically determined by a series of cyclic load tests.

METHOD

To determine the non-dimensional function used in the prediction model a centrifuge test series is designed. A model pile subject to idealized load cycles representing a monopile supporting an offshore wind turbine is used. In order to model the response correctly, it is important to design a load setup, which applies the load

in a way similar to a wind turbine foundation, (Klinkvort, Leth & Hededal 2010). Here, the combined cyclic loads acting on a wind turbine is simplified to a single total force resultant acting between sea level and nacelle height, see Figure 2.

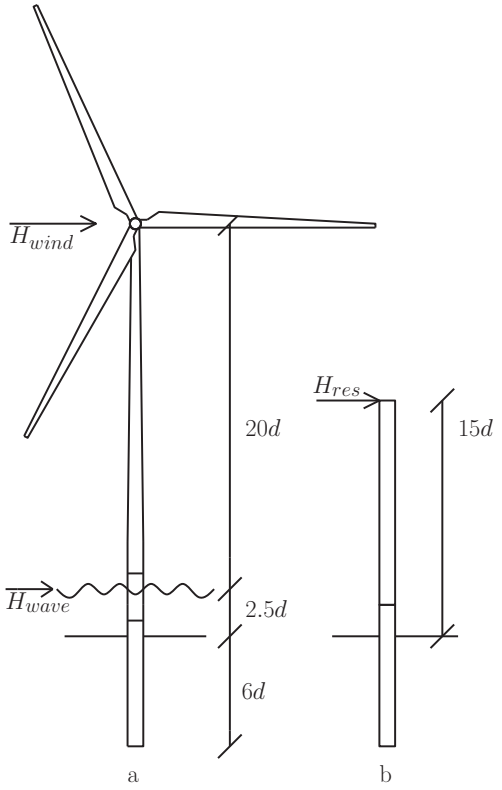

Figure 2 Non-dimensional drawing of offshore wind turbine and centrifuge model pile

A sketch of the centrifuge pile setup is shown in Figure 3. A circular barrel with an inner diameter d_b=500mm is used. The soil sample consists of a homogenous dense sand layer with a height of h_b=388mm. The cyclic tests series was performed with two different solid steel piles. The piles are made of respectively 24 and 36 mm steel core with a 2 mm epoxy coating leading to a total diameter of d = 28 mm and d = 40 mm. The load eccentricity and the penetration depth of the piles were kept constant, l_e = 15d and l_L = 6d for the all tests. The load is measured at pile head and lateral displacements are measured 2d above sand surface.

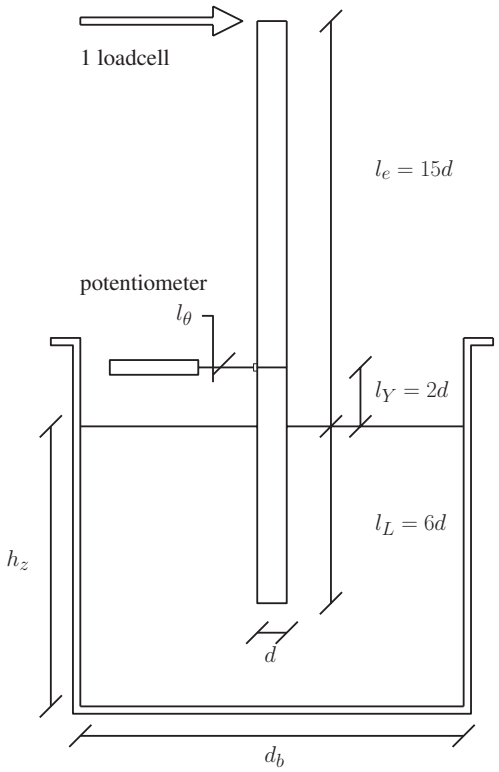

Figure 3 Sketch of the centrifuge setup

The sand was prepared in the centrifuge container by dry pluvation using a single spot hopper. An average relative density is calculated from the weight of the sand sample. The saturated tests samples were flooded from below with de-aired water after pluvation. All centrifuge tests were performed in dense Fontainebleau sand with a relative density of approximate 90 %. The triaxial results showed a maximum angle of friction corresponding with the observations done by (Bolton 1986) using a critical state angle of $\varphi'_{cr}=30^{o}$. The classification and triaxial parameters are shown in Table 1, (Leth, Krogsbøll & Hededal 2008).

The pile was installed by jacking. All d = 28 mm piles were installed at 1g while all d = 40 mm piles were installed at an elevated g-level in order to minimize installation effects. Installation at full stress level is preferable, but a 20 kN limit on the jack precluded full in-flight installation. The procedure for the test sequence was to spin the centrifuge up; install the pile and then stop the centrifuge.

Table 1 Classification and triaxial parameters for the Fontainebleau sand

Specific gravity of particles, G_s	2.646
Minimum void ratio, e_{min}	0.548
Maximum void ratio, e_{max}	0.859
Average grain size, d_{50}, mm	0.18
Coefficient of uniformity, C_u	1,6
d/d_{50}	156-222
$\varphi'_{max} \approx \varphi'_{cr} + 3(I_D(10 - ln(p')) - 1)$	

After the pile was installed the jack was removed and the lateral loading equipment was placed. Finally the centrifuge was accelerated to the prescribed g-level, and the load tests were performed.

The centrifuge is used to increase the effective density of the soil corresponding to a offshore prototype pile with a diameter of approximately 3 meters. The centrifuge technique can be seen e.g. (Schofield 1980) & (Garnier et al. 2007). The increase in g-field, η and the geometrical scaling factor, N_s does not have to be the same if no excess pore pressure is generated, (Li, Haigh & Bolton 2010). To verify the effective stress scaling approach, four monotonic tests were performed, two in saturated sand and two in dry sand, with effective stress levels corresponding to a prototype pile with a diameter of respectively 1 and 3 meters. As seen in Figure 4, there is practical no differences between the responses of a pile in saturated and dry sand. This validates the scaling approach as long as fully drained conditions are maintained during loading.

Results

Five monotonic and twelve cyclic tests have been performed, see Table 2;. The monotonic tests were used as validation of the scaling approach and as a reference for the cyclic tests. First seven cyclic tests on the d=28 mm pile in dry sand was performed. From these test, the non-dimensional functions was established. This was done by first changing the load amplitude of the cyclic loading (ζ_b), while keeping the characteristic of the cyclic loading (ζ_c) constant. Afterwards the effect of the characteristic of the cyclic loading was investigated by changing ζ_c while keeping ζ_b constant. Later, two tests on a d=40 mm pile were performed to see the influence of number of cycles and three tests were used to see the influence from performing cyclic

test in saturated sand. Although tests were performed on different sized piles and in dry or saturated conditions, the non-dimensional functions determined from the first 7 tests proved representative for the entire test series.

Monotonic test

All monotonic tests were performed with deformation controlled loading of the pile with a constant rate of one diameter per minute. This was so slow that fully drained loading conditions were ensured, as seen in Figure 4.

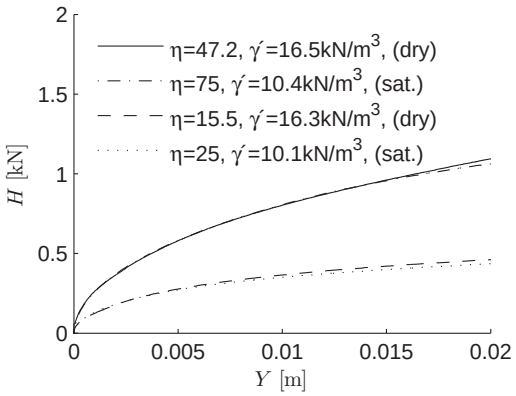

Figure 4 Validation of scaling approach, d=40mm

In Figure 5 the result from the monotonic load tests can be seen. Here the normalised displacement of the pile is plotted against the applied normalised force. The two monotonic tests performed on the model pile with a diameter of d = 40 mm show identical results. The pile with a diameter of d = 28 mm shows initially the same response as the two other piles, but the response starts to deviate from a pile head displacement above 0.05 d. A reason for the deviation could be that the d = 28 mm piles is installed at 1g, whereas the d = 40 m piles are installed at an elevated stress field. As demonstrated by (Dyson, Randolph 2001) 1g installation leads to a softer response.

It can be seen from Figure 5 that the ultimate capacity was not reached for any of the tests. Therefore a rotation criterion was used to define the reference bearing capacity, $\tilde{P}_{mon}$. Failure was defined at a rotation of 4 degrees for the piles with a diameter of d = 40 mm. The maximum normalised force was found to be

$\tilde{P}_{mon} = 19$. This is shown in Figure 5 as a dotted line. At load level less than $0.4\,\tilde{P}_{mon}$, the monotonic response from the three tests is identical. Since all cyclic tests were performed below this level. it is chosen to use the results from the different pile diameter to calibrate the model.

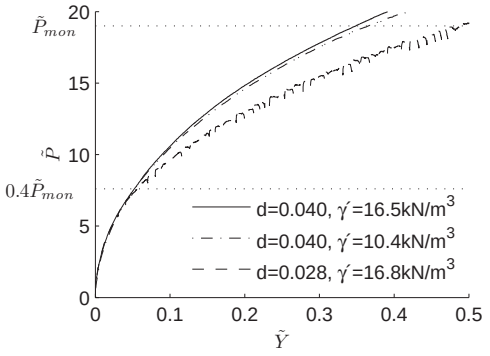

Figure 5 Normalised monotonic test results

Calibration of model

The cyclic tests series consist of 12 tests performed with a setup which subjects the piles with load controlled cycles with a period of 10 sec. The tests were designed so the cyclic loading of the pile was performed with a magnitude comparable to the serviceability load of an offshore wind turbine, according to (LeBlanc, Houlsby & Byrne 2010).

Evolution of deflection

The accumulation of displacement may be described by a power function. The maximum deflection for all cycles plotted together with the power fit is shown in Figure 6. It can be seen that the power fit captures the accumulation of displacement well. The results together with the non-dimensional cyclic load characteristics can be seen in Table 2.

Table 2 Test program

Test nr.	Type	Diameter [mm]	Saturated	I_D	ζ_c	ζ_b	*no. of cycles*	α	$\tilde{K}_0$	κ
1	Monotonic	28	No	0.88	1	1	-	-	-	-
2	Monotonic	40	No	0.94	1	1	-	-	-	-
3	Monotonic	40	Yes	0.96	1	1	-	-	-	-
4	Monotonic	40	No	0.83	1	1	-	-	-	-
5	Monotonic	40	Yes	0.80	1	1	-	-	-	-
6	Cyclic	28	No	0.86	0.54	0.27	500	0.068	1185	-0.017
7	Cyclic	28	No	0.93	0.16	0.25	500	0.097	881	-0.021
8	Cyclic	28	No	0.86	-0.41	0.29	500	0.117	486	0.10
9	Cyclic	28	No	0.84	-0.84	0.28	500	-0.115	304	0.27
10	Cyclic	28	No	0.84	-0.37	0.08	500	0.032	1618	0.09
11	Cyclic	28	No	0.86	-0.32	0.18	1000	0.077	557	0.06
12	Cyclic	28	No	0.79	-0.46	0.36	500	0.088	360	0.13
13	Cyclic	40	No	0.93	-0.50	0.33	10000	0.089	332	0.16
14	Cyclic	40	No	0.94	-0.96	0.34	3000	-0.349	193	0.29
15	Cyclic	40	Yes	0.96	-0.39	0.36	250	0.137	309	0.14
16	Cyclic	40	Yes	0.87	-0.47	0.36	250	0.126	424	0.07
17	Cyclic	40	Yes	0.95	0.05	0.15	300	0.087	968	-0.023

The value of α can be calculated using two non-dimensional cyclic functions as shown in Equation 4. By normalising $T_c = 1$ for pure one-way loading, $\zeta_c = 0$, the non-dimensional function T_b can be found from a series of test where ζ_b is changed while $\zeta_c = 0$.

$$\alpha\left(\zeta_c = 0, \zeta_b\right) = 1 \cdot T_b(\zeta_b)$$

Equation 9

When T_b is created the function T_c may be found by performing a series of test with a constant ζ_b and then dividing the results with the T_b function, i.e.

$$T_c(\zeta_c) = \frac{\alpha}{T_b(\zeta_b)}$$

Equation 10

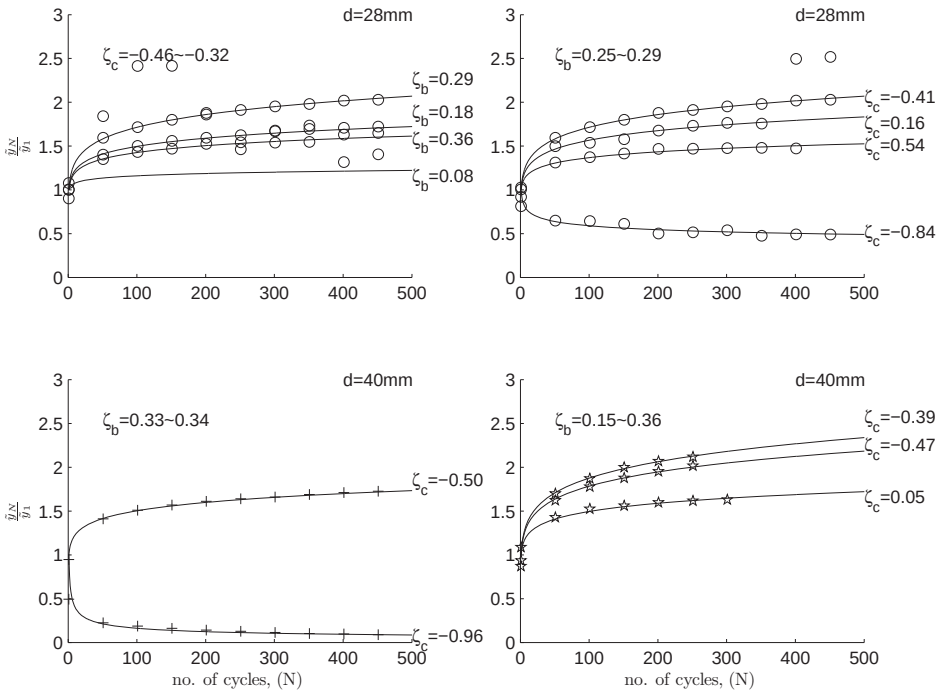

Figure 6 Accumulation of displacement from cyclic tests

The result of this analysis can be seen in Figure 7. It was chosen to force the values of T_b to be a straight line and then to plot the corresponding value of T_c. The linear dependency of the load magnitude can be seen in Equation 11.

$$T_b(\zeta_b) = 0.61\zeta_b - 0.013$$

Equation 11

The function T_b cannot be negative, hence cyclic loading with a small magnitude $\zeta_b \leq 0.02$, will lead to a value $T_b = 0$, implying that the pile-soil interaction is reversible and no accumulation of displacements will occur.

Figure 7 shows results for the cyclic load characteristic function T_c. The results seem to follow a third order polynomial, see Equation 12.

$$T_c(\zeta_c) = (\zeta_c + 0.63)(\zeta_c - 1)(\zeta_c - 1.64)$$

Equation 12

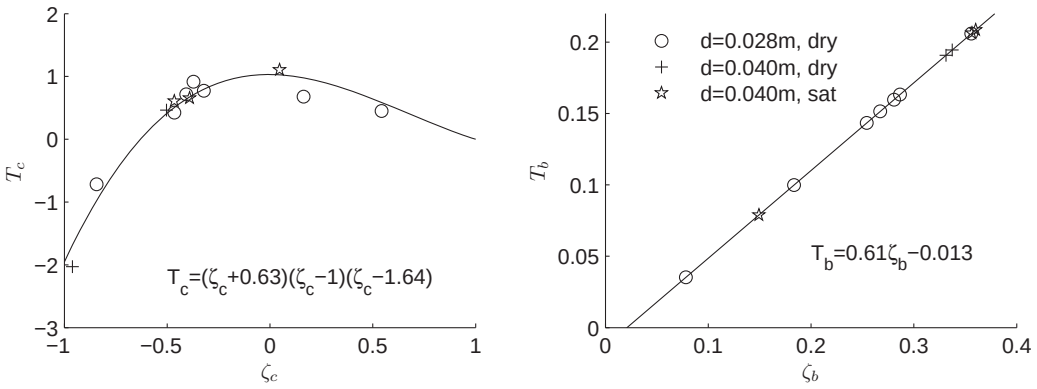

Figure 7 Cyclic dimensionenless functions for accumulation of displacements

The function secures that $\alpha = 0$ for monotonic loading, $\zeta_c = 1$. The maximum value of the function is found $\zeta_c = -0.01$, which means that the most damaging load situation is when the monopile is loaded in a more or less pure one-way loading. When $\zeta_c \leq -0.63$ the function T_c becomes negative, which means that the accumulation of displacement is reversed and the pile moves towards its initial position.

Since both dry and saturated condition have been used in the tests, this shows that all tests are fully drained and the chosen scaling approach seems valid also for quasi static cyclic loading. From the non-dimensional functions we can conclude that the accumulation coefficient, α, is increasing with increasing magnitude of the cyclic loading, and that the most damaging cyclic load orientation is in the interval of $-0.4 \leq \zeta_c \leq 0$.

The displacement for the first cycle is easily found from a monotonic test, and is only depending on the load magnitude. Having the monotonic load-displacement curve together with the non-dimensional functions shown in Equation 11 and Equation 12 thus makes it possible to estimate the displacement to a given number of cycles using Equation 3.

Evolution of secant stiffness

In Figure 8, the secant stiffness is plotted against the number of cycles. It shows that the logarithmic function seems to describe the changes in secant stiffness reasonably. The results of the logarithmic fits can be also been seen in Table 2.

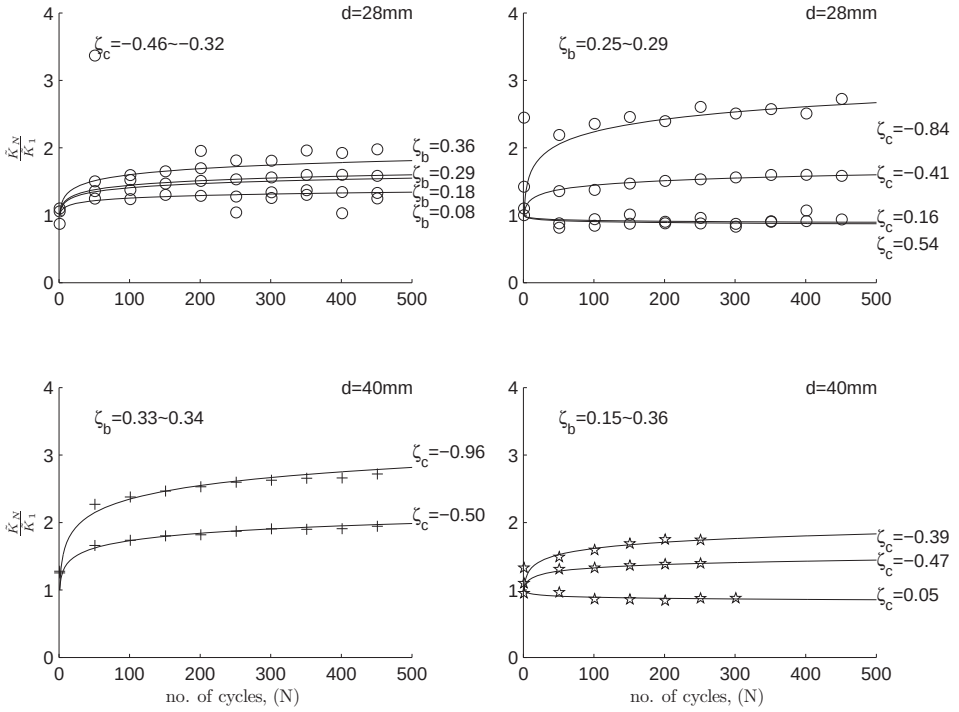

Figure 8 Change in secant stiffness from cyclic tests

The determination of the non-dimensional functions follows the same methodology as described for the displacements. The results are shown in Figure 9.

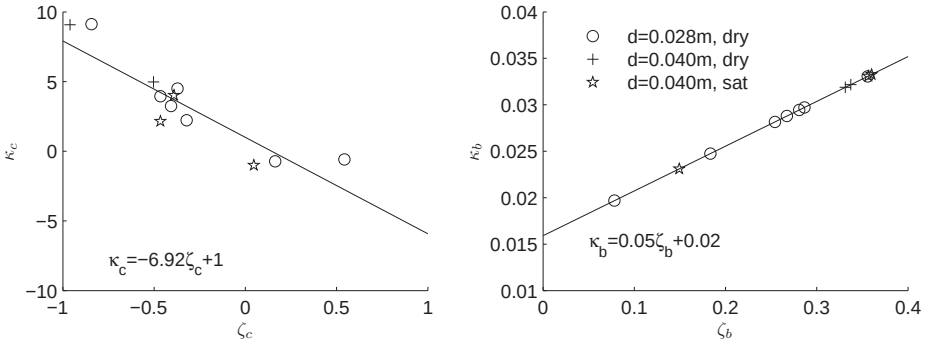

Figure 9 Cyclic dimensionenless functions for change in secant stiffness

A linear dependency of the load magnitude is found;

$$\kappa_b(\zeta_b) = 0.05\zeta_b + 0.02$$

Equation 13

Equation 13 implies that an increase in the cyclic load magnitude leads to an increase in the accumulation secant stiffness accumulation rate, κ . Having determined κ_b , the values of κ_c are plotted and it is seen that a linear fit seems to capture the trend, see Equation 14.

$$\kappa_c(\zeta_c) = -6.92\zeta_c + 1$$

Equation 14

It can be seen that going from one-way to two-way loading will lead to an increasing accumulation of stiffness.

The initial cyclic secant stiffness is found by considering the results of a monotonic test and cyclic tests with varying amplitude. The function $\tilde{K}_s(\zeta_b)$ is established directly from the monotonic load-displacement curve. The function $\tilde{K}_c(\zeta_c)$ is then evaluated from the cyclic tests. The results are shown in Figure 10, and it can be seen that a second order polynomial describe the variation of $\tilde{K}_c(\zeta_c)$,

$$\tilde{K}_c(\zeta_c) = 1.64\zeta_c^{\,2} + 3.27\zeta_c + 3.27$$

Equation 15

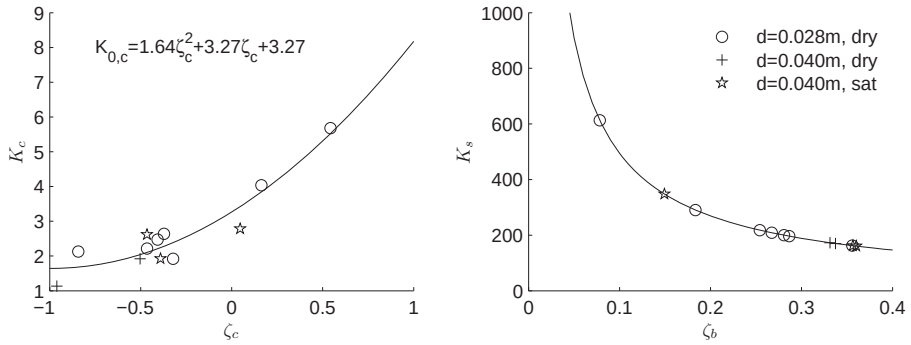

Figure 10 Cyclic dimensionenless functions for initial stiffness

From this equation, it should be recognized that the initial stiffness due to cyclic loading is stiffer than the monotonic stiffness. Depending on the characteristic of the cyclic loading, the initial cyclic secant stiffness may be 2 to 8 times the monotonic secant stiffness.

DISCUSSION

We have proposed a simple framework for the predication of displacements and stiffness from cyclic loading for monopiles supporting offshore wind turbines. This framework was calibrated by a set of centrifuge tests in order to determine a set of non-dimensional functions. The centrifuge tests represent simplifications of the complex wind-water-structure-soil interaction problem and these simplifications are discussed in connection with offshore prototype monopile conditions.

First of all, an offshore monopile is situated in saturated soil conditions. The centrifuge test series was carried out in primarily dry dense sand. Choosing an effective stress scaling approach enables us to model piles situated in saturated conditions using dry sand. This was demonstrated by four monotonic tests. A direct comparison between cyclic tests performed in dry and saturated conditions was not carried out, but looking at the non-dimensional functions derived from testing in dry and saturated condition, no difference is

registered. The scaling approach therefore seems valid. It is important to recognize that the results only are valid for drained loading conditions. Testing in water saturated sand does not represent full scale drainage which means that the water flow in the centrifuge setup is occurring N_s times faster compared to the prototype and it is therefore unlikely that pore pressures can build up at the current rate of loading. The possible accumulation of pore pressure has to be studied in more details.

Secondly, monopile diameters for offshore wind turbine foundations are ranging from 4 - 6 meters and are continuously increasing. The cyclic investigation was performed at a stress level corresponding to a d = 3 meter pile. Pilot tests carried out at The Technical University of Denmark indicate that the normalized response for centrifuge monopiles is identical, when the stress field is equal or larger than the stress field for a 3 meter in diameter pile. The reason for this can be recognized using the equation from the maximum angle of friction by (Bolton 1986) shown in Table 1. From this equation it can be seen that the maximum angle of friction at pile tip reduces only from 38^o to 37^o going from a stress field for 3 meter in diameter pile to 6 meter in diameter pile. It is therefore believed that the results of this tests series also can be used for larger diameters than 3 meters.

At last, the main part of the tests in this study involved 250-500 load cycles. Three tests were performed with more than 500 cycles; one test with 1000 cycles on the d=28mm pile and two tests on the d=40mm pile with respectively 3000 and 10000 numbers of cycles. From these tests it was seen that accumulation of displacement and secant stiffness was well described with the predictions based on the first 500 cycles. It therefore seems reasonable to use the results for up to 10000 cycles. This is still below the number of cycles for the fatigue limit state ($N = 10^7$), but it is an improvement compared to the original design method, (API 2007), which is based on tests with fewer than 50 cycles (Murchison, O'Neill 1984).

We have discussed some of the limitations of our simplified model. In general, the model framework is similar to the one proposed by (LeBlanc, Houlsby & Byrne 2010), but differences between the models are seen. One of the main findings from the 1g experiments was that the most damaging load situation was for two-way loading, i.e. $\zeta_c \approx -0.6$. The present centrifuge test series does not show this trend, instead it

indicates that one-way loading, $\zeta_c \approx 0$, is the most damaging one. From the tests by (LeBlanc, Houlsby & Byrne 2010) accumulation of rotation was seen regardless of the characteristic of the loading. This is also in contrast to the observation done in this study, where it was seen that the pile starts to move back against its initial position for pure two-way loading. This observation was also done by (Rosquët 2004) who performed centrifuge tests on long slender piles. One explanation of these disagreements can be the fact that the tests performed by (LeBlanc, Houlsby & Byrne 2010) was carried out in loose sand in order to model the maximum angle of friction correctly. The sand in the 1g experiments thus most likely starts to compact when loaded. Tests performed in a centrifuge model stresses and relative densities correctly, so the dilatant behaviour of sand is therefore better accounted for.

The correct modelling of stresses together with the chosen simplification indicates that the findings from our study are reliable and can be used in the predications of prototype monopiles.

CONCLUSION

The design of monopiles supporting offshore wind turbine is today one of the great geotechnical challenges for renewable energy, if this foundation concept shall succeed to deeper waters. The prediction of accumulation of displacements and change in pile-soil stiffness from cyclic loading are some of the main design drivers and models have to be improved. In order to establish a better design methodology, a series of centrifuge tests was carried out at the Technical University of Denmark. A setup simulating load conditions for an offshore monopile supporting a wind turbine was used to investigate the response.

Two key issues for the design of a monopile for wind turbine were investigated, accumulation of displacements and the change in secant stiffness. It was clearly seen that the accumulation of displacement and secant stiffness is affected by the characteristic of the cyclic loading, and by the load amplitude.

An empirically based design procedure for a monopile installed in dense saturated sand has been given, but should only be used for drained conditions. The design procedure can be applied for any load amplitude, load characteristic and number of cycles. Together with three sets of non-dimensional functions, the procedure

only needs a monotonic response in order to an address the accumulation of displacement and the change in stiffness. This gives a very simple design procedure which is superior the given methodology used in the industry today.

REFERENCES

API 2007, "API RP 2A-WSD Recommended practice for planning, designing, and constructing fixed offshore platforms - Working stress design,".

Bolton, M.D. 1986, "Strength and dilatancy of sands", *Geotechnique,* vol. 36, no. 1, pp. 65-78.

Briaud, J., Smith, T.D. & Meyer, B.J. 1983, "USING THE PRESSUREMETER CURVE TO DESIGN LATERALLY LOADED PILES", *Proceedings - Annual Offshore Technology Conference,* vol. 1, pp. 495-502.

Byrne & Houlsby 2003, "Foundations for offshore wind turbines", *Philosophical Transactions of the Royal Society London, Series A (Mathematical, Physical and Engineering Sciences),* vol. 361, no. 1813, pp. 2909-2930.

Dyson, G.J. & Randolph, M.F. 2001, "Monotonic lateral loading of piles in calcareous sand", *Journal of Geotechnical and Geoenvironmental Engineering,* vol. 127, no. 4, pp. 346-352.

Garnier, J., Gaudin, C., Springman, S.M., Culligan, P.J., Goodings, D., Konig, D., Kutter, B., Phillips, R., Randolph, M.F. & Thorel, L. 2007, "Catalogue of scaling laws and similitude questions in geotechnical centrifuge modelling", *International Journal of Physical Modelling in Geotechnics,* vol. 7, no. 3, pp. 1-23.

Klinkvort, R.T., Leth, C.T. & Hededal, O. 2010, "Centrifuge modelling of a laterally cyclic loaded pile", *Physical Modelling in Geotechnics,* pp. 959-964.

LeBlanc, C., Houlsby, G.T. & Byrne, B.W. 2010, "Response of stiff piles in sand to long-term cyclic lateral loading", *Geotechnique,* vol. 60, no. 2, pp. 79-90.

Leth, C.T., Krogsbøll, A.S. & Hededal, O. 2008, "Centrifuge facilities at Technical University of Denmark", *Proceedings Nordisk Geoteknikermøte nr.15,* pp. 335-342.

Li, Z., Haigh, S.K. & Bolton, M.D. 2010, "Centrifuge modelling of mono-pile under cyclic lateral loads", *Physical Modelling in Geotechnics, ,* pp. 965-970.

Lin, S. & Liao, J. 1999, "Permanent strains of piles in sand due to cyclic lateral loads", *Journal of Geotechnical and Geoenvironmental Engineering,* vol. 125, no. 9, pp. 798-802.

Long, J.H. & Vanneste, G. 1994, "Effects of Cyclic Lateral Loads on Piles in Sand", *Journal of Geotechnical and Geoenvironmental Engineering,* vol. 120, no. 1.

McClelland, B. & Focht, J., J.A. 1956, "Soil modulus for laterally loaded piles", *American Society of Civil Engineers -- Proceedings -- Journal of the Soil Mechanics and Foundations Division,* vol. 82.

Murchison, J.M. & O'Neill, M.W. 1984, "EVALUATION OF P-Y RELATIONSHIPS IN COHESIONLESS SOILS", *Analysis and Design of Pile Foundations.Proceedings of a Symposium in conjunction with the ASCE National Convention.,* , pp. 174-191.

Rosquët, F. 2004, *PIEUX SOUS CHARGE LATERALE CYCLIQUE*, L'École Centrale de Nantes et l'Université de Nantes.

Schofield, A.N. 1980, "Cambridge geotechnical centrifuge operations", *Geotechnique,* vol. 30, no. 3, pp. 227-268.

Paper VII

"An elasto-plastic spring element for cyclic loading of piles using the p-y-curve concept"

O. Hededal & R. T. Klinkvort

Published in: *Numerical Methods in Geotechnical Engineering, 2010*

Numerical Methods in Geotechnical Engineering – Benz & Nordal (eds)
© 2010 Taylor & Francis Group, London, ISBN 978-0-415-59239-0

A new elasto-plastic spring element for cyclic loading of piles using the p-y-curve concept

Ole Hededal & Rasmus Klinkvort
Department of Civil Engineering, Technical University of Denmark

ABSTRACT: Modeling the response of large diameter piles subjected to lateral loading is most often done by means of p-y-curves in combination with Winkler beam models. Traditionally the p-y curves are formulated as non-linear (elastic) relations between the lateral movement y and the soil response pressure p in terms of monotonic loading (until failure) as e.g. prescribed by API (2000). However, the cyclic and dynamic performance is only to a limited degree accounted for. Here the elasto-plastic framework is applied allowing definition of unloading-reloading branches, hence enabling modeling of cyclic response. The present model can account for effects like pre-consolidation and creation of gaps between pile and soil at reversed loading. Results indicate that the model is able to capture hysteresis during loading with full cycles and model the accumulated displacement observed on piles subjected to "half cycles" as e.g. seen from centrifuge tests carried out. This article presents the theoretical formulations, discusses numerical implementation and finally presents simulations.

1 INTRODUCTION

Modeling the response of large diameter piles subjected to lateral loading is most often done by means of p-y-curves in combination with Winkler beam models. Traditionally, the p-y curves are formulated in terms of non-linear (elastic) relations between the lateral movement y and the soil response pressure p in terms of monotonic loading (until failure). These curves were established by back-analysis of a series of tests carried out in the 1950es by Matlock and co-workers. The tests were primarily static, monotonic load tests, but also a few cyclic tests were carried out.

Matlock (1970) carried out further cyclic tests on piles in clay that revealed a general reduction of the ultimate capacity for piles subjected cyclic loading compared to monotonic loading. This led to a general reduction of the cyclic ultimate capacity compared to the monotonic ultimate capacity. This reduction or cyclic degradation as it is commonly denoted is incorporated in almost all design codes, e.g. API (2000), as a formal reduction of the ultimate capacity. Still, the models does not directly correlate the reduction to the characteristics of the cyclic loading, i.e. number of cycles, loading amplitude or frequency.

Matlock (1970) and later Mayoral et al. (2005) set up a conceptual model for pile-soil interaction from these observations, cf. Figure 1. The model consists of 3 parts. Firstly, a loading phase where the soil-pile interaction follows the virgin curve. Secondly, an unloading phase that due to irreversible deformations in the soil will imply the development of a gap between the pile and the soil. Finally, a phase where the pile moves towards the initial position and into the opposite

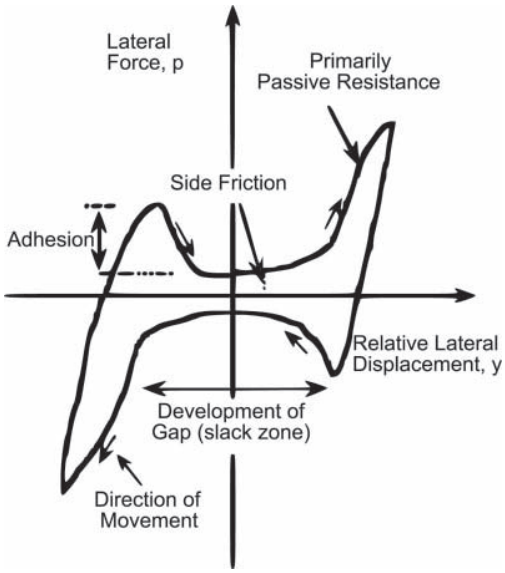

Figure 1. Typical loading cyclic for a model pile in clay, from Mayoral et al. (2005).

soil face in the cavity created behind the pile during initial loading. In this phase it may be assumed that there exists a drag or friction along the side of piles. Whether or not the gap will develop may depend on the type of soil type. El-Naggar et al. (2005) assumes that the gap will develop for cohesive soils, whereas for cohesionless soils, the soil will cave in and close the gap. Still, centrifuge tests carried out on a pile in

dry sand indicate that this cave-in effect may not be fully developed, Klinkvort (2009), thus there is probably a need to include the drag effect in a model even for cohesionless soils. Klinkvort (2009).

One of the first attempts in formulating p-y-curves that reflected the observed behavior was done by Matlock et al. (1978). Later, Boulanger et al. (1999) proposed an elasto-plastic p-y model based on a two component set-up in which the loading response is handled by a series connection of springs – one spring handling loading (passive failure mode) and another spring handling the unloading-reloading properties of a pile subjected to cyclic loading that is gradually creating a gap behind the pile. Taciroglu et al. (2006) further developed these ideas and proposed a macro-element consisting of three components; leading-face element, rear-face element and drag-element. The two face-elements are formulated in terms of elasto-plastic springs supplemented with a tension cut-off. The drag element controls the side friction, when the pile is moving inside the cavity during unloading.

In the present work, the principles of the above-mentioned models are incorporated in a single spring element that can be directly incorporated in a standard finite element code. In the following the elasto-plastic constitutive relations will be presented. Then follows a discussion about the implementation and finally some results from simulations.

2 ELASTO-PLASTIC MODEL

A simple one-dimensional elasto-plastic spring is defined. The model is expressed in terms of the earth resistant force p and the associated displacement u.

The standard procedure for development of elasto-plastic models are used. First the operator split between elastic and plastic components is assumed.

$$du = du^e + du^p \tag{1}$$

where du^e is the elastic part and du^p is the plastic part of the total displacement increment du.

The plastic displacement component is defined in terms of the gradient to the plastic potential, i.e.

$$du^p = d\lambda \frac{\partial g}{\partial p} \tag{2}$$

with $d\lambda$ as the plastic multiplier. The direction of the plastic displacement increment is fixed to the loading plane, implying that the plastic flow potential is by definition associated to the yield surface, i.e. $f = g$.

The simplest yield function may be written as

$$f = |p| - p_u(\boldsymbol{\alpha}) = 0 \tag{3}$$

in which $p_u(\boldsymbol{\alpha})$ is the current strength yield strength and $\boldsymbol{\alpha} = (\alpha_1, \alpha_2, \dots)$ are the hardening parameters (to be defined later).

As mentioned above the flow rule is associated to the yield function, hence rewriting Eqn. (2) by use of Eqn. (3), we find

$$du^p = d\lambda \frac{\partial f}{\partial p} = \frac{p}{|p|} d\lambda \tag{4}$$

In case of plastic loading $f = 0$ the consistency requirement requires the stress point to remain on the yield surface, hence

$$df = \frac{\partial f}{\partial p} dp + \frac{\partial f}{\partial \boldsymbol{\alpha}} \frac{\partial \boldsymbol{\alpha}}{\partial \lambda} d\lambda = \frac{p}{|p|} dp - H\, d\lambda = 0 \tag{5}$$

where the hardening modulus H is the scalar contraction of the partial derivatives of the yield function with respect to $\boldsymbol{\alpha}$. For isotropic hardening, only a single hardening parameter is needed, i.e. $\boldsymbol{\alpha} \equiv \alpha$, but since we need to account for the development of a gap on the front and on the rear of the pile, respectively, it is necessary to introduce two hardening parameters as is presented in the coming sections.

As always the fundamental assumption of common elastic and plastic stress is used, hence

$$dp = k\, du^e = k(du - du^p) = k\left(du - \frac{p}{|p|} d\lambda\right) \tag{6}$$

where k is the elastic stiffness. Combining Eqn. (5) and Eqn. (6) yields the definition of the plastic multiplier $d\lambda$,

$$d\lambda = \frac{p}{|p|} \frac{k}{k+H} du = \frac{k}{k+H} |du| \tag{7}$$

Here it is used that the displacement increment is associated to the loading direction, hence $p \cdot du = 1$.

This relation is then entered back into Eqn. (6) to produce the elasto-plastic tangent stiffness,

$$k^{ep} = \frac{k\,H}{k+H} \tag{8}$$

This completes the formal definition of the plasticity model. Remaining is now to define the yield strength as a function of the hardening parameters.

2.1 *Yield function*

Following the terminology of Mayoral et al. (2005) and Matlock (1970) we divide the current yield strength into two parts; one relating to the drag contribution and one relating to the earth pressure.

$$p_u(\boldsymbol{\alpha}) = p_u^{\text{drag}} + p_u^{\text{face}}(\boldsymbol{\alpha}) \tag{9}$$

The first term p_u^{drag} is the drag capacity, which in this version of the model is assumed to be constant. Below this value, the spring is assumed linear elastic with a stiffness k. The second term must account for the

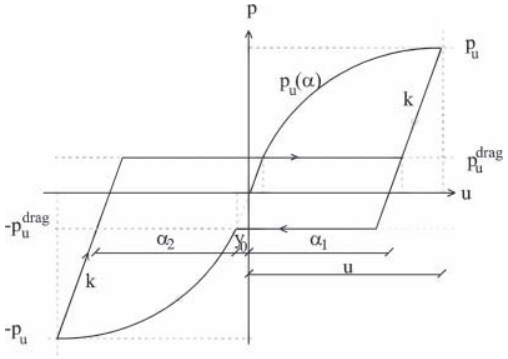

Figure 2. Schematic drawing of the spring element.

earth pressure when either of the pile faces are in contact with the soil. If there is no contact, this term must vanish. This can be achieved by introducing a multiplier to the virgin curve. The obvious candidate is a smooth step function,

$$S(x) = \frac{1}{1 + e^{-2\beta x}} \tag{10}$$

The parameter β defines the curvature and the coordinate x is

$$\begin{aligned} x_1 &= u - p_u^{\text{drag}}/k - \alpha_1 \quad \text{for} \quad u > 0 \\ x_2 &= -u + p_u^{\text{drag}}/k + \alpha_2 \quad \text{for} \quad u < 0 \end{aligned} \tag{11}$$

A typical value for β would be around 1.000.000. The coordinate x thus defines the current position of the pile relative to the soil. If the pile is in contact with the soil $x \geq 0$ and if there is a gap $x < 0$. Using Eqn. (9) we can write the yield function as

$$p_u^{\text{face}}(\boldsymbol{\alpha}) = \sum_i S(x_i)\, p_u^{\text{virgin}}(\alpha_i) \tag{12}$$

The hardening parameters α_i, $i = 1, 2$ represents either loading of the front or rear face of the pile. The virgin curve $p_u^{\text{virgin}}(\alpha)$ depends on the soil conditions as e.g. given by API (2000).

2.2 *Evolution law for hardening parameters*

Referring to Figure 2 it is easily seen that the hardening parameter α_i is defined as the plastic displacement accumulated during contact between soil and pile. Physically α is representing the progressive development of the gap. Using the experience from contact mechanics, it is deemed that a formulation of unloading and reloading in terms of a displacement criterion (rather than the usual stress based criterion) allows us to keep the formulation simple, even for the discontinuous phase when the pile is moving in the developed cavity.

The evolution law for the hardening parameters should thus be defined in such a way that they only develop when the pile is in contact with the soil. As long as the pile is sliding in the cavity created by the cyclic motion, the model should behave ideally plastic. Introducing once again the step function we may find

$$d\alpha_i = S(x_i) du^p = \frac{p}{|p|} S(x_i)\, d\lambda \tag{13}$$

in which the definition of the plastic displacement, Eqn. (4), is utilized. Having established the evolution law, it is finally possible to identify the model specific hardening modulus, H, by revisiting the consistency equation, Eqn. (5). After some manipulation we find that

$$\frac{p}{|p|}\, dp + \underbrace{\frac{p}{|p|} \sum_i \left[\frac{\partial p_u^{\text{virgin}}}{\partial \alpha_i} S^2 + p_u^{\text{virgin}} \frac{\partial S}{\partial \alpha_i} S \right]}_{-H} d\lambda = 0 \tag{14}$$

Note that the arguments α_i and x_i has been omitted in the formula. Analyzing Eqn. (14), it is noted half of the contributions vanishes if the soil is in contact with either the front face or the rear face of the pile, since the for the unloaded face $S = 0$. Likewise this relation ensures that $H = 0$ in the cavity since $S = 0$ for all terms.

3 IMPLEMENTATION

The proposed spring element is implemented in an in-house MATLAB based FE code, Hededal and Krenk (1995). The implementation consists of two parts. Firstly implementation of the spring element using a backward Euler integration scheme for integration of the constitutive relation. Secondly, a Winkler model based on the proposed model has been defined and analyzed using a Newton Raphson based non-linear solver.

For this specific application it has been chosen to use the (API 2000) definition of the p-y curves for sand,

$$p_u^{\text{virgin}}(u) = A\, p_{ult} \tanh\left(\frac{kX}{A\, p_{ult}} u \right) \tag{15}$$

Here p_{ult} is the ultimate capacity, A is a strength reduction parameter, k is the subgrade reaction modulus, X is the depth and u is the total lateral displacement.

Still, in order to implement this relation into the proposed format, it is necessary to divide the total resistance into a drag contribution and a face loading contribution, i.e.

$$p_u^{\text{virgin}}(u) = p_u^{\text{drag}} + p_u^{\text{face}}(\boldsymbol{\alpha}) \tag{16}$$

This is not a trivial task, since the hyperbolic function can not be easily inverted in order to allow

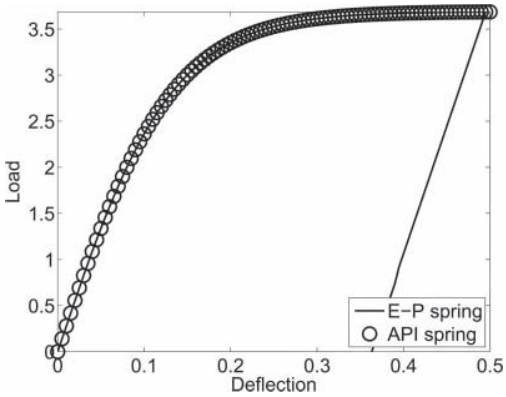

Figure 3. API curve versus the elasto-plastic curve.

Table 1. Pile soil properties.

Pile diameter	D	$1\,m$
Pile length	L	$6\,m$
Load eccentricity	e	$2.5\,m$
Frictional angle	ϕ	$42°$
Soil density	γ	$16\,kN/m^3$

for a split of elastic and plastic contribution. In the present situation, it has be chosen to use the following approximation,

$$p_u^{\text{face}}(\alpha_i) = A\,p_{ult}\tanh\left(\frac{kX}{A\,p_{ult}}u\right) - p_u^{\text{drag}} \tag{17}$$

Eqn. (17) is a implicit function in α since we have $u = \alpha + p/k$. This implies that the derivative with respect to α is not trivial. Here we use

$$\frac{\partial p_u}{\partial \alpha} \approx \frac{\partial p_u}{\partial u} \tag{18}$$

as a first order approximation. Comparing the API curve to the prediction of the model, Figure 3, this approximation appears to be acceptable.

4 RESULTS

To demonstrate the ability of the model to capture the pile-soil interaction as observed by Matlock (1970) and Mayoral et al. (2005), three test simulations have been carried out.

The material properties used in the three test examples are shown in Table 1. The three tests have been performed with a monotonic or cyclic laterally load applied in the top of the pile. A rather large stiffness has been used for the sand in order to clearly demonstrate the capability of the spring element.

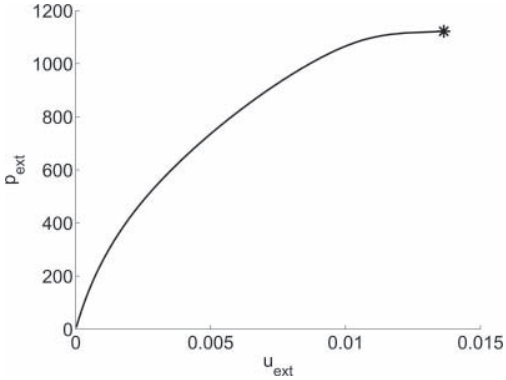

Figure 4. Overall response on a pile subjected to monotonic loading loading.

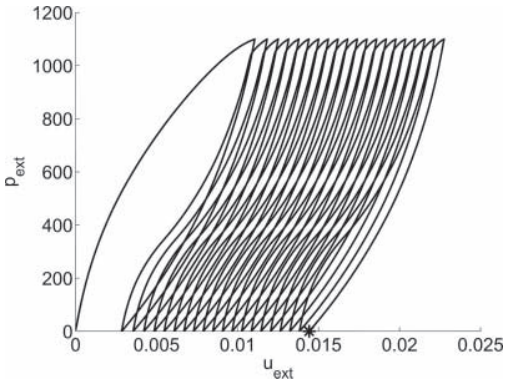

Figure 5. Overall response on a pile subjected to one-way loading.

4.1 *Example 1 – monotonic loading*

The spring element presented here is capable of performing cyclic tests. As demonstrated in Figure 3 the elasto-plastic element follows the virgin curve recommended by API (2000). Monotonic tests can therefore also easily be performed with this element. In Figure 4 the result as pile head deflection versus applied laterally load from a monotonic test can be seen. The maximum bearing capacity of the pile is calculated to $P_{max} = 1122\,kN$. Using the theory from Hansen (1961), the maximum bearing capacity can be calculated to $P_{max} = 1152\,kN$. This results fits very well with the calculation performed in the model.

4.2 *Example 2 – one way loading*

The second example illustrates a pile that is subjected to a load varying from zero and to a given value in the same direction, this is called one-way loading. The maximum load during the cycles is close to the ultimate capacity, so that the accumulation effect is clearly seen.

The overall pile response can be seen in Figure 5. This figure shows the pile top deflection versus the

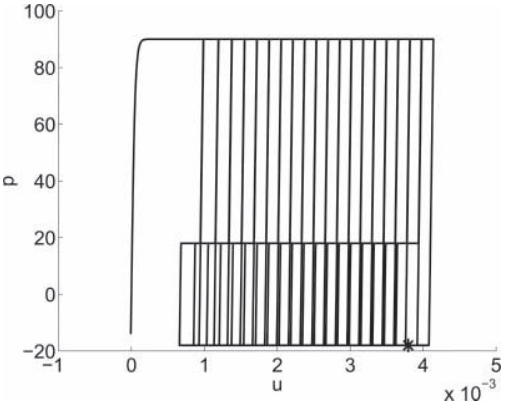

Figure 6. Spring response on a pile subjected to one-way loading.

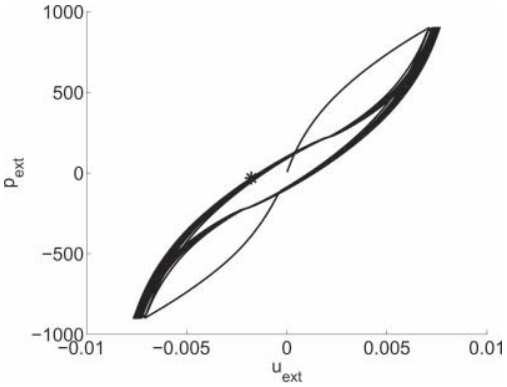

Figure 7. Overall response on a pile subjected to two-way loading.

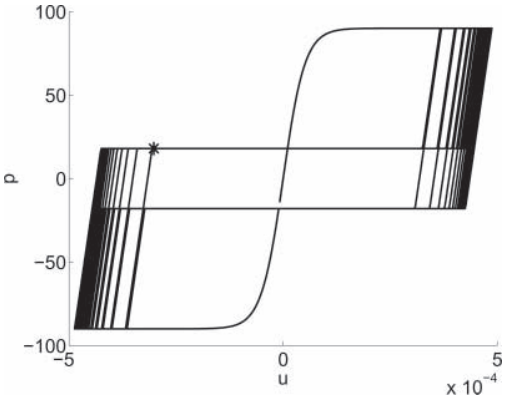

Figure 8. Spring response on a pile subjected to two-way loading.

applied force. The model simulates a load controlled test with constant load amplitude in a total of ten cycles. It can be seen from Figure 5 that the deflection increases with every cycle. Still, the rate of increase for every cycle is getting smaller and smaller. This shows that the model is able to take account for the accumulation of displacement when the model is subjected to one-way loading.

The response from one of the springs near the soil surface can be seen in Figure 6. The spring reaches fast the maximum bearing capacity. This is due to the high stiffness. It unloads elastically and then the development of a cavity can be seen. As described in section 2.2, no hardening occurs when the pile is moving in this cavity. It can also be seen that after the first cycle the the spring does not go back to its initial position, but exhibits a permanent deformation. This is due to the accumulation of deflection. The accumulation of deflections occurs due to the development of cavity in several springs and the subsequent redistribution of the force therefore occurs.

4.3 *Example 3 – two way loading*

In this example the pile is subjected to a given load varying between negative and positive values, this is called two-way loading. The overall pile response can be seen in figure Figure 7. The pile is loaded five full cycles. The same maximum force is applied for both direction. It can be seen from Figure 7 that the deflection is getting larger and larger from every load cycle. This is valid for both sides and the increase in deflection is also the same for both sides. This means that the average deflection of the load cycles is constant and equal to zero. It is though interesting that the deflection amplitude increases, hence the secant stiffness will decrease as a consequence of cyclic loading. This effect is extremely important if we are to model the cyclic response of monopile foundations for wind turbine, since the load here is frequency dependent.

It should be noted that the number of iterations increases dramatically after the first half cycle when the pile is in a position around the mean deflection. This is due to the development of a cavity in nearly all spring elements. In this position the system have very low stiffness. A simple remedy to this could be to include a small amount of kinematic hardening to the drag-term in a manner as proposed by Hededal and Strandgaard (2008).

The response from one of the springs can be seen in Figure 8. It can be seen that a cavity develops as expected. As for the overall pile response, an increase in deflection of the single spring for every load cycle is observed. Also here the average deflection for an overall load cycle is constant and equal to zero. There is no degradation of the springs which can be seen in one-way loading example.

5 DISCUSSION

The cyclic spring presented in this paper is capable of capture physical aspects as seen in tests Matlock (1970), Mayoral et al. (2005) and Klinkvort (2009). Still, improvements are needed. In this section ideas

which will improve the performance of the spring element and the representation of the physical world.

The presented model operates with the same virgin stiffness as un-/reloading stiffness. This could be changed and it must also be expected that a soil not will load and unload with the same stiffness. With a change like this the model will probeable start to accumulate displacements in a smaller loading range.

When springs moving in the cavity some sort of hardening should occur. This can also be seen in the Figure 1 by Mayoral et al. (2005). As a side effect an introduction of hardening in the cavity will help the global iterations to converge faster.

Other effects which should be incorporated in the future is suction release for clay springs and the fall back of sand particle when dealing with sand springs.

6 CONCLUSION

An elasto-plastic spring element has been defined. The spring element embeds two fundamental features of cyclically loaded piles. It is able to account for preloading of the soil by tracing the virgin curve. Secondly, the creation of a gap after reloading, which is undeniably developing in cohesive soils, is accounted for by introducing a smoothed step function that keeps track of the current position of the pile-soil interfaces. The element is not only relevant for the quasi-static loading with random time series, but also has a potential in dynamic analysis, where it will provide a physically based hysteretic damping.

REFERENCES

API (2000). American petroleum institute. recommended practice for planning, designing and constructing fixed offshore platforms- working stress design, api recommended practice 2a-wsd (rp2a-wsd), 21st edition, dallas.

Boulanger, R. W., C. J. Curras, B. L. Kutter, D. W. Wilson, and A. Abghari (1999). Seismic soil-pile-structure interaction experiments and analyses. *Journal of Geotechnical and Geoenvironmental Engineering 125*(9), 750–759.

El-Naggar, M. H., M. A. Shayanfar, M. Kimiaei, and A. A. Aghakouchak (2005). Simplified bnwf model for nonlinear seismic response analysis of offshore piles with nonlinear input ground motion analysis. *Canadian Geotechnical Journal 42*, 365–380.

Hansen, J. B. (1961). The ultimate resistance of rigid piles against transversal forces. *Danish Geotechnical Institute, Copenhagen, Denmark Bulletin NO. 12*, 5–9.

Hededal, O. and S. Krenk (1995). *FEMLAB – matlab toolbox for the Finite Element Method*. Aalborg University.

Hededal, O. and T. Strandgaard (2008). A 3d elasto-plastic soil model for lateral buckling analysis. In *Proc. 18th International Offshore and Polar Engineering Conference, ISOPE 2008*.

Klinkvort, R. T. (2009). Laterally loaded piles – centrifuge and numerical modelling. Master's thesis, Technical University of Denmark.

Matlock, H. (1970). Correlations for design of laterally loaded piles in soft clay. In *Offshore Technology Conference*, pp. 577–594.

Matlock, H., H. C. Foo, and L. M. Bryant (1978). Simulation of lateral pile behavior under earthquake motion. In *Proc. American Society of Civil Engineers Specialty Conference on Earthquake Engineering and Soil Dynamics*, Volume 2, pp. 600–619.

Mayoral, J. M., J. M. Pestana, and R. B. Seed (2005). Determination of multidirectional p-y curves for soft clays. *Geotechnical Testing Journal of Computational Mechanics Vol. 28*, No.3.

Taciroglu, E., C. Rha, and J. Wallace (2006). A robust macroelement model for soil-pile interaction under cyclic loads. *Journal of Geotechnical and Geoenvironmental Engineering, ASCE 132*(10), 1304–1314.

The installation and foundation cost of offshore wind turbines is substantial, and today energy from offshore wind is not competitive with energy from more classical energy production methods. The goal of this research project has been to develop simple engineering tools, which can be used in the design of a technical optimal and cost beneficial solution for monopiles supporting offshore wind turbines. The methodologies developed in this thesis can be directly used in the design of offshore monopiles, with a scientific justification based on centrifuge model scale tests.

DTU Civil Engineering
Department of Civil Engineering
Technical University of Denmark

Brovej, Building 118
2800 Kgs. Lyngby
Telephone 45 25 17 00

www.byg.dtu.dk

ISBN: 9788778773579
ISSN: 1601-2917